THE FINITE ELEMENT METHOD APPLIED TO THE THIN SHELLS AND BOX STRUCTURES

Author: M.J.Todd, B.A.

Supervisor: Dr. R.J.Allwood, Ph.D., M.I.C.E.

Submitted for Ph.D. of Loughborough
University of Technology

April 1970

SUMMARY

Using the assumed stress approach first presented by T.H.H.Pian, two finite elements have been developed which may be used for the analysis of thin shells and box structures. One has seven degrees of freedom at each node, the other has twelve. In addition, improved elements for two-dimensional membrane analyses have also been produced and compared. An existing program for the handling of the computation involved in such analyses has been developed to allow the large number of equations resulting from practical three-dimensional problems.

A wide ranging comparison of the new shell elements with existing knowledge of a variety of structures is presented in the thesis which enables the user-engineer to select the appropriate element in any given set of circumstances. Also there are included the results of analysing some practical problems, in particular a motorway bridge deck of cellular construction.

In general, good results are achieved although the improvements over existing methods is more significant for box structures, for which less is known, than the thin shells about which more is known.

Acknowledgements

The author wishes to thank Dr. R.J.Allwood for the advice and direction he has given, particularly during the period of the work reported in this thesis.

Thanks are also due to Professor G.C.Brock for making the facilities of the Civil Engineering Department available, to the staff of the University Computer Centre for their help and cooperation, in particular Mr. D.C.Hogg and Mr. J.E.Sawbridge for their assistance in overcoming many programming difficulties, to the Board of Managers of the University of London Computer Centre for making available the facilities of their Computer Centre, to Mr. J.R.Turner for providing the results quoted in chapter eight, and to the Science Research Council who provided financial support.

In addition, the author would like to thank his wife, Christine, for her understanding and tolerance throughout this project.

TABLE OF CONTENTS

INDEX OF FIGURES

Introduction

The design of structures involves at some stage a determination - analysis - of the stresses or strains throughout the structure under a variety of loading cases. For many years engineers have sought methods which will improve their knowledge of and ability to analyse structures. In all cases, the theories produced are limited in their scope of application. At the outset of any analysis the real-life structure has to be simplified to a greater or lesser extent and it is one of the aims of research to reduce the difference between reality and theory as much as possible.

Of the many techniques developed to determine stress and strain distributions in linearly elastic structures, the Finite Element Method is one which is capable of general application. (For a full description of the method see Zienkiewicz [1] or Holand & Bell [2])

This technique consists, in principle, of dividing a complex problem into small parts each of which is analysed separately. These small parts, called "Finite elements", are assembled together to produce an analysis of the whole. Whilst, ideally, each element would be analysed exactly, it is not in general possible to do this; some degree of approximation is involved. This is done by chosing a finite set of basic solution patterns each of which satisfies the boundary conditions of the element. Since we may use the Principle of Superposition, the best approximate solution to a particular loading may be obtained by linear combinations of this basic set. The extent to which this solution matches the exact distribution depends on the choice of the basic set.

The basic patterns are expressed in terms of the values of the distribution at certain discrete points, known as nodes, and the values are referred to as "degrees of freedom". This expresses the fact that these values are to be determined independently, the values at all other points in the problem are interpolated between them by the basic distribution patterns. The greater the number of degrees of freedom in the whole problem the greater the complexity of variation that can be generated from linear combinations of the basic patterns within each element.

As an illustration of these fundamental principles, consider the one-dimensional distribution of stress shown in fig. 1(a). We first divide the region of the problem, in this case the horizontal axis, into, say, four segements, (finite elements). Taking next as the basic set in each segment only the constant distribution we can approximate to the original by such as in fig. 1(b).

If, instead, we allow a linear variation through each element we can obtain a better approximation, fig. 1(c). If, in addition, we divide the problem into a greater number of segments, or elements, we have an even better result, fig. 1(d). We say that by further subdivision the solution is "converging" to the exact distribution. Of course, had the original distribution - the "exact" solution - been composed of straight lines, we could have complete convergence simply by suitable choice of elements. This is important to note since with most elements there are special loading or boundary conditions for which they can provide an exact solution. This in no way improves

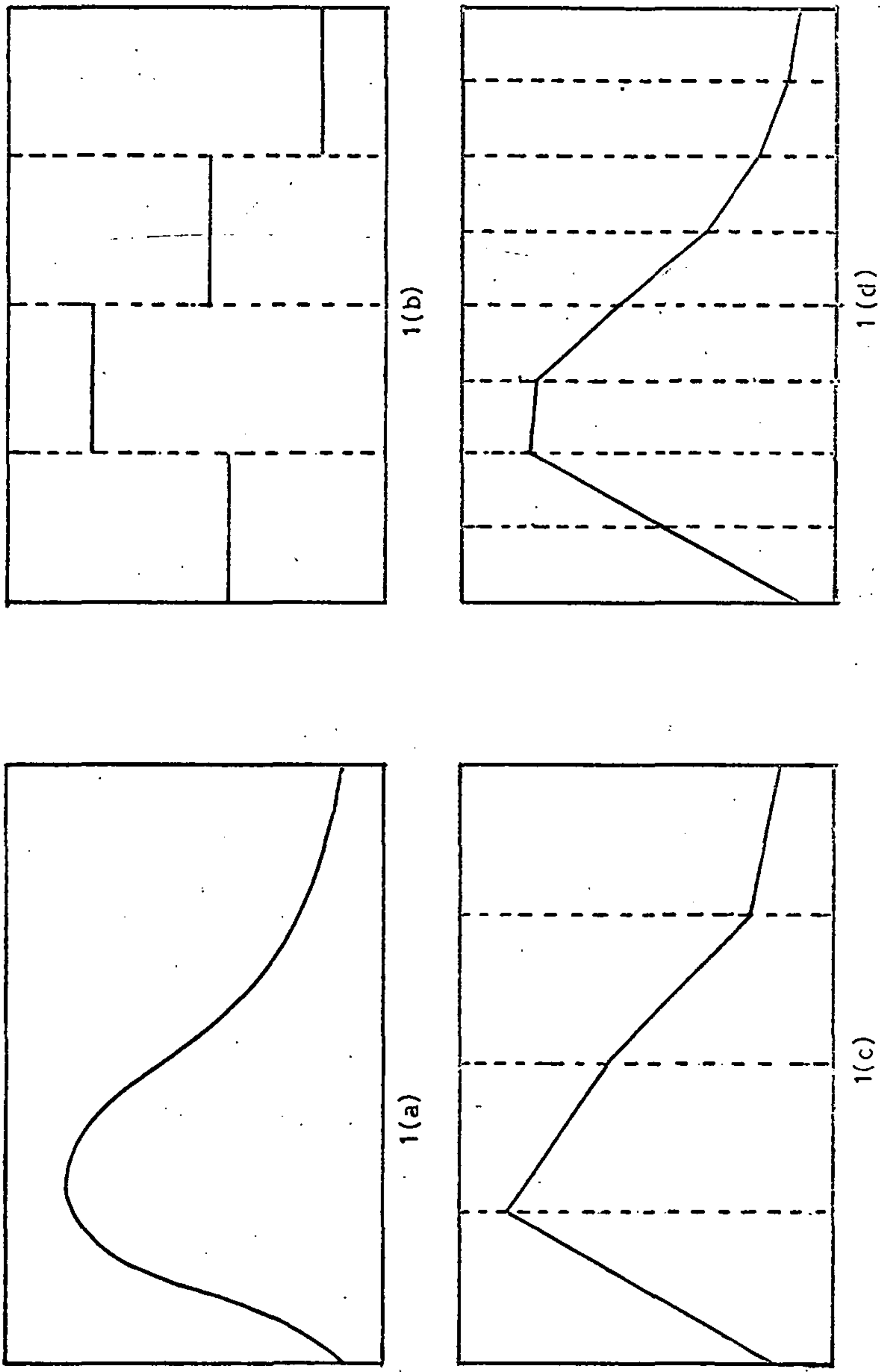

Fig.1 One dimensional distribution

its ability to match any other, more general, stress or strain distribution.

This then is the basis of the Finite Element Method: that by sufficient subdivision of the original problem we can obtain as exact a solution as we require. To improve an approximate solution two approaches are possible. Either improve the variation of stress/strain within each element, keeping the same number of elements, or increase the number of elements with the same degree of approximation within each element.

A great deal of success has been achieved by pursuing the latter course, but many problems remain unsolved and thus, in this thesis, we are concerned with the former approach. A considerable amount of effort has been devoted to the development of a wide range of two dimensional elements of varying sophistication, from the earliest Taig element - a membrane triangular element with two degrees of freedom at each node [6] - to the complex iso-parametric elements of Zienkiewicz.[8] These are all limited to in-plane (membrane) forces. Correspondingly, elements have also been developed to solve problems with forces wholly out-of-plane (bending).[5]

Work by Douthwaite[7] on a rectangular membrane element has shown that benefits can be gained from the use of additional degrees of freedom at each node. Following this, this thesis begins with an examination of this aspect of membrane element improvement. Whilst some interest derives from this particular problem, the primary object of this author's work is the combination of membrane and bending effects into a shell element. This field has received some attention yet lacks features essential for the routine analysis of shell structures. Whilst much design work has been carried out using plane analogies for essentially three dimensional problems, there are many instances in which such calculations are barely justifiable and a genuine need exists for analyses which properly represent three dimensional interactions. One class of such problems includes those in which the thicknesses of the structural elements are small in relation to their other dimensions. This allows not only the classical shell problems such as cylinders, but also problems containing a sharp discontinuity in the slope of the geometry at, for example, the corner of a box. An illustration of this is the typical cellular construction of motorway bridges popular today. The object of this work is to allow the engineer to solve both of these types of problem with the same shell finite element, using as coarse a mesh as possible. Ultimately, each structural element would be represented by a single element unless geometrical considerations ruled otherwise. For example, in a motorway bridge the webs of the cells would be represented by a single element from top to bottom. (Present limitations insist that longitudinal subdivision be used, although only a few elements should, ideally be required.) All this arises from a complementary ideal, which is that as far as possible the user-engineer should have to specify as little data as possible that is not normally generated in an engineering definition of the problem on, say, a drawing. In fairness, it should also be pointed out that it is possible that in the future automatic mesh generation will provide another answer to this problem.

Smooth curved shells, such as a cylindrical roof, will have to be represented by multi-faceted polyhedra in which each face is an element, but again the object is to reduce to a minimum the number of elements. The generation of the data for the definition of each facet is tedious and error-prone.

Whilst several elements have been developed to solve thin shell problems, quite successfully in many cases, they lack, in general, one important feature. This is, see fig. 2, the transmission of out-of-plane bending moments from one element into the in-plane moment of an adjacent element. In a membrane shell this effect is not, of course, present, nor would it be if all elements lay in the same plane. However, flat two dimensional elements, when used to approximate to a smooth curved shell, do not lie so and the absence of this effect can be quite marked.

Such elements are capable of solving problems of smooth curved shells using a large mesh of elements to reduce the angle between neighbouring elements as much as possible. In the box-type of structure this effect cannot be ignored, indeed it dominates much of the stress distribution. An element capable of representing this effect is required for the analysis of present day structures.

Plate elements have been developed which include out-of-plane rotations as independent degrees of freedom. In particular, that of Allwood and Cornes[5] has been used in this work. In order to complete the full shell effect a membrane element is required that will combine with this plate element to produce the interconnection. The first of two shell elements, called S7, includes rotations about all three rectangular axes as independent degrees of

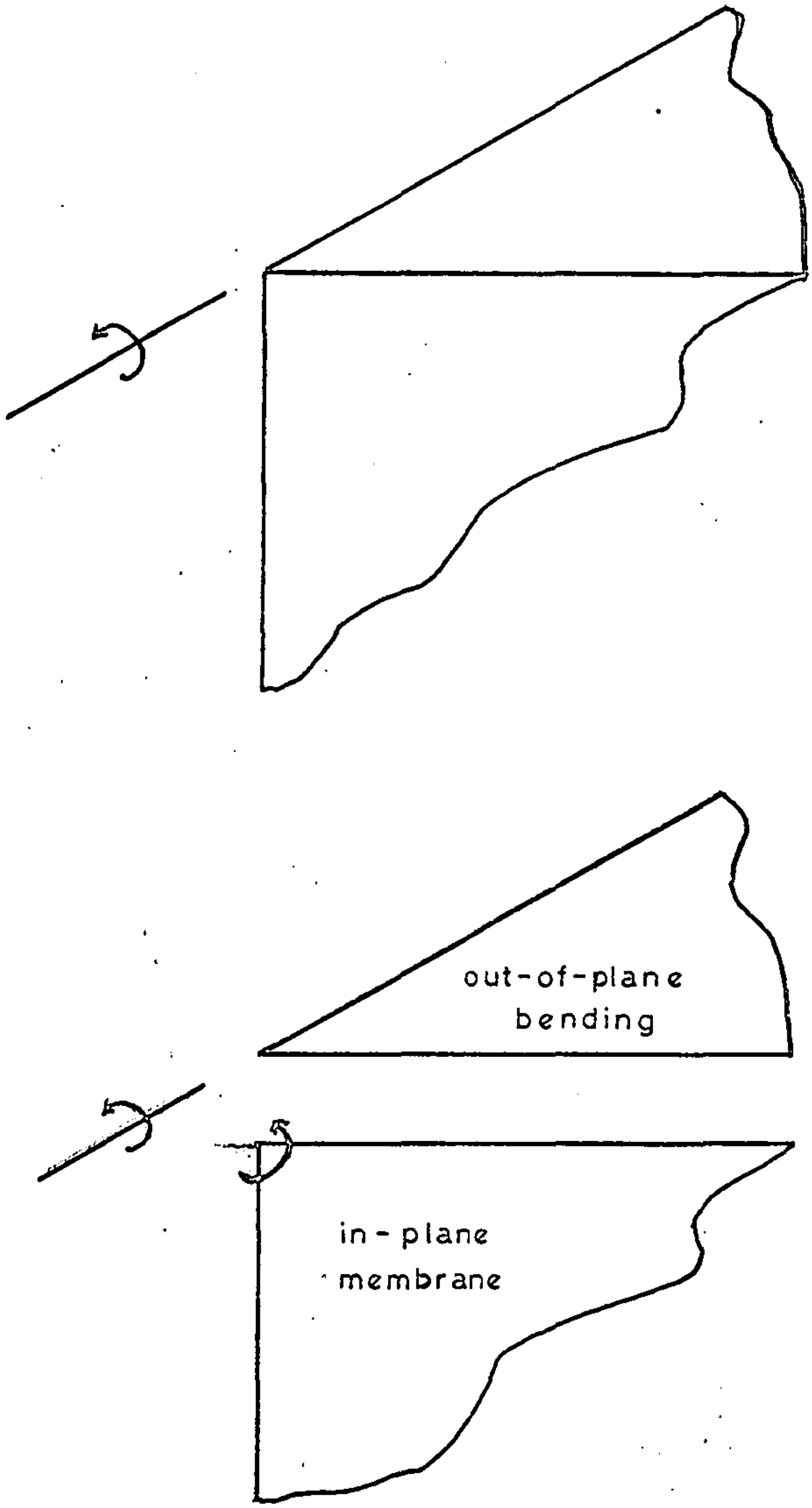

Fig. 2 Interaction between bending and membrane action at a box corner

freedom. Considering only the average rotation about a given direction at any point as a degree of freedom has one serious implication. That is, that the rotation of any line drawn in the plane of the element through that point is the same and consequently no shear strain is allowed to develop. In terms of derivatives the average rotation, $\theta = \frac{1}{2}(\frac{\partial v}{\partial x} - \frac{\partial u}{\partial y})$ and the shear strain, $\gamma = (\frac{\partial u}{\partial x} + \frac{\partial v}{\partial y})$ In some instances the enforced zero shear strain at the nodes can be particularly serious, although it will be demonstrated that for many practical problems quite adequate solutions are obtained despite this error.

On the other hand, it will also be shown that there are important cases when this shear strain is so significant in the distribution of stresses that solutions cannot be approached without allowing shear to develop. For these problems a more sophisticated element has been developed, called S12, which uses derivatives such as $\frac{\partial u}{\partial x}, \frac{\partial v}{\partial y}$ as independent degrees of freedom. (The significance of these names will become apparent later.) In both elements the bending effects are represented by the same plate element in combination with different membrane elements.

The contents of this thesis are divided into two parts. The first examines a range of membrane elements, two of which are selected as suitable for shell elements. These latter are then compared in the second half and the circumstances under which the simpler S7 element is applicable are largely delimited and one important example of the use of the S12 element concludes the work. It is the object of research such as this to provide the user-engineer with rules under which he may use any particular element with some measure of confidence in the results, without having to reconsider the underlying assumptions on every occasion.

Chapter One Derivation of plane stress elements

1.1 Displacement approach

Historically, the first finite element approach consisted of determining the minimum potential energy solution from a basic set of displacement patterns. It was considered an important condition for convergence, indeed later proved as sufficient [10] that these basic patterns be compatible. That is to say, the values of displacements along a common boundary should not be different for adjacent elements. Put another way, the displacements along such a boundary should depend only on the values of the degrees of freedom at either end of it.

Whilst this condition of compatibility is not a necessary condition, (see, for instance, Bazeley et.al.[11]) it is often difficult to predict the results of using non-compatibly formulated elements. The more complex the element, the more difficult it becomes to devise fully compatible displacement patterns. There is even no guarantee of the existence of such patterns. Newer improvements to this method, such as area coordinates, (see Bazeley et.al. [11]) and iso-parametric elements,[8] have enabled the development of compatible elements at the expense of a greater quantity of computation.

1.2 Assumed stress approach

An alternative solution to the problem of compatibility was put forward in 1964 by Pian.[4] This hybrid method assumes displacement patterns around the boundary alone. Within the element, stress distribution patterns are assumed instead. As a result, there is no difficulty in ensuring compatibility between elements.

In contrast with the displacement approach this method minimises the complementary energy functional, π :

$$\pi = U - \sum_i \int u_i S_i ds \qquad \text{........ (1)}$$

where

U = strain energy

u_i = boundary displacement produced by ith nodal degree of freedom

S_i = corresponding boundary force

By expressing the stresses, $\underline{\sigma}$, as polynomials with unknown coefficients, $\underline{\beta}$,

$$\underline{\sigma} = P.\underline{\beta} \qquad \text{........ (2)}$$

Pian showed that

$$U = \tfrac{1}{2}\underline{\beta}^t.H.\underline{\beta}$$

where

$$H = \int P^t.N.P \; dv \qquad \text{........ (3)}$$

and N is the elasticity matrix:

$$\underline{\epsilon} = N.\underline{\sigma} \qquad \text{........ (4)}$$

Further, he showed that by assuming polynomial interpolation functions for the boundary displacements in terms of the nodal displacements, $\underline{q}$

$$\underline{u} = L.\underline{q}$$

the work done by the boundary forces can be expressed as:

$$\underline{\beta}^t.T.\underline{q}$$

where

$$T = \oint P_s^t.L.ds \qquad \text{........ (5)}$$

and P_s is derived from P and represents the stresses along the boundary.

Minimising the complementary energy, Pian finally arrived at the stiffness matrix, k .

$$k = T^t . H^{-1} . T \qquad \text{........ (6)}$$

Whilst for the Pian method, unlike the displacement approach, there is no rigid constraint on the number of unknown stress coefficients, β , that can be used with a given configuration of element degrees of freedom, there is one important factor to be borne in mind, which was first pointed out by Tong and Pian.[13]

This concerns the lower limit of the number of coefficients, NSTREC. If we denote the rank of a matrix by r( ), we have, from equation (5) above:

$$r(k) \leq \min(r(T^t), r(H^{-1}), r(T))$$
$$= \min(r(T), r(H)) \qquad \text{........ (7)}$$

since column rank = row rank: $r(T^t) = r(T)$

and H is non-singular: $r(H^{-1}) = r(H) = \text{NSTREC}$

If, for a given type of element, there are m degrees of freedom which are required to represent rigid body motion then

$$r(k) \geq k_1 - m \qquad \text{........ (8)}$$

where k_1 is the number of degrees of freedom of the element. Thus from equations (7) & (8) we have that:

$$\text{NSTREC} \geq k_1 - m$$

For example, consider the element Pian first derived which was a rectangular element with two degrees of freedom at each node. For this element:

$$k_1 = 8 \quad \text{and} \quad m = 3$$

Thus to ensure that the element will always provide a solution when only rigid body motion has been constrained from the element:

$$\text{NSTREC} \geq 5$$

In practice this requirement is not entirely necessary, for in an assembly of elements there may be sufficient independent equations to provide a solution even with the minimum constraints. In some of the elements to be considered in later chapters, a value of NSTREC less than the strict minimum has been used without any undue harm other than the failure with an artificial problem of one element with three constraints.

There is no rigid upper limit on NSTREC, but as the stress functions increase in length, the element will converge to the equivalent displacement element. It appears, however, that there is no real benefit in continuing beyond a relatively short function. This has been discussed by Cornes[14] and so will not be pursued further here. As far as possible the minimum practical value has been used throughout.

Pian's original paper [4] only considered a rectangular element in plane stress but subsequently rectangular and right-angled triangular elements for plate bending have been developed. (See Severn and Taylor [15]) However, it is necessary for the adequate representation of problem geometries to have elements which are either general triangles or quadrilaterals. Such an element has been produced for the plate bending case and is quite successful. (See Allwood and Cornes [5])

For the general polygonal element, it is simpler to work in terms of each side of the element in turn, the final element stiffness matrix being the combination of contributions from each. This method was first used by Allwood and Cornes[5] for the plate bending element. The only restriction imposed by this approach is that each nodal degree of freedom must introduce displacements along the two adjacent boundaries only. In practice this means that the interpolation polynomials must be functions of x' alone and not of y'. (See fig. 3 for notation.)

For the H matrix (equation (3)) we calculate the HI matrix which is the integral of the H matrix under the side in question. The integral for the whole area of the element is then the sum of the individual HI matrices.

The TI matrix, similarly, is the integral along the one edge of the element of the T matrix. (equation (5)) It is convenient to work in terms of the stresses and displacements related to the set of axes parallel and normal to the side itself. If M is the matrix which transforms the global stresses into these axes and L interpolates the corresponding displacements from the nodal displacements, we have that

$$TI = \int_{N_1}^{N_2} P_s{}^t . M^t . L \, ds \qquad \ldots\ldots\ldots (9)$$

Further, we may consider L as being composed of two other matrices L' and W, where

$$L = L'.W$$

and L' interpolates the edge displacements from the nodal displacements given in local terms and W transforms the nodal displacements from global to local axes.

1.3 New plane stress elements

The work of Douthwaite [7] showed that considerable benefits can accrue from the increasing of the degrees of freedom per node from two to four, especially in problems which contain a measure of in-plane bending, such as in a cantilever. However, the particular degrees of freedom he

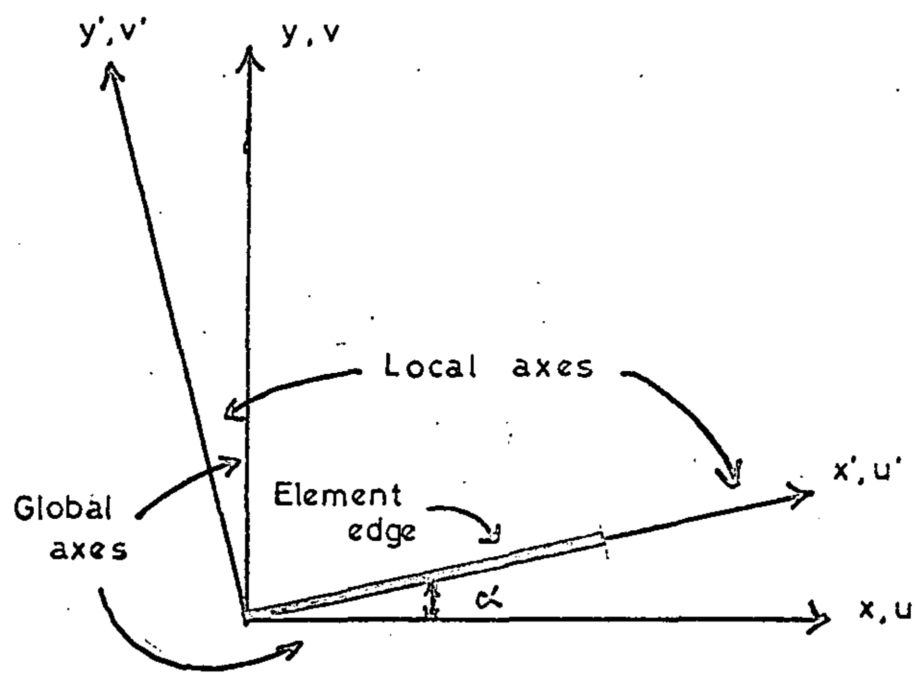

Fig. 3 Axis notation

chose, $u, v, \frac{\partial v}{\partial x}, \frac{\partial u}{\partial y}$, are applicable only to rectangular elements. This is because that for the general polygon in the Pian method it is necessary to express the nodal degrees of freedom in the global axes in terms of those in the local axes parallel and normal to each edge in turn. However, the four first derivatives of displacement, $\frac{\partial u}{\partial x}, \frac{\partial u}{\partial y}, \frac{\partial v}{\partial x}, \frac{\partial v}{\partial y}$, each individually give rise to components of all four of the "rotated" derivatives. (See section 1.4) Logically, the next element to be considered after the simple "u-v" element is that with the full set of six degrees of freedom at each node, including all the derivatives of displacement as independent degrees: $u, v, \frac{\partial u}{\partial x}, \frac{\partial u}{\partial y}, \frac{\partial v}{\partial x}, \frac{\partial v}{\partial y}$ (The derivatives may be interpreted thus:

$\frac{\partial v}{\partial x}, \frac{\partial u}{\partial y}$: rotations of x and y axes respectively

$\frac{\partial u}{\partial x}, \frac{\partial v}{\partial y}$: direct strains in x and y directions respectively)

However, it is important to realise that for a given number of elements in a mesh, the computation involved in producing a solution from start to finish including both the calculation of the element stiffness matrices and the solution of the assembled equations, increases more than proportionally with the number of degrees of freedom at each node. It is, thus, essential to keep these to a minimum, balancing this against the improvements to be gained from more sophisticated displacements and stress patterns.

The choice of a set of degrees of freedom between the simple two and the complete six is limited by the one important factor already mentioned. Since we are concerned with the general polygonal element, it is essential that the solution of any problem in one set of axes is the same as in a rotated set of axes. This in turn implies that the set of nodal degrees of freedom expressed in one set of axes, must be related to the corresponding degrees of freedom in another set of axes at an angle to the first set. The set of four degrees of freedom used by Douthwaite (7), for example, cannot be so expressed and is thus not suitable for a general polygonal element. Two variables are significant in this context in that they are invariant under an axis rotation and are thus emminently suitable as degrees of freedom. These are:

(i) average rotation, $\theta = \frac{1}{2}\left(\frac{\partial v}{\partial x} - \frac{\partial u}{\partial y}\right)$

(ii) dilation, $e = \left(\frac{\partial u}{\partial x} + \frac{\partial v}{\partial y}\right)$

and two further elements have been derived, one using three degrees of freedom and the other four. The former takes the average rotation in addition to the two direct displacements and the latter both of the above.

To summarise, the elements to be considered are:-

TAIG	u, v
PIAN	u, v
RECT4	$u, v, \frac{\partial v}{\partial x}, \frac{\partial u}{\partial y}$
GEN6	$u, v, \frac{\partial u}{\partial x}, \frac{\partial u}{\partial y}, \frac{\partial v}{\partial x}, \frac{\partial v}{\partial y}$
GEN3	u, v, θ
GEN4	u, v, e, θ

In section 1.4 below the stiffness matrix for the six degree of freedom element, GEN6 will be derived in detail. In this derivation the only changes that need be made for the other nodal configurations are in the L matrix. The changes to this are elementary and need no elaboration. The differences in the behaviour of these elements will be examined in detail in chapter three.

1.4 Derivation of element stiffness matrix

Following Mallick and Severn [16], the stress patterns assumed for this element are based on the Airy stress function. This is defined such that the function ϕ leads to:

$$\sigma_x = \frac{\partial^2\phi}{\partial y^2} \qquad \sigma_y = \frac{\partial^2\phi}{\partial x^2} \qquad \tau_{xy} = \frac{\partial^2\phi}{\partial x \partial y}$$

The following form is assumed for ϕ:

$$\begin{aligned}\phi = {} & A_1(y^2/2) + A_2(y^3/6) + A_3(x^2/2) + A_4(x^3/6) + A_5(xy) \\ & + A_6(xy^2/2) + A_7(x^2y/2) + A_8(y^4/12) + A_9(x^4/12) \\ & + A_{10}(x^2y^2/2) + A_{11}(x^3y/6) + A_{12}(xy^3/6) + A_{13}(y^5/20) \\ & + A_{14}(xy^4/12) + A_{15}(x^2y^3/2) + A_{16}(x^3y^2/2) + A_{17}(x^4y/12) \\ & + A_{18}(x^5/20)\end{aligned} \qquad \ldots\ldots\ldots (10)$$

However, ϕ must satisfy the biharmonic equation which gives us:

$$\left.\begin{aligned} A_{10} &= -\tfrac{1}{2}(A_9 + A_8) \\ A_{16} &= -A_{14}/6 - \tfrac{1}{2}A_{18} \\ A_{15} &= -A_{17}/6 - \tfrac{1}{2}A_{13} \end{aligned}\right\} \qquad \ldots\ldots\ldots (11)$$

We thus have 15 independent stress coefficients. (i.e. NSTREC = 15). Noting what was said earlier about the value of NSTREC this, strictly, allows us to use only a triangle. (3 nodes * 6 d.f. - 3 rigid body = 15). For a quadrilateral we would need 21 independent stress coefficients, a considerable jump in the quantity of computation required. As a consequence, although there is no theoretical reason why not, six degree of freedom quadrilateral elements have not been considered in this thesis.

From equations (2), (10), & (11) we have the following P matrix:

$$
\left(\begin{array}{ccccccccccc}
1 & y & 0 & 0 & 0 & x & 0 & y^2-\frac{1}{2}x^2 & -\frac{1}{2}x^2 & 0 & xy \\
0 & 0 & 1 & x & 0 & 0 & y & -\frac{1}{2}y^2 & x^2-\frac{1}{2}y^2 & xy & 0 \\
0 & 0 & 0 & 0 & 1 & -y & -x & xy & xy & -\frac{1}{2}x^2 & -\frac{1}{2}y^2
\end{array}\right. :
$$

$$
: \left.\begin{array}{cccc}
y^3-3x^2y/2 & xy^2-x^3/6 & -\frac{1}{2}x^2y & -\frac{1}{2}x^3 \\
-\frac{1}{2}y^3 & -\frac{1}{2}y^2x & x^2y-y^3/6 & x^3-3xy^2/2 \\
3xy^2/2 & \frac{1}{2}x^2y-y^3/3 & \frac{1}{2}xy^2-x^3/3 & 3x^2y/2
\end{array}\right)
$$

We also have from the equation of elasticity:

$$
\begin{aligned}
\epsilon_x &= \frac{1}{E}\cdot(\sigma_x - \nu.\sigma_y) \\
\epsilon_y &= \frac{1}{E}\cdot(\sigma_y - \nu.\sigma_x) \\
\gamma_{xy} &= \frac{2(1+\nu)}{E}\cdot \tau_{xy}
\end{aligned}
\qquad \ldots\ldots\ldots (12)
$$

which gives us the N matrix of equation (4) as:

$$
\frac{1}{E}\cdot \begin{pmatrix} 1 & -\nu & 0 \\ -\nu & 1 & 0 \\ 0 & 0 & 2(1+\nu) \end{pmatrix}
$$

The P_s matrix is derived from the above P matrix by making the following substitution:

$$
\begin{aligned}
x &= X_1 + sL\cos\alpha \\
y &= Y_1 + sL\sin\alpha
\end{aligned}
\qquad s = x/L
$$

where (X_1, Y_1) are the coordinates of the first node of the side and L is the length of the side. This gives the stress, in global axes, along the boundary. The transformation of these stresses into those in local axes is given by:

$$\sigma = \sin^2\alpha.\sigma_x + \cos^2\alpha.\sigma_y - 2\sin\alpha\cos\alpha.\tau_{xy}$$

$$\tau = -\sin\alpha\cos\alpha.\sigma_x + \sin\alpha\cos\alpha.\sigma_y - \tau_{xy}(\sin^2\alpha - \cos^2\alpha)$$

From this the matrix M is obtained:

$$\begin{pmatrix} -\sin\alpha\cos\alpha & \sin\alpha\cos\alpha & \cos^2\alpha - \sin^2\alpha \\ \sin^2\alpha & \cos^2\alpha & -2\sin\alpha\cos\alpha \end{pmatrix}$$

For the L matrix we shall consider the following set of degrees of freedom:

$$u,\ v,\ \frac{\partial u}{\partial x},\ \frac{\partial u}{\partial y},\ \frac{\partial v}{\partial x},\ \frac{\partial v}{\partial y}\ .$$

The matrix L is compounded from two other matrices L' and W where:

L' are the interpolation polynomials for the degrees of freedom in local axes and

W is the transformation of these into global axes.

Using the notation of fig.3 we have the following relations:

$$\left.\begin{aligned} u' &= u.\cos\alpha + v.\sin\alpha \\ v' &= -u.\sin\alpha + v.\cos\alpha \end{aligned}\right)\quad \left(\begin{aligned} x &= x'.\cos\alpha - y'\sin\alpha \\ y &= x'.\sin\alpha + y'\cos\alpha \end{aligned}\right.$$

Therefore:

$$\frac{\partial u'}{\partial x'} = \cos^2\alpha.\frac{\partial u}{\partial x} + \sin\alpha\cos\alpha.\frac{\partial u}{\partial y} + \sin\alpha\cos\alpha.\frac{\partial v}{\partial x} + \sin^2\alpha.\frac{\partial v}{\partial y}$$

$$\frac{\partial u'}{\partial y'} = -\sin\alpha\cos\alpha.\frac{\partial u}{\partial x} + \cos^2\alpha.\frac{\partial u}{\partial y} - \sin^2\alpha.\frac{\partial v}{\partial x} + \sin\alpha\cos\alpha.\frac{\partial v}{\partial y}$$

$$\frac{\partial v'}{\partial x'} = -\sin\alpha\cos\alpha.\frac{\partial u}{\partial x} - \sin^2\alpha.\frac{\partial u}{\partial y} + \cos^2\alpha.\frac{\partial v}{\partial x} + \sin\alpha\cos\alpha.\frac{\partial v}{\partial y}$$

$$\frac{\partial v'}{\partial y'} = \sin^2\alpha.\frac{\partial u}{\partial x} - \sin\alpha\cos\alpha.\frac{\partial u}{\partial y} - \sin\alpha\cos\alpha.\frac{\partial v}{\partial x} + \cos^2\alpha.\frac{\partial v}{\partial y}$$

.... (13)

From these relations we can obtain the matrix W:

$$
\left(
\begin{array}{cccccc:c}
c & s & 0 & 0 & 0 & 0 & \\
-s & c & 0 & 0 & 0 & 0 & \\
0 & 0 & c^2 & sc & sc & s^2 & \\
0 & 0 & -sc & c^2 & -s^2 & sc & O \\
0 & 0 & -sc & -s^2 & c^2 & sc & \\
0 & 0 & s^2 & -sc & -sc & c^2 & \\
\hdashline
 & & O & & & & \text{DITTO}
\end{array}
\right)
$$

where $c = \cos\alpha$

$s = \sin\alpha$

We now have to calculate the interpolation polynomials for L'. Assume the following forms for u' & v' along the edge:

$$u'(s) = as^3 + bs^2 + cs + d$$

$$v'(s) = ks^3 + ls^2 + ms + n$$

where $s = x'/L$

Thus, if we substitute

$f \equiv 2s^3 - 3s^2 + 1$

$g \equiv s^3 - 2s^2 + s$

$h \equiv 3s^2 - 2s^3$

$k \equiv s^3 - s^2$

we have for L':

$$
\left(
\begin{array}{cccccc:cccccc}
f & 0 & L.g & 0 & 0 & 0 & h & 0 & L.k & 0 & 0 & 0 \\
0 & f & 0 & 0 & L.g & 0 & 0 & h & 0 & 0 & L.k & 0
\end{array}
\right)
$$

Thus all the component matrices have been derived and the next chapter considers the problem of generating an element stiffness matrix from them.

Chapter Two The technique of setting up an element stiffness matrix

2.1 Introduction

The next stage of the development of a finite element is to produce a program capable of generating a particular element stiffness matrix from the data. In the previous chapter, the components of the element stiffness matrix were derived. Whilst it is possible to proceed to an explicit form of the H and T matrices, this is not ideal. For, although the work involved in producing the early regular element stiffness matrices was not cumbersome, that for the general polygon is. Not only are lengthy expressions involved in deriving the components of the stiffness matrix, but the program which results is also tedious, error-prone, and difficult to test.

Furthermore, it was known in advance that several different formulations of the plane stress stiffness matrix were to be tried, so that several alternative approaches to the element stiffness program were followed to find that which is most amenable to modification.

2.2 Algebraic technique

The first of these consisted of the provision of a package of subroutines for the algebraic manipulation of polynomials.[17] This proved to be feasible and such a package, albeit rudimentary, was written. Commands and data for this package were set up which would compute the H and T matrices and produce the algebraic results. These were then input into a program which interpreted them and produced a suitable FORTRAN subroutine.

Although capable of achieving its object, the process itself, and the resulting subroutines, proved too cumbersome to be of anything but academic value.

2.3 Numerical technique

The next attempt was to use an entirely numerical technique, defining all the basic functions using the FORTRAN arithmetic statement function facility, which allows the programmer to define functions which can then be used in a manner similar to the internal functions such as SIN or COS. Each of the basic matrices used in calculating the H and T matrices is supplied as an array of integers which refer to one of the built-in functions. The integrations over the area and along the boundary are carried out numerically using a five-point Gaussian algorithm.(18) This algorithm was used since it is almost twice as accurate as the Simpson rule of the same degree.

This technique proved more successful and was used for some time to produce solutions to simple problems. Although the resulting program was more concise than any previous, execution times were excessive. However, it should be noted that this technique of defining the basic matrices by integer arrays leads to a program which does not expand proportionally when including further formulations of elements in the same basic program. The execution times were largely the result of evaluating each of the component matrices each time that any array element was computed.

2.4 Mixed technique

The third and present version is a combination of the two techniques. The functions which are polynomials are stored by specifying only the number of terms and the coefficient and powers of each term. Trigonometric functions are stored in much the same way as before. In the calculation of both H and T the product of three basic matrices is required to be integrated. In this program the first part of the product is formed algebraically and the individual terms stored dynamically in a linear array with an integer matrix of pointers. The final product is integrated numerically using the same algorithm as before.

The three basic matrices for each of H and T are specified by integer arrays which refer to the list of available functions. These, and the polynomials themselves, are stored in DATA areas. The trigonometric functions are built into the program itself. The DATA areas are kept in separate overlay areas for each element and are brought in from backing store as required, and then transferred to a common area of core store.

For instance, the polynomial $x^3 - 3xy^2/2$ would be represented by the following seven numbers:

2	1	3	0	-1.5	2	1
number of terms	coefficient	power of x	power of y	second term		

For the elasticity matrix, say, the following list of built-in functions is required:

$1 \quad -v \quad 2(1+v)$ (where v is Poisson's Ratio)

The integer matrix defining the elasticity matrix is then:

$$\left\{ \begin{matrix} 1 & 2 & 0 \\ 2 & 1 & 0 \\ 0 & 0 & 3 \end{matrix} \right\}$$

where 0 refers to the zero function.

In both the H and T matrices the middle of the three component matrices is independent of x and y and involves only the basic properties and geometry of the element itself, such as Poisson's Ratio, thickness and so on. This matrix is formed first and then used to pre-multiply the next matrix to form an algebraic form of the intermediate product. This product is stored in a linear array in the same way as the basic polynomials. The final product is formed one array element at a time, with the integration being carried out numerically as described in the next section. No final algebraic product is formed. **(For details see Appendix Three)**

2.5 Simplification of HI matrix

If the HI matrix is numerically evaluated directly as a double integral, the number of Gaussian points at which the value of the integrand is required is 21. However, the integration is simplified, and in computer terms, shortened by a transformation which splits the double integral over an area into two single integrals. The first, an improper integral (that is, one between algebraic not numeric limits) is evaluated algebraically from the powers of each term and the coefficients. The second integral is evaluated numerically. This latter, being now a single line integral, requires only five Gaussian points. Since the integrand has to be evaluated at each Gaussian point this transformation reduces quite considerably the computation required. Notable savings were in fact achieved.

The mathematics of the transformation are as follows:

$$\int_{x=a}^{x=b} \int_{y=0}^{y=h(x)} f(x,y)\,dx\,dy = \int_{x=a}^{x=b} F(x)\,dx$$

where $\quad F(x) = \left[G(x,y) \right]_{y=0}^{y=h(x)}$

& $\quad G(x,y) = \int f(x,y)\,dy$

2.6 Segmentation of program

Having written the program for one element, any other element only requires minor changes to the program in addition to a new segment of DATA statements. In fact, a complete new element can be generated, incorporated into the program and tested in a single computer run with a considerable degree of confidence that it will be correct.

The block layout of the element calculation is as shown in fig.4. The development of this program was greatly facilitated by a considerable division into subroutines, each of which could be written and tested independently and then "plugged-in" to the rest of the developing program. In addition, this approach made it easier to try out the three methods discussed above, by a simple replacement of relevant subroutines.

The same can be said of the control system, described in more detail in Appendix One. The value of dividing a large program into as many small segments as reasonable is indisputable.

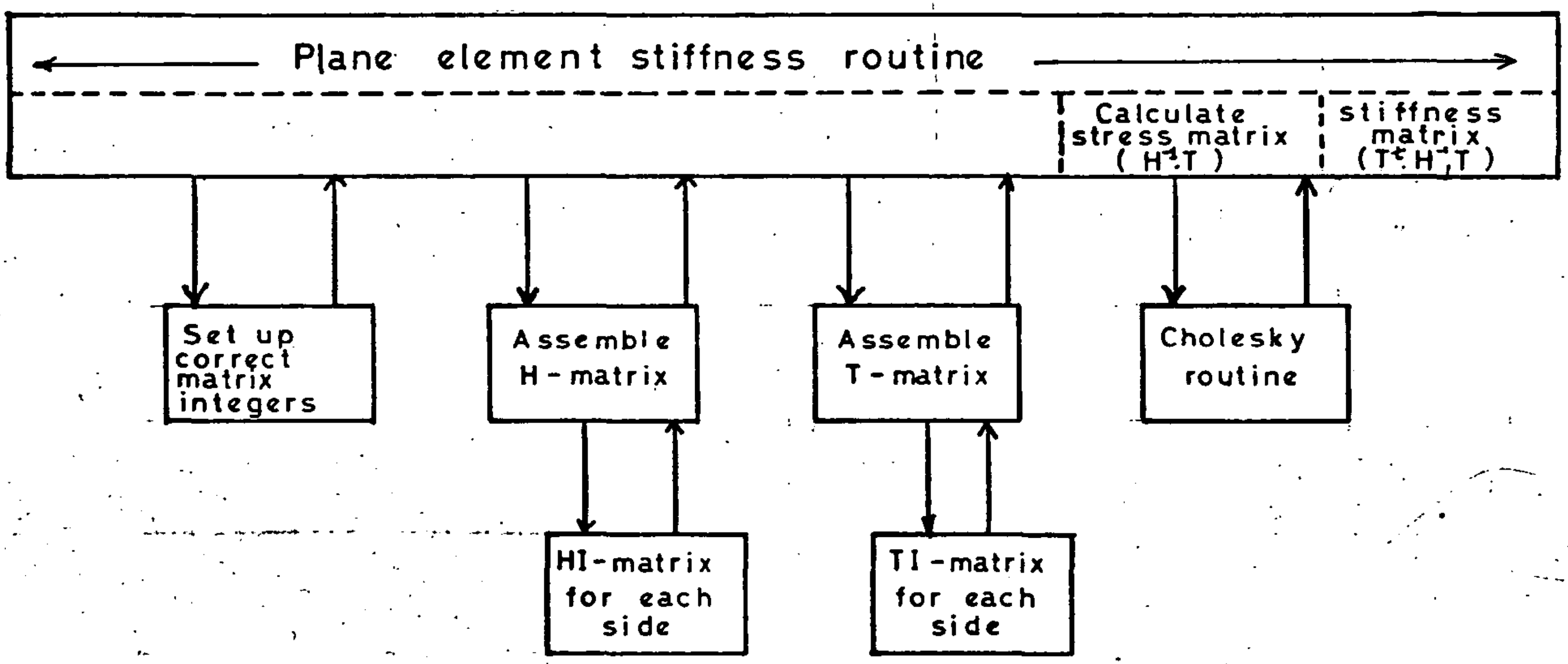

Fig. 4 Block diagram of plane element calculation

Chapter Three Comparison of plane stress elements

3.1 Introduction

Whilst some efforts have been made to produce a criterion for the comparison of finite elements, these have so far had only limited success.(19) Until it is possible to make a more impartial and direct comparison of differently formulated stiffness matrices, it is still necessary to select a set of fundamental problems on which to base an evaluation. The selection of such problems can, and indeed does, influence the apparent relative merits of individual elements. This is particularly so if problems which can be solved exactly by one element and not by another are chosen. In this case, it is left to judgement as to the severity and significance of the errors. Such judgement must include an assessment of the likelihood of encountering in real life a situation in which the relevant problem occurs.

3.2 Basis for comparison

Five types of problem were selected for the comparative tests on the various plane stress elements considered:

1 The bending of a short rectangular (2:1) cantilever with various meshes

2 The stretching of the same plate with various meshes

3 The pure shear of a square plate with various meshes

4 The bending of a cantilever of varying aspect ratio with a single mesh

5 The stretching of the same plate with varying aspect ratio and a single mesh

These problems are shown in figs. 5,6 & 7.

3.3 Results of comparative tests

The results of these tests for all elements are plotted in figs. 8,9,11,15,& 16 and listed in tables 2 - 6.

Whilst it can be seen from these figures that all the elements are convergent - indeed they must be so, following the proof of this by Pian[13] - the rates of convergence are not the same and differ according to the type of problem attempted.

3.3.1

Convergence in test 1 is extremely rapid for all elements. Almost all the results, apart from those from a single element, mesh A, are within 15% of the convergent result.

3.3.2

Not so rapid is the convergence in the second test. In addition, the convergence for GEN3 and GEN4 is not monotonic. The deflected shape of the plate when stretched, (fig. 10) is somewhat different from the usual "necking" noted with a larger aspect ratio. However, the same effect - outward displacement of horizontal edges near loaded end - was just noticeable in the experiments carried out by Douthwaite.[7] This effect is because, with the small aspect ratio, the load has become more distinctly two point loads rather than a distributed load over the whole end of the plate.

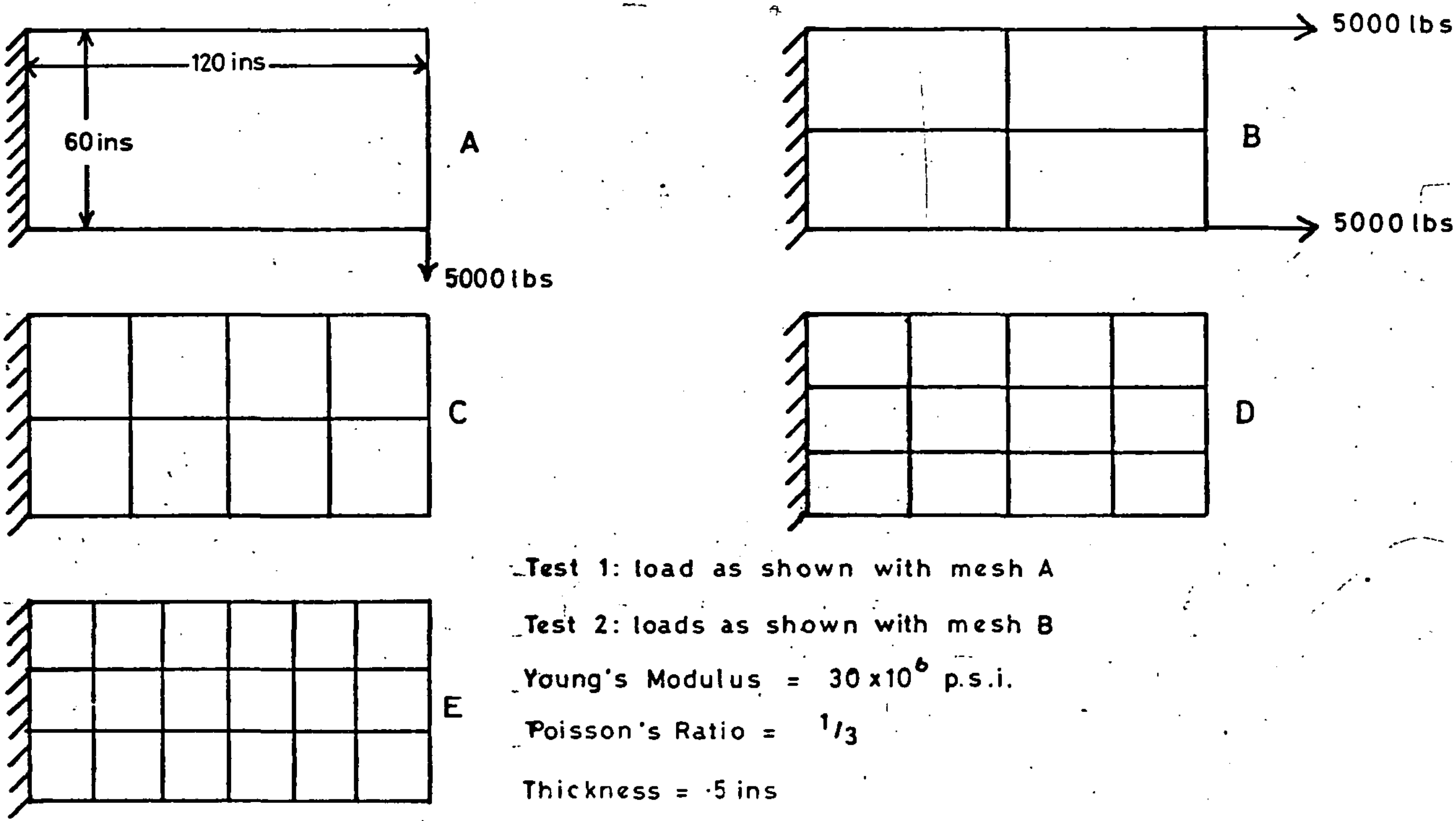

Test 1: load as shown with mesh A

Test 2: loads as shown with mesh B

Young's Modulus = 30×10^6 p.s.i.

Poisson's Ratio = $^1/_3$

Thickness = ·5 ins

Fig. 5 Meshes used for tests 1 & 2

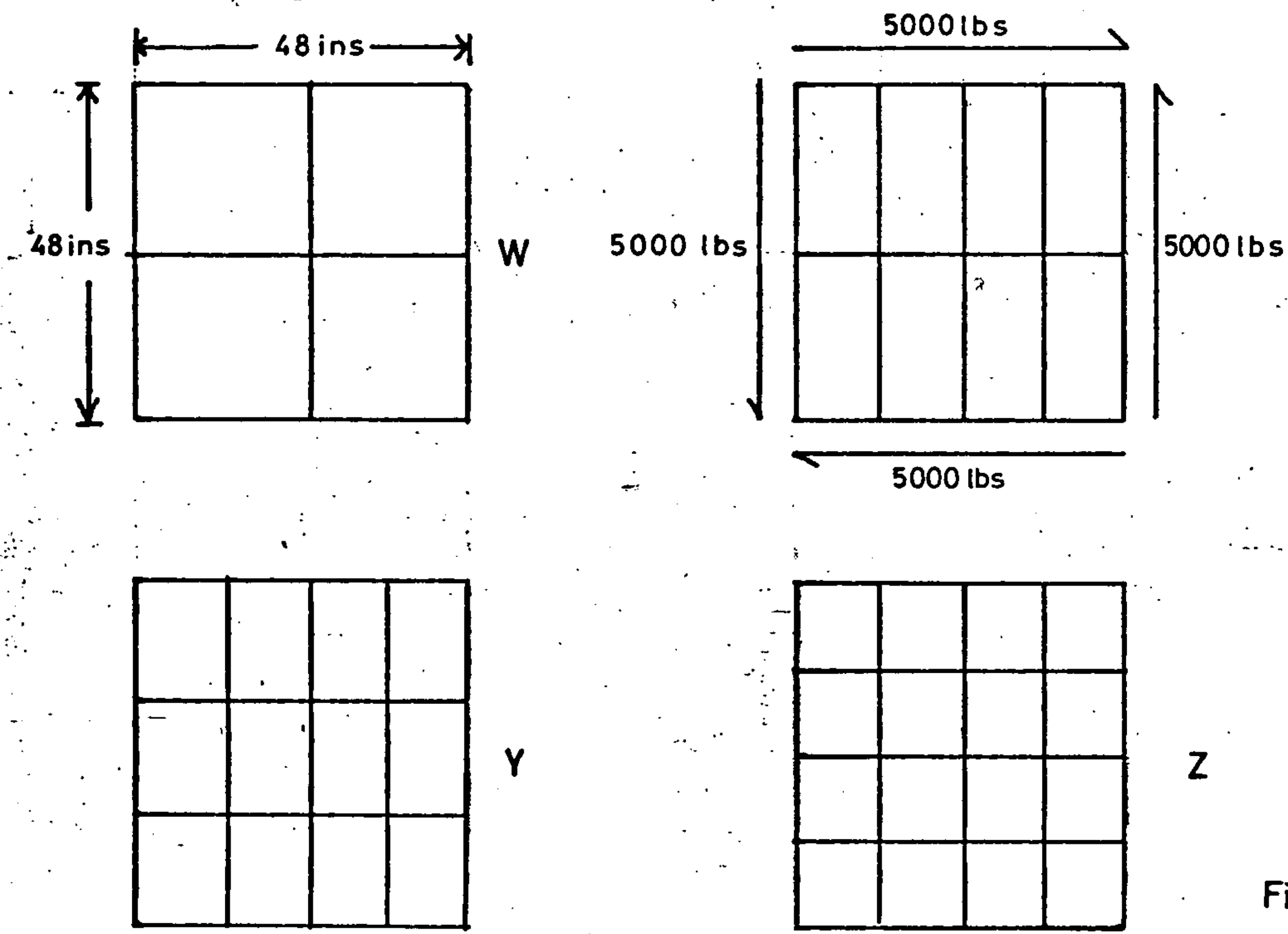

Young's Modulus = 30×10^6 p.s.i.

Poisson's Ratio = $1/3$

Thickness = ·5 ins

Fig. 6 Meshes used for test 3

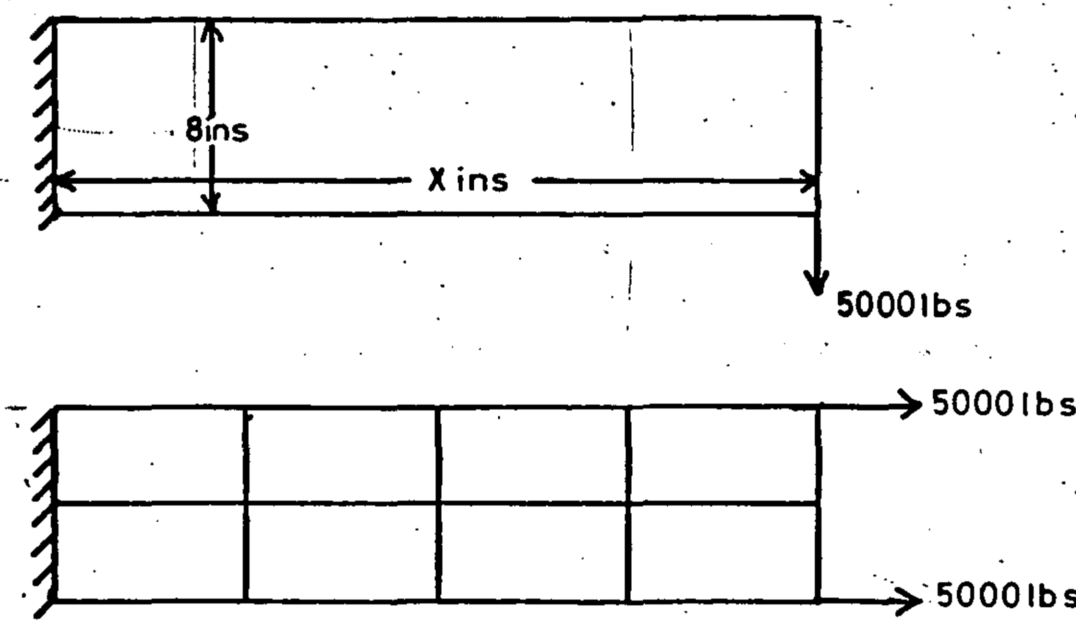

Test 4 load

Test 5 loads

Young's Modulus = 30×10^6 p.s.i.

Poisson's Ratio = $1/3$

Thickness = ·5 ins

5 cases: X = 24, 36, 48, 60, 120

Fig. 7 Problems used for tests 4 & 5

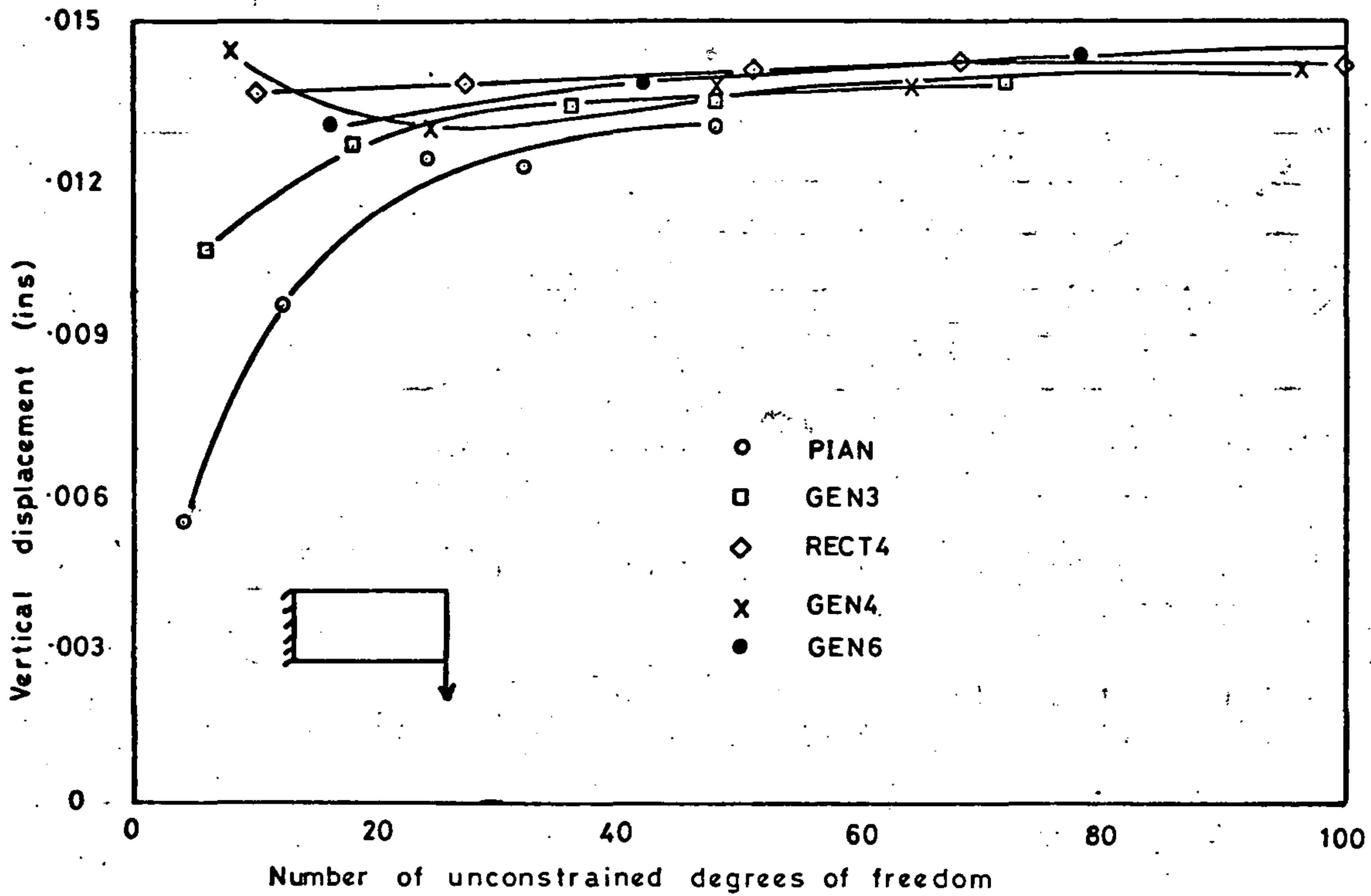

Fig. 8 Vertical displacement of loaded corner for test 1

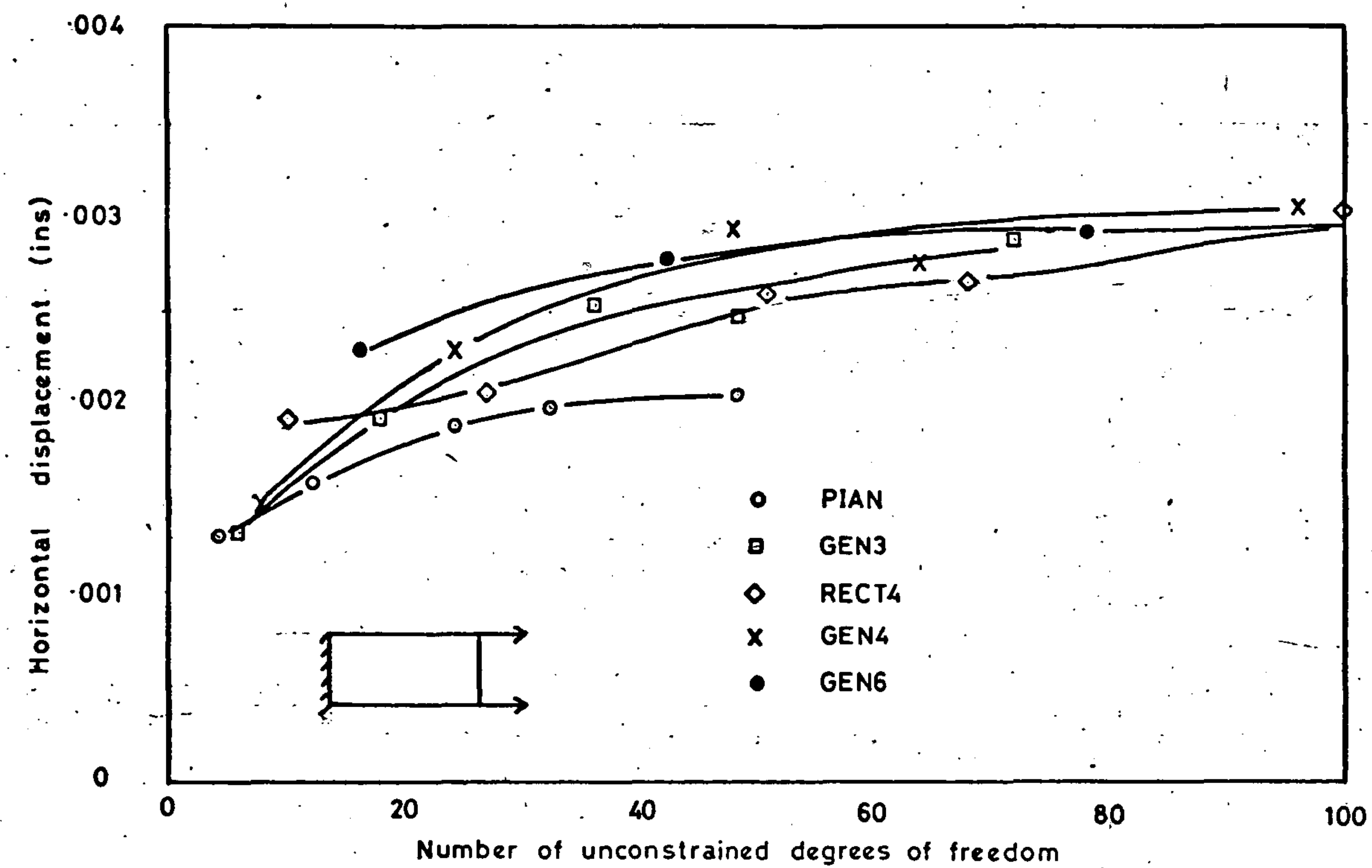

Fig. 9 Horizontal displacement of loaded corners for test 2

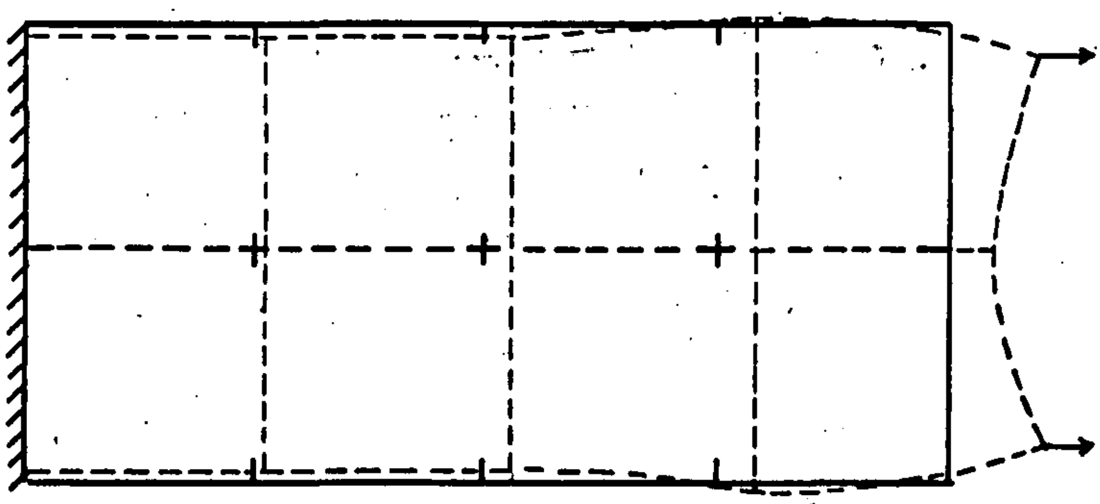

Fig. 10 Deflected shape - test 2, mesh C

3.3.3

Success in the shear test (test 3) depends primarily upon whether the actual edge displacement pattern is present in those available to any particular element - that is to say, whether or not the sides may take up a linear displacement and whether the sides may rotate relative to each other at each node. This is possible for all these elements except those in which the average rotation is considered as a degree of freedom, GEN3 and GEN4. In these cases the "corners" of each element are considered as being "rigid joints" as in, say, a plane frame analysis.

Although the solution obtained from these elements converges, (fig.11) the edge displacement which corresponds to this is as shown in fig. 12 and further, direct stresses are induced in addition to a varying shear stress. (see fig.13) The overall effect of this varies depending on the extent to which shear dominates the action of any particular problem considered. In addition, it should be noted that both the GEN4 and GEN6 elements require generalised dilation forces to represent properly a shear force. These result from the fact that the shear force produces a displacement in the same direction as the dilation degree of freedom. The effect of neglecting these is shown in the results for the GEN4 element and can be seen to be rather marked.

3.3.4

The effect of using an average rotation can also be seen in the deflected shape of the lower edge of the cantilever problem, test 1. Take, for instance, the mesh C. The deflection for this case is shown in fig. 14(a) for the element GEN4. Definite errors can be seen which result from

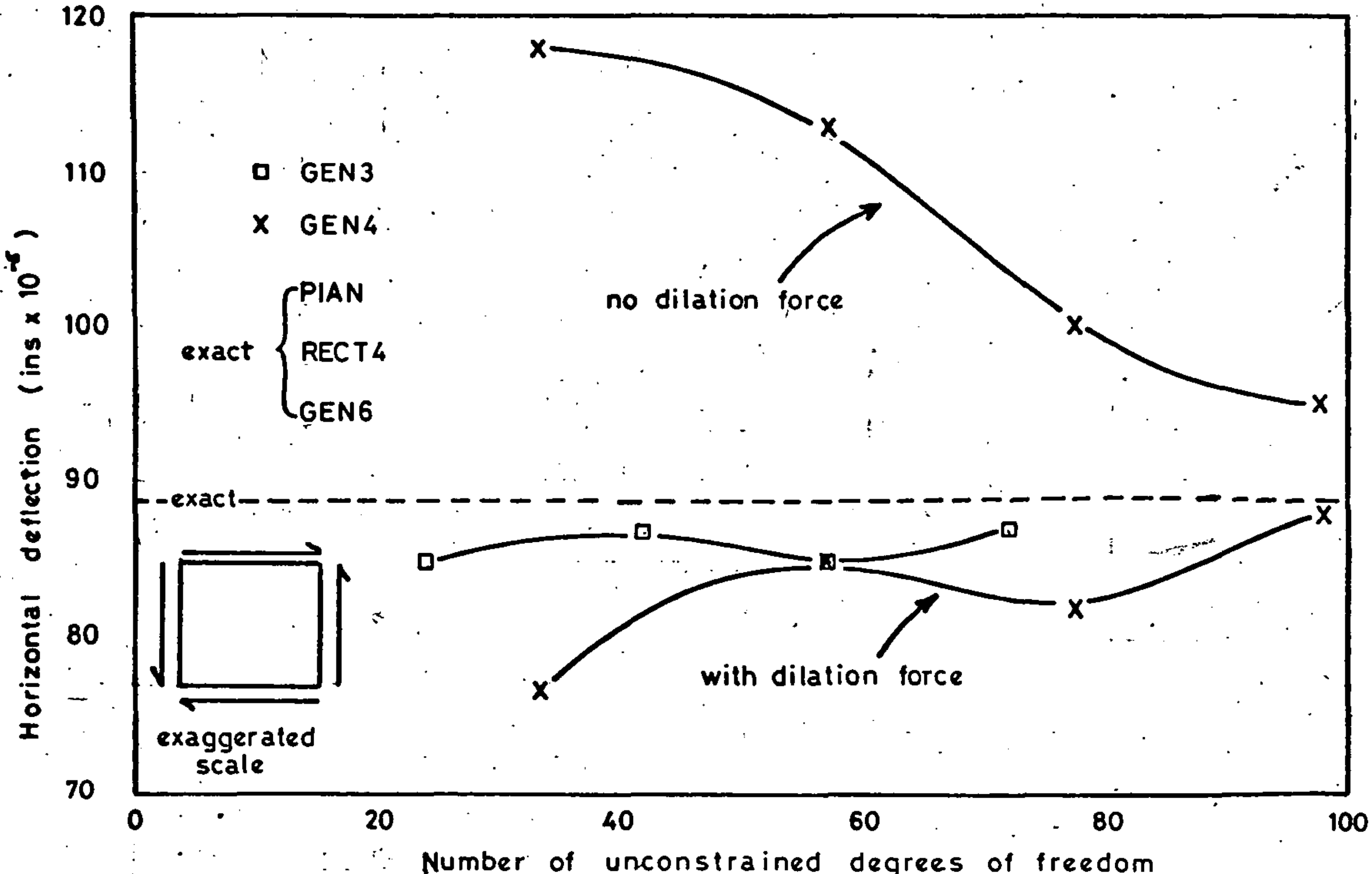

Fig. 11 Horizontal shear deflection for test 3

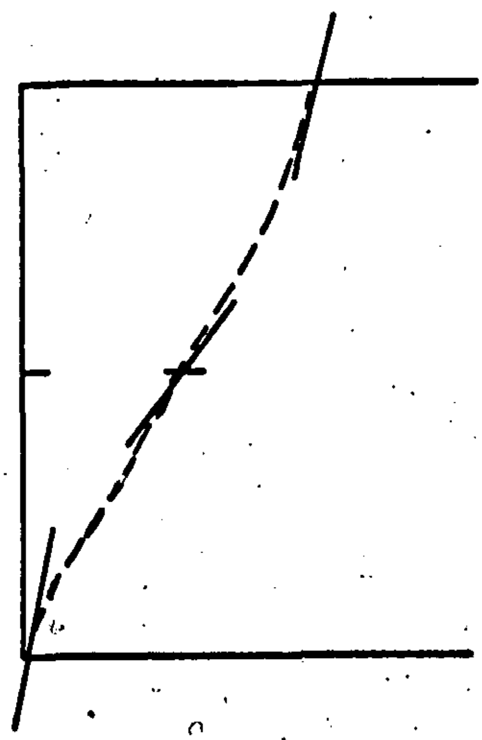

Fig. 12 Deflected edge shape - test 3, mesh W

-17	0	55	-55	0	17
19		9	-9		-19
16	-49	-75	75	49	-16
-16	49	75	-75	-49	16
-19		-9	9		19
17	0	-55	55	0	-17

exact value = 0

Horizontal stress in p.s.i.

227	204	140	140	204	227
204		194	194		204
140	194	207	207	194	140
140	194	207	207	194	140
204		194	194		204
227	204	140	140	204	227

exact value = 208

Shear stress in p.s.i.

Fig. 13 Stresses in shear problem W using element GEN4

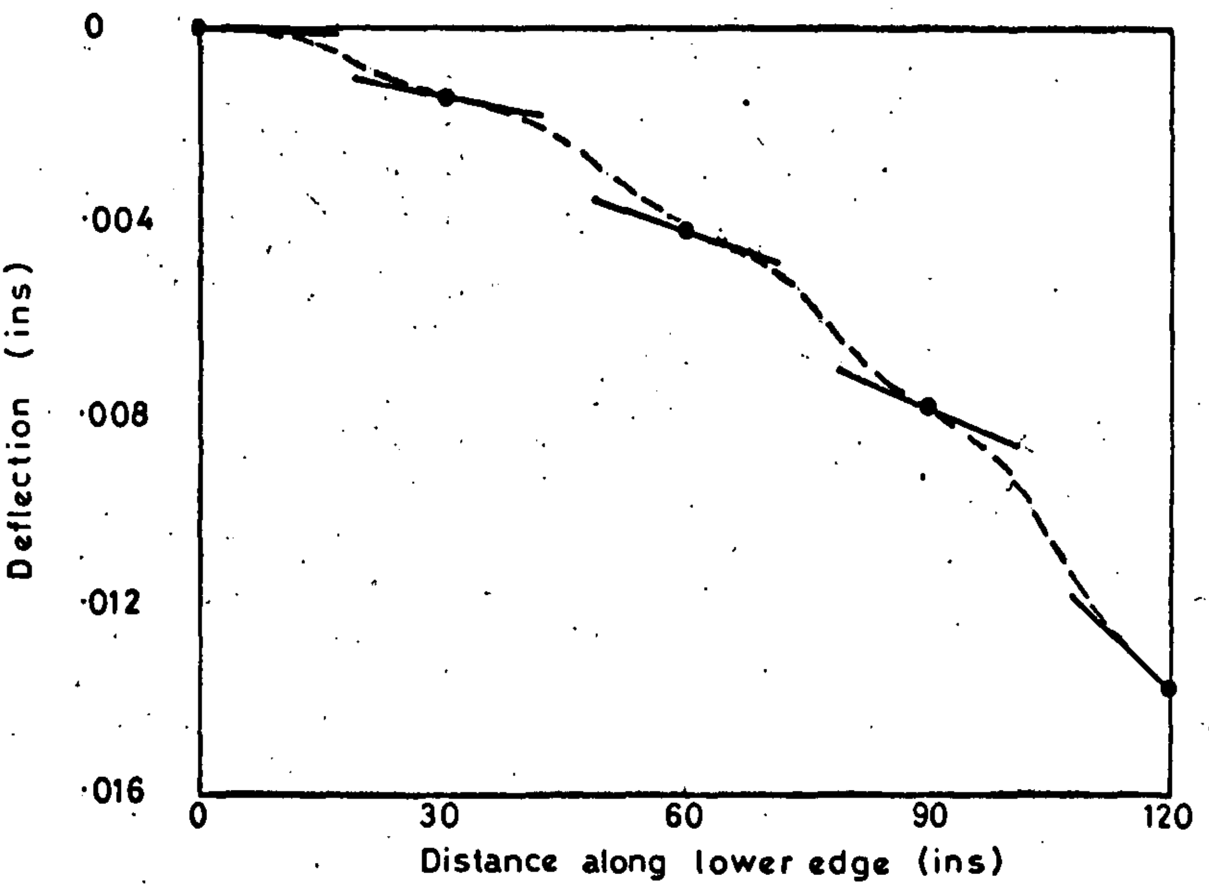

Fig. 14(a) Solution using GEN4

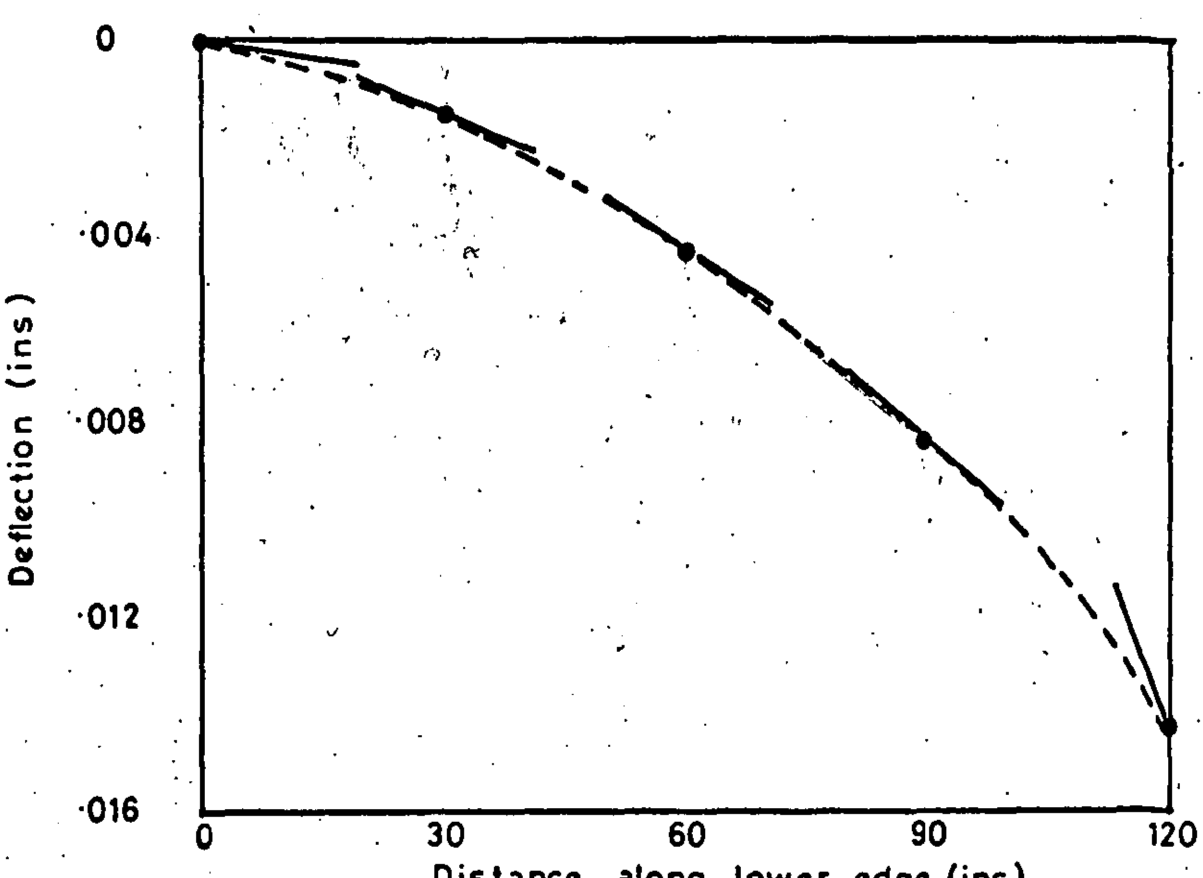

Fig. 14(b) Solution using GEN6

Fig. 14 Deflected shape of lower edge - test1, mesh C the fact that the slopes at each node are considerably less than the correct values. However, the GEN6 solution, fig. 14(b), does not contain this particular error.

3.3.5

The results of the tests 4 and 5 (figs. 15 & 16) are not unimportant. In effect, these tests measure the ability of the elements to cope with situations in which the stress in one direction is varying considerably more rapidly than in the other. The large aspect ratio used means that the resulting stiffness equations might be ill-conditioned, but errors are unlikely to have arisen from this source - see chapter six where this question will be examined.

The basic Pian element performs particularly poorly in this context. The consequence is that any element subdivision of a problem for this element must be such that all the elements are as near "square" as possible. This can cause quite a considerable increase in the number of nodal points if the mesh is to be refined more in one region than in another.

The three degree of freedom element, GEN3, is a marked improvement on the basic element but nevertheless, up to 25% errors were recorded. This is in contrast to the 9% errors of the GEN4 element. The very good behaviour of the RECT4 element is, as always, restricted by the limited type of problem open to it, and that of the GEN6 element is achieved at an increased cost in computing time. The GEN4 as a general element is thus an acceptable compromise.

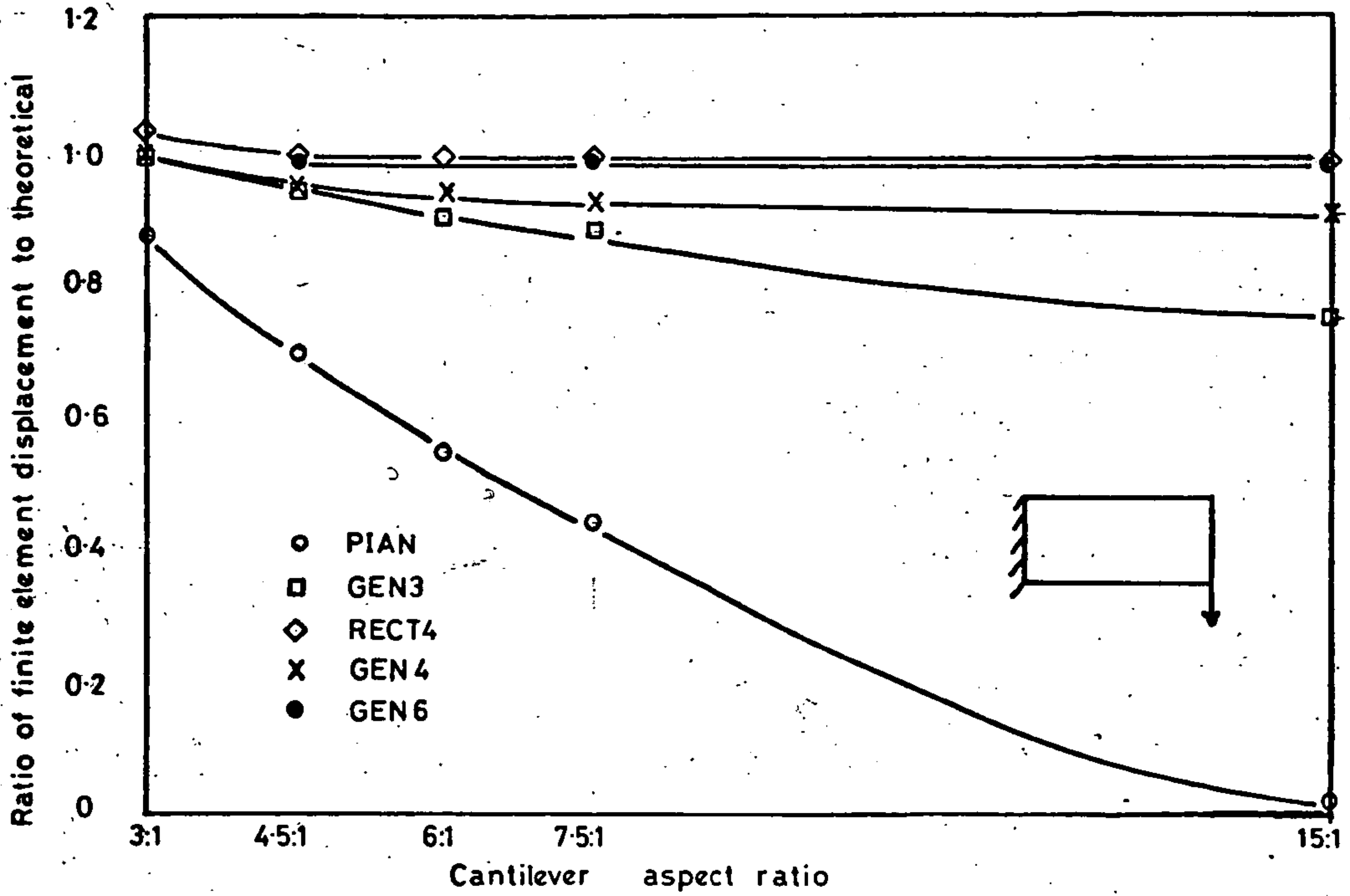

Fig. 15 Vertical displacement of loaded corner of cantilever for varying aspect ratio - test 4

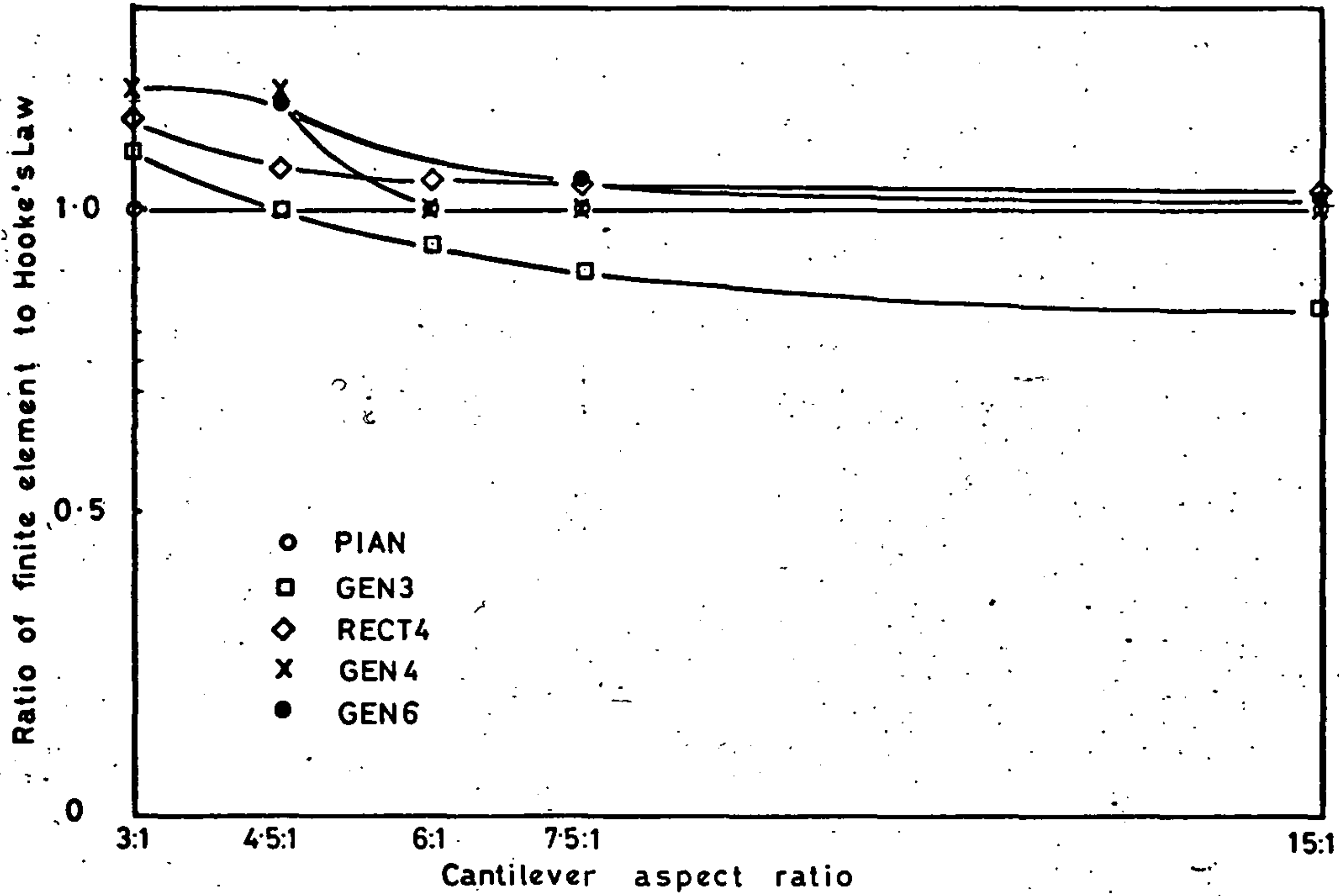

Fig. 16 Horizontal displacement of loaded corners for varying aspect ratio - test 5

3.4 Triangles versus quadrilaterals

It was shown by Allwood[21] that, for the displacement method, it is always better to use a general quadrilateral element subdivision than one into triangles with the same node positions. The argument, substantiated by example, was based on the number of unknown coefficients in the displacement patterns which were available for independent evaluation. It is found that the stress distribution of the quadrilateral can be linear, whilst that of the triangle is constant. Two triangles can only produce a step function not a linear variation.

It is not possible to argue in the same way for the assumed stress approach since the same stress patterns are available to both the triangle and the quadrilateral. Nevertheless, examples (see figs. 17 & 18) indicate that the same theorem may be true. In this case the fact probably stems from the incompatibility between the edge displacements and the stress distributions; the discrepancy will be greater for the two triangles than an equivalent quadrilateral since the former include a contribution from the common boundary between the two elements in addition to the external boundary.

Since only a triangle has been made available for the GEN6 configuration, this element has been omitted from this comparison.

3.4.1

From these results it can also be seen that, as expected, the PIAN element as a triangle is exactly the same as the Taig triangle. This is because the two elements require the same stress distributions - constant - and these

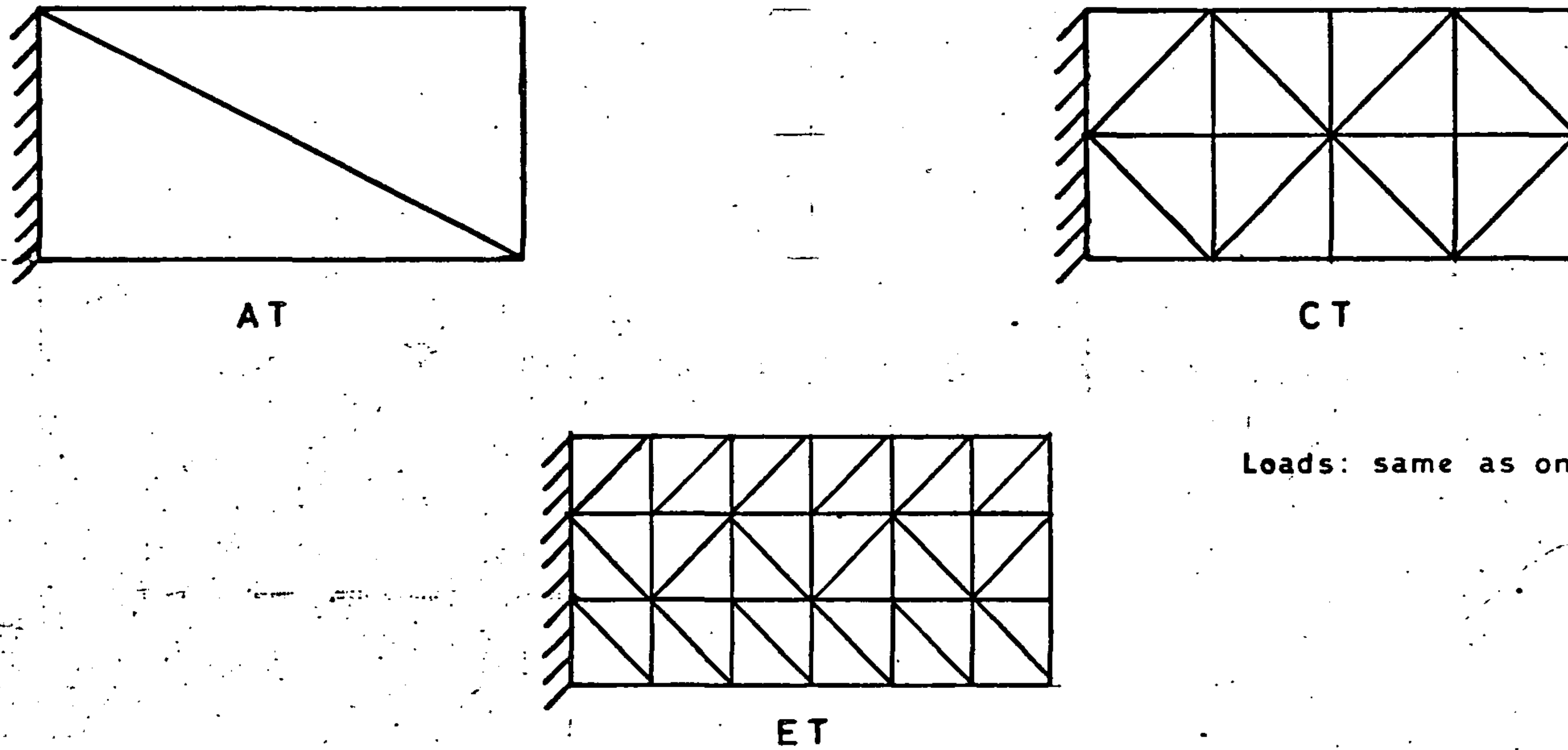

Loads: same as on fig. 4

Fig. 17 Meshes used for comparison of quadrilaterals & triangles

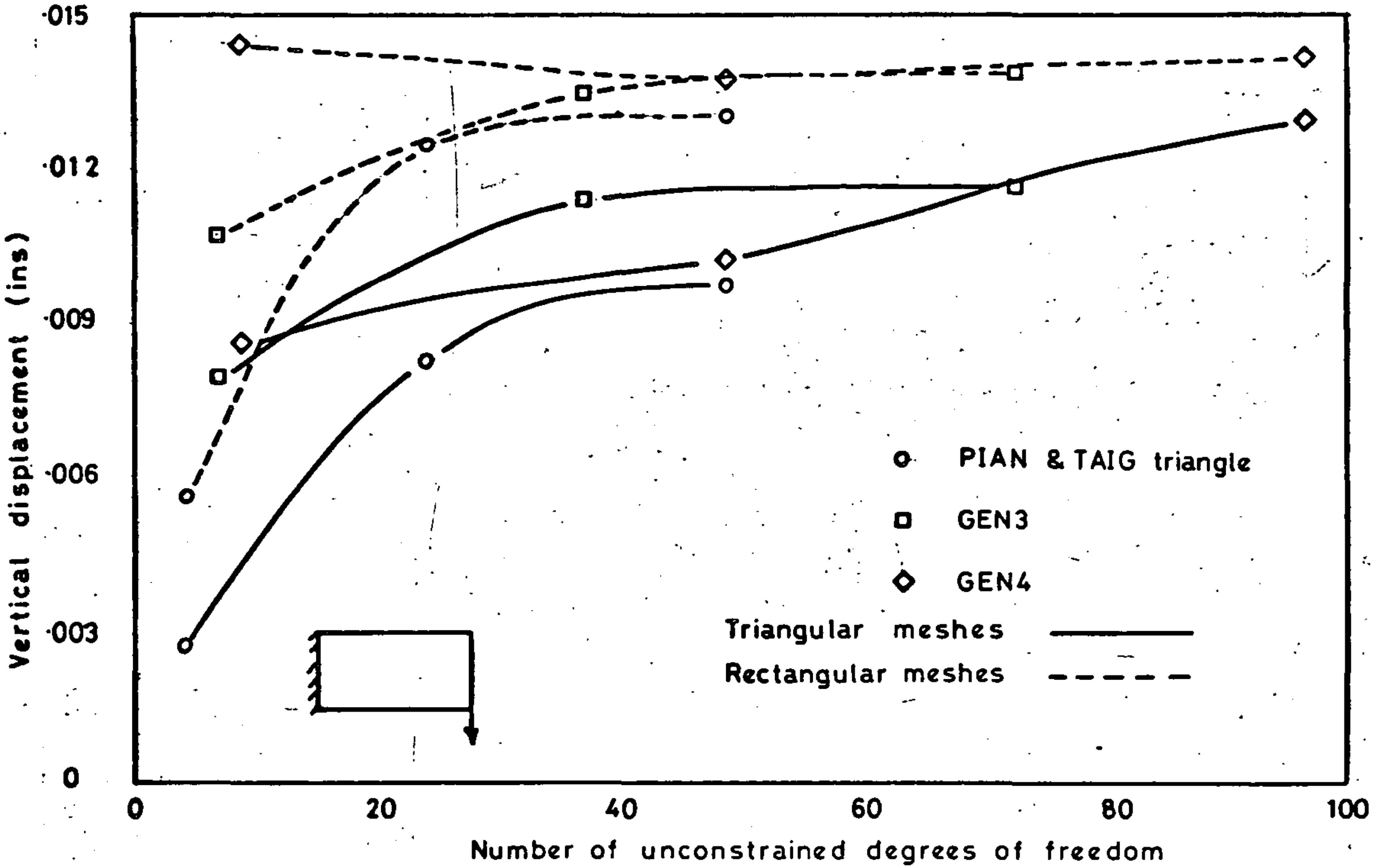

Fig. 18 Comparison of triangles and rectangles

match the edge displacements exactly. This is the only case amongst the elements examined where this is so. The same effect would not be observed, for example, with the Pian element and the Taig rectangle.

3.5 Calculation of stresses

3.5.1

In chapter one, equation (6), where the element stiffness matrix was shown to be:

$$k = T^t . H^{-1} . T$$

we can also see how to calculate stresses, using the stress assumption. For:

$$\underline{\beta} = H^{-1} . T . \underline{q} \qquad \ldots\ldots\ldots \quad (14)$$

where $\underline{q}$ are the nodal displacements for the element. The matrix $H^{-1}.T$ is known as the stress matrix. From equation (14) we can calculate the stress at any point within the element using the appropriate coordinates in equation (2):

$$\underline{\sigma} = P . \underline{\beta}$$

The subroutine which calculates the stresses is written to print out the values of the stresses at the nodes and midsides. Alternative points could have been used and, in fact, a stress plotting program has been written (see appendix two) which allows this facility.

3.5.2

For the GEN6 element an alternative is available since the strains are calculated as independent degrees of freedom at each node. The stresses may be calculated (equation (4)) from them usingthe relation:

$$\underline{\sigma} = N^{-1} . \underline{\epsilon}$$

In addition, this feature of the GEN6 element allows an implied constraint of stress as well as displacement;

3.5.3

For those elements which have constant, or near constant, stress bases, the value calculated from the stress functions for each element is most logically assigned to the centroid of that element. This creates difficulties in plotting stresses on the boundary of the problem. The best that can be done is some form of extrapolation. Nothing more sophisticated than manual extrapolation has been attempted in this work, although others have investigated this. (see Wilson[22])

3.5.4

As a comparison, consider the longitudinal stress along the lower edge of the 15:1 cantilever in test 4. (Cant. 4/15) The results for this from four different elements are shown in table 1. The notes (a) - (c) refer to section 3.5.5)

x ins	node	"exact"	Rect16 (i)	GEN4 (ii)	GEN6 (iii)	GEN6 (ii)
0	1	-11250	-10497	-3275 (c)	-11850	-11450
30	4	-8437	-8656	-8402	-8650	-8550
60	7	-5625	-5769	-5727	-5550	-5600
90	10	-2812	-2883	-2749	-2785	-2770
120	13	0	-1373 (a)	+66	+740 (b)	+8

x = distance from supported end

Table 1: Longitudinal stress (p.s.i.) along lower edge of cantilever 4/15

(i) Stresses calculated from an interpolation of the nodal degrees of freedom

(i) Stresses from stress polynomials

(iii) Stresses from nodal strain degrees of freedom

3.5.5

(a) The stresses from the Rect16 elements are virtually constant across the whole element and thus the values quoted at nodes 4,7 & 10 are averaged values coming from a step function distribution which is discontinuous at these points. This accounts for the non-zero stress at x = 120. In reality the value -1373 should be considered as the value at the point x = 105. The same applies to the value at the other end, x = 0.

(b) This non-zero stress arises from a zero horizontal strain and a non-zero vertical strain multiplied by Poisson's Ratio. It is reasonable to expect a non-zero strain locally under the point load and hence the positive longitudinal stress. This is a feature of the stress distribution not picked up by any of the element stresses derived from nodal displacements or assumed stress distributions which average out many such local variations.

(c) This value at the root of the cantilever is in error as the result of the difficulty in correctly representing the constraint condition at this point. The strain in the vertical direction should be zero and that horizontally, non-zero. This implies that the dilation is non-zero. However, in the converse situation, a non-zero value of dilation is attributed equally to the strain in each direction making the stresses incorrect. However, the effect is very local and appears not to impair the results elsewhere. The quoted values were obtained, in fact, by constraining the dilation to be zero.

3.6 Stress free boundaries

It is possible in this particular method to constrain certain boundary stresses to zero by the imposition of zeros in the assumed stresses. (See Pian [23]) This introduces one or more zero columns into the P matrix. Conflicting opinions have been expressed (Dungar & Severn[24], and Pian[23]), it is not apparent that this refinement significantly alters the solutions obtained by the standard element, other than at the boundary itself. Provided that intelligence is employed in the interpretation of the results when zero stresses are expected but small values are printed out, no trouble should arise from the use of standard elements. Since the stress pattern selected from the basic set by the energy minimisation process is a smoothed out version of the exact distribution, it is not clear that this process of imposing a stress value at a particular point is correct. In general, the stress calculated at any point by the assumed stress approach refers to a small region around that point and not just at that point itself.

3.7 Conclusions

3.7.1

For problems in which in-plane bending (cantilever) action dominates then GEN4 provides a marked improvement over basic two degree of freedom elements. However, the inability of this element to represent shear is a drawback although the PIAN or Taig elements are quite satisfactory for such situations.

3.7.2

The GEN6 element combines the virtues of the two and four degree of freedom elements but at a considerable increase in expense. For many situations this expense may not be paralleled with a similar improvement in the results, compared with the GEN4 element. Provided it is possible to determine in advance which to use, PIAN and GEN4 are to be preferred on the grounds of economy.

3.6.3

As a prospective membrane component of a shell element GEN4 is immediately attractive in that its average rotation degrees of freedom fit well with the out-of-plane rotations of a bending element. However, the effect of the distorted shear stress under some circumstances resulting from the use of GEN4 may be a problem and will be investigated in later chapters. For situations in which shear is present at a significant level, GEN6 can be used also in conjunction with the same bending element to produce a more sophisticated shell element capable of representing shear more correctly.

Element		A	B	C	D	E
PIAN	D1	.00560	.00966	.01241	.01233	.01309
	D2	.00193	.00318	.00406	.00405	.00431
	N	4	12	24	32	48
GEN3	D1	.01077	.01276	.01352	.01369	.01394
	D2	.00[illegible]49	.00459	.00492	.00503	.00512
	N	6	18	36	48	72
RECT4	D1	.01377	.01384	.01416	.01434	.01415
	D2	.00582	.00474	.00494	.00496	.00510
	N	10	27	51	68	100
GEN4	D1	.01452	.01302	.01378	.01394	.01417
	D2	.00483	.00460	.00506	.00504	.00523
	N	8	24	48	64	96
GEN6	D1	.01315	.01378	.01446		.01478
	D2	.00399	.00446	.00468		.00487
	N	16	42	78		152
Rect 16	D1	.00960	.01267	.01335	.01371	.01390
	D2	.00385	.00436	.00459	.00473	.00485
	N	10	27	51	68	100

"exact" solution for D1 = .01333 (See supplement to chapter 3)

D1 = vertical deflection at loaded node
D2 = horizontal deflection at loaded node
N = number of unconstrained equations

Table 2: Results of bending loadcase (test 1)

Element		A	B	C	D	E
PLAN	D1	.00130	.00164	.00187	.00199	.00211
	D2	.00017	.00021	.00038	.00043	.00057
	N	4	12	24	32	48
GEN3	D1	.00136	.00190	.00254	.00246	.00285
	D2	.00041	.00094	.00112	.00112	.00131
	N	6	18	36	48	72
RECT4	D1	.00189	.00211	.00263	.00269	.00305
	D2	.00062	.00067	.00096	.00105	.00123
	N	10	27	51	68	100
GEN4	D1	.00145	.00230	.00290	.00272	.00306
	D2	.00054	.00091	.00138	.00122	.00144
	N	8	24	48	64	96
GEN6	D1	.00230	.00275	.00288		.00313
	D2	.00042	.00071	.00090		.00106
	N	16	42	78		154
Rect	D1	.00159	.00197	.00244	.00249	.00274
16	D2	.00032	.00061	.00087	.00093	.00106
	N	10	27	51	68	100

D1 = horizontal deflection of loaded nodes

D2 = vertical deflection of loaded nodes

N = number of unconstrained equations

Table 3: Results of stretching case (test 2)

Element		W	X	Y	Z
PLAN		←	exact		→
GEN3	D	.00085	.00087	.00085	.00086
	N	24	42	57	72
RECT4		←	exact		→
GEN4	D1	.00118	.00113	.00100	.00095
	D2	.00076	.00085	.00082	.00088
	N	33	57	77	97
GEN6		←	exact		→
Rect 16		←	exact		→

exact solution = .00089 ins.

D = horizontal deflection of upper left corner
D1 = same deflection without dilation force
D2 = as D1 but including dilation force.

Exact solution is obtained from:-

$$\tau_{xy} = \frac{5000}{48*\frac{1}{2}}$$

$$\gamma_{xy} = \frac{10^4}{48} * \frac{2*4/3}{30*10^6}$$

$$D = \frac{10^4*8*48}{48*9*10^7}$$

$$= .00089 \text{ ins}$$

Table 4: Results from shear problem (test 3)

Element		3:1	4.5:1	6:1	7.5:1	15:1
PIAN	D	.00338	.00887	.01636	.02498	.07127
	R1	.94	.73	.57	.44	.02
	R2	.87	.70	.55	.44	.02
GEN3	D	.00388	.01192	.02677	.05013	.33745
	R1	1.08	.98	.93	.89	.75
	R2	.99	.94	.90	.88	.75
RECT4	D	.00402	.01266	.02937	.05684	.44977
	R1	1.12	1.04	1.02	1.01	1.00
	R2	1.03	.99	.99	.99	1.00
GEN4	D	.00391	.01212	.02782	.05337	.40908
	R1	1.09	1.00	.97	.95	.91
	R2	1.00	.95	.94	.93	.91
GEN6	D		.01263		.05670	.44861
	R1		1.04		1.00	1.00
	R2		.99		.99	.99
Rect 16	D		.01217	.02824	.05466	.43257
	R1		1.00	.98	.97	.96
	R2		.95	.95	.95	.96
	E1	.00360	.01215	.02880	.05625	.44997
	E2	.00390	.01273	.02958	.05721	.45177

D = Finite element Vertical deflection at load
E1 = Simple beam theory average deflection
E2 = Shear-corrected deflection at load

R1 = $^{D}/_{E1}$ R2 = $^{D}/_{E2}$

Table 5: Results from test 4.

Element		3:1	4.5:1	6:1	7.5:1	15:1
PLAN	D	.00020	.00030	.00040	.00050	.00099
	R	1.00	1.00	1.00	1.00	.99
GEN3	D	.00022	.00030	.00038	.00045	.00085
	R	1.10	1.00	.95	.90	.85
RECT4	D	.00023	.00032	.00042	.00052	.00103
	R	1.15	1.07	1.05	1.04	1.03
GEN4	D	.00024	.00036	.00040	.00050	.00097
	R	1.20	1.20	1.00	1.00	.97
GEN6	D		.00035		.00053	.00102
	R		1.17		1.06	1.02
Rect 16	D		.00032	.00041	.00050	.00100
	R		1.07	1.02	1.00	1.00
Exact		.00020	.00030	.00040	.00050	.00100

D = finite element average horizontal deflection

R = D/exact

"Exact" deflection obtained from Hooke's Law

Table 6: Results from test 5.

Element	A	AT	C	CT	E	ET
PIAN	.00560	.00230	.01241	.00812	.01309	.00985
GEN3	.01077	.00771	.01352	.01131	.01394	.01149
GEN4	.01452	.00857	.01378	.01034	.01417	.01296
Taig		.00282		.00812		.00985

Table 7: Results from comparison of triangles quadrilaterals for bending problem. (see test 1)

Supplement To Chapter Three:

Deflection of cantilever loaded vertically at lower end corner.

From Timoshenko & Goodier [25] we have the following formula for the "effect of shearing force":

$$\text{deflection, } d_2, = \frac{Pl^3}{3EI} + \frac{Pc^2}{2IG}*l$$

$$\text{But } G = \frac{E}{2(1+v)}$$

$$\text{Let } d_1 = \text{usual value} = \frac{Pl^3}{3EI}$$

$$\text{Then } d_2 = d_1(1 + \frac{3(1+v)}{4}*(\frac{b}{l})^2)$$

If we have that $v = {}^1/_3$

$$\text{then } d_2 = d_1(1 + (\frac{b}{l})^2)$$

Chapter Four Miscellaneous Plane Stress Problems

4.1 Introduction

In addition to the comparative tests of chapter three, a selection of problems was solved using the GEN4 element. This not only provides further validity to the process, but also demonstrates the range of suitable problems.

4.2 Simply supported deep beam

The problem of determining the stresses in a deep beam with simple supports (see fig.19) is one which does not have a simple solution. A finite difference technique and experimental model results have been compared with other approximate analyses (See Iyengar et.al.[27]) The results here for the GEN4 element using a coarse mesh of 3 x 4 elements are compared with those of the authors of [27] usinga 4 x 8 finite difference mesh. For a comparison, the elementary bending theory results are also shown. (figs. 20 & 21)

Although the finite element mesh is rather coarse, the agreement is good. The point of greatest discrepancy, the horizontal stress at the bottom of the centre-line section, is that result most contested by all the analyses quoted in (27). The range of results quoted is 1.0 - 1.5 p.s.i. whilst the maximum in the GEN4 distribution is 0.8 p.s.i. Otherwise the results are very similar and show well the deviation from the simple theory.

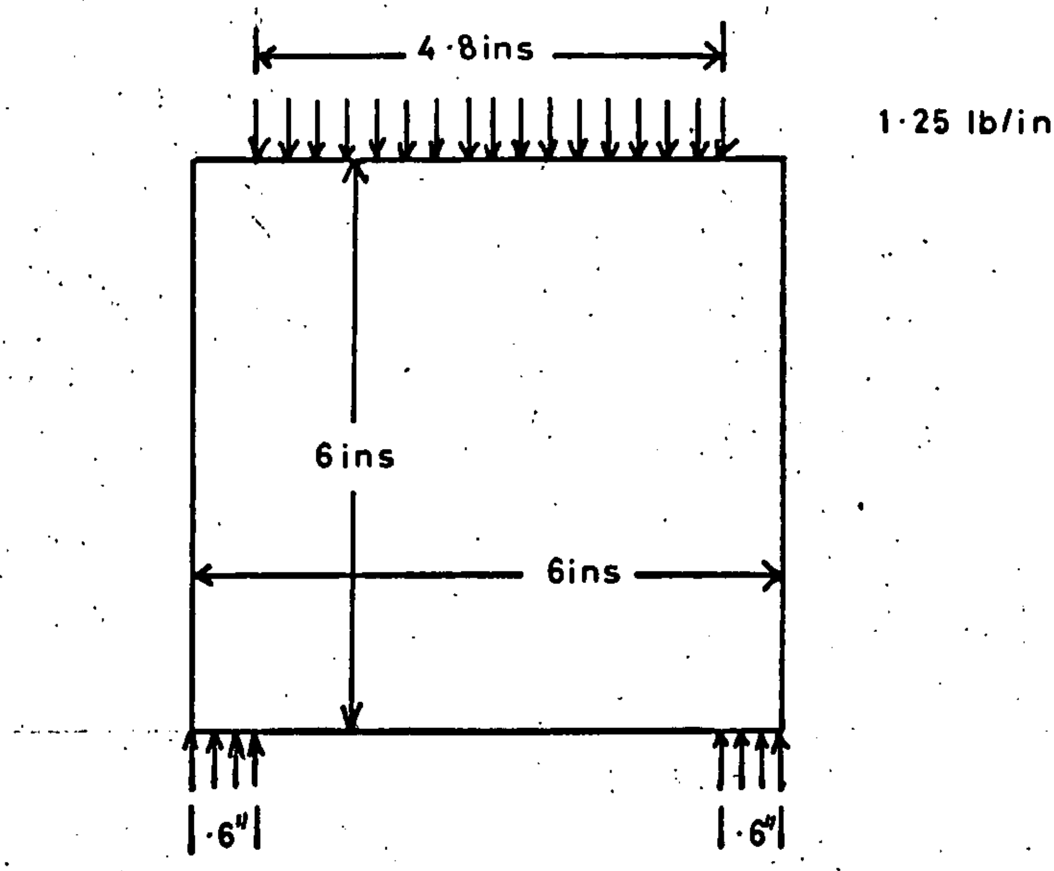

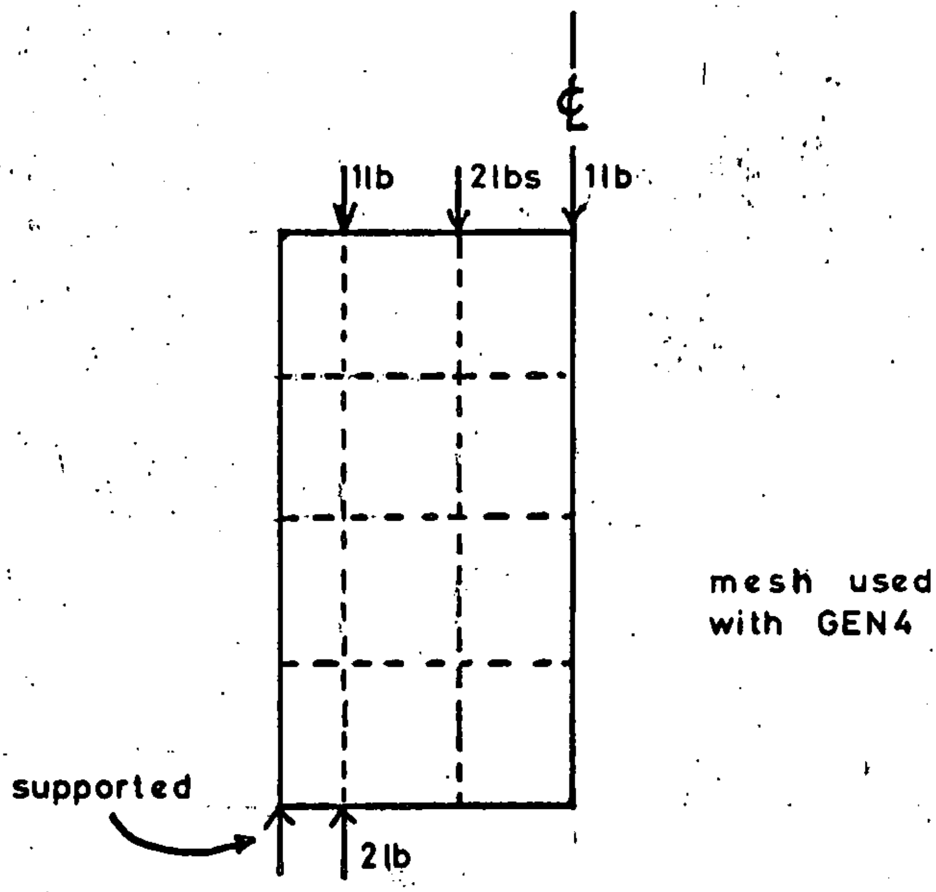

Fig. 19 Simply supported deep beam

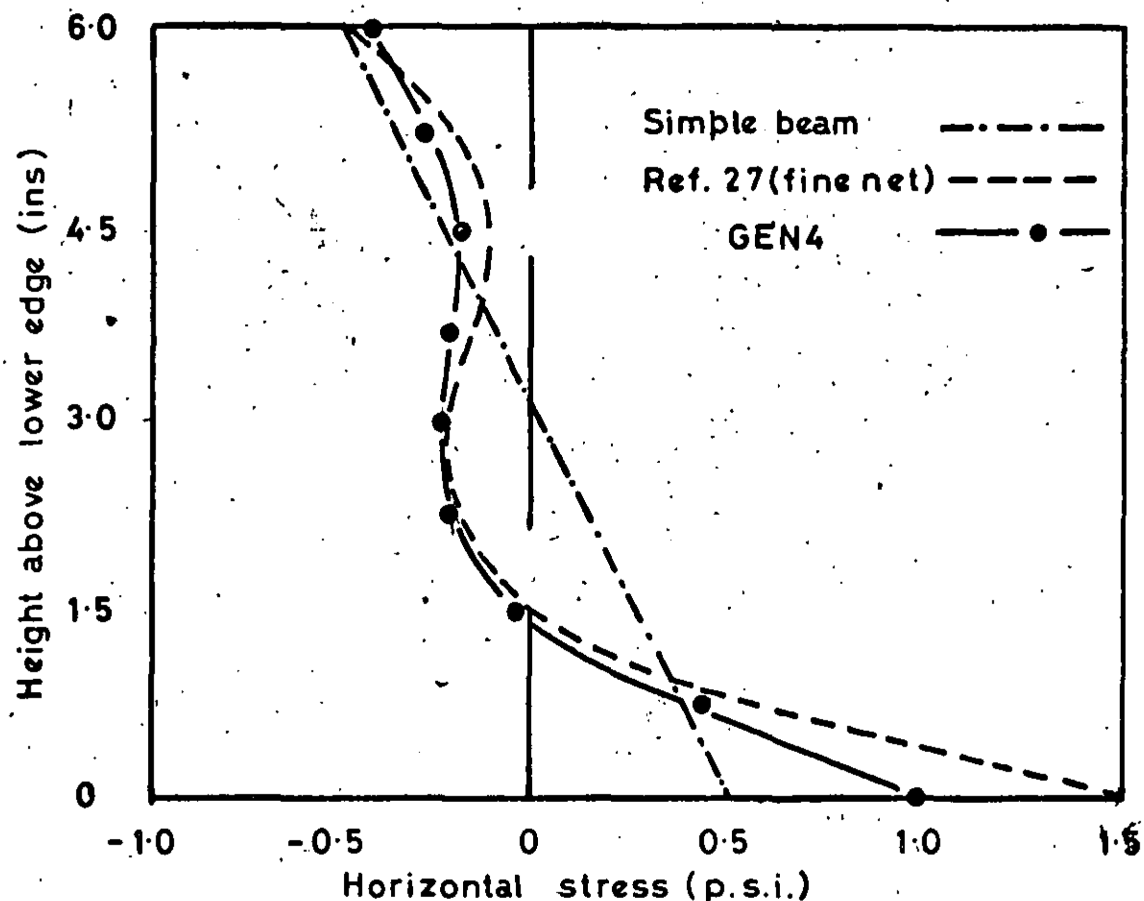

Fig. 20 Horizontal stress across centre line of deep beam

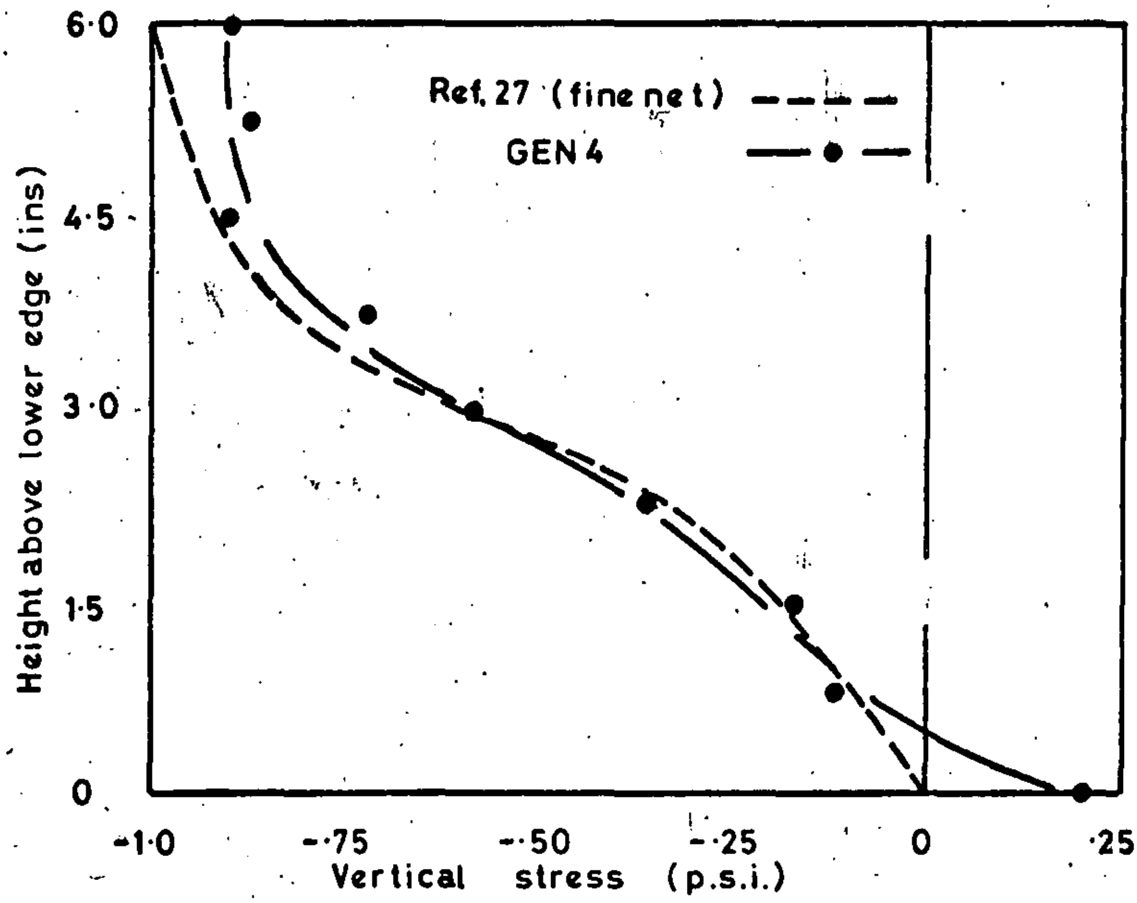

Fig. 21 Vertical stress across centre line of deep beam

4.3 Diametrically opposed point loads on a circular disc

This problem has a solution by Timoshenko and Goodier[25] and quite a successful solution was obtained using the GEN4 element. The mesh is shown in fig. 22. Similar meshes have been used with other finite elements. (See, for example, (27),(28))

Since the problem has symmetry about both the vertical and horizontal axes, it is only necessary to consider one quadrant.

The results, see figs. 23 & 24, are quoted in the non-dimensional units of $^{d.t}/_{P}$. It should be noted that the scale of fig.24 is much greater than that of fig.23 and that small variations in the major stress will introduce proportionally more significant errors in the minor stress. In view of this the finite element results are quite close to the "exact" solution, bearing in mind that this is an example of the difficulty in the Finite Element method of solving problems with point loads. Such loading cases introduce infinite discontinuities in the exact stress distributions which have to be rounded to a finite quantity in the finite process. Nevertheless, reasonable solutions are usually obtained in all regions not too close to the discontinuity. Again, it must be remembered that the stresses calculated for any point are the result of a process which averages the stress over the region around that point, thus obscuring the discontinuities in the exact distributions.

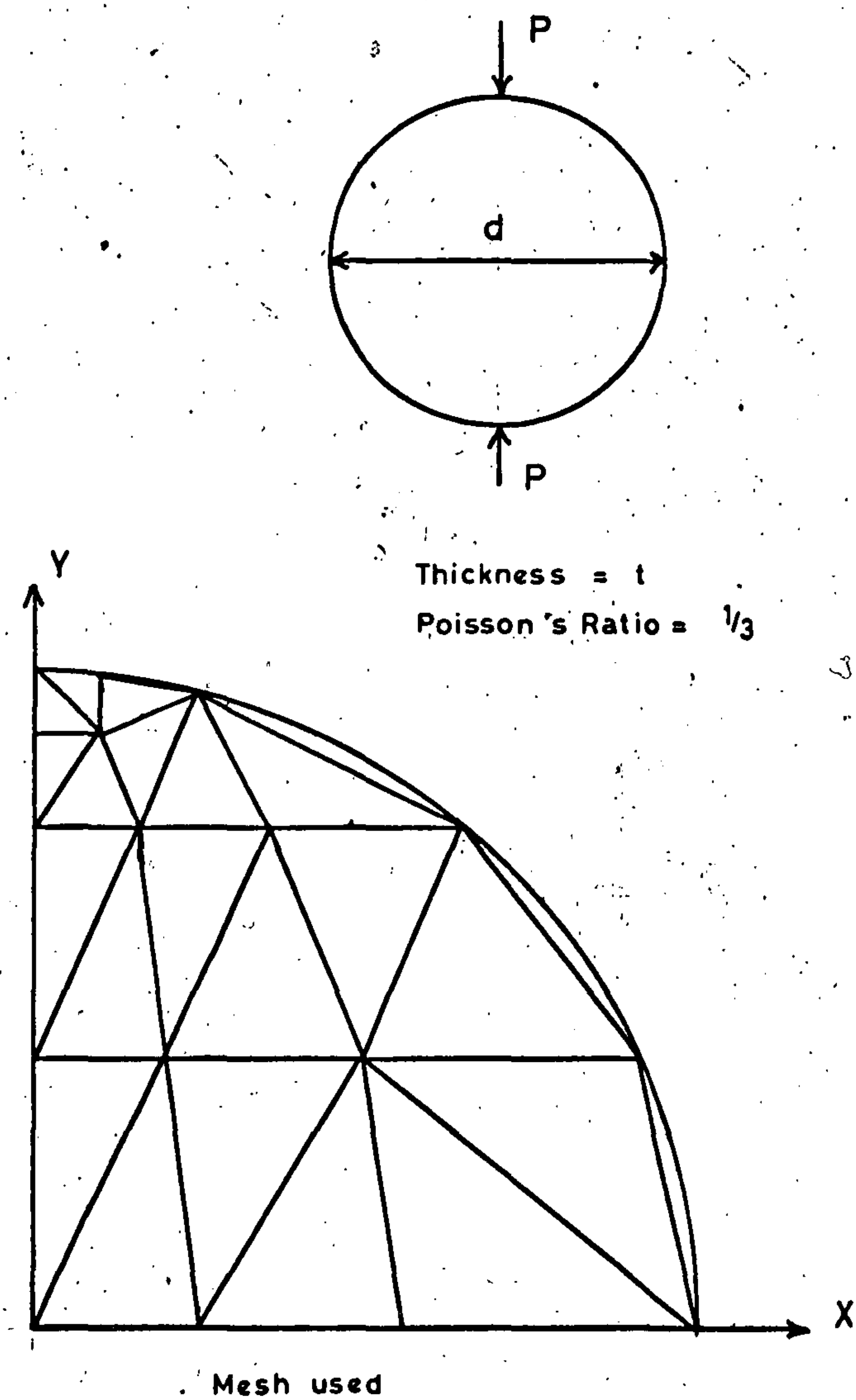

Fig. 22 Concentrated load on circular disc

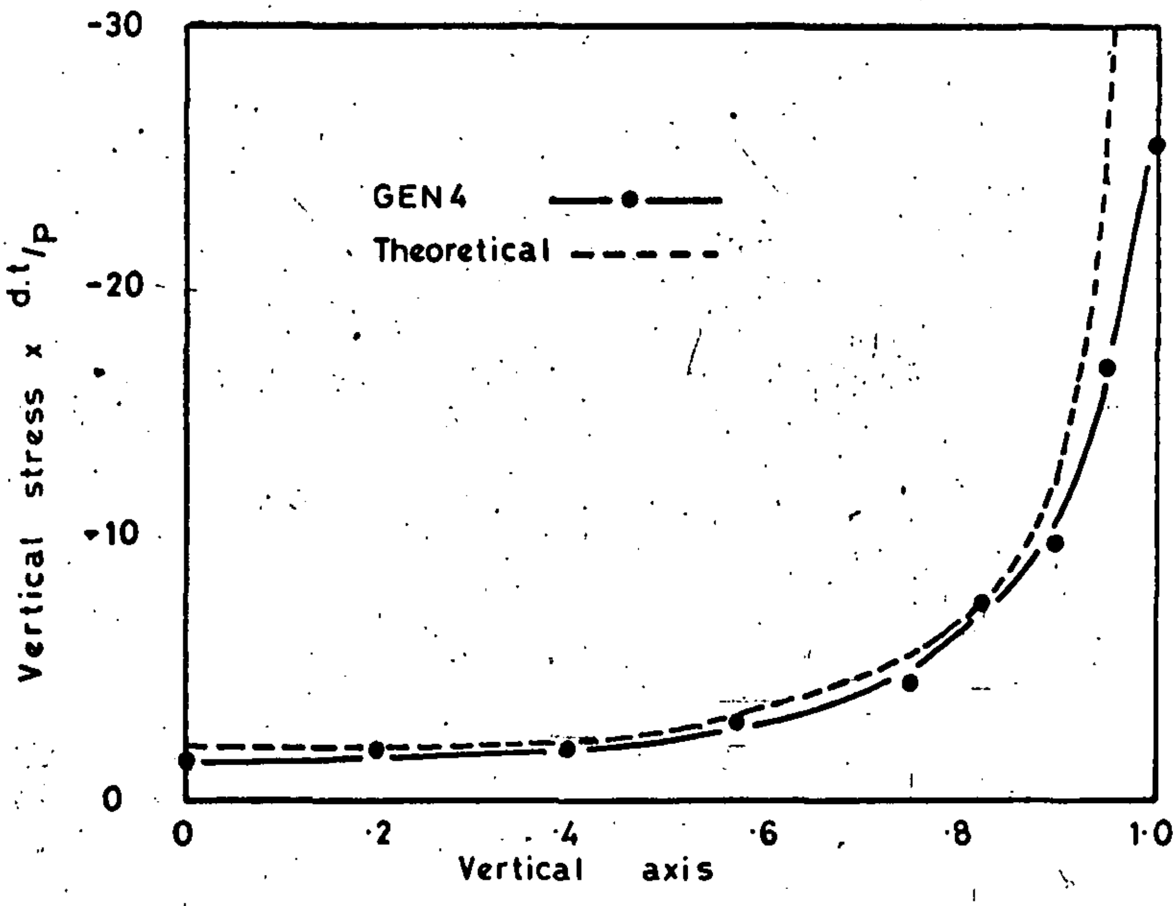

Fig. 23 Vertical stress along vertical axis of circular disc

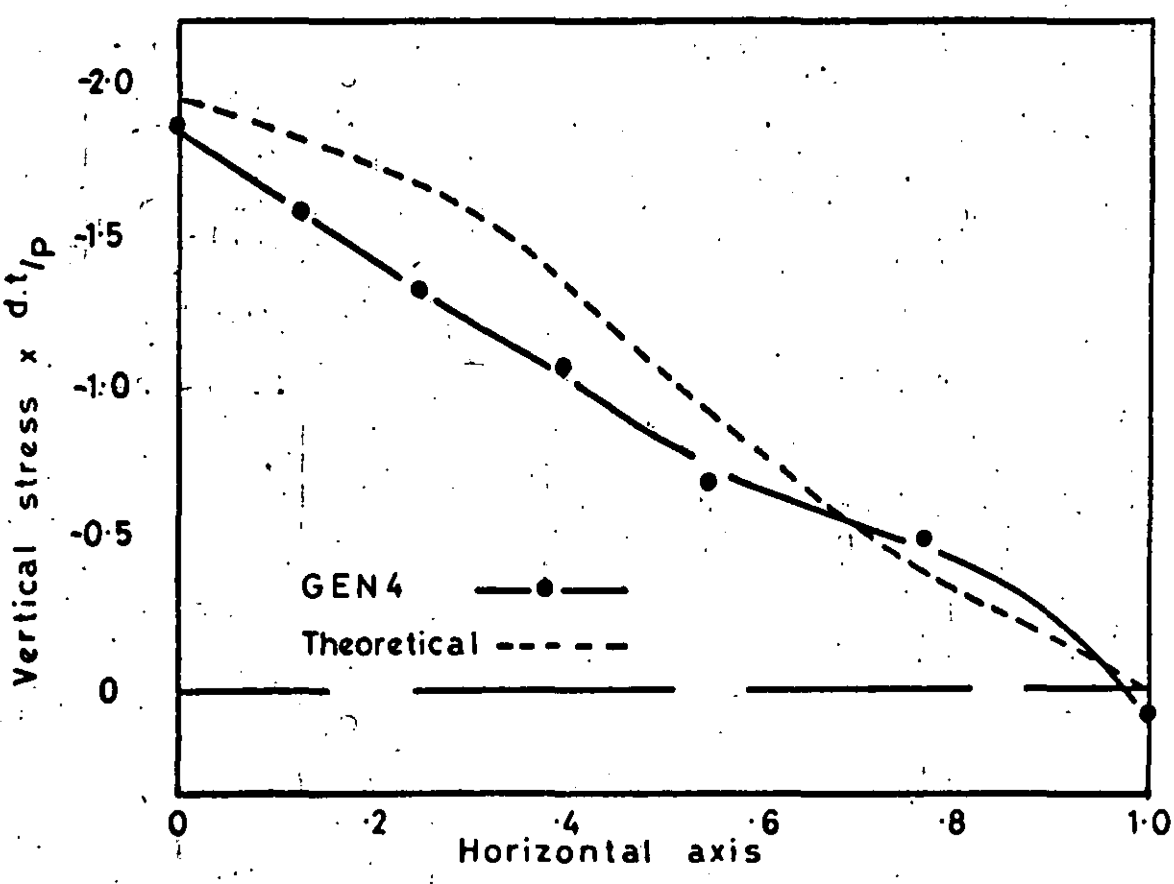

Fig. 24 Vertical stress along horizontal axis of circular disc

4.4 Pian's stretched plate problem

This problem was selected by Pian[23] as a test of his original element and a comparison with his "stress free boundary" elements. (See section 3.6) It is included here because shear effects were expected to be quite significant in the region of the loads and the effect of this on the GEN4 solution is of some interest. The mesh used by Pian (fig. 25) was very much finer than that used here - 48 elements instead of 15, 112 equations instead of 68 - and the results obtained are shown in figs.26 - 28.

Apart from the 2ins. nearest to the load, the results for the deflection of the panel centre line are barely distinguisable. In the remaining small region, the analytic solution quoted by Pian ceases to exist and there is a difference between the two finite element solutions. (For the analytical solution, see Warren, et.al.[24]) Also there is general agreement between the results for the direct stress distribution (fig.27) across a transverse section 5ins. from the load. Small negative stresses occur at the outer edge for both finite element solutions in comparison with the analytic solution which has a small positive value.

Turning to examine the shear stress across the same section, fig. 22, we find that both finite element solutions have discrepancies between themselves and the analytic solution. On the one hand, the Pian solution has a non-zero shear at the centre line of the section whilst it agrees with the analytic solution away from this edge. On the other hand, the GEN4 solution has a nearly zero shear stress at this point, but in the adjoining region the shear stress is somewhat lower than the analytic solution. This might

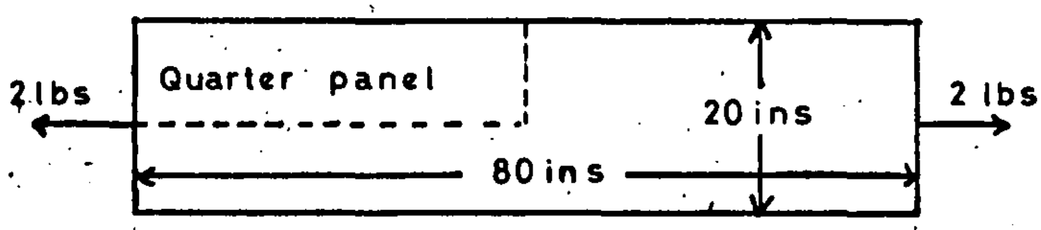

Young's Modulus = 10^7 p.s.i.

Poisson's Ratio = $^1/_3$

Thickness = ·25 ins

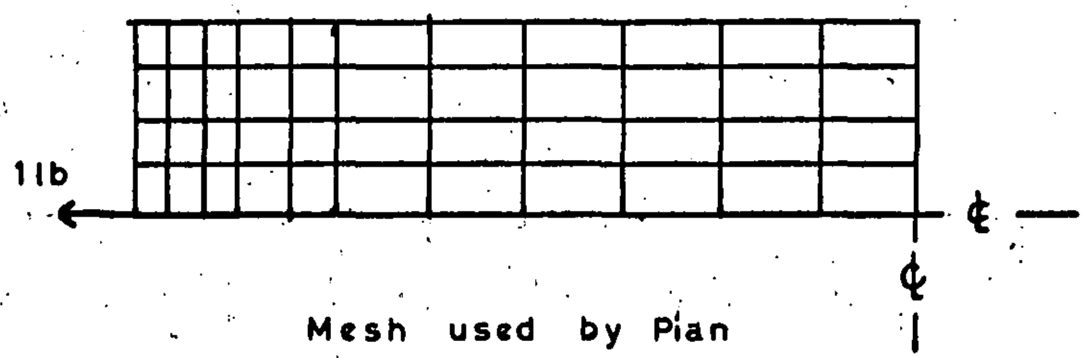

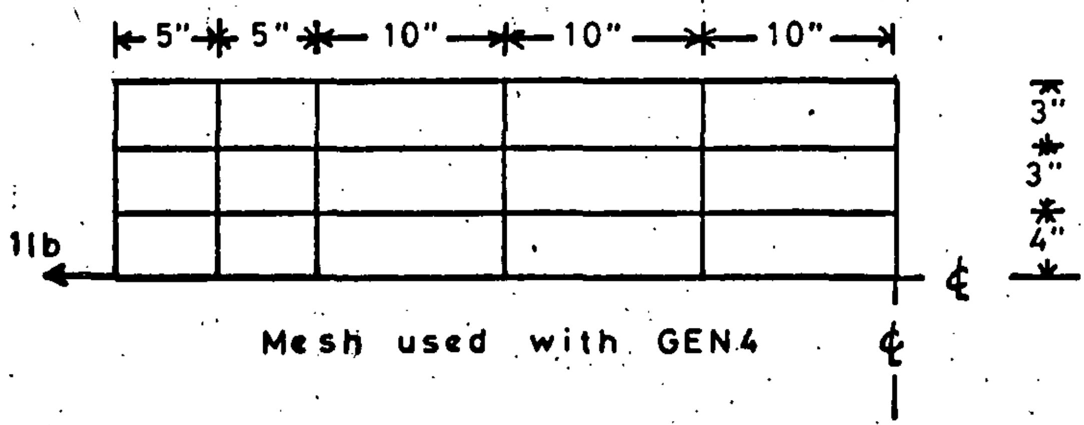

Fig. 25 Pian's stretched panel problem

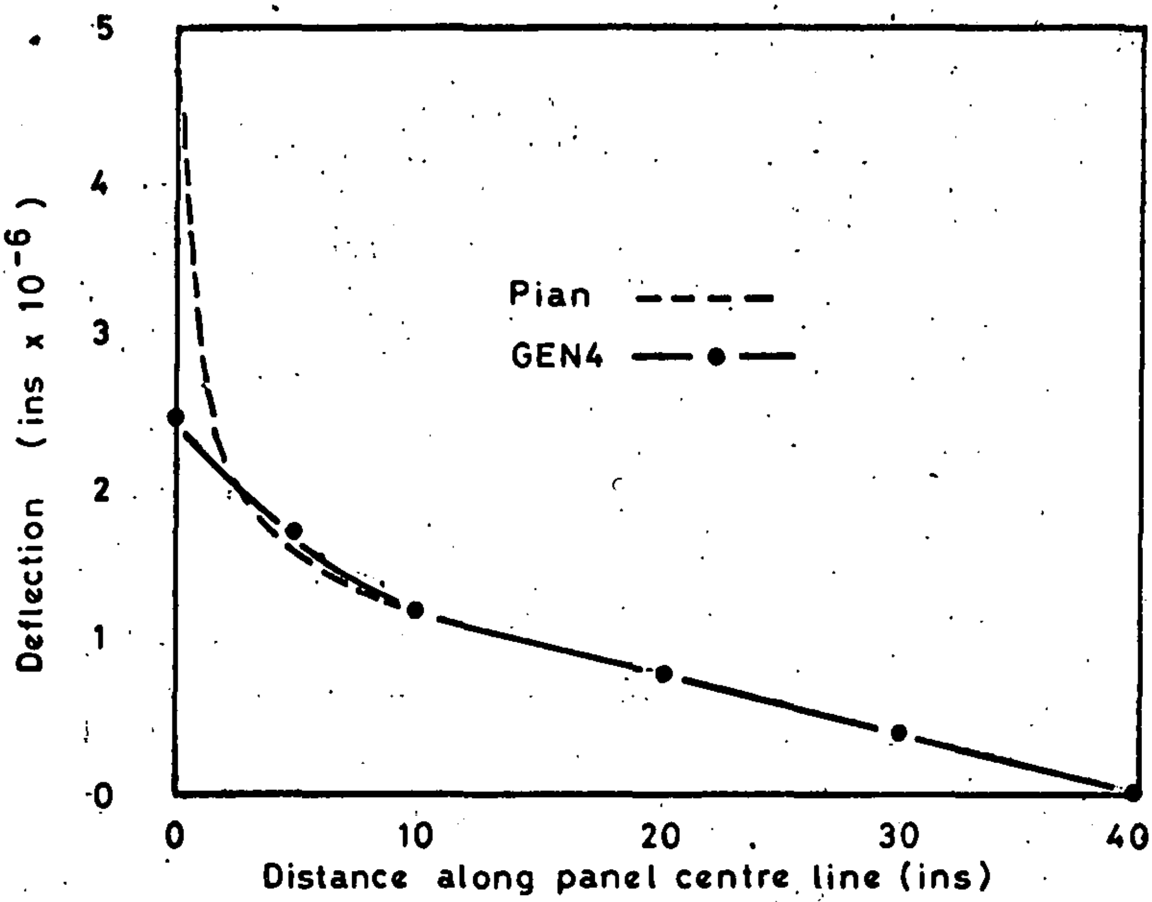

Fig.26 Deflection of panel centre line

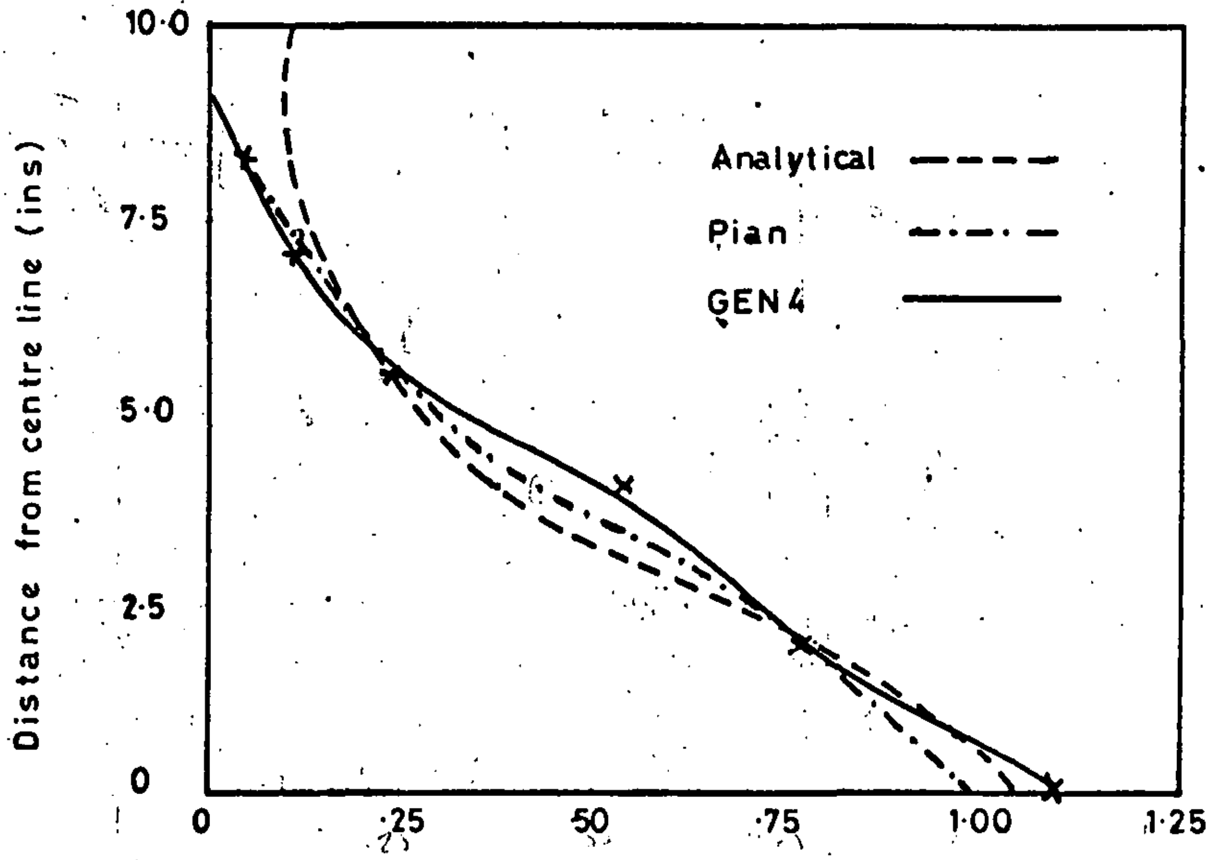

Fig. 27 Direct stress across section 5" from load (p.s.i)

Fig. 28 Shear stress across section 5" from load (p.s.i.)

have been expected since it is shear which the GEN4 element is poor at representing. Nevertheless, although the individual element stresses vary quite considerably, fig.29, the averaged nodal values are considerably better. (fig.28)

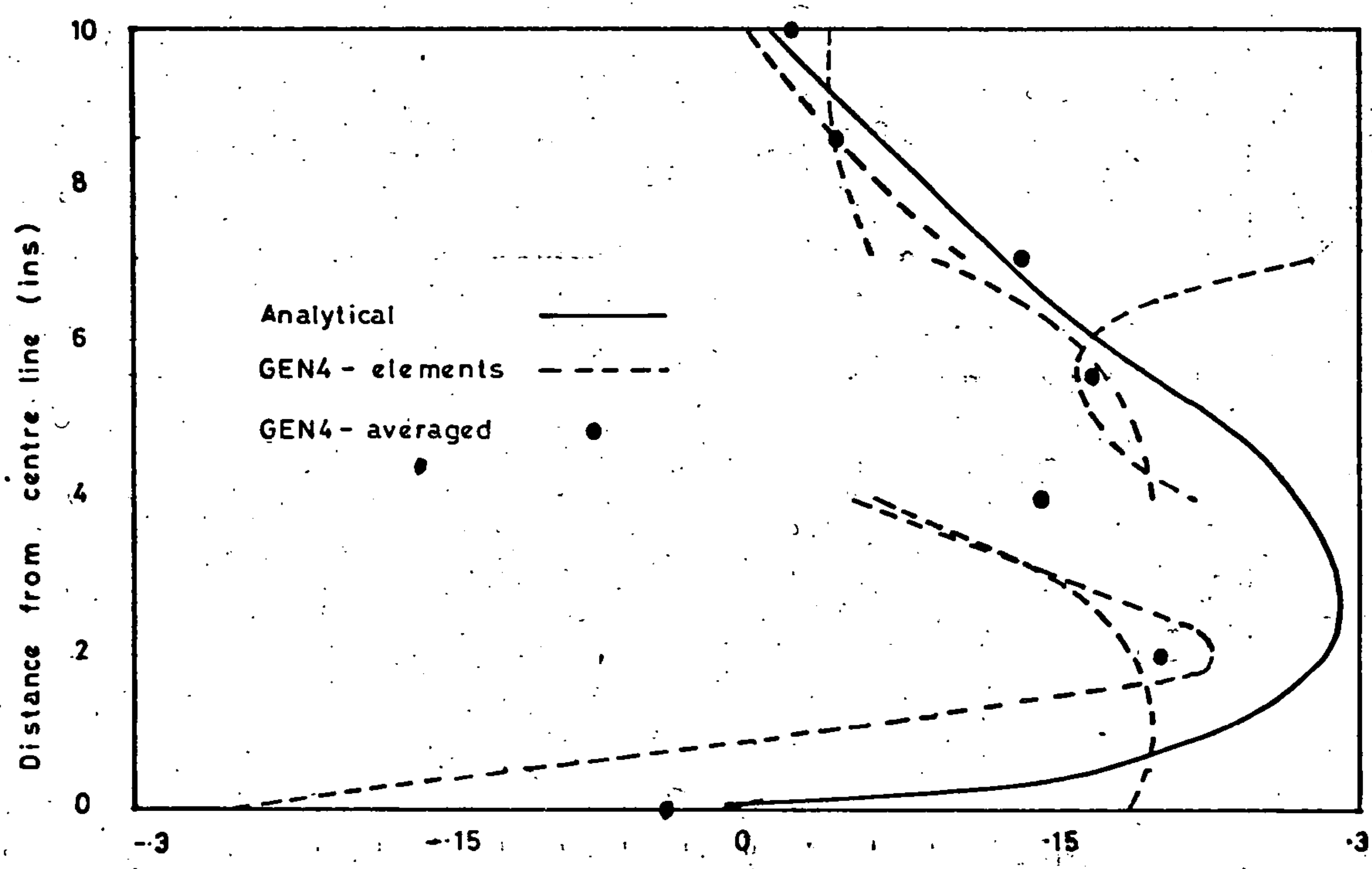

Fig.29 Shear stress across section - values from each element

Chapter Five Shell element derivation

5.1 Basic shell assumptions

A fundamental concept in the development of a shell element is the division of the stress distribution into two parts - in-plane (membrane) and out-of-plane (bending) - which can be first considerede separately and then combined together. (See Bogner et.al.[31]). Timoshenko [32] defines a shell as being thin when its thickness is small in relation to its other dimensions. To be more specific, the elements developed in this work satisfy the following conditions:

(a) No shear between the inside and outside surfaces is allowed to develop. Put another way, normals to the mid-plane remain normal in the stressed state.

(b) Direct and shear stresses in the plane of the element vary linearly across the thickness of the element.

(c) Out of plane shear stresses vary parabolically across the thickess, having zero value on the surfaces, reaching a maximum on the mid-plane.

Both the Cornes bending element[14] and the two membrane elements, GEN4 and GEN6, satisfy these conditions. We now prodeed to consider the combination of bending and membrane elements into a shell element

5.2 Seven degree of freedom shell element, S7

This element combines the GEN4 membrane element having four degrees of freedom at each node with the bending element, having three degrees of freedom per node.

The set of seven degrees of freedom for the shell element, in its own plane, is

$$u,\ v,\ w,\ \theta_x,\ \theta_y,\ \theta_z,\ e$$

Thus these separate easily into two subsets:

$$u,\ v,\ e,\ \theta_z \qquad\qquad w,\ \theta_x,\ \theta_y$$

the first of which is the set of GEN4 degrees of freedom and the second those of the bending element. The combination of the two separate elements is thus simply a case of re-ordering the degrees of freedom in the sequence set out above. These then have to be rotated into the same set of degrees of freedom, but in the global axes. In fact, the re-ordering is incorporated into the same transformation as the rotation to produce a single operation, the details of which are set out in section 5.4.

5.3 Twelve degree of freedom shell element, S12

The second shell element combines the same bending element with GEN6 for the membrane contribution. For this shell element the twelve dgrees of freedom are:

$$u,\ v,\ w,\ \frac{\partial u}{\partial x},\ \frac{\partial u}{\partial y},\ \frac{\partial u}{\partial z},\ \frac{\partial v}{\partial x},\ \frac{\partial v}{\partial y},\ \frac{\partial v}{\partial z},\ \frac{\partial w}{\partial x},\ \frac{\partial w}{\partial y},\ \frac{\partial w}{\partial z}$$

However, in this case the degrees of freedom of the two component matrices are:

membrane: $\quad u,\ v,\ \frac{\partial u}{\partial x},\ \frac{\partial u}{\partial y},\ \frac{\partial v}{\partial x},\ \frac{\partial v}{\partial y}$

bending: $\quad w,\ \theta_x,\ \theta_y$

The first step in relating these two subsets to the set of twelve degrees of freedom is to realise that:

$$\theta_x = \tfrac{1}{2}\left(\frac{\partial w}{\partial y} - \frac{\partial v}{\partial z}\right)$$

$$\theta_y = \tfrac{1}{2}\left(\frac{\partial w}{\partial x} - \frac{\partial u}{\partial z}\right)$$

However, for the thin shell bending only out-of-plane, the two component derivatives in each of θ_x and θ_y are numerically equal. Consider fig. 30(a). Here $\theta_1 = \frac{\partial w}{\partial x}$.

and $\theta_2 = -\frac{\partial u}{\delta z}$. Under our assumptions, (see 5.1) we have that $\theta_1 = \theta_2$. Consequently, we must have a stiffness relation which constrains the shear strain $\gamma_{xz} = \frac{\partial w}{\delta x} + \frac{\partial u}{\delta z}$ to be zero, in addition to the previous equations for θ_y. (Correspondingly, γ_{yz} must also be zero.)

Further, no consideration has yet been given to the out-of-plane direct strain $\epsilon_z = \frac{\partial w}{\delta z}$. In order that we satisfy the thin shell assumptions, we must also have this zero. Thus we must include in the shell element three extra stiffness equations in addition to the original nine from the membrane (K_1) and bending (K_2) stiffness matrices. These are:

$$\gamma_{xz} = \left(\frac{\partial w}{\delta x} + \frac{\partial u}{\delta z}\right) = 0$$

$$\gamma_{yz} = \left(\frac{\partial w}{\delta y} + \frac{\partial v}{\delta z}\right) = 0$$

$$\epsilon_z = \frac{\partial w}{\delta z} = 0$$

Provided no "forces" are made to act on these degrees of freedom, we may write these equations in the standard stiffness matrix form:

$$\underline{P}_3 = K_3 . \underline{d}_3$$

where $\underline{P}_3 = 0$, $\underline{d}_3 = \begin{Bmatrix} \gamma_{xz} \\ \gamma_{yz} \\ \epsilon_z \end{Bmatrix}$ and $K_3 = \begin{pmatrix} \delta & 0 & 0 \\ 0 & \delta & 0 \\ 0 & 0 & \delta \end{pmatrix}$

where the value of δ is, so far, immaterial, say $\delta = 1$.

K_1, K_2 & K_3 can be assembled together to make the full local shell element. This is now expressed in terms of the following degrees of freedom:

$$u, v, \frac{\partial u}{\delta x}, \frac{\partial u}{\delta y}, \frac{\partial v}{\delta x}, \frac{\partial v}{\delta y}, w, \theta_x, \theta_y, \gamma_{xz}, \gamma_{yz}, \epsilon_z$$

These can be transformed uniquely into the set of twelve that we require.

This is again incorporated with the rotation into global axes and the details are given in section 5.5.

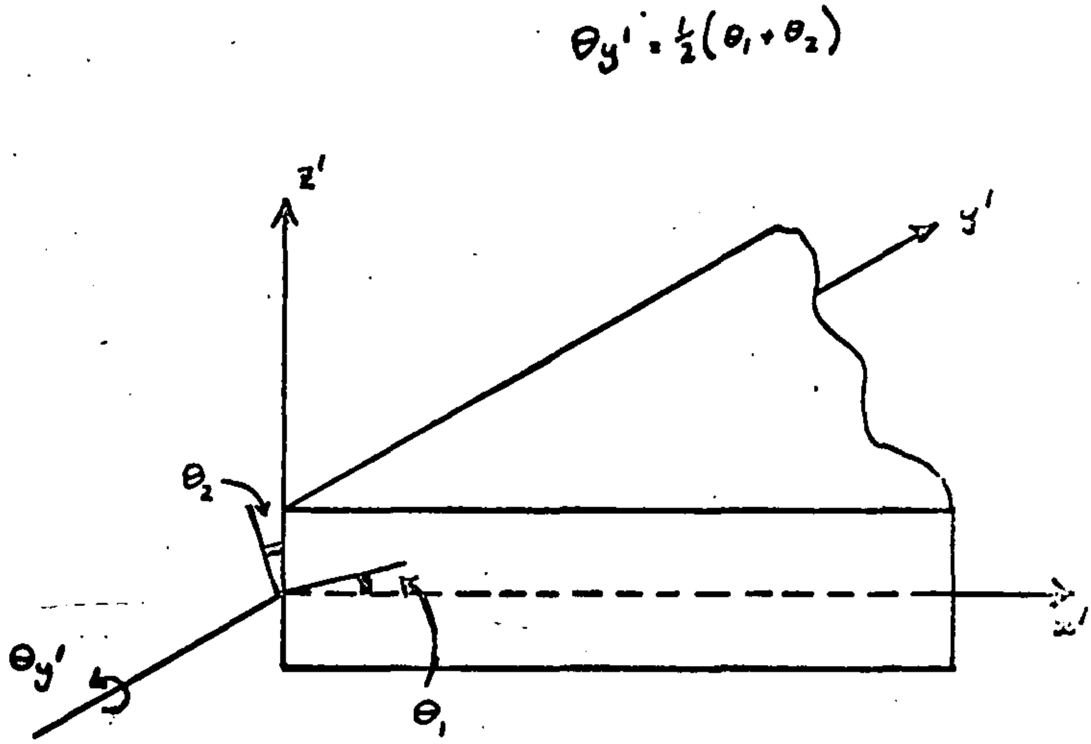

(a) Bending case

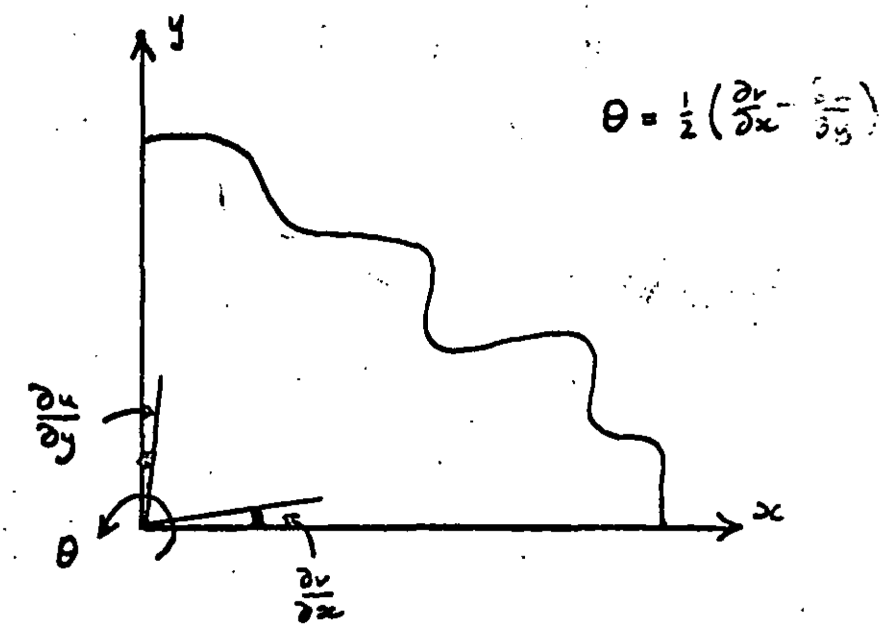

(b) Membrane case

Fig. 30 Components of average rotation

5.4 Transformation of S7 from local to global axes

Let:

$\underline{q}$ = global degrees of freedom for one node

$\underline{q}'$ = local " " " " " "

The transformation between the two can be written:

$$\underline{q}' = B.\underline{q}$$

If the element has, say, three nodes the full transformation is:

$$\underline{q}_e' = \begin{pmatrix} B & 0 & 0 \\ 0 & B & 0 \\ 0 & 0 & B \end{pmatrix} . \underline{q}_e$$

or: $\underline{q}_e' = C.\underline{q}_e$

If K' = local element stiffness matrix

K = global " " "

then

$$K = C^t.K'.C$$

For the S7 shell element the K' matrix is composed of:

K_1 = in-plane stiffness matrix

K_2 = out-of-plane stiffness matrix

and then:

$$K' = \begin{pmatrix} K_1 & 0 \\ 0 & K_2 \end{pmatrix} \qquad \text{........ (15)}$$

In detail, the transformation, including the re-ordering of the degrees of freedom, is shown in table 8, which is expressed in terms of the direction cosines in the following way:

$$u' = l_1.u + l_2.v + l_3.w$$
$$v' = m_1.u + m_2.v + m_3.w$$
$$w' = n_1.u + n_2.v + n_3.w$$

where l_i, m_i, n_i are direction cosines.

$$
\begin{pmatrix}
l_1 & l_2 & l_3 & 0 & 0 & 0 & 0 \\
m_1 & m_2 & m_3 & 0 & 0 & 0 & 0 \\
0 & 0 & 0 & 0 & 0 & 0 & 1 \\
0 & 0 & 0 & m_3l_2-l_3m_2 & m_1l_3-l_1m_3 & m_2l_1-l_2m_1 & 0 \\
n_1 & n_2 & n_3 & 0 & 0 & 0 & 0 \\
0 & 0 & 0 & m_3n_2-n_3m_2 & m_1n_3-n_1m_3 & m_2n_1-n_2m_1 & 0 \\
0 & 0 & 0 & n_3l_2-l_3n_2 & n_1l_3-l_1n_3 & n_2l_1-l_2n_1 & 0
\end{pmatrix}
$$

Table 8: Transformation matrix, B for S7 element

5.5 Transformation of S12 from local to global axes

This is the same as for S7 but with $K' = \begin{pmatrix} K_1 & 0 & 0 \\ 0 & K_2 & 0 \\ 0 & 0 & K_3 \end{pmatrix}$

and the transformation is given in table 9, at the end of this section. However, one significant point still remains to be considered. When two elements meet at an angle, the special degrees of freedom γ_{xz}, γ_{yz}, ϵ_z will not be the same for each and indeed, in global terms, the matrix K_3 will by now be transformed into different parts of the assembled equations. Furthermore, although it is essential that for the bending case (fig. 30(a)) these terms be zero, for an element at, say, right angles to this, these degrees of freedom now become membrane degrees of freedom (fig. 30(b)), and are allowed to develop independently as befits a membrane problem.

A fundamental technique in the stiffness method is that specific equations can be made to "dominate" and become independent of the rest simply by the numerical technique of multiplying them by a large factor. This, for example, can be used to impose finite or zero settlements upon certain direct displacements. Similarly here, if normal stiffness equations are superimposed on the special equations introduced in 5.3, and the value of δ is made sufficiently small, the effect of the special "constraints" will be insignificant in the presence of ordinary stiffness. In this way we are able to make elements meeting at an angle remain rigidly connected together by these peculiar constraints unless there is a real element which is capable of taking these strains and which allow these shear and direct strains to develop.

l_1	l_2	l_3									
m_1	m_2	m_3									
			l_1^2	l_1l_2	l_1l_3	l_2l_1	l_2^2	l_2l_3	l_3l_1	l_3l_2	l_3^2
			l_1m_1	l_1m_2	l_1m_3	l_2m_1	l_2m_2	l_2m_3	l_3m_1	l_3m_2	l_3m_3
			m_1l_1	m_1l_2	m_1l_3	m_2l_1	m_2l_2	m_2l_3	m_3l_1	m_3l_2	m_3l_3
			m_1^2	m_1m_2	m_1m_3	m_2m_1	m_2^2	m_2m_3	m_3m_1	m_3m_2	m_3^2
n_1	n_2	n_3									
				$\frac{1}{2}(n_1m_2 - m_1n_2)$	$\frac{1}{2}(n_1m_3 - m_1n_3)$	$\frac{1}{2}(n_2m_1 - m_2n_1$		$\frac{1}{2}(n_2m_3 - m_2n_3)$	$\frac{1}{2}(n_3m_1 - m_3n_1)$	$\frac{1}{2}(n_3m_2 - m_3n_2)$	
				$\frac{1}{2}(l_1n_2 - n_1l_2)$	$\frac{1}{2}(l_1n_3 - n_1l_3)$	$\frac{1}{2}(l_2n_1 - n_2l_1)$		$\frac{1}{2}(l_2m_3 - n_2l_3)$	$\frac{1}{2}(l_3n_1 - n_3l_1)$	$\frac{1}{2}(l_3n_2 - n_3l_2)$	
			$2l_1n_1$	$l_1n_2 + n_1l_2$	$l_1n_3 + n_1l_3$	$l_2n_1 + n_2l_1$	$2l_2n_2$	$l_2n_3 + n_2l_3$	$l_3n_1 + n_3l_1$	$l_3n_2 + n_3l_2$	$2l_3n_3$
			$2n_1m_1$	$n_1m_2 + m_1n_2$	$n_1m_3 + m_1n_3$	$n_2m_1 + m_2n_1$	$2n_2m_2$	$n_2m_3 + m_2n_3$	$n_3m_1 + m_3n_1$	$n_3m_2 + m_3n_2$	$2n_3m_3$
			n_1^2	n_1n_2	n_1n_3	n_2n_1	n_2^2	n_2n_3	n_3n_1	n_3n_2	n_3^2

Table 9: Transformation matrix, B for S12 element

Chapter Six Basic tests on the shell element, S7

6.1 Introduction

The testing of the plane stress elements as reported in Chapter Three and that of the bending element by Cornes[14] has validated the behaviour of the component elements under a variety of practical situations. It is not necessary to perform exactly the same tests on the shell elements. Two points remain, however, which need consideration. Firstly, it is hoped that the S7 and S12 elements can be used with particularly coarse meshes. The degree to which this is possible has to be determined particularly in relation to the geometric approximation of curved surfaces. Additionally, the effect of using plane elements and polyhedra to represent curved elements and doubly curved shells need examination. Secondly, the inability of the S7 element to represent shear correctly needs to be assessed in the shell condition.

The element S7 involves considerably less computation than the twelve degree of freedom element, S12, especially in situations where geometric considerations prevent the use of a coarser mesh by the S12 element than the S7. As a consequence, it is intended to use the latter as far as possible, resorting to the more sophisticated element in problems for which the S7 element is not capable of producing a good solution.

6.2 Basis of evaluation

Six problems were selected for the basis of evaluating the S7 element and these cover a wide range of aspects of the use of the element. These problems are:

I Simple portal

This problem demonstrates that this element correctly represents rigid joints between elements meeting at right angles.

II Cantilevers

This set of three cantilevers covers a variety of problems in which elements again meet at right angles. Also included is an example in which beam elements are combined with the shell element.

III Numerical stability

A sequence of channel cantilevers with an increasing stiffness ratio is examined to establish the numerical stability of the combination of element and method of solution of the equations.

IV Simply supported box beam with end diaphragms

This problem is included in order to demonstrate the care required in assessing the implications of using the average rotation in the shell element S7.

V Cylindrical shell

A sequence of cylindrical shells with increasing fineness of subdivision of the curved direction is compared in order to determine the degree of geometrical approximation required for a given stress accuracy.

VI Spherical cap

This problem is a thin shell with double curvature and considerable bending effects.

6.3 Results of evaluation

6.3.1 Simple portal

A simple portal (see fig.31) was analysed with three finite elements, one for each of the structural elements. The results are compared with a two dimensional area-moment analysis of the equivalent portal frame.

Deflection of upper right corner

=	.025 ins	S7 shell element
=	.025 ins	Area moment analysis

Bending moment at supports

=	13.74×10^4 lb-in	S7 shell element
=	13.71×10^4 lb-in	Area moment analysis

6.3.2 Cantilevers

Three cantilevers of various cross-sections have been analysed, the first two using shell elements only, the last with a mixture of shell elements and beams. These also illustrate the ability of the S7 element to represent "corner" situations.

A I-beam

B Square hollow box beam

C Channel beam

In all cases the depth was relatively large in relation to the length as this represents a more exacting task and the results quoted for comparison include the shear correction term given in chapter three.

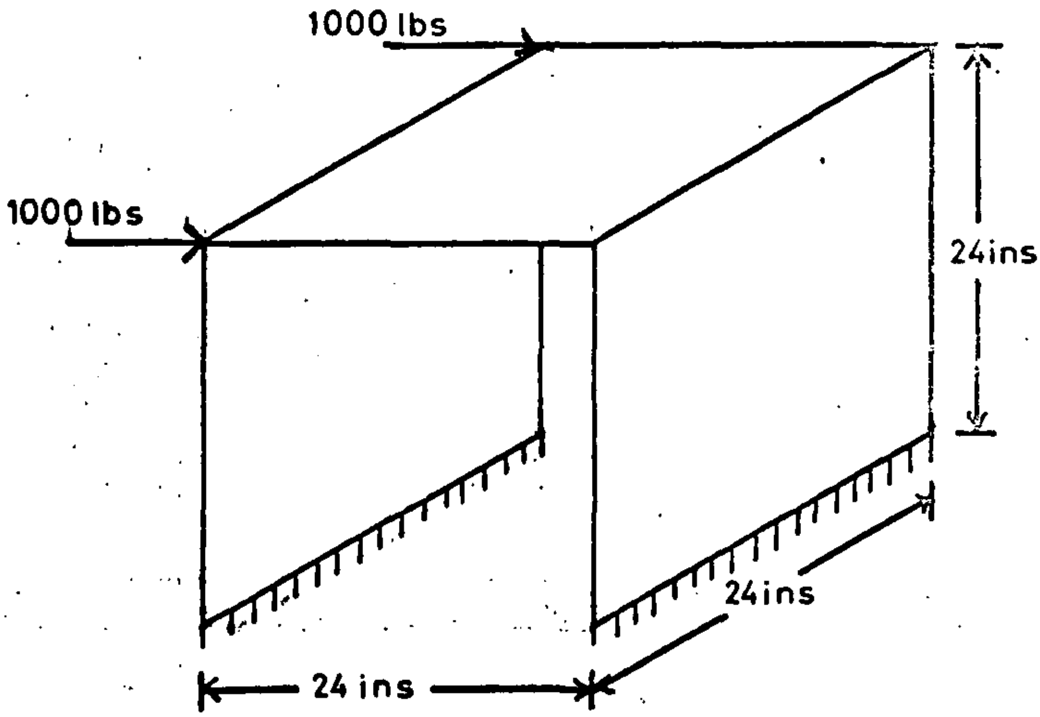

Young's Modulus = 30×10^6 p.s.i.

Poisson's Ratio = ·3

Thickness = 1in

Fig. 31 Simple portal - test 1

Cantilever A

For this problem the length of the cantilever was divided into three equal sections. The depth of the web was a single element whilst the flanges were two elements each, one on either side of the web. (See fig. 32) The load was placed centrally on the flange.

Second moment of area	=	5.636×10^6 ins^4
Number of equations	=	126
Maximum deflection	=	.00169 ins simple theory
	=	.00170 ins S7 shell element
End rotation	=	.00001 radians simple theory
	=	.00001 radians S7 shell element

Cantilever B

For this problem the length of the cantilever was divided into four elements but otherwise the division was that dictated by the geometry of the problem. Two load cases were considered, bending and torsion, which introduce quite different stress patterns.

Second moment of area	=	148 ins^4
Number of equations	=	112
Bending load case:		
Maximum deflection	=	.00225 ins simple theory
	=	.00219 ins S7 shell element
Torsional load case:		
End rotation	=	.00006 radians simple theory
	=	.00005 radians S7 shell element

For the second load case the simple theory does not include the effect due to the end deformations being different from each other.

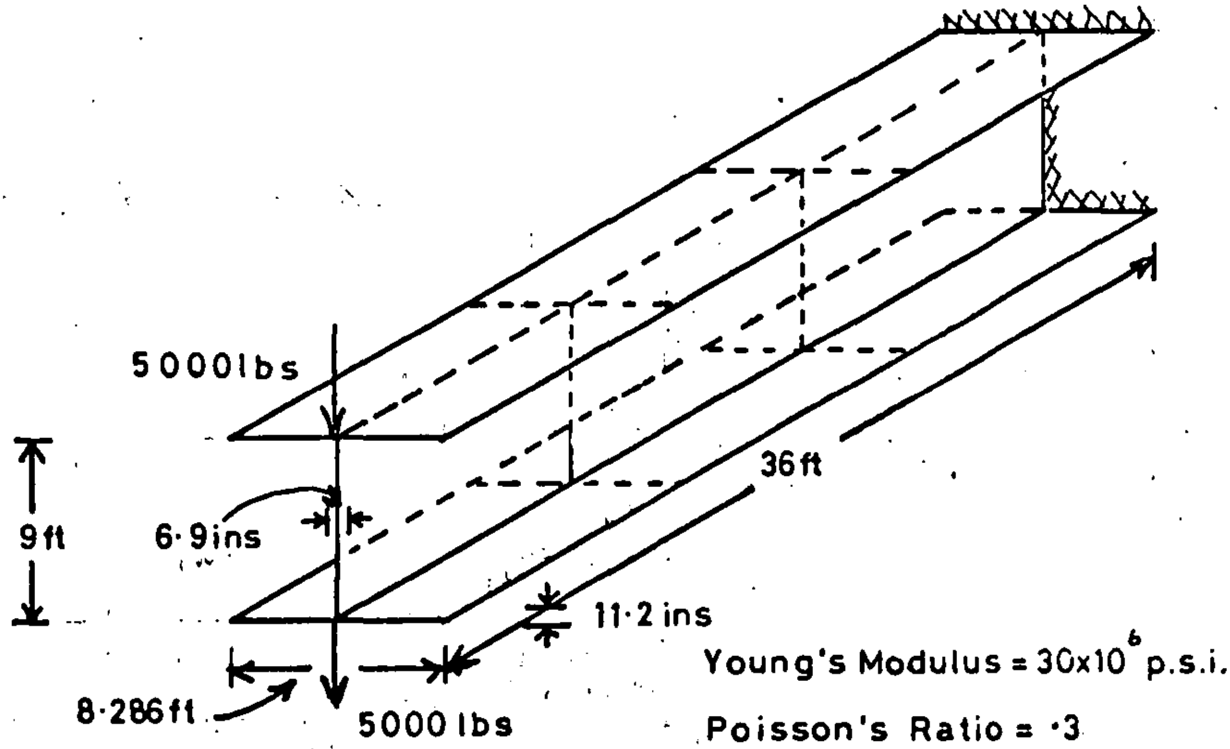

Fig. 32 Cantilever A - test 2

Young's Modulus = 30×10^6 p.s.i.

Poisson's Ratio = ·3

Thickness = 2 ins

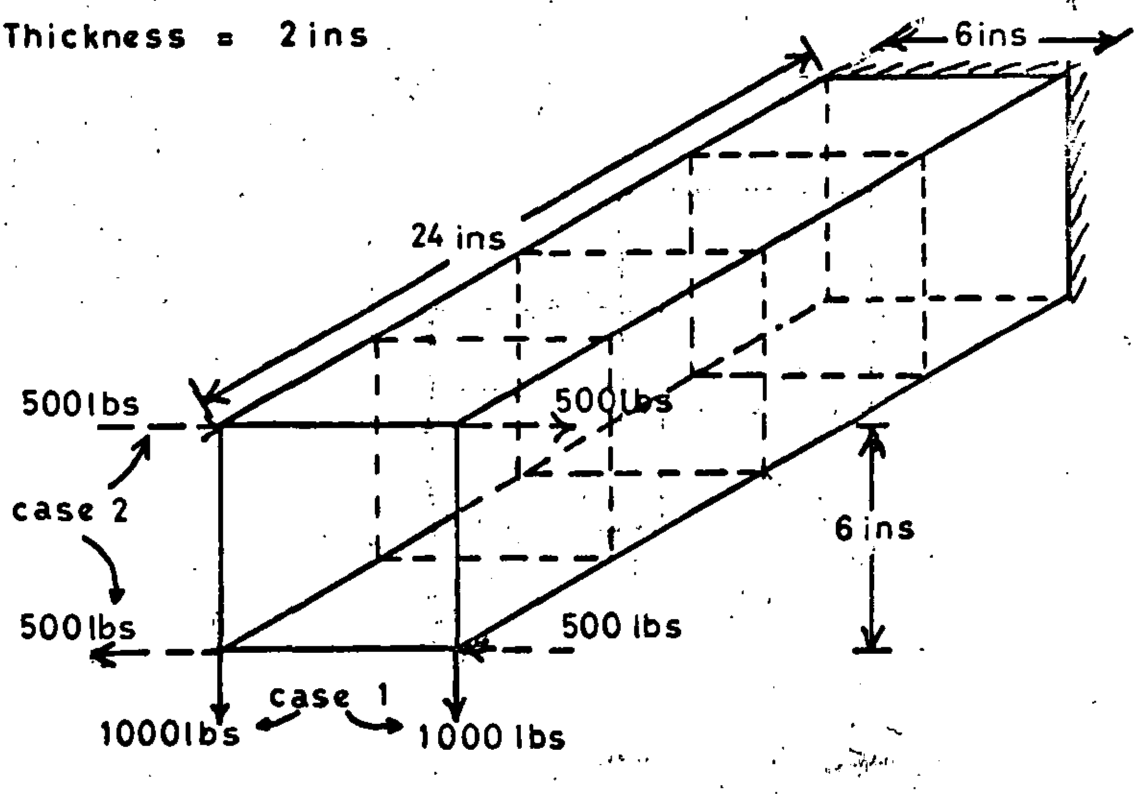

Fig. 33 Cantilever B - test 2

Cantilever C

For this problem (see fig. 34) the web is represented by a shell element and the two flanges by beam elements eccentrically placed along the edges i.e. the neutral axes of the beams are offset from the edges of the elements comprising the web. This example is included here to establish the validity of the method prior to its use in one of the problems of Chapter Seven. An oblique load was considered and so for a theoretical solution we superimpose two separate calculations. These are only approximate since some of the load is taken in torsion and the end conditions of this example cannot be matched correctly by simple theory.

For the vertical deflection:

P = 939.7 lbs. Second moment = 19.46 ins^4

Using the rotation and deflection of node A we can obtain the average vertical deflection for the top flange.

vertical deflection (ins)	=	.025	simple theory
	=	.023	S7 shell solution

For the horizontal deflection:

P = 375.0 lbs Second moment = 5.06 ins^4

Horizontal

horizontal deflection (ins)	=	.037	simple theory
	=	.028	S7 shell solution

6.3.3 Numerical stability problem

A channel cantilever was examined, with a longitudinal division of the flange into two instead of one as for cantilever B above. The point P (see fig.35) was varied in position in order to induce an increasing

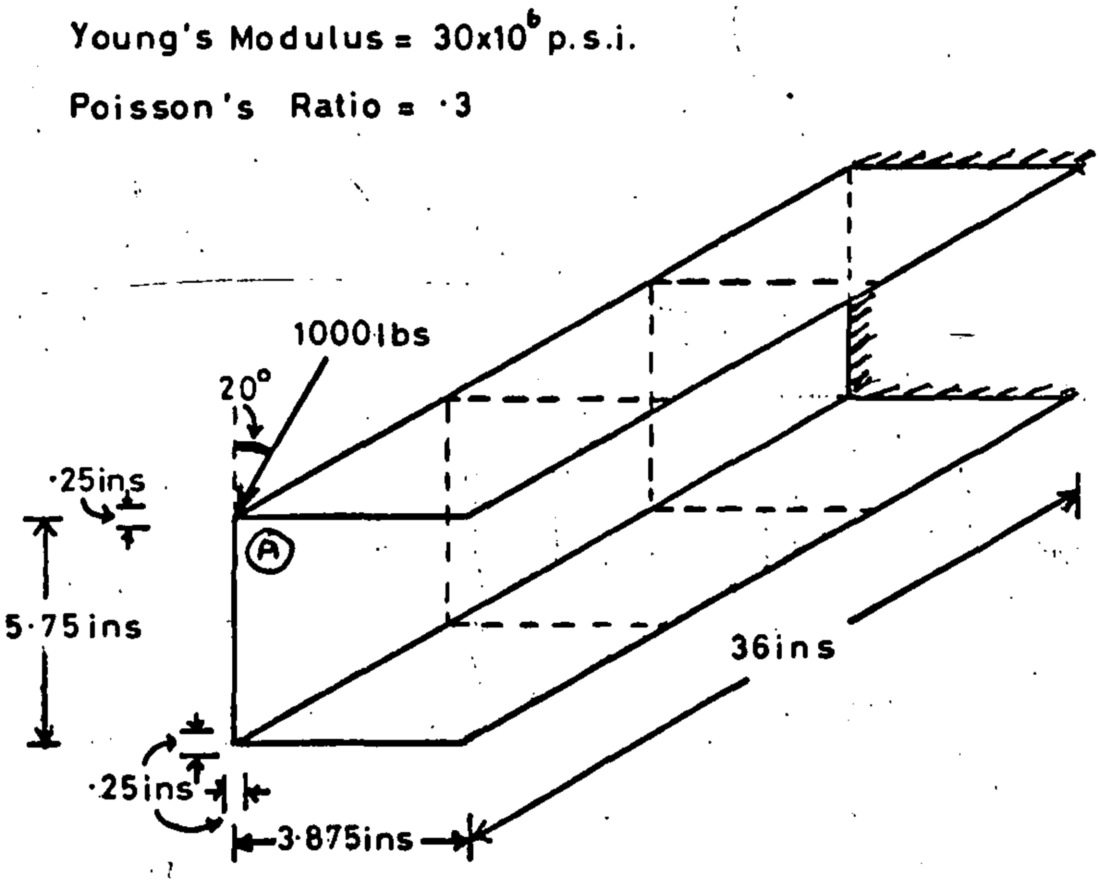

Fig. 34 Cantilever C - test 2

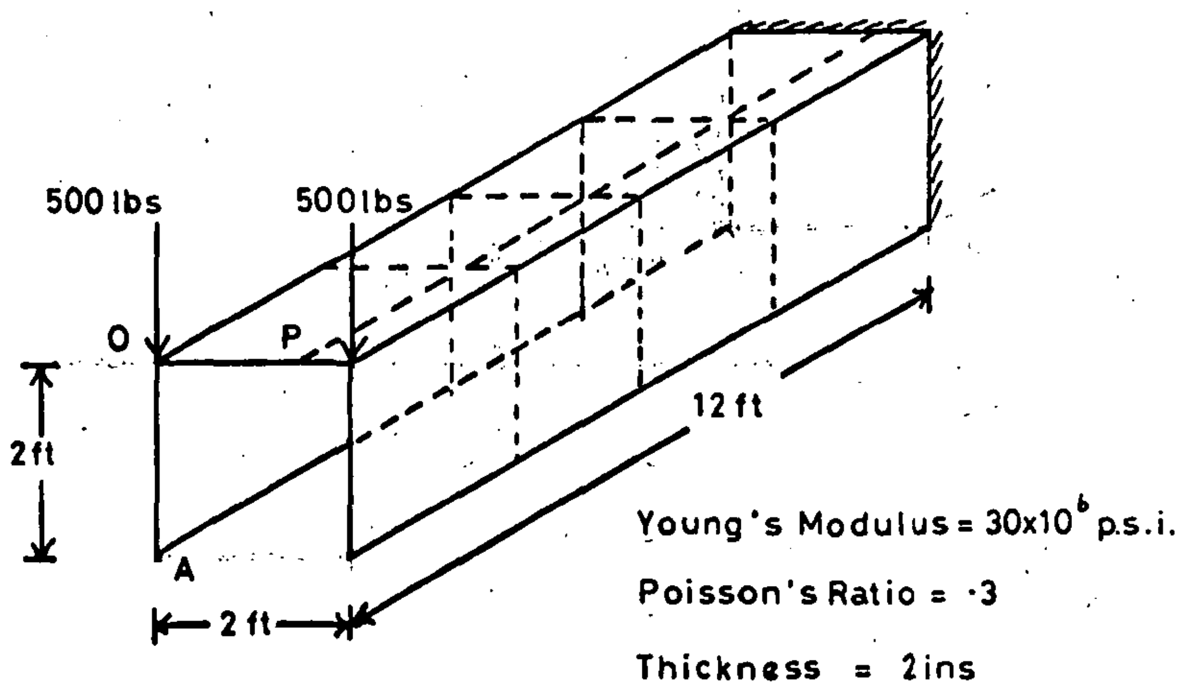

Fig. 35 Channel cantilever - numerical stability (test 3)

stiffness ratio. The variation in the solutions - see table 10 below - is remarkably slight despite the aspect ratio of the slender element reaching 30,000:1. This indicates that any errors in the solution of problems using this shell element with this method of solving the resulting equations are unlikely to be the result of numerical inaccuracy or near singularity. The causes are more likely to arise from the basic theoretical problems which are, in part, discussed in the succeeding sections.

OP (ft)	deflection (ins x 10^{-5})	forces at node A (lbs/in)		
		horiz	vertical	shear
1.0	366	476	83	15
1.5	366	476	83	15
1.7	365	479	84	16
1.9	364	474	83	17
1.99	359	467	83	18
1.9999	356	466	82	18
Exact deflection = 370 x 10^{-5} ins.				

Table 10: Numerical stability problem: end results for deflection and forces.

6.3.4 Simply supported box beam with end diaphragms

The problem to be considered in this section is shown in fig.36 and consists of a simply supported box beam with transverse diaphragms across the ends and a line load across the centre line.

Without the end diaphragms the S7 element gives a good solution to the central deflection, see table 11. Although the stresses at the free edge are usually small but non-zero, this makes little difference normally to the overall deflections. This is the result produced here.

solution	no.of nodes	deflection (ins)
S7 (no diaphragm)	16	.326
S7 (0.5" diaphragm)	16	.288
S7 (5.0" diaphragm)	16	.139
S7 (mesh (i))	24	.337
S7 (mesh (ii))	18	.286
S12 (no diaphragm)	16	.343
S12 (5.0" diaphragm)	16	.342
Theoretical		.312

Table 11: Central deflection of simply supported box beam.

In reality, the addition of a diaphragm at the free ends of the box should make but little difference to the results. However, the second result in table 11 shows that for the S7 element this is just not so: the addition of the diaphragm reduces the central deflection quite considerably. Further, the thicker the diaphragm the greater this effect. (It should be noted that diaphragms of the relative proportions of the thicker diaphragm are today being used in bridge structures - see chapters 8 & 9) We now seek an explanation for this effect.

Although, on the simple beam theory no shear effects are included in this problem, in any beam with finite depth a certain amount of shear must take place, particularly over the supports. On the other hand, the variety of problems so far considered in this thesis demonstrate that the local distortions which result from the use of S7 and GEN4 in these circumstances do not contribute appreciably to the overall results. (See, for example, fig. 14(a) chapter three, where the vertical deflection along the horizontal edges was examined in detail.) Under pure in-plane shear the edge shape adopted by GEN4 and S7 is shown in fig. 12. At the supported vertical edges of the webs in the present problem, this shape is superimposed on the correct pure rotation of the beam at this point. As before, the result without the diaphragm shows that this does not produce global errors. However, if an end diaphragm is now added, this will tend to be bent to the same shape, see fig. 37. This shape involves out-of-plane bending and the diaphragm is likely to be particularly stiff against this deformation pattern, and so will introduce large negative moments at the corners of the free end as it resists this bending. These moments reduce the central deflection.

In addition, thicker diaphragms will be even more stiff and contribute larger moments. This is borne out by the results already quoted. Two remedies for this problem were pursued and will now be considered.

(a) finer mesh with S7

(b) same mesh with S12

The first line of attack requires further understanding of the S7 deformation in order to refine the mesh most successfully. The distribution of $\hat{\theta}$ across the element, as shown in fig.37 is assumed by the Cornes bending element – and hence S7 also – to be linear between the values at the ends. Since, here, these end values are the same, $\hat{\theta}$ must be constant across the element. If, by some means, the distribution of $\hat{\theta}$ could be made so that the resultant moment across the end can be zero, we can confine the effect of these negative moments to local distortions, rather than the present overall effect.

The simplest way of improving the distribution of $\hat{\theta}$ is by making the diaphragm of two elements and the distribution can then be bi-linear. Two different meshes which include this are shown in fig. 38 and the results for these are included in table 11. These are much closer to the expected results and the above explanation seems justified. However, the penalty imposed by this is twofold. A considerable increase in the computation is required for both meshes and even so we are left with important erroneous distortions of the diaphragm. The second remedy must now be considered.

As will be recalled from previous chapters, the GEN6 and S12 elements allow in-plane shear to take place at the corners of an element. As was shown for GEN6 in fig. 14(b), this removes the local distortions introduced by GEN4.

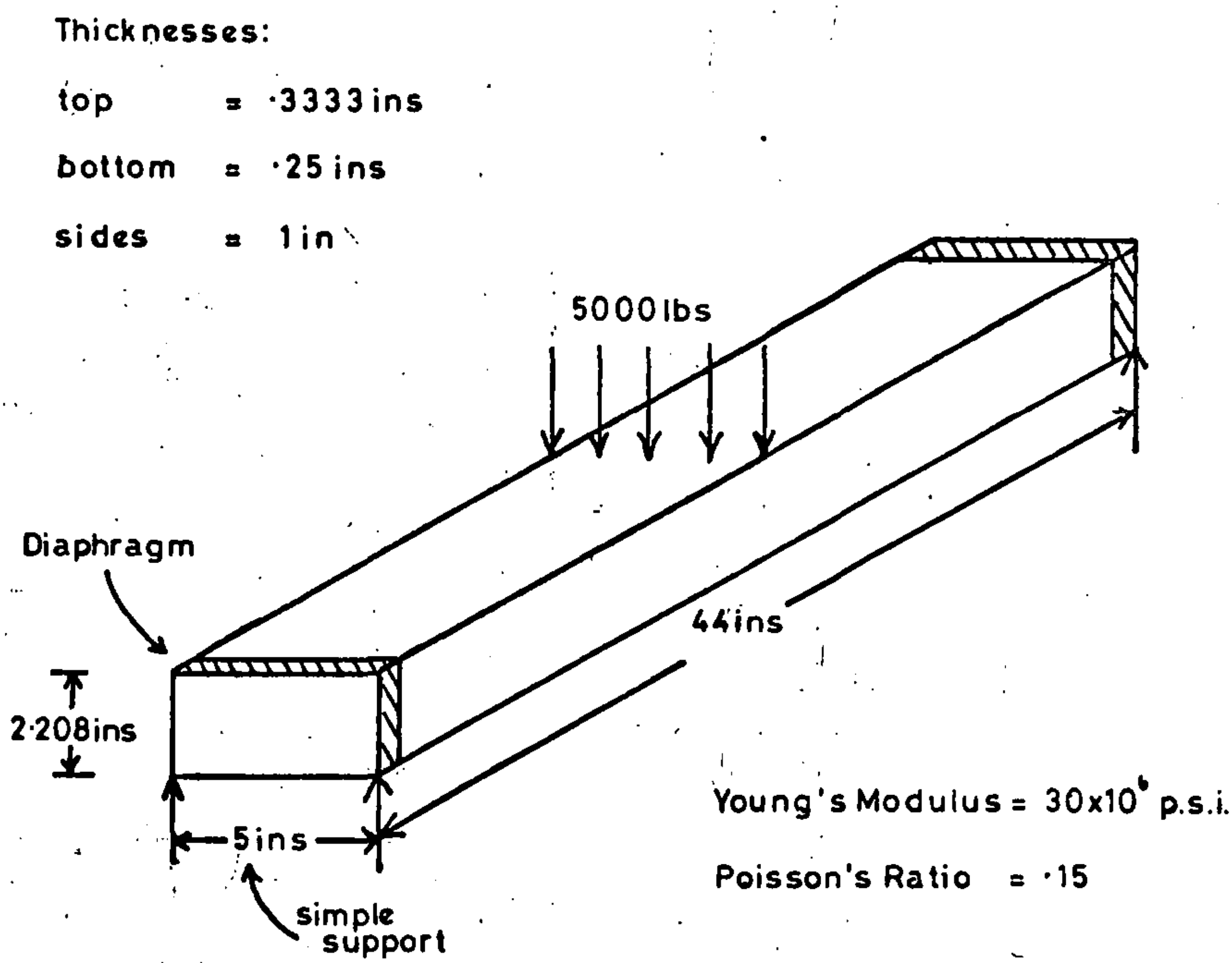

Fig. 36 Simply supported box beam with end diaphragm - test 4

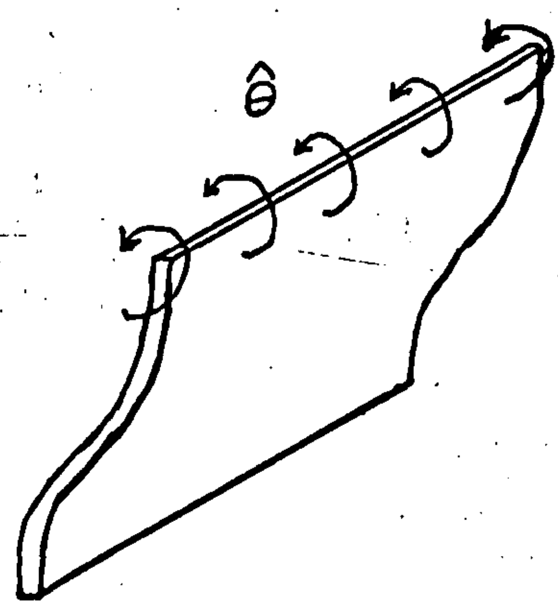

Fig. 37 Deflected shape of end diaphragm using S7

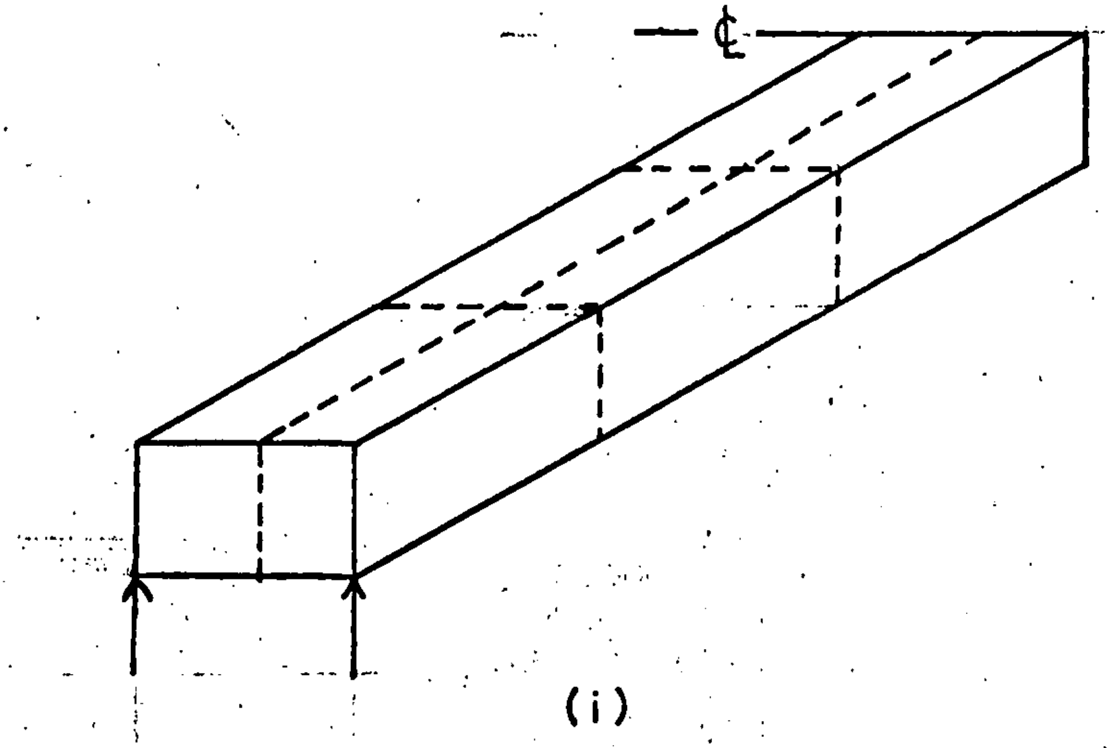

(i)

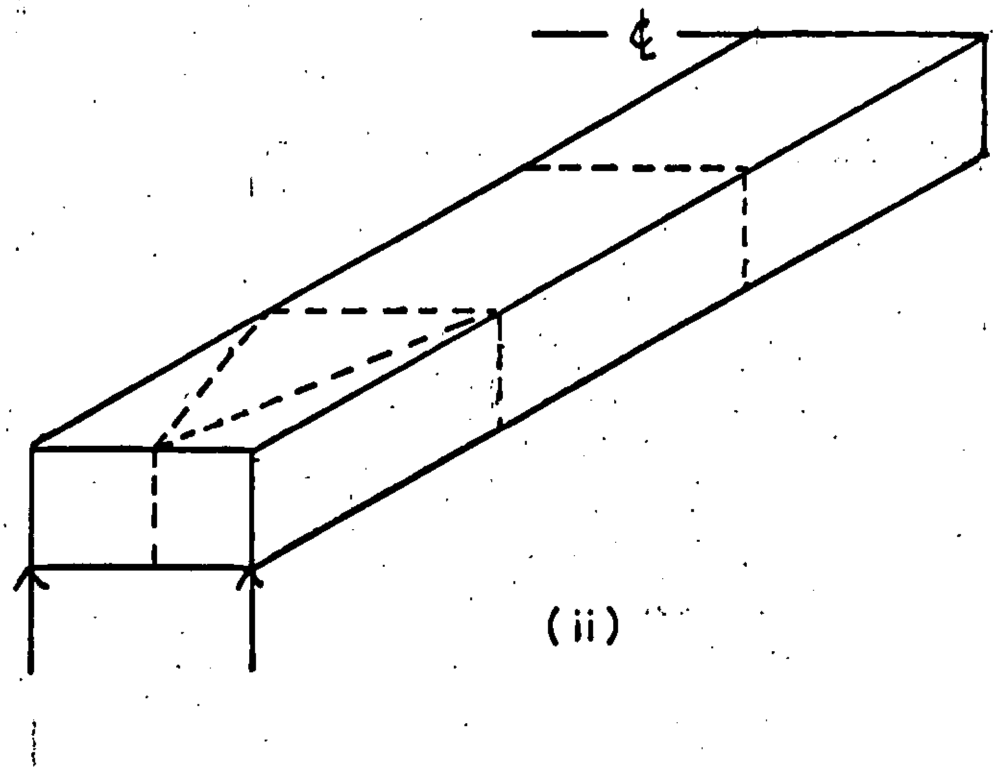

(ii)

Fig. 38 Additional meshes used with S7

Correspondingly, since the correct effects should now be represented by S12 at the corners of the beam, we expect better results than from S7 and -table 11 - this is so. The end diaphragm can now rotate as expected without the additional deformation introduced by S7.

In general, this latter approach is the more acceptable since even with mesh refinement, S7 still has erroneous stresses locally. Thus we must expect to have to resort to using S12 for box-type problems in which diaphragms are included at stress-free boundaries.

6.3.5 Cylindrical shell with line load

This problem was included to discover the degree of geometric accuracy required for a given stress accuracy. A cylindrical shell with a line load along the crown and supported rigidly along the edges was divided into four elements along the generator of the surface and into a varying number - N - in the other direction. Four cases were analysed with N = 2,3,4,6. The problem is shown in fig. 39 and the results obtained for the crown deflection are given in table 12. The resulting distributions of bending moment along the free edge are shown in fig.40. These results show that even the coarsest representation gives a reasonable solution and for many purposes would be quite sufficient, but for further accuracy four subdivisions would appear quite adequate.

This example also shows that for shells curved in one direction only, the element S7 can provide efficient and accurate solutions.

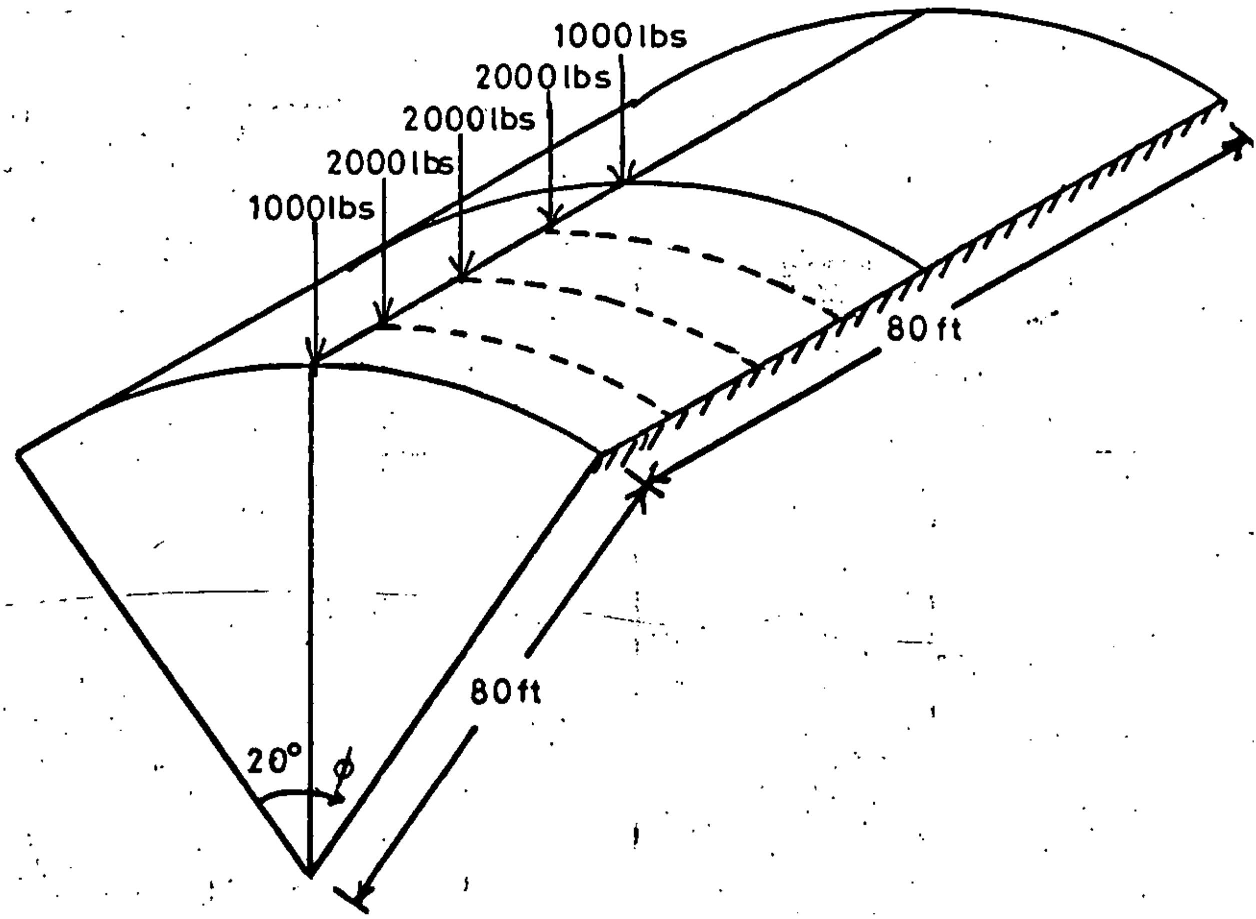

Young's Modulus = 30×10^6 p.s.i.

Poisson's Ratio = ·3

Thickness = 4 ins

Fig. 39 Cylindrical shell with line load - test 5

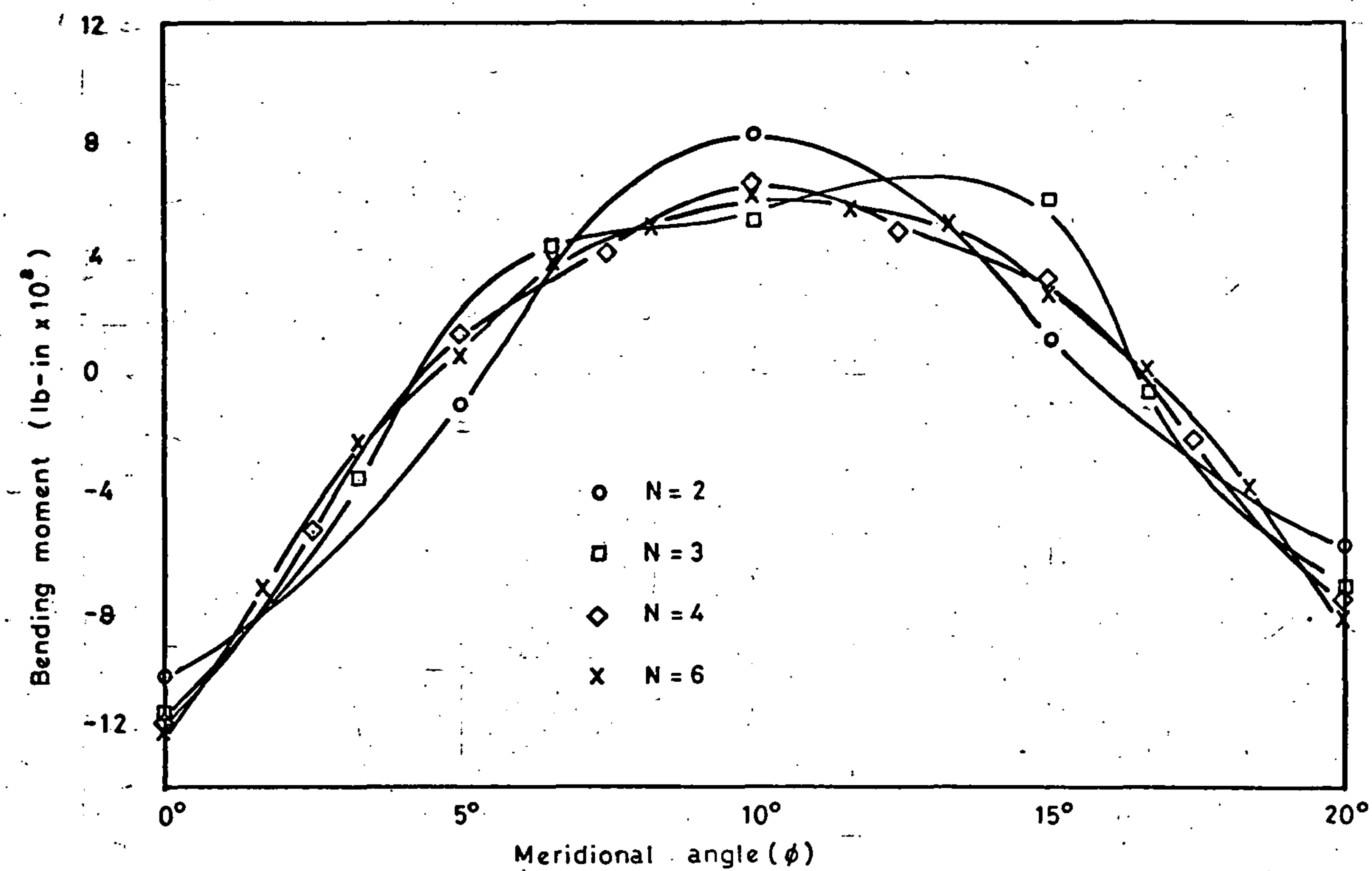

Fig.40 Bending moment along free edge of cylindrical shell with line load - test 5

N	Average central deflection (in)
2	.01913
3	.02054
4	.02074
6	.02120

Table 12: Average central deflection of crown of cylindrical shell with line load

6.3.6 Spherical cap

This problem, fig.41, which has a Timoshenko solution (32), is a standard test case for shell finite elements and has been solved quite successfully with a number of quite elementary elements. These elements require a fine mesh, not necessary with the S7 element. We should expect this element to be capable of quite good solutions, with far fewer elements.

Being axially symmetric, only a slice of the problem need be analysed, as shown in fig. 41. Two meshes were used, the first considered a $22\frac{1}{2}^{o}$ slice of the shell and used only three elements; the second considered a 10^{o} slice and 10 elements. The results are plotted in figs. 42 - 45.

The principal discrepancy occurs at the crown of the shell where, according to Timoshenko, no bending takes place, only membrane action. That is to say, the inside and outside stresses should be equal. However, it can be seen from the results that the finite element solution introduces quite an amount of bending at this point. This stems from the fact that the geometric approximation used, when the full shell is considered, introduces a "point" at the crown which can withstand the bending which a "flat" crown cannot. This

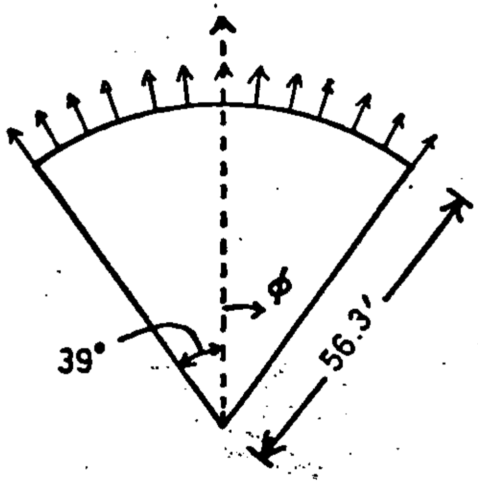

Young's Modulus = 10×10^6 p.s.i.

Poisson's Ratio = ·2

Thickness = 2·36 ins.

Normal pressure = 284 p.s.i.

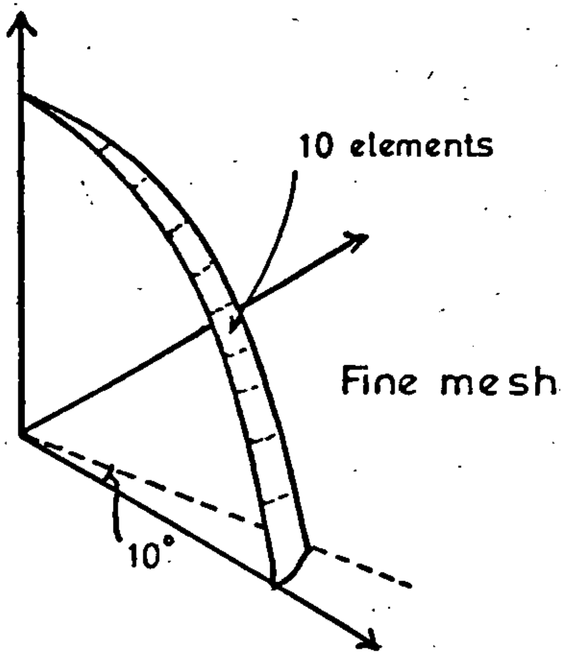

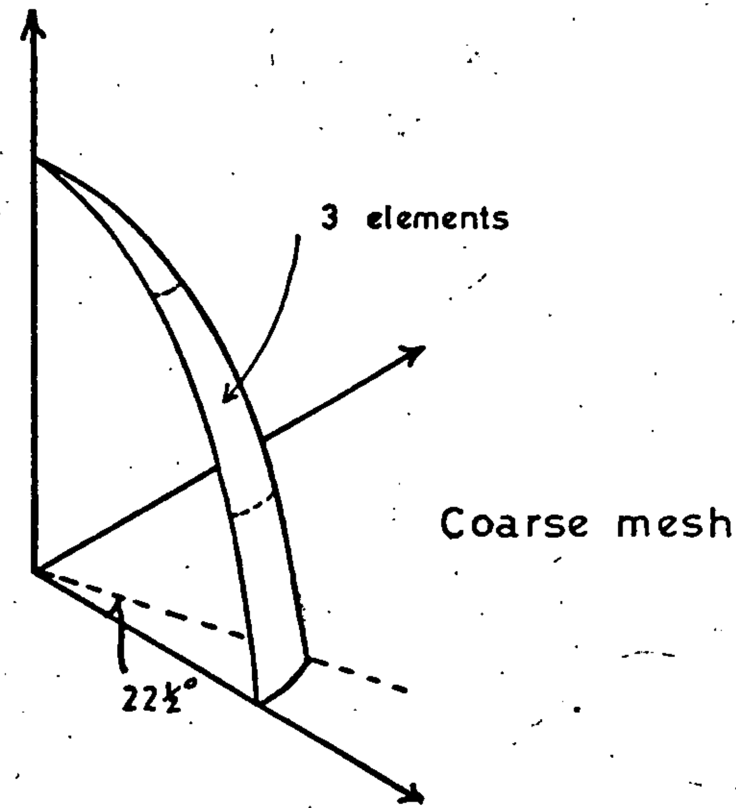

Fig. 41 Spherical cap

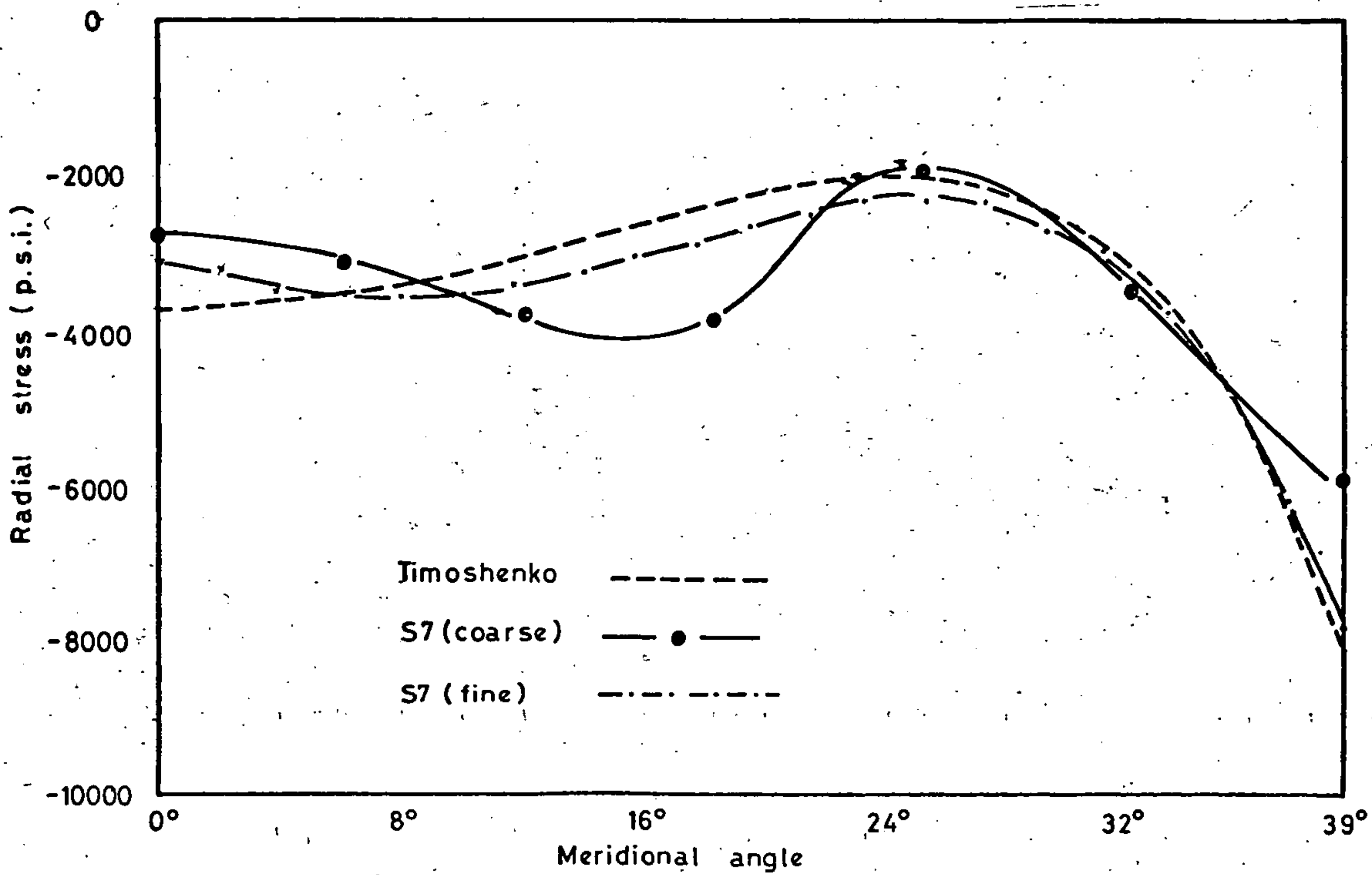

Fig. 42 Radial stress on inside of spherical cap

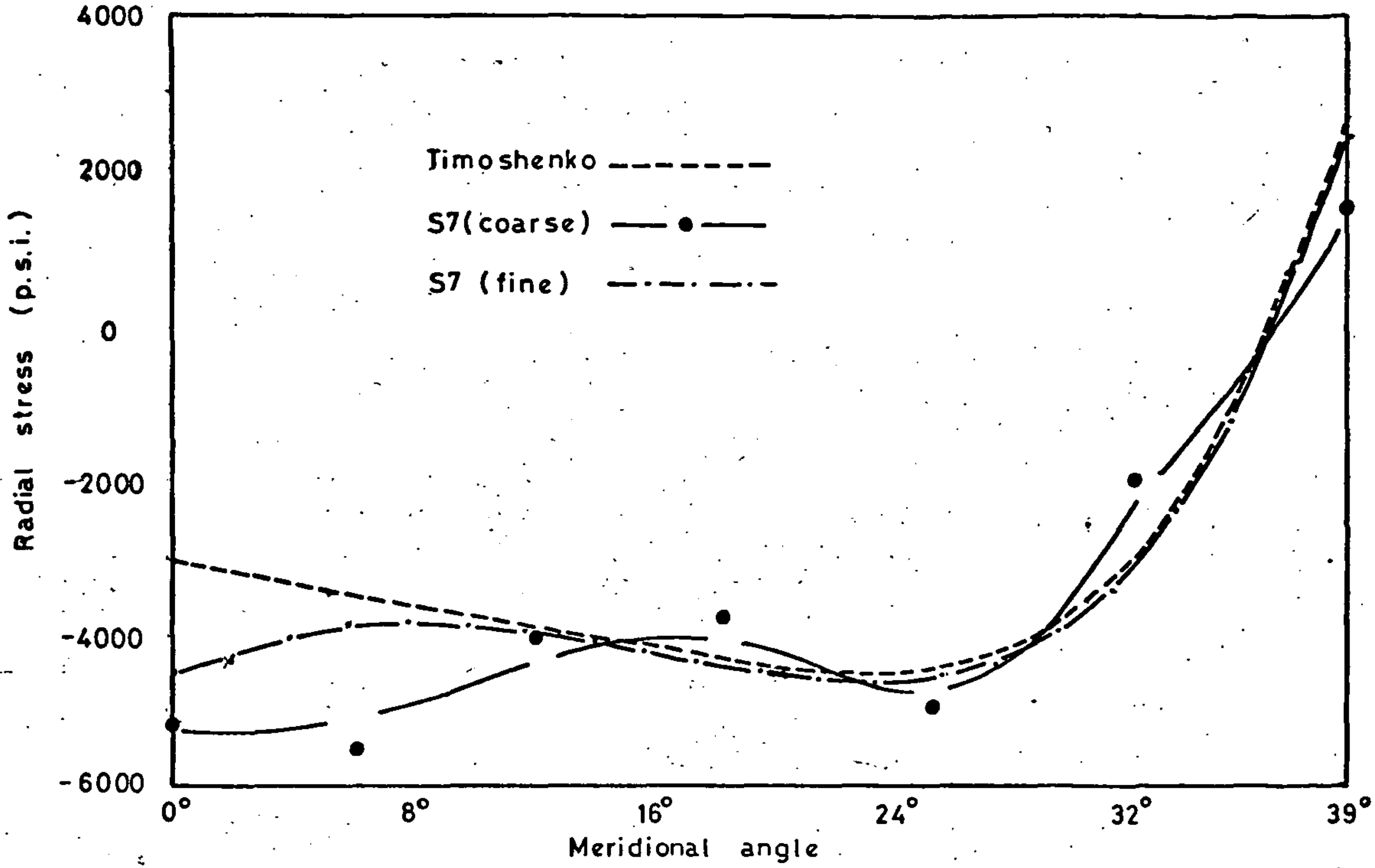

Fig. 43 Radial stress on outside of spherical cap

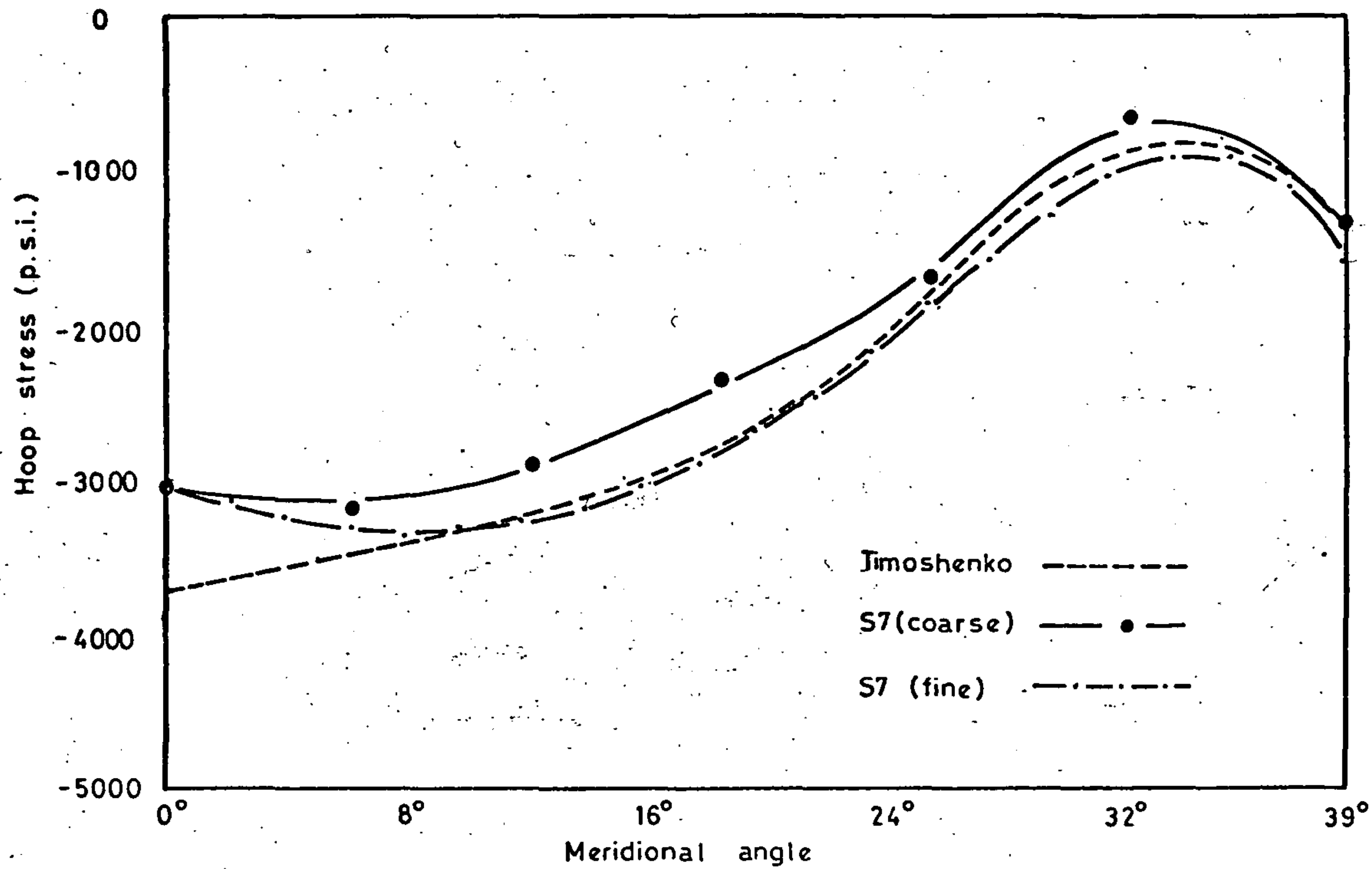

Fig. 44 Hoop stress on inside of spherical cap

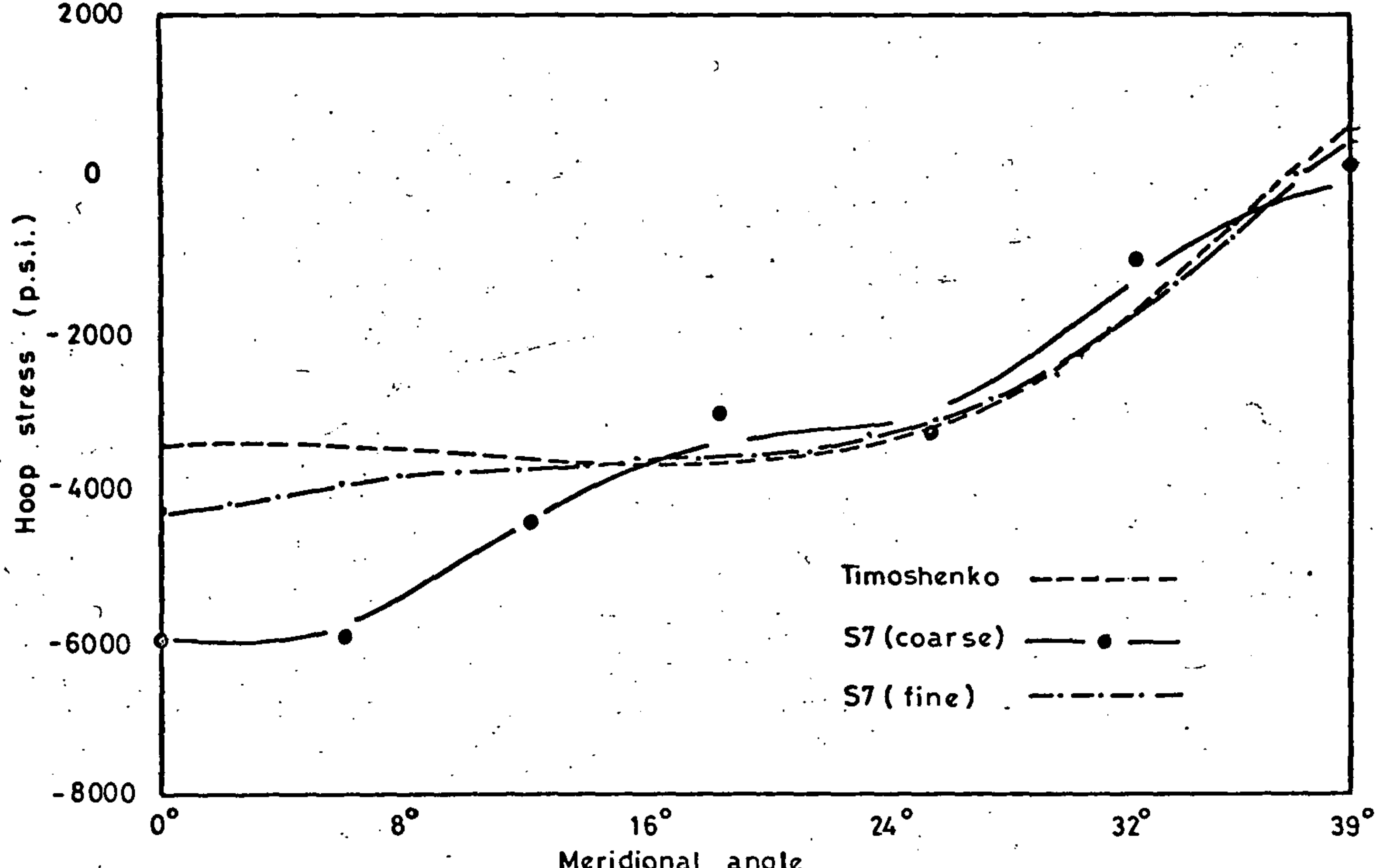

Fig. 45 Hoop stress on outside of spherical cap

error can be reduced markedly by making the topmost element small and horizontal.

The results for maximum stresses, table 13, can be compared with the solution quoted by Argyris [33] which used 200 elements but no advantage was taken of the radial symmetry of the problem. The correct maxima are, naturally, the more difficult to obtain being, for some, at a boundary. The alteration to the mesh suggested above would considerably improve these results - the error occurring at the point of maximum stress.

		Timoshenko	Argyris	S7 coarse	S7 fine
radial stress	inside	8170	7360	6404	7876
	outside	4600	4520	5637	4593
hoop stress	inside	3500	3550	5687	4593
	outside	3740	3710	5579	4372

Table 13: Maximum stresses in spherical cap

6.4 Conclusions

In this chapter, six tests have been discussed. The S7 element produced acceptable solutions to five of these. Indeed, efficient and encouraging results were obtained. In the remaining case of a simply supported box beam with diaphragms over the supports, the problems encountered were best resolved by resorting to the more sophisticated S12 element.

In all other circumstances, however, remarkably efficient solutions can be obtained with quite coarse geometric representation. (test V) The full effects of transmitting stresses around box corners are well catered for (tests I & II) and there is high numerical stability in the solution process and the element so that large and small, long and thin elements can be used in conjunction with each other (test III). In addition, if the full details of stresses in flanges, reductions in the computation can be obtained by use of beams in conjunction with elements.(test II)

Chapter Seven Thin shells and box structures analysed

7.1 Introduction

In this chapter we shall consider some practical problems selected to cover a wide range of engineering applications to confirm the abilities of the S7 element. No such wide ranging collection of problems has been found in the literature and so this collection could form the basis on which to test any further elements which might be developed.

In all cases the mesh was chosen to be the minimum feasible for practical use. An increase in the number of elements would produce an improvement in the results quoted in this thesis.

These examples are divided into two sections and within each the complexity increases from that examined in chapter six. The first section contains those problems which have previously been categorised as shells. These problems may be solved by elements which ignore the transmission of in-plane rotations from one element to another as a bending rotation. This is not serious if the adjacent elements meet at a sufficiently small angle and the mesh is fine. These elements have been used with some success in such situations but are not of any use where the angle between elements is significant, such as at a corner of a box.

The second category contains those problems for which the type of element mentioned in the previous paragraph are not applicable i.e. box-like structures. This is the type of problem to which this study makes a particular contribution.

7.2 Cylindrical shell with dead load

This problem has already been solved by finite elements, but these have been relatively elementary. It is important that any more developed element should provide an adequate solution, preferably with a coarser mesh.

Being doubly symmetric (see fig. 46) only a quarter need be considered and here a 4 x 4 mesh was used. The basic tests in Chapter Six indicate that this should be adequate.

The shell is loaded by its own dead weight and supported by rigid diaphragms at either end, but free along the sides. The diaphragms were rigid only in their own plane and infinitely flexible in bending. The results from the S7 shell element are compared with a solution by Clough & Johnson[34] using a mesh 16 x 22. They also quote an "exact" solution of the Donnell-Jenkins shell equation which is barely distinguishable from the finite element solution

It can be seen from figs. 47 & 48 that the displacement solutions agree quite well and the stresses, figs. 49 & 50, moderately well. The greatest discrepancy occurs along the free edge where such errors, whilst not large, might be expected.(Values at boundary nodes do not possess the same advantage of nodel averaging or interpolation as internal nodes.) In addition, of course, the loading by point loads only contribute an error at the edge as a result of ignoring moment resultants. The ease with which such loads can be imposed must be balanced against the penalty of introducing innaccuracies; the former may often be felt to be the more important.

Young's Modulus = 3×10^6 p.s.i.

Poisson's Ratio = 0

Thickness = 3 ins.

Dead Load = 90 p.s.i.

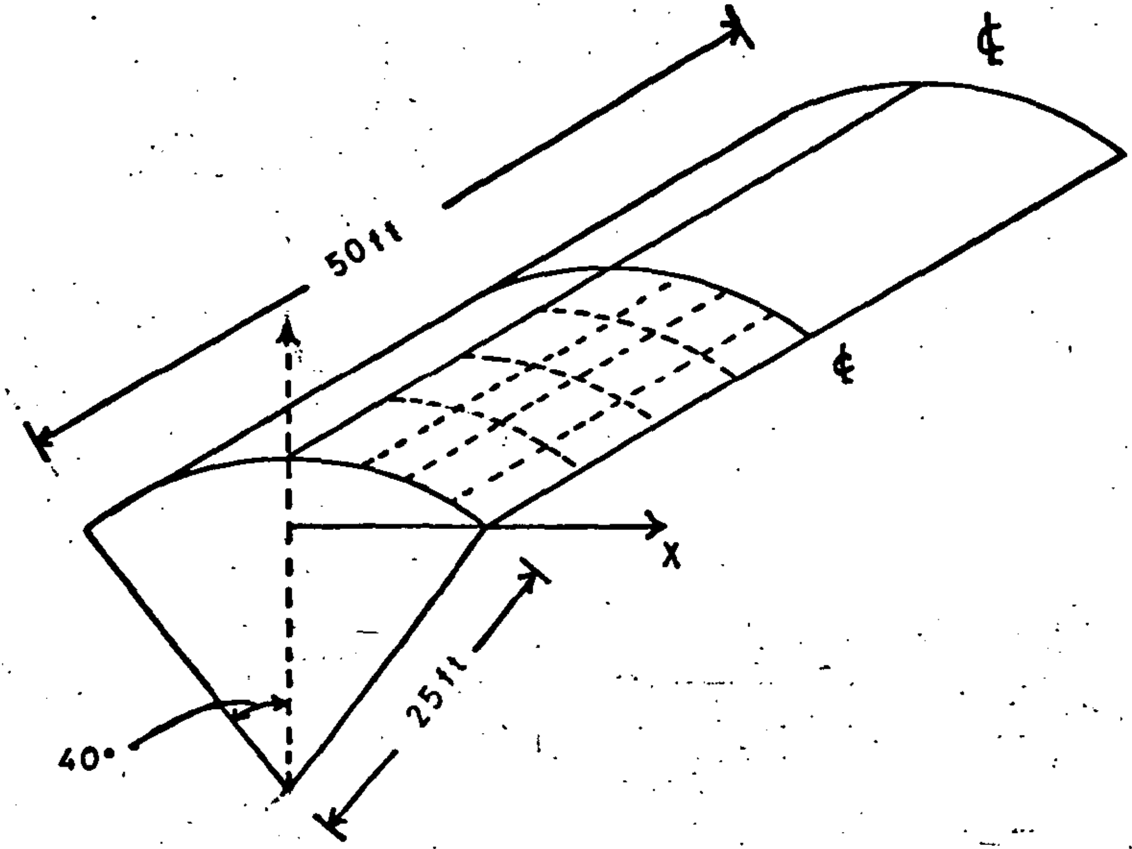

Fig.46 Cylindrical shell under dead load.

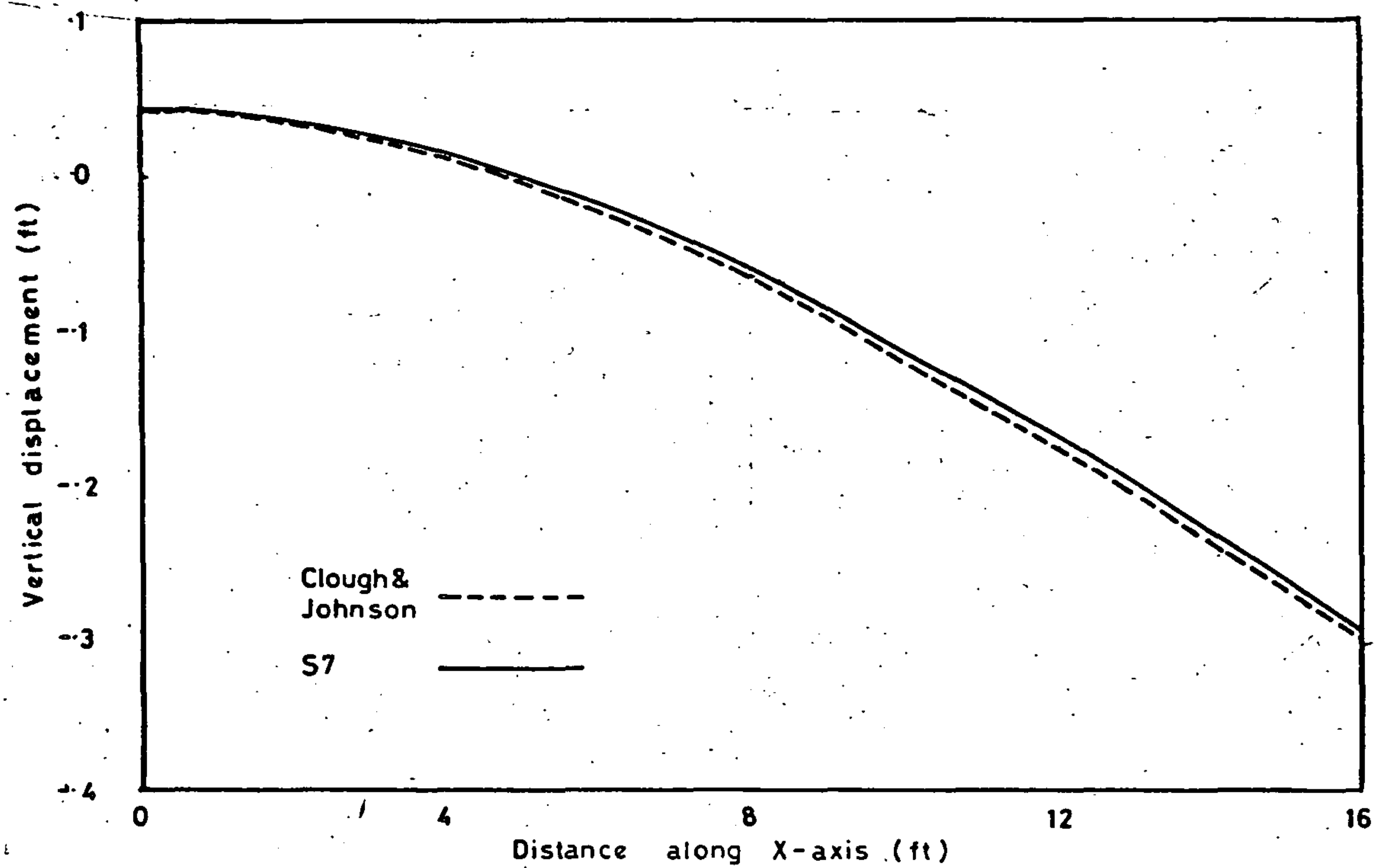

Fig. 47 Vertical displacement of centre section

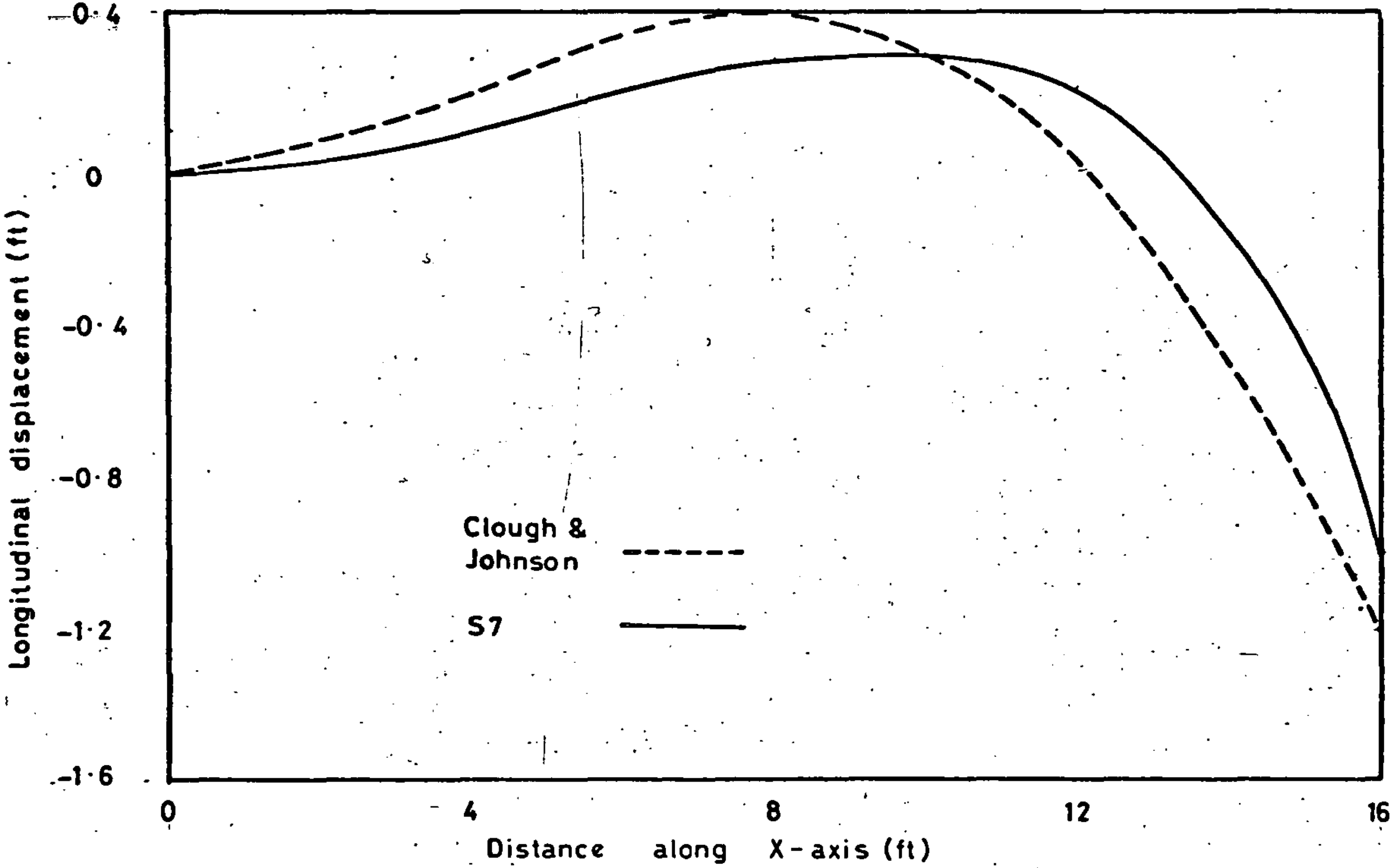

Fig.48 Longitudinal displacement at diaphragm

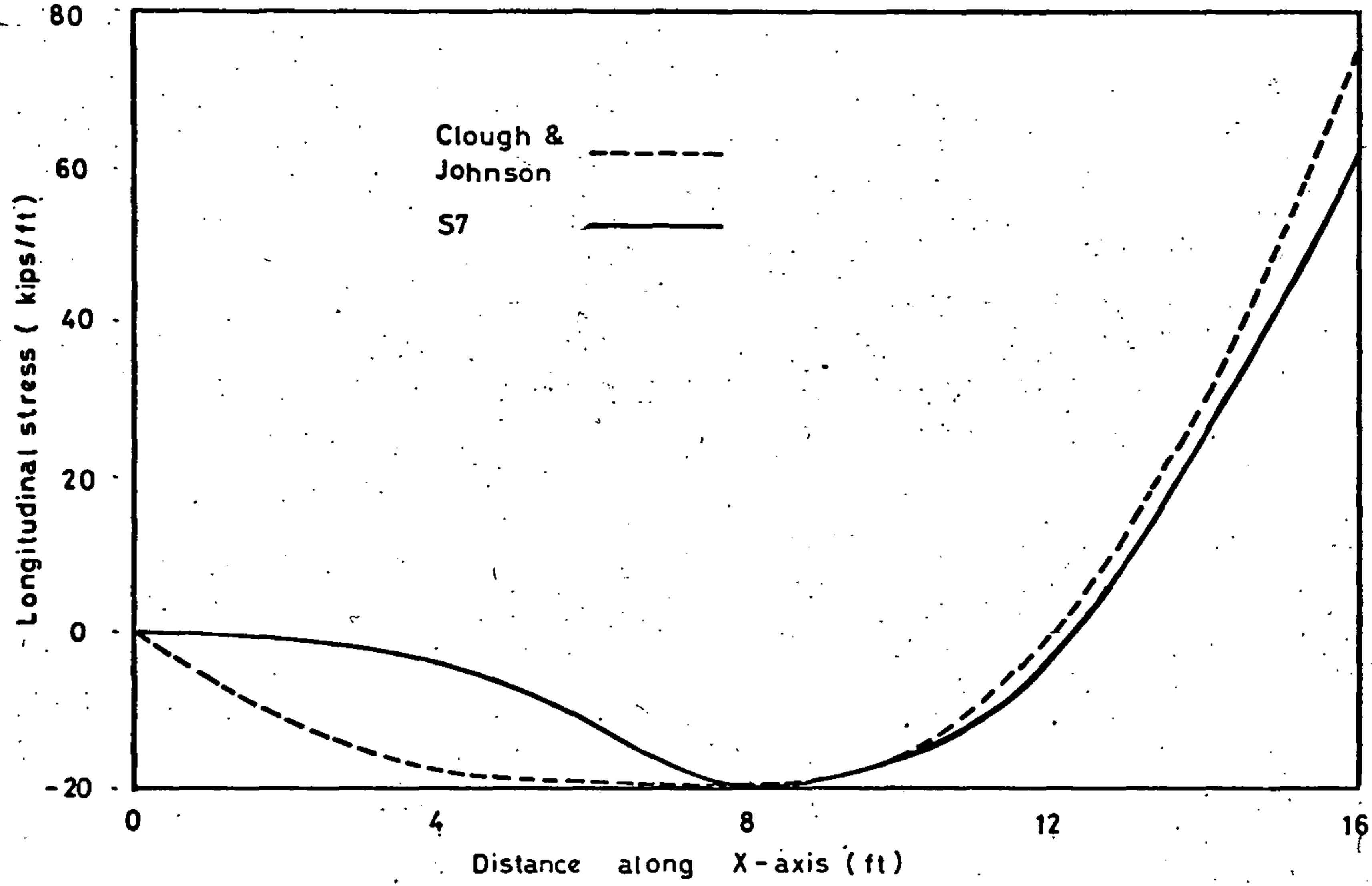

Fig.49 Longitudinal stress at centre section

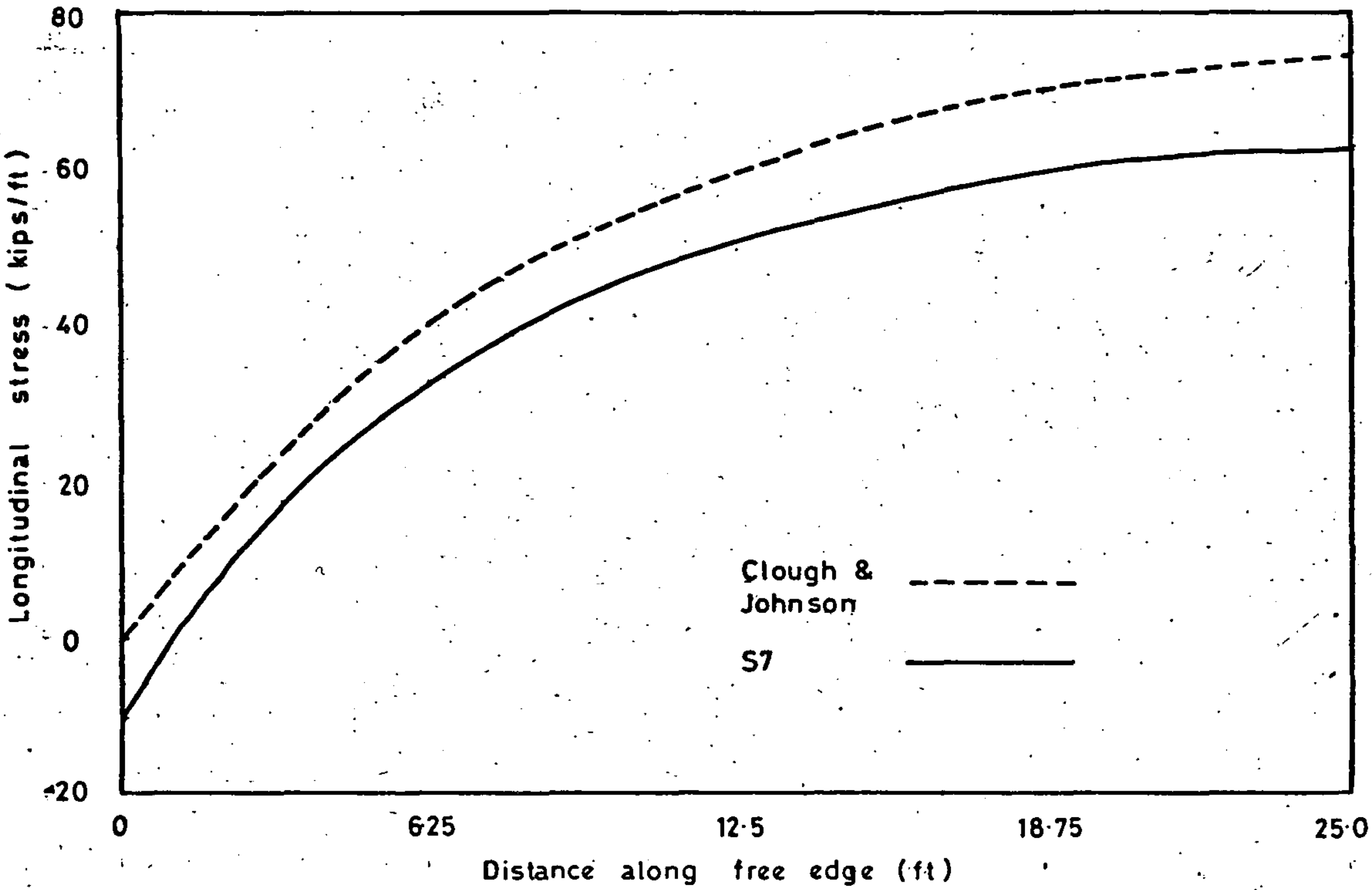

Fig.50 Longitudinal stress along free edge

7.3 Arch dams

The calculation of stresses in arch dams is one which has received much attention by the profession in recent years. Several methods of analysis have been compared[35][36] and, in general, the finite element technique appears to be the most accurate and adaptable in a wide range of situations. It cannot be hoped that, in view of the specialised attention the problem has received, this new element will provide cheaper or more exact solutions. However, it is advantageous if the same element that is capable of solving very different problems can also perform adequately here.

The pressure loading facility of the Loughborough program is capable of the calculation of a hydrostatic load but on the following simple basis. The depth of the centroid of each element is calculated and hence, from the height of the surface of the liquid given in the data, the pressure at this point obtained. The total force on the element, provided it is below the water level, is calculated assuming that this pressure is constant over the whole element. This force is then applied in equal parts to all the nodes of the element in the appropriate normal direction.

7.3.1 Arch dam 1

The first dam to be considered (see fig.51) was used by Hansteen[37] to demonstrate a finite difference technique. The same dam was also solved using finite elements by Holand & Åldstadt[38] with a fine mesh of triangles, 11 x 9 (i.e. 180 elements) - these are the results quoted. A later finite element solution by Megard[39]

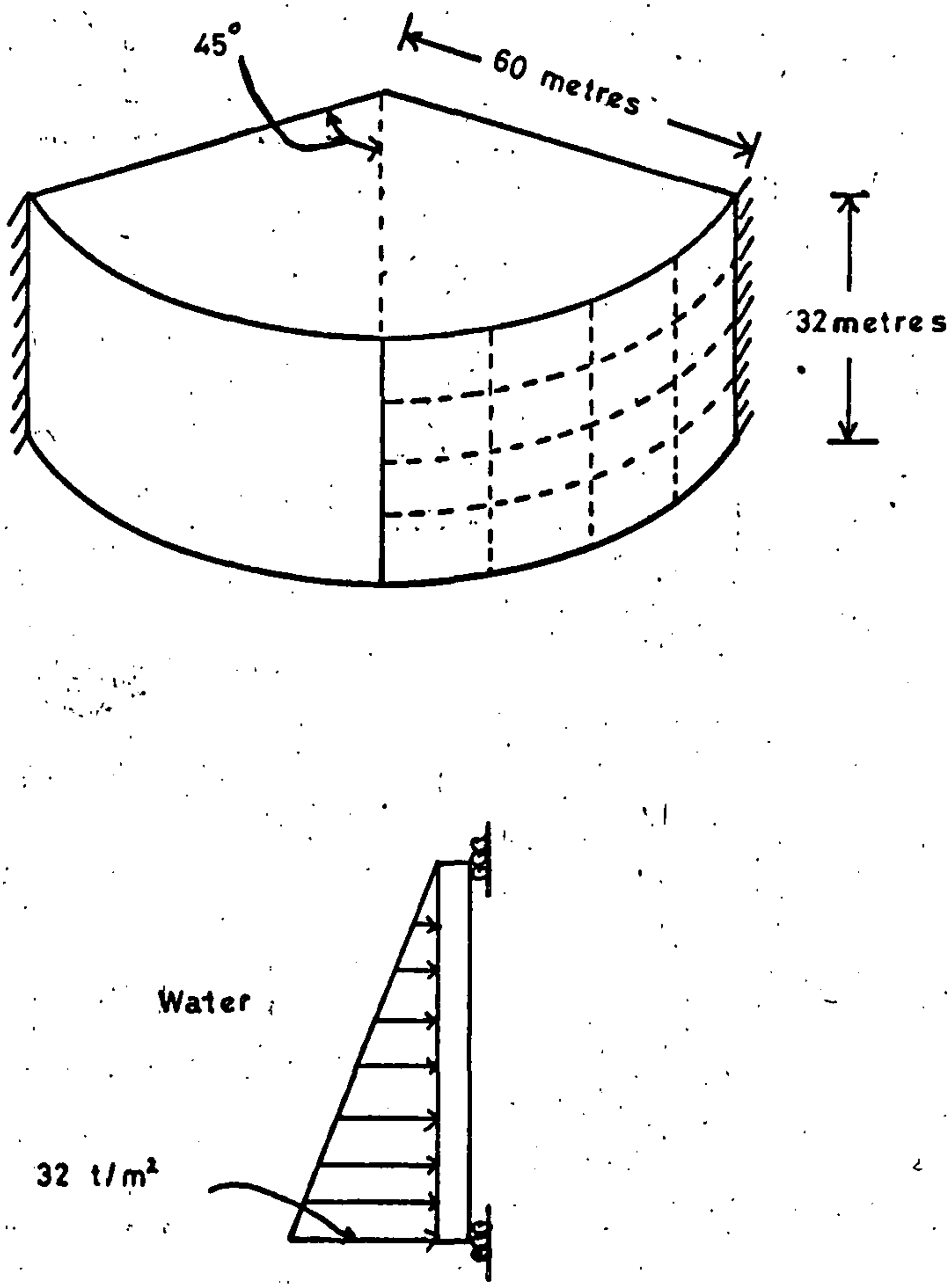

Young's Modulus = 2×10^6 p.s.i.

Poisson's Ratio = ·2

Thickness = 2·4 metres

Fig. 51 Idealised dam (No. 1)

of the same dam used only 6 x 4 rectangular elements, both plane and curved. All three of these solutions are essentially the same. The mesh employed for the S7 shell solution used 4 x 4 plane rectanglar elements. The results, shown in figs. 52 - 55, indicate a generally correct solution. Although the method of representing the hydrostatic loads gives the correct resultant force for this regular mesh, it is erroneous in its distribution, particularly at the boundaries. As a consequence we find that the moments, figs. 54 & 55, are much better than the deflections and forces, figs. 52 & 53. For a greater accuracy a finer mesh should be used. In contrast with the cylinder under uniform pressure or point loads, a greater degree of geometrical accuracy is required for a similar stress accuracy. (For further discussion of this see section 7.5)

7.3.2 Arch dam 2

The second, somewhat more realistic, dam was first analysed by Zienkiewicz[36] but then taken as the design type 1 for the Inst. of Civil Engineers' review of techniques for arch dam analysis.[35] The mesh used (see fig.56) here is substantially the same as that by Zienkiewicz except that the sloping boundary is represented exactly by extra triangles rather than an approximate step boundary. This in itself will introduce some differences in addition to other approximations.

The solutions as presented in figs. 57 - 59 differ from Zienkiewicz's solution by a similar quantity as other solutions presented in [35]. There is no "exact" solution with which to make a comparison. In the absence of such an arbiter, the S7 solution may be considered acceptable.

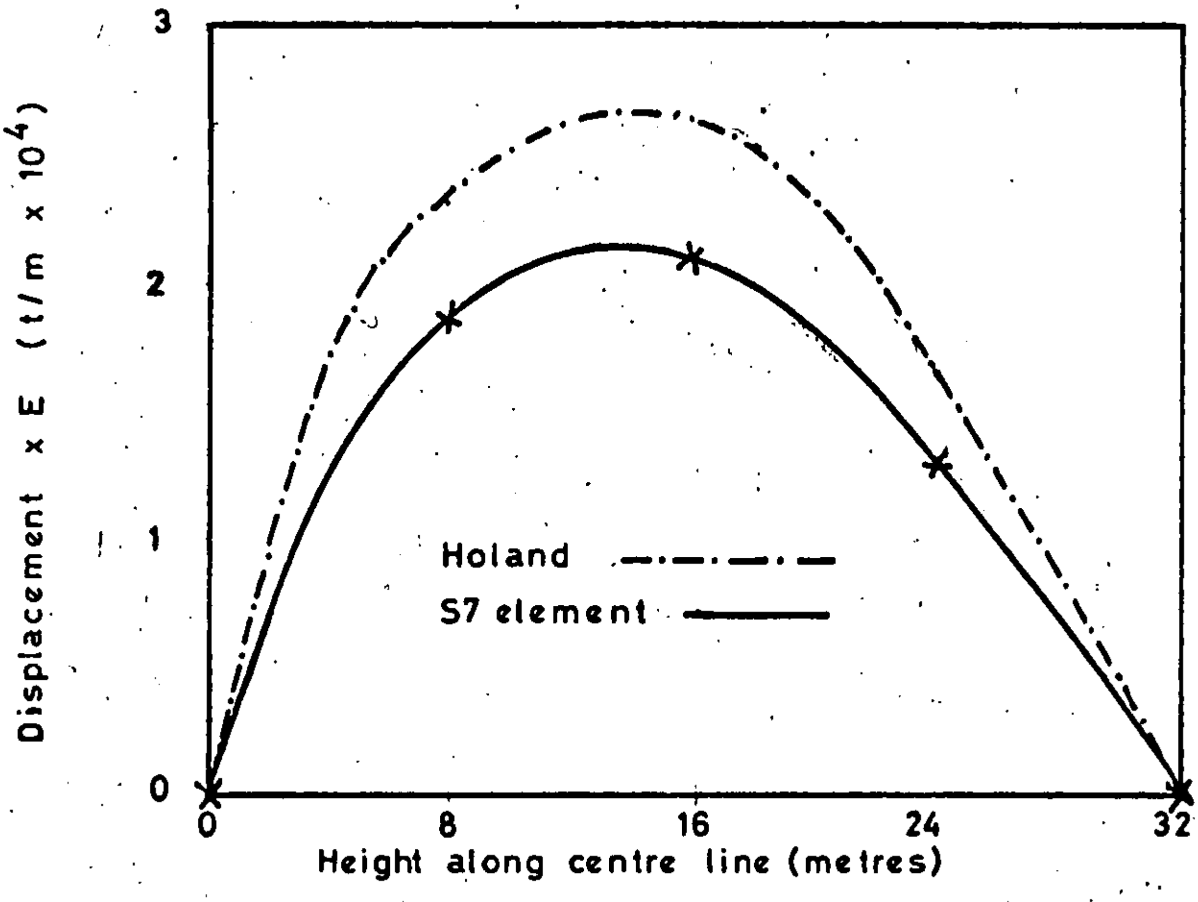

Fig. 52 Displacement of centre line outwards

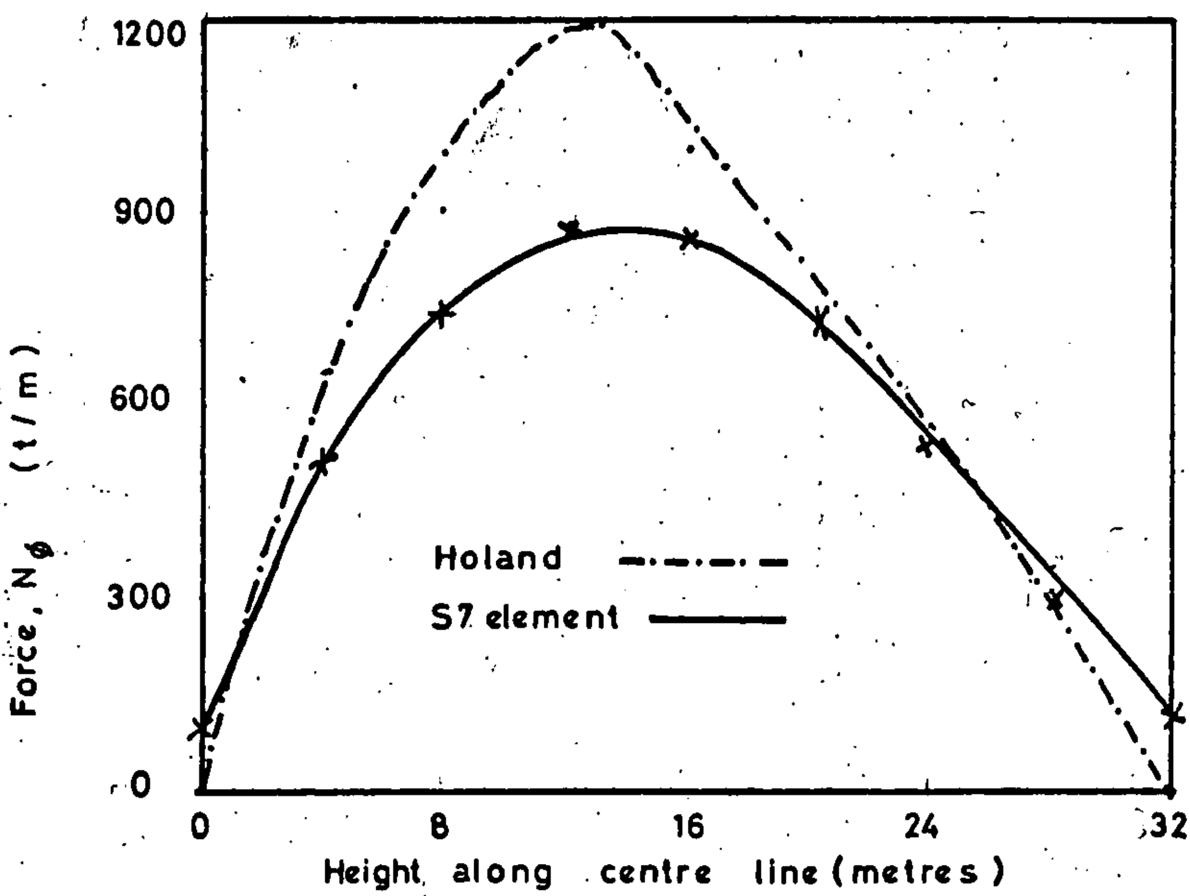

Fig. 53 Force N_ϕ along centre line

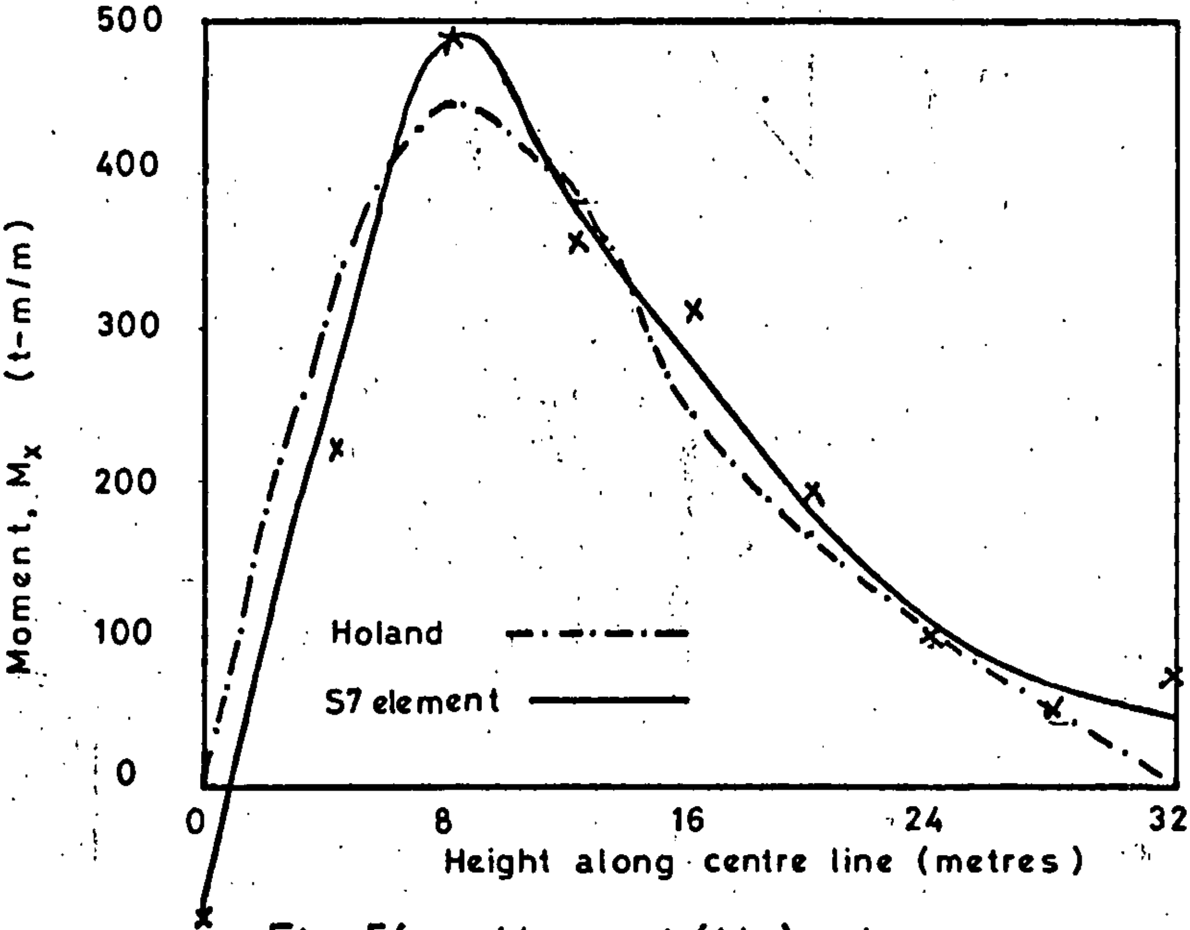

Fig. 54 Moment (M_x) along centre line

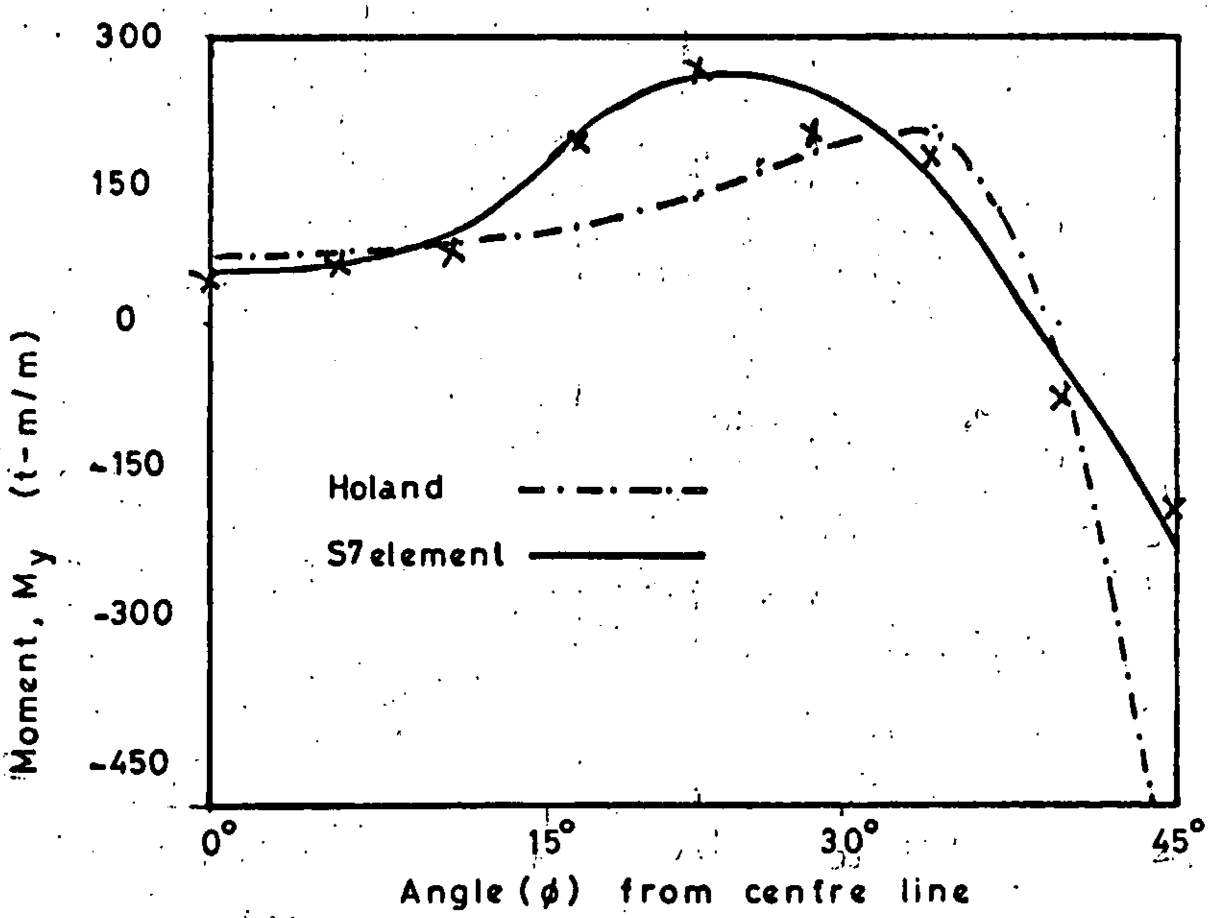

Fig. 55 Moment (M_y) at height 26·25 metres

water level

Young's Modulus = 2×10^{6} kg/ m^2

Poisson's Ratio = ·15

Thickness = 3 metres

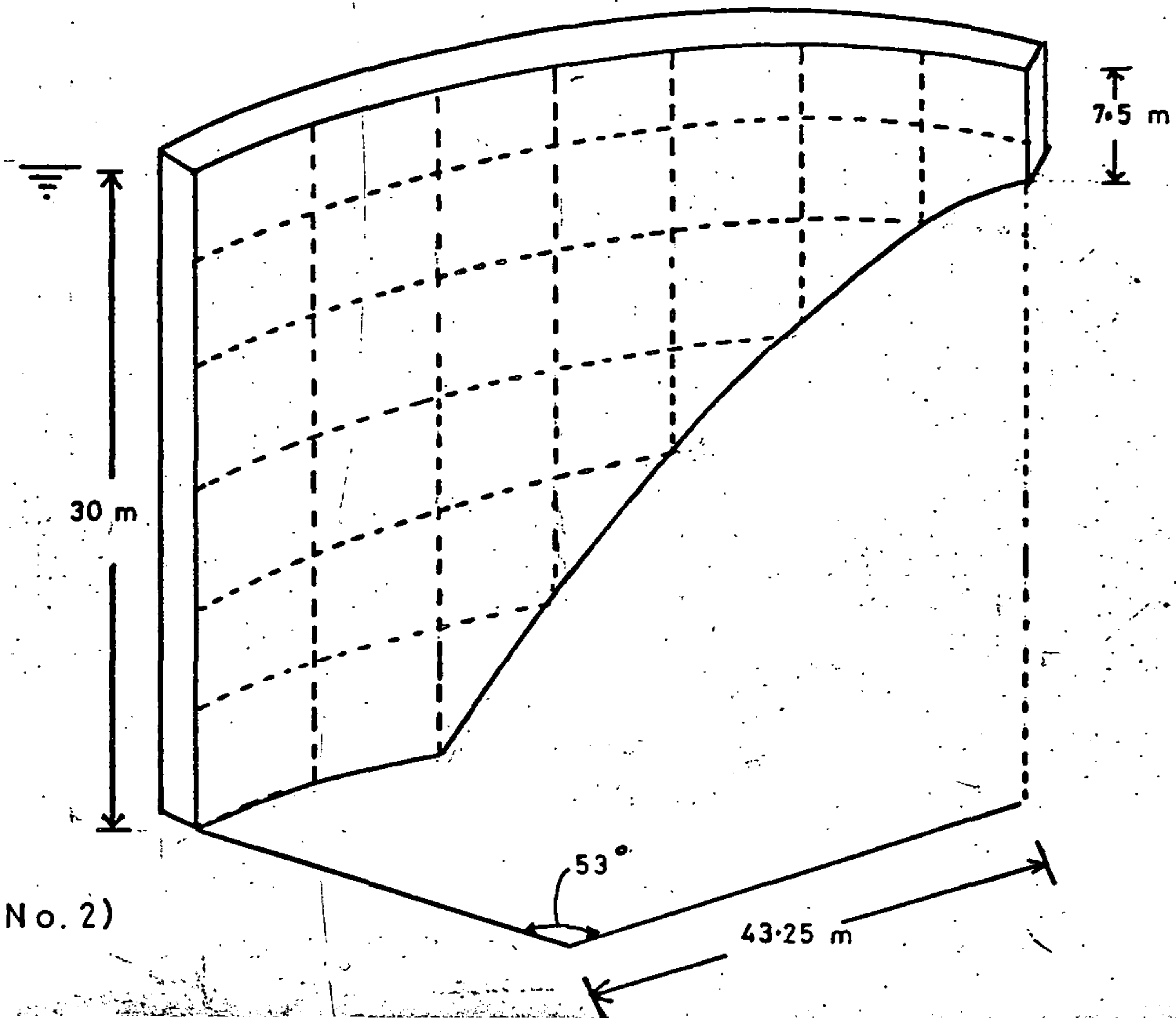

Fig. 56 Arch dam (No. 2)

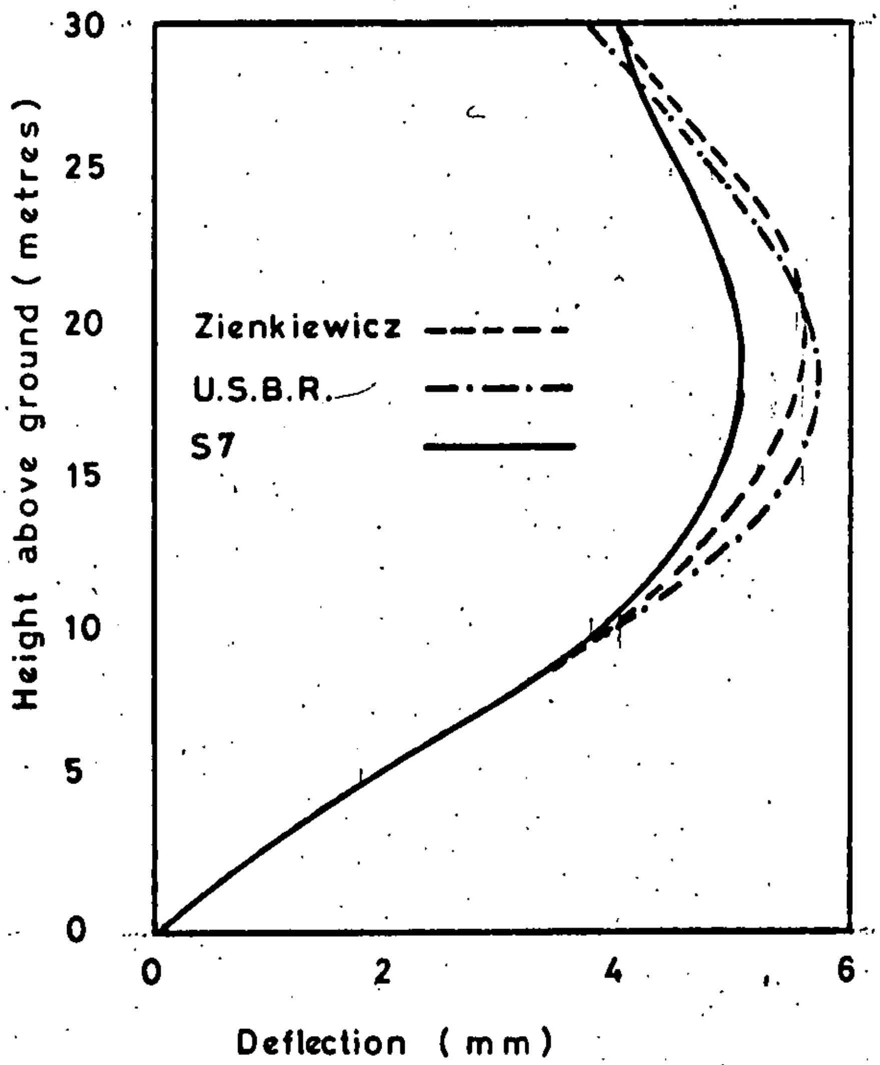

Fig. 57 Radial deflection of centre line of arch dam no. 2

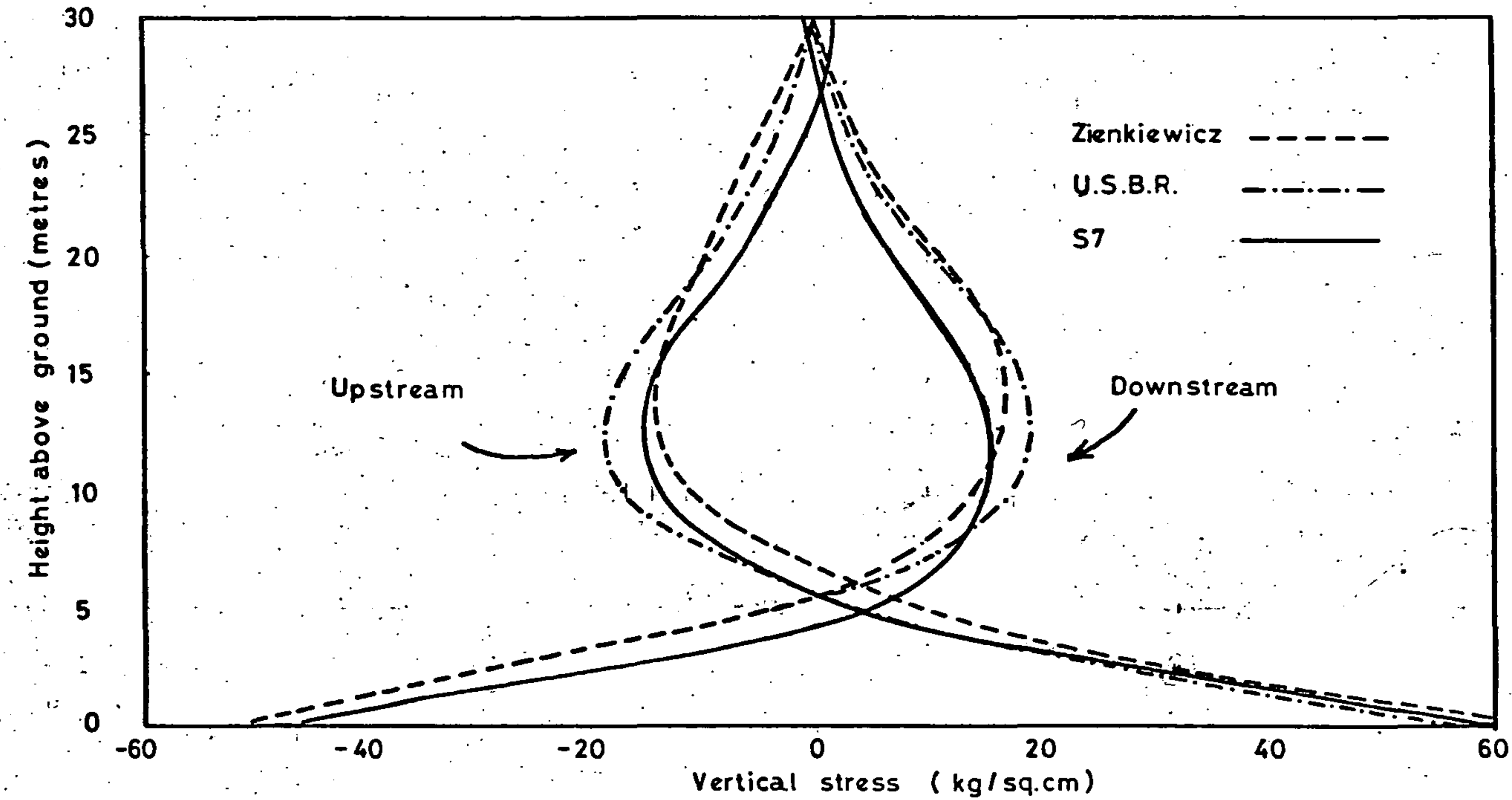

Fig. 58 Vertical stresses along centre line of arch dam no. 2

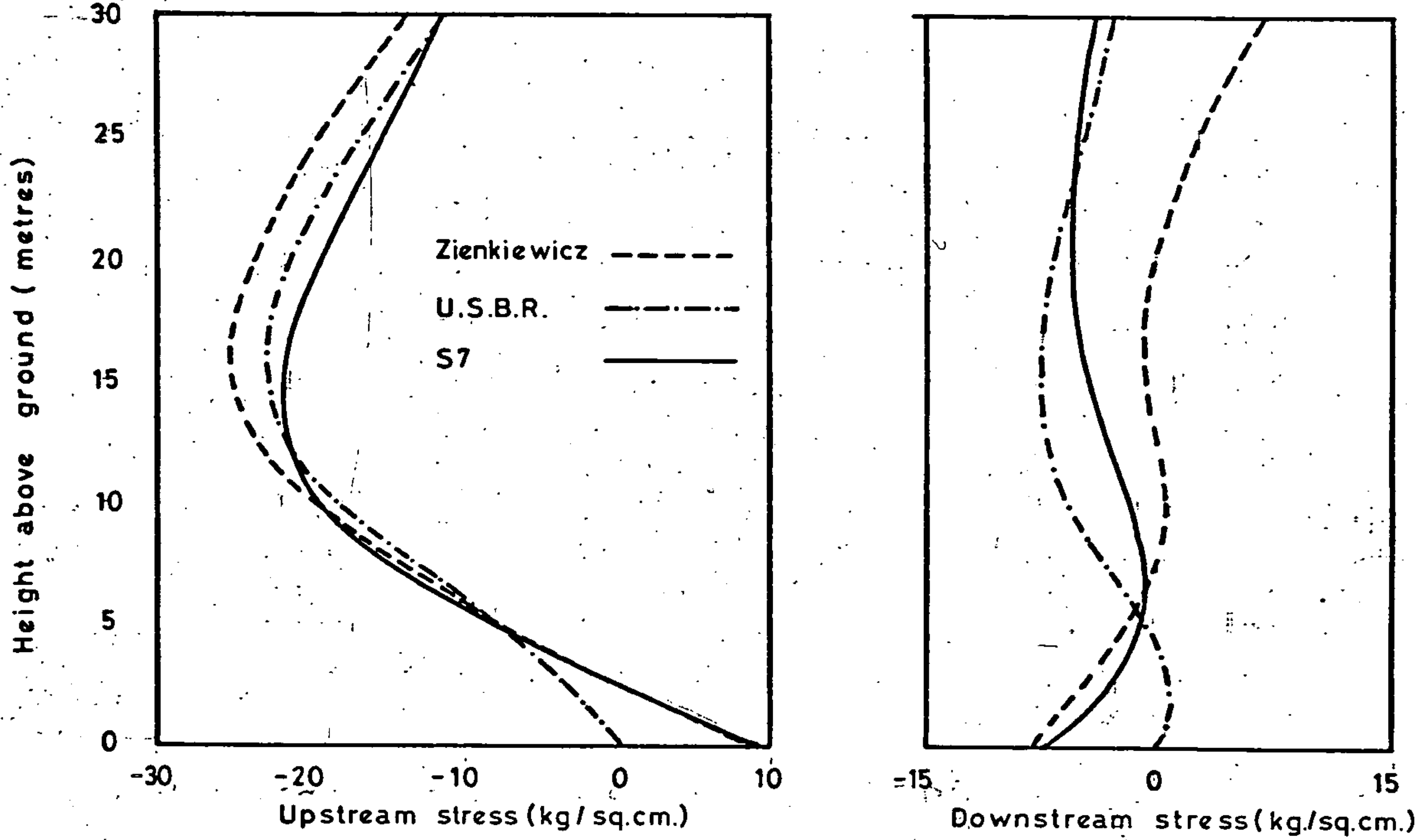

Fig. 59 Hoop stresses along centre line of arch dam no. 2

7.4 Cylindrical shells with edge beams

Tables of stresses in a range of practical cylindrical shells with edge beams rigidly supported at the ends of the beams have been produced by Gibson.[40] Two typical shells were selcted for a comparison with the finite element method: one, fig.60, a multishell of fairly large longitudinal span, the other, fig. 62, a single shell much shorter in comparison. In both cases a uniform vertical load of 56 lb/sq.ft.was applied to the shell surfaces and the corresponding dead+live load to the beams.

For the first case, the finite element analysis was carried out for the symmetric half of a three span roof and the results for the transverse bending moment across the centre line are shown in fig. 61. These compare quite closely with those of Gibson except near the edge beams where the finite elements may have difficulty in providing the correct representation.

For the second shell, two finite element analyses were used. One represented the edge beams by finite elements and the other by beams eccentrically placed to the main shell. The results are shown in figs. 63 - 65. Thec principle discrepancy between the finite element and Gibson's results is in the transverse bending moment at the crown of the centre line (fig. 65) where the latter results give zero but both the finite element results are distinctly non-zero.

The main point to notice is that the multi-shell roof has a much larger length/depth ratio than this single shell roof and we already know that S7 (and GEN4) has difficulty in representing the shear in problems where this is significant. It is quite possible that the differences in

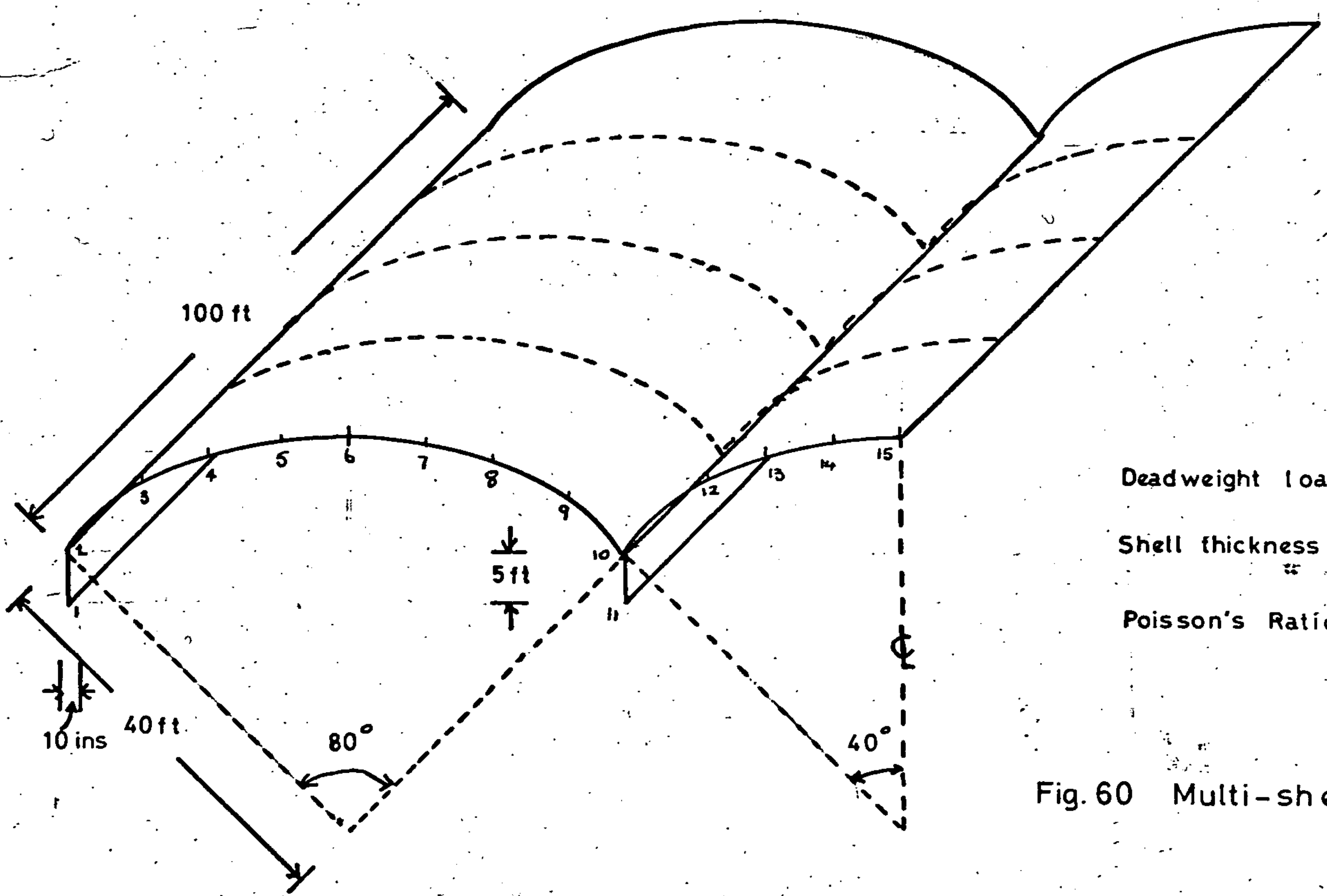

Deadweight load = 56 lb/sq.ft.

Shell thickness = ·3 ins

Poisson's Ratio = ·3

Fig. 60 Multi-shell roof

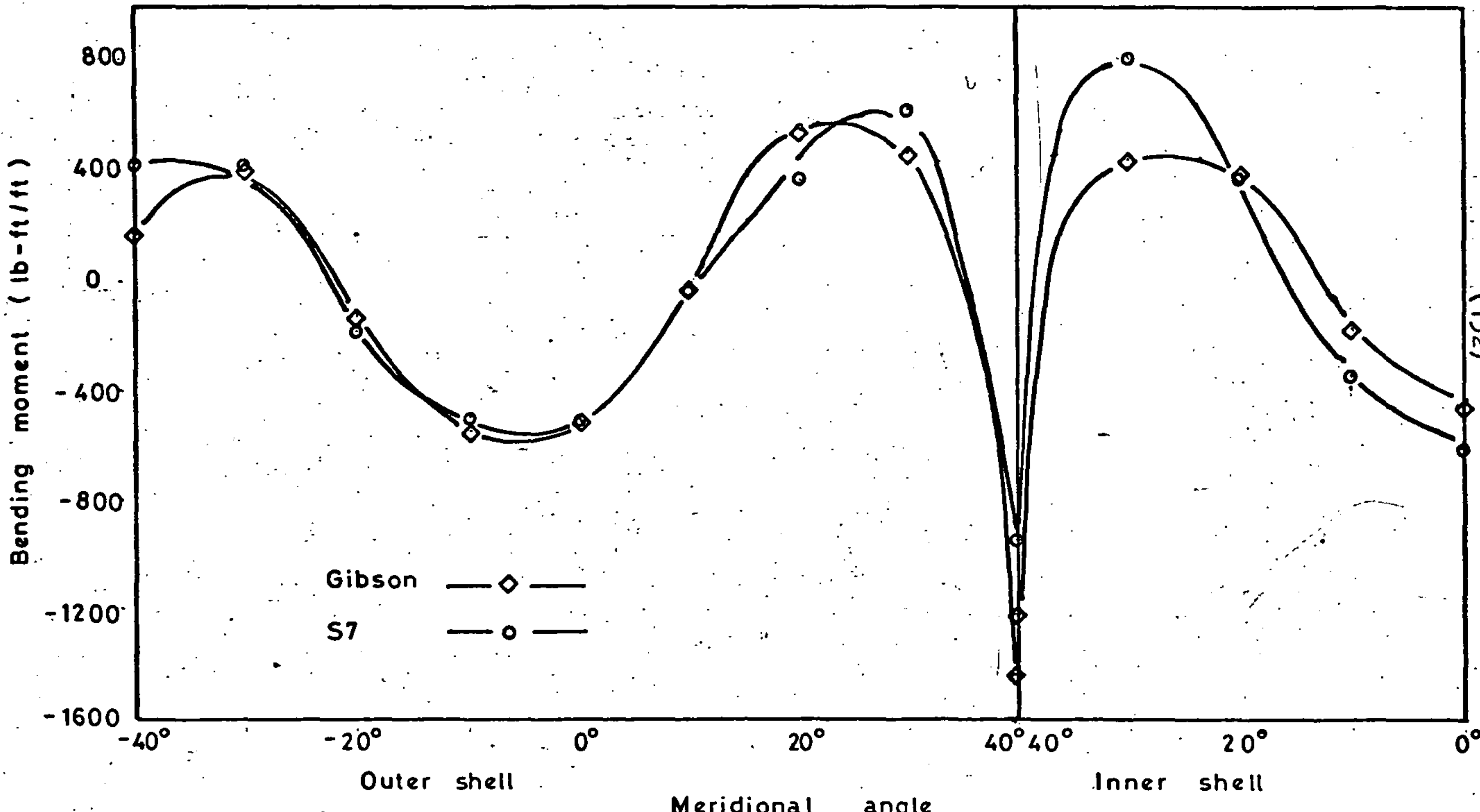

Fig. 61 Bending moment across centre section

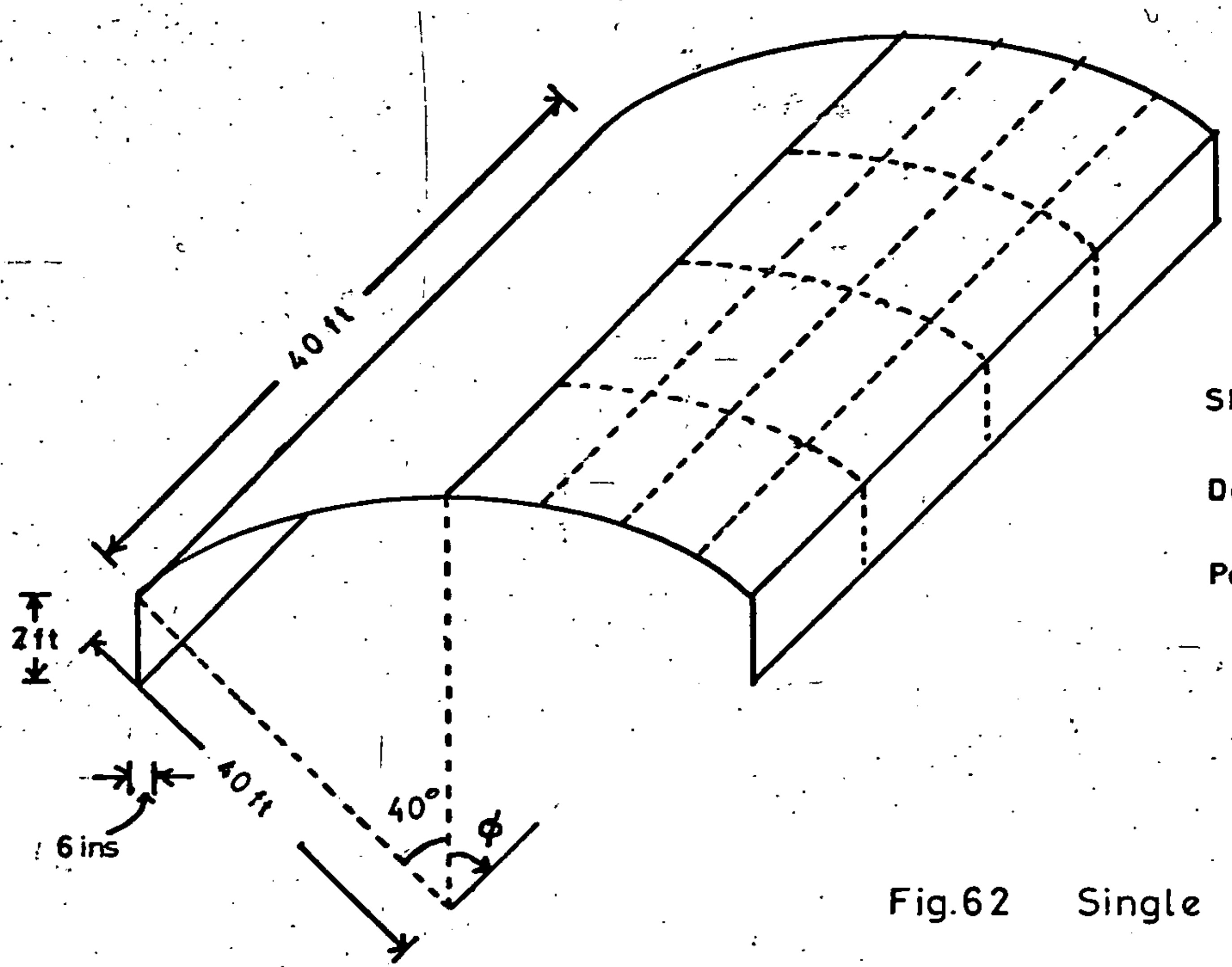

Shell thickness = 3 ins

Dead weight = 56 lb/sq.ft.

Poisson's Ratio = .3

Fig.62 Single shell cylindrical roof

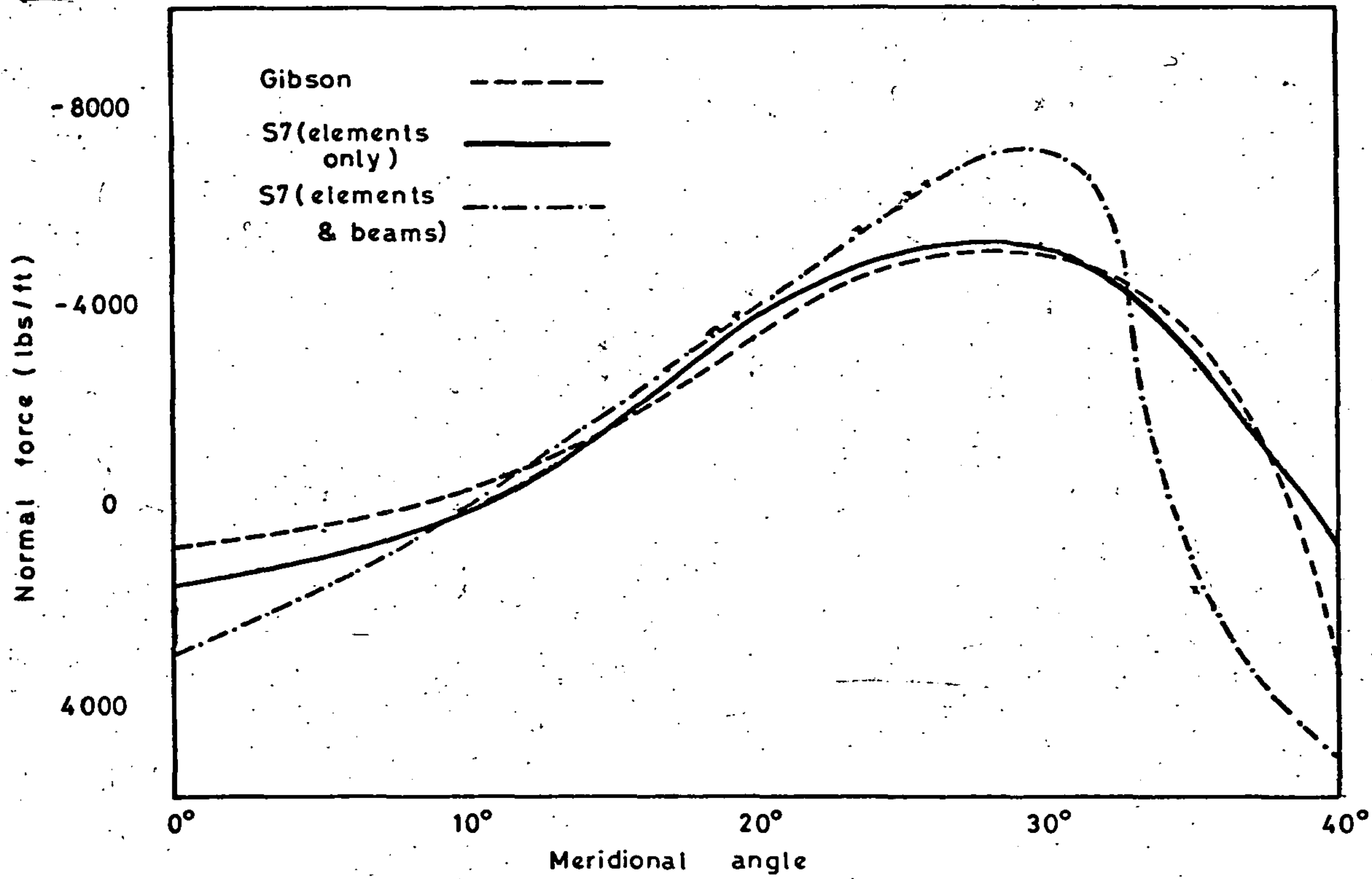

Fig.63 Longitudinal normal force across centre section (single shell)

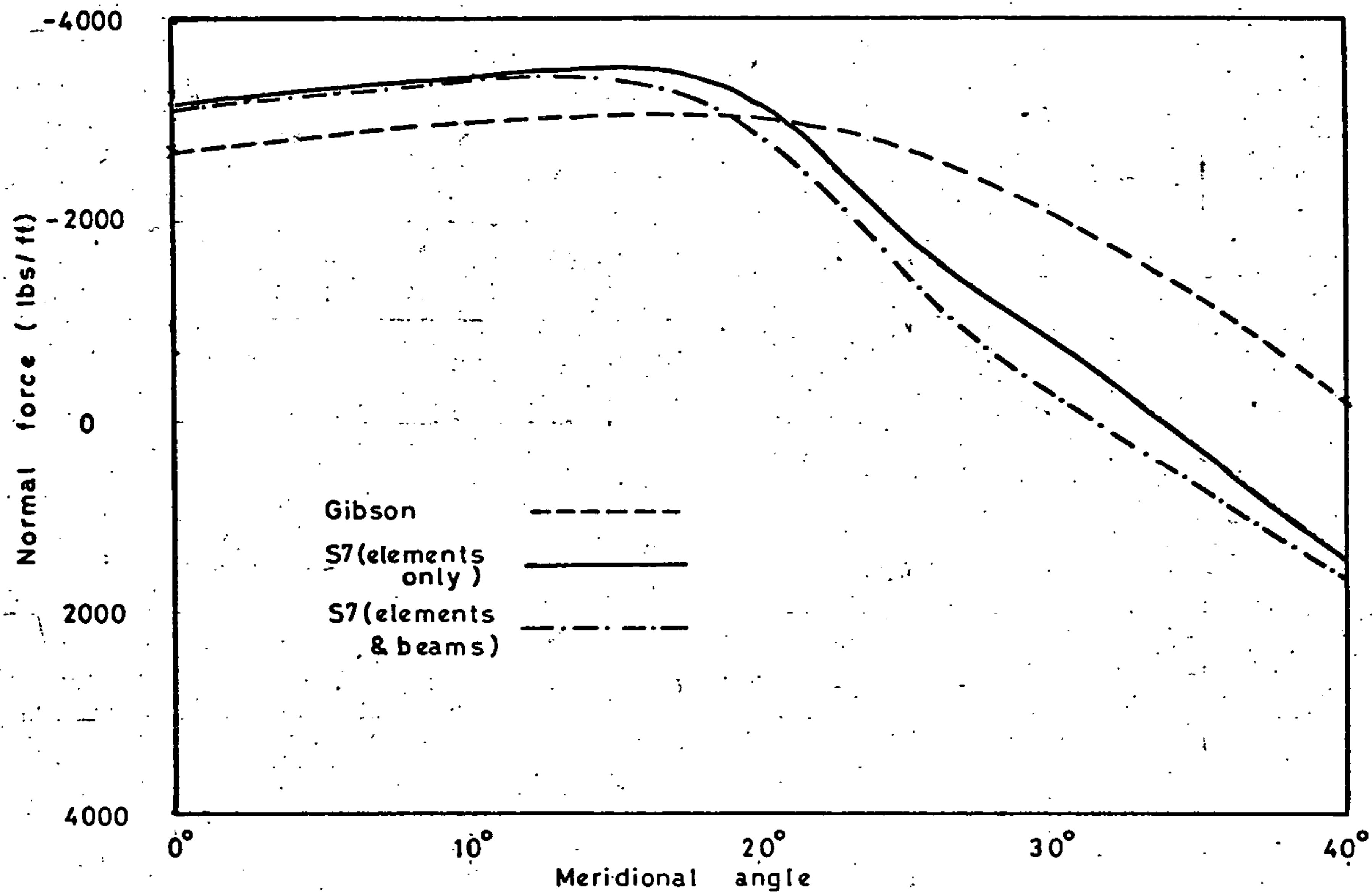

Fig.64 Transverse normal force across centre section (single shell)

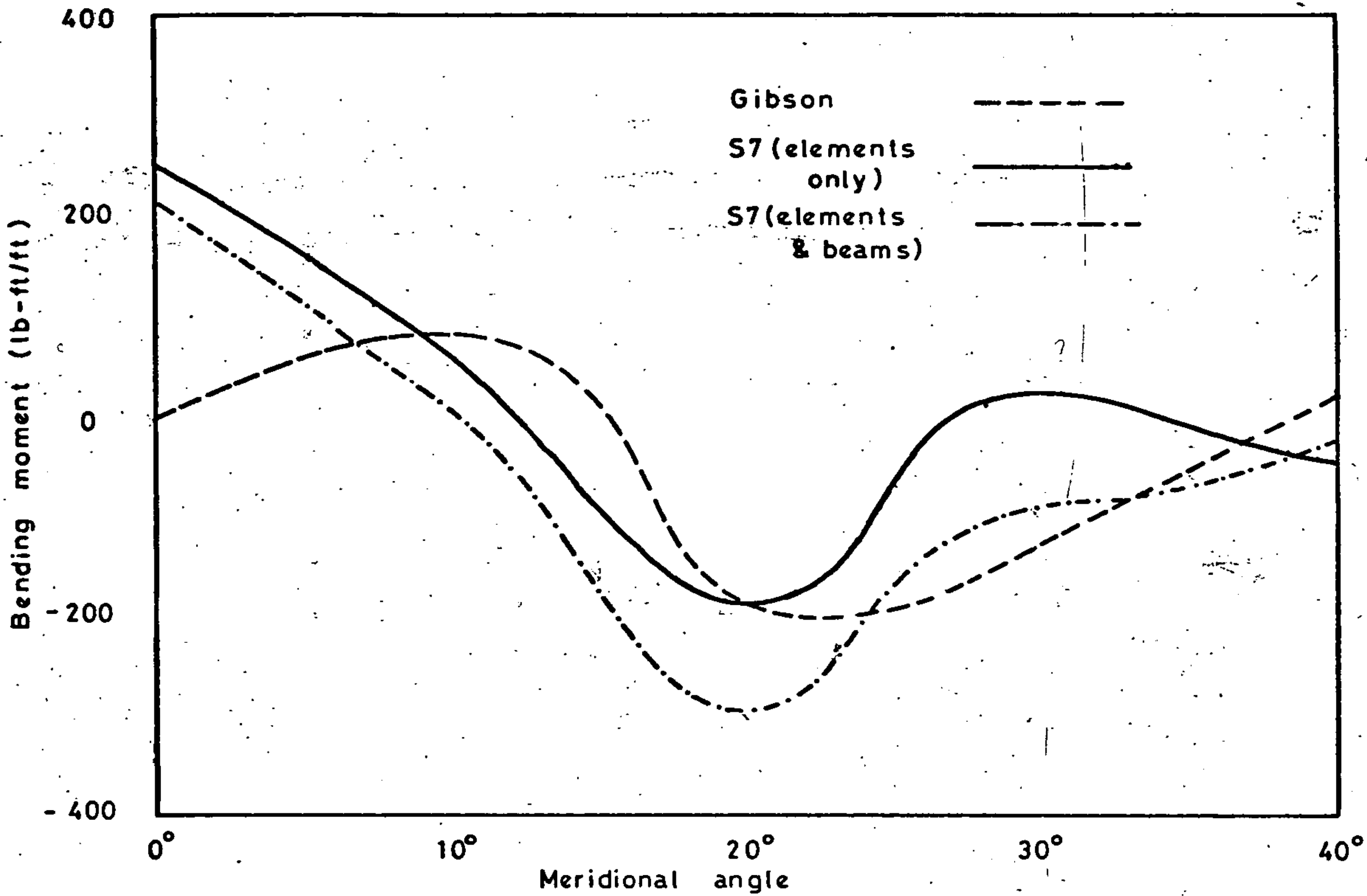

Fig.65 Transverse bending moment across centre section

the results are due to this.

7.5 Rectangular tank filled with liquid

We now turn to the solution of problems in which structural elements meet at angles too large to be ignored, in particular those meeting at right angles.

The first problem to be considered is a simple shell problem involving a distinct "corner" in the shell. The tank is made of uniform thickness material, rigidly constrained at the base and filled with water. Because of symmetry only a quarter of the original problem need be analysed here. Two meshes are compared in order to assess the degree of subdivision required for a given degree of accuracy in the results. The pressure loading due to the water was calculated using the crude facilities available and, although quite adequate for the fine mesh, does introduce some errors for the coarse mesh. In particular, the load at the upper free edges is too large - resulting in an increase in deflection. The use of accurately calculated loads would improve this solution. Nevertheless, the cruder results are shown here in order to demonstrate what may be achieved by elementary techniques and meshes.

The problem and meshes are shown in fig.66 and the results compared in figs. 67 & 68 with an experimental result and another finite element solution by Cheung & Davies.[41] As a comparison, the value of deflection outwards at the top of the centre line in the longer side (fig.67) can be estimated using the solution by Timoshenko[32] for a plate fully restrained on three sides and loaded hydrostartically. The value obtained from this is 1.1×10^{-2} which is close to that determined for the complete tank by the finite elements. (1.2×10^{-2}) The corresponding

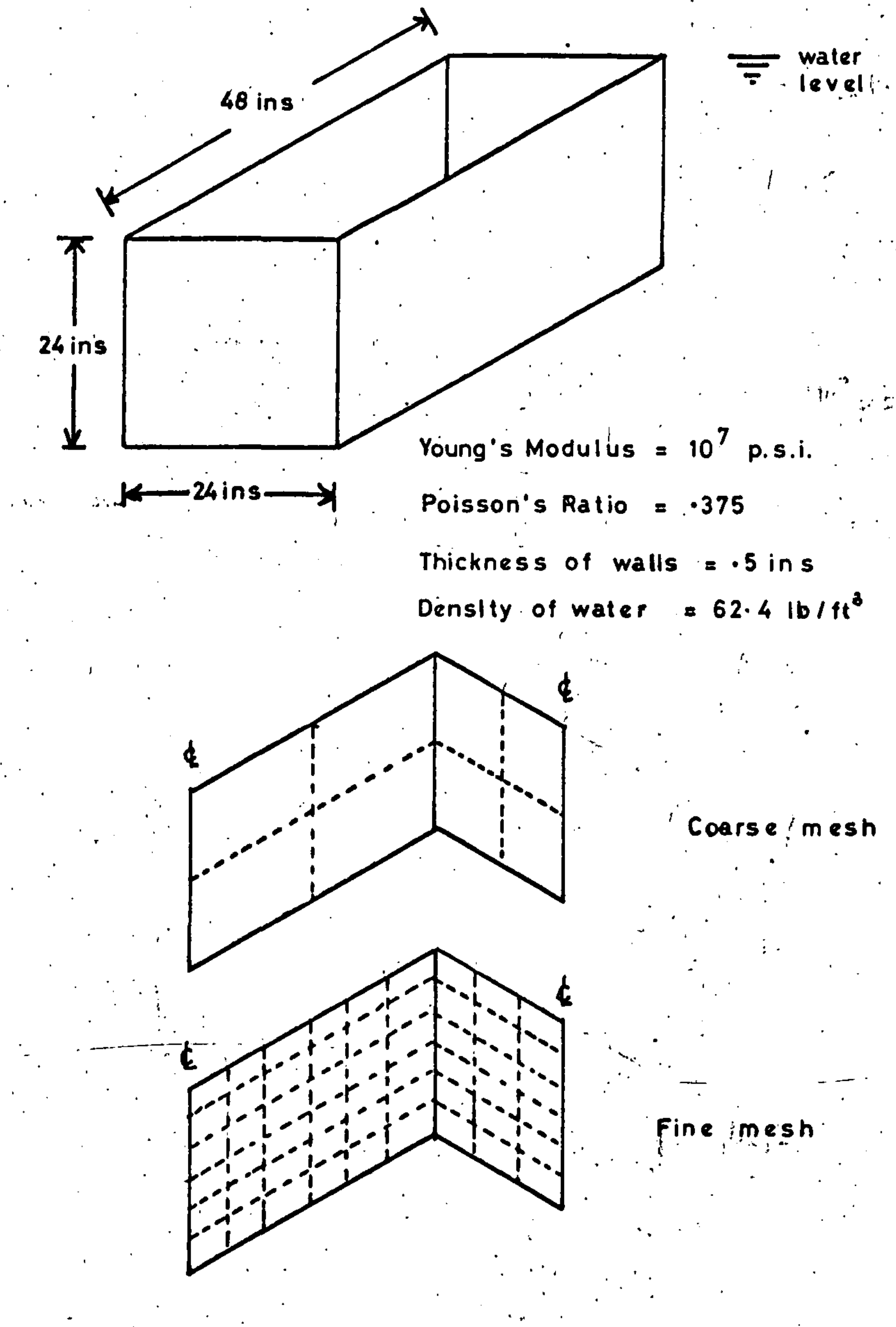

Fig. 66 Rectangular tank

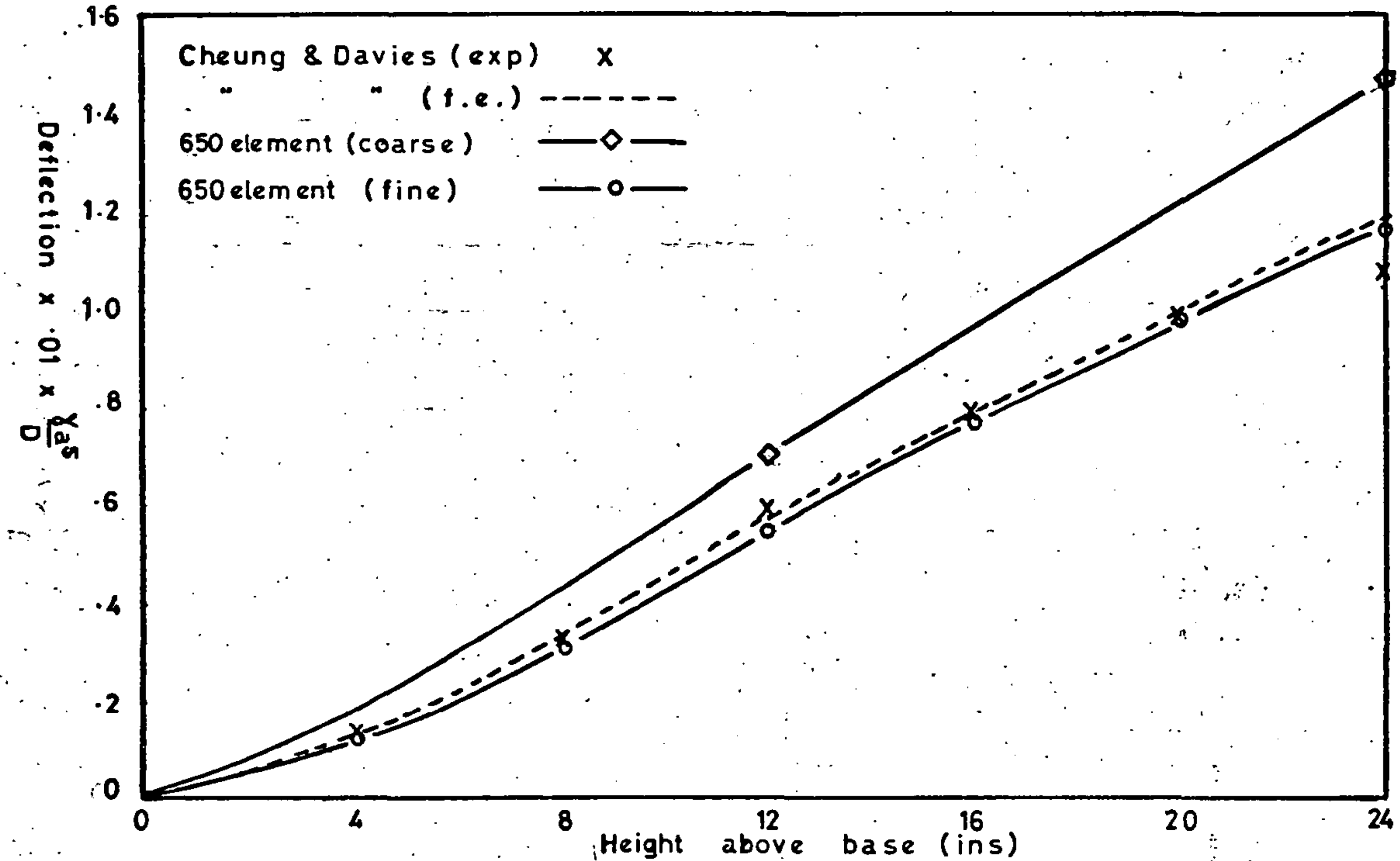

Fig. 67 Deflection outwards of vertical centre line (longer side)

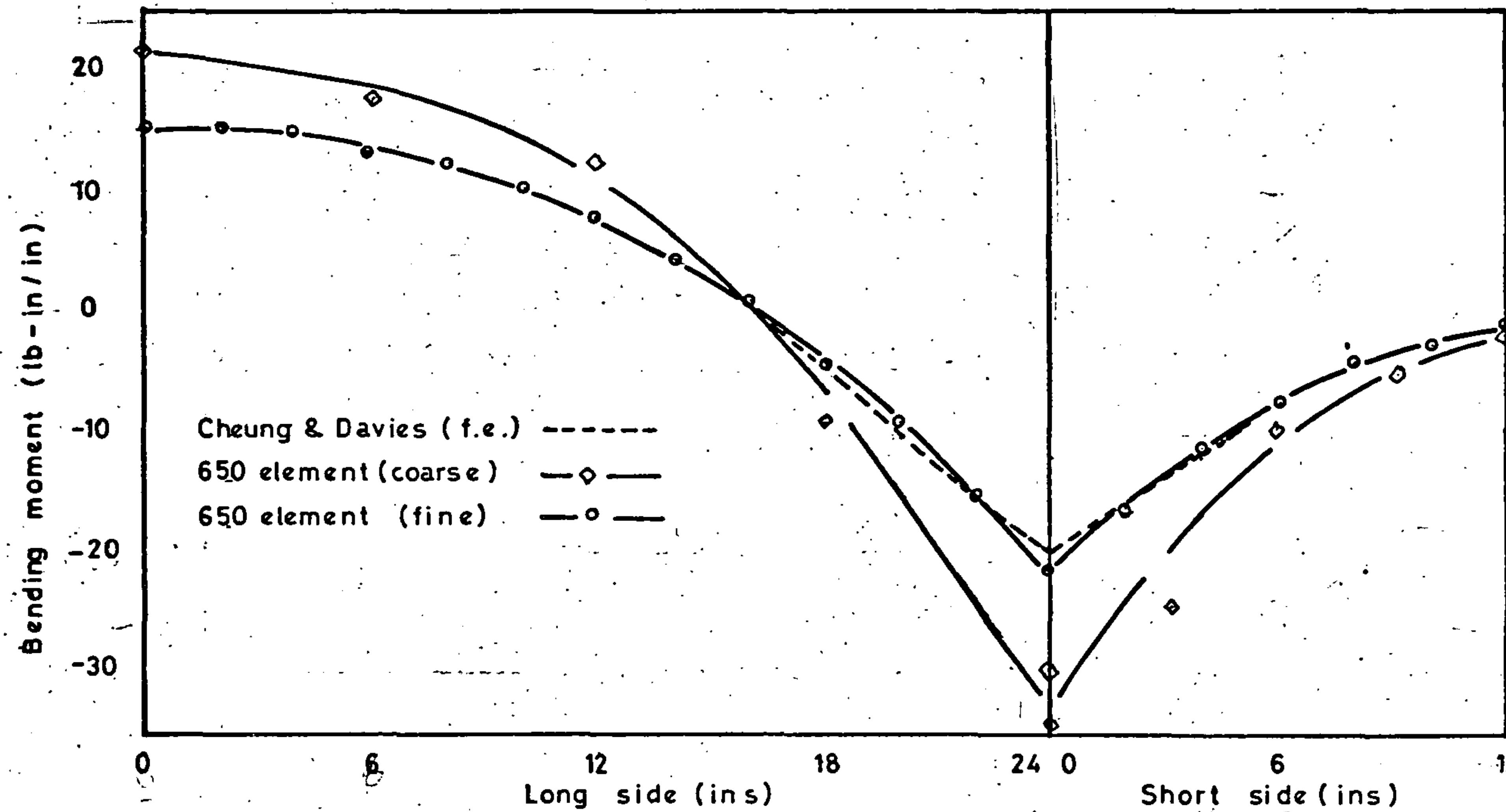

Fig. 68 Horizontal bending moment along top edge

calculation is not valid at all for the shorter side since this deflects inwards in this problem whilst as an independent plate it would deflect outwards. The bending moment at the top of the longer side centre line is estimated as 12 lb-in/in and at the corner 36 lb-n/in.

The experimental results validate the finite element calculations but the finite element used by Cheung & Davies includes only bending effects translated into three dimensional terms. They neglect any in-plane membrane effects arising from a moment generated in an element at right angles to another. A reasonable solution is achieved by Cheung and Davies because these effects are small. Comparing the horizontal and vertical bending moments at the corner from the S7 shell solution (see fig.69) confirms that the vertical, whilst being non-zero, is much smaller than the horizontal moment. It is this vertical moment which is transmitted into the in-plane of the other side. This is an important principle to note yet again, that a more elementary element may give equally good results to the more sophisticated elements developed in this thesis.

7.6 Folded plate beam

Although for most purposes a beam of peculiar cross section, such as shown in fig. 70, need not be analysed on any other basis than as a simple beam, it may be necessary at times to obtain the detailed variation of stresses across the beam section. For the purposes of comparison, the two span continuous beam analysed by Scordelis & Lo[42] was considered. Using a finite segment technique they calculated the stresses at points A & D at various sections along the beam.

The finite element analysis here used only a basic mesh

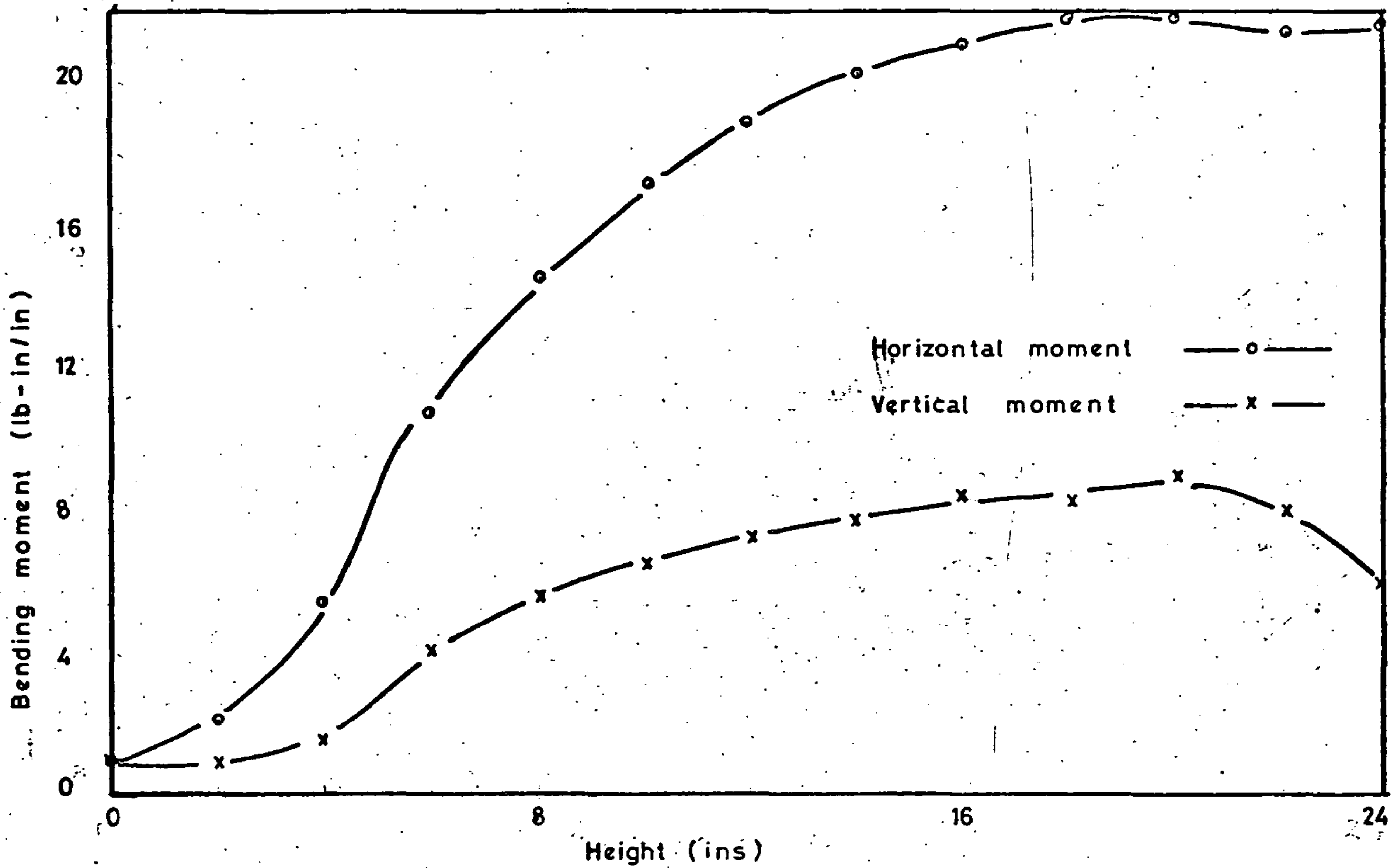

Fig. 69 Bending moments in short side at corner

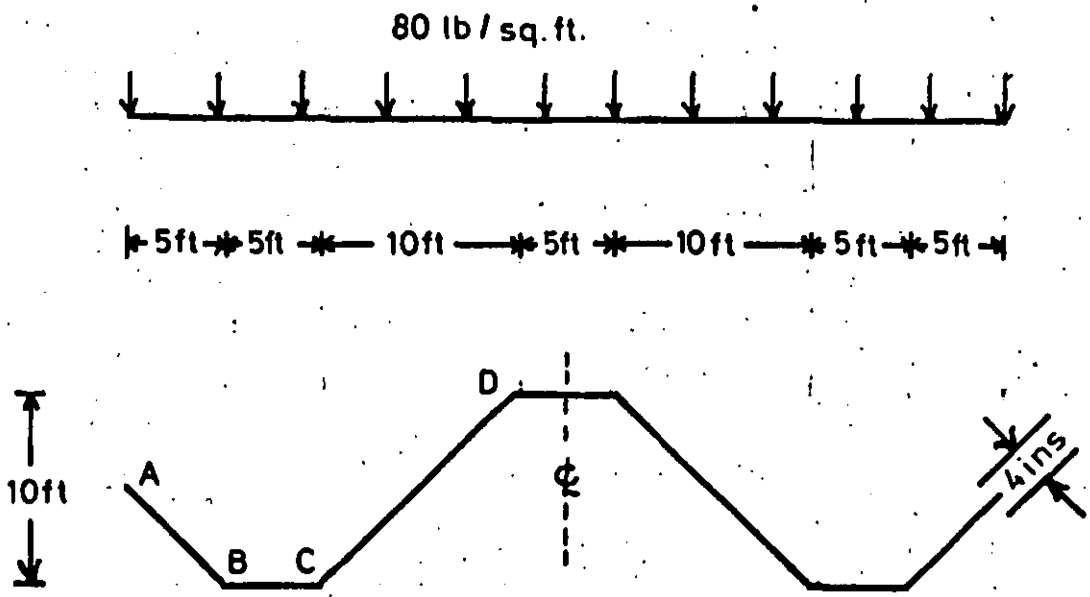

Transverse section

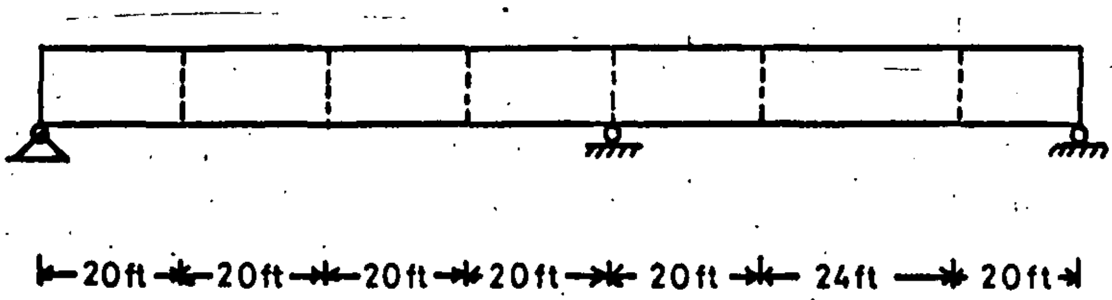

Longitudinal section

Young's Modulus = 3·66 p.s.i.

Poisson's Ratio = 0

Fig. 70 Folded plate beam

of 28 elements for the symmetric half of the beam. Each plane part of the cross section was represented by a single element, i.e. four in the half section, and the longer span divided into four and the shorter into three.

The beam was subjected to a uniform load of one pound per square foot of projected area. At all three supports all nodes at that section were constrained, at one as a pin, and the others as rollers. The results for both deflections and longitudinal stresses at the points A - D along the beam aretabulated along with the comparative results in tables 14 & 15 and graphically in figs. 71 & 72.

The finite element here provides quite an efficient solution bearing in mind the amount of information available for a minimal mesh.

These detailed results should be compared with the results which would have been obtained from a simple beam theory.

Central deflection longer span = 109×10^{-6}ft

Central deflection shorter span = 35×10^{-6}ft

These predict quite well the deflection of the central part of the beam but do not include the deflection arising from the deformation of the cross section: the outer edges deflect considerably more.

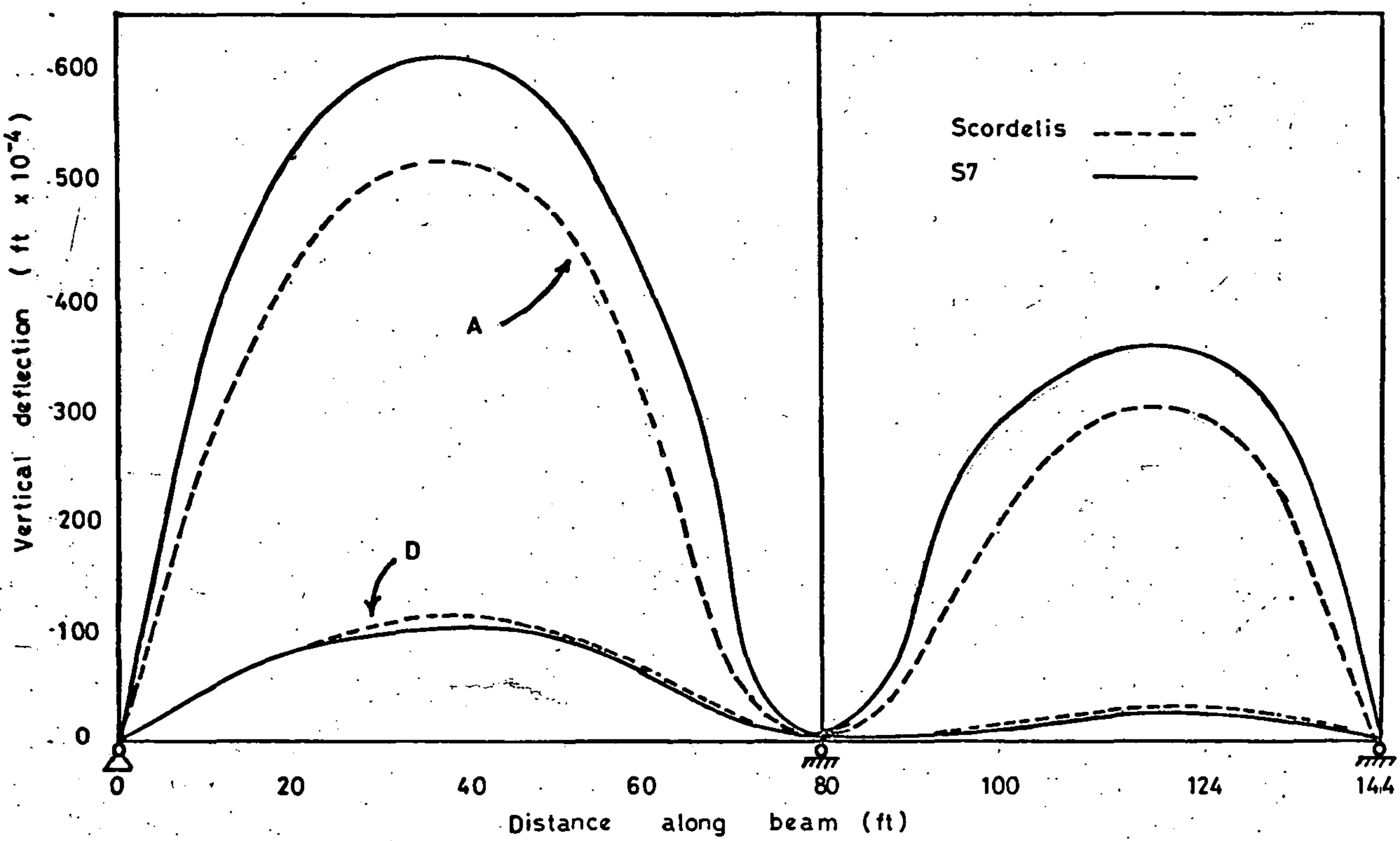

Fig. 71 Vertical deflection of folded plate beam

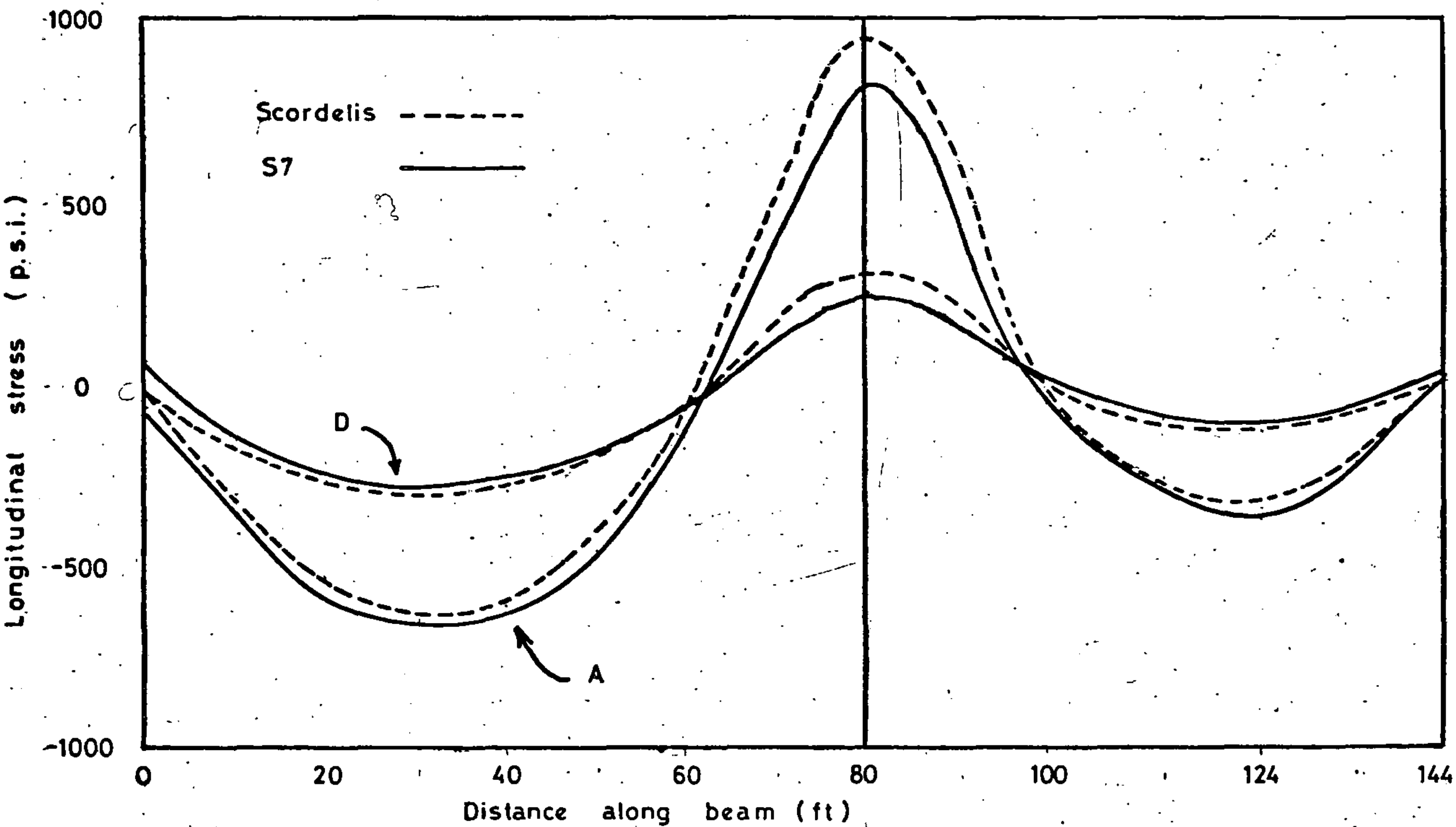

Fig.72 Longitudinal stress in folded plate beam

X (ft)	Point A		Point B		Point C		Point D	
	S7	S&L	S7	S&L	S7	S&L	S7	S&L
0	0	0	0	0	0	0	0	0
20	524	411	237	216	82	89	82	82
40	615	514	302	281	101	121	103	111
60	422	308	169	159	61	73	61	66
80	0	0	0	0	0	0	0	0
100	290	198	75	66	-12	-3	9	13
124	354	282	111	110	-5	6	19	25
144	0	0	0	0	0	0	0	0

Table 14: Deflections along folded plate beam (ft x 10^{-4})

0	-53	0	-50	0	-56	0	85	0
10	-305	-400	150		169		-142	
20	-556	-525	262	257	253	262	-210	-232
30	-643		327		323		-289	
40	-618	-584	294	279	266	213	-221	-273
50	-450		243		206		·192	
60	-183	-135	104	75	75	70	-76	-68
70	379		-216		-126		123	
80	817	960	-451	-527	-267	-360	255	340
90	437		-228		-185		167	
100	-60	-17	80	43	-27	-33	-95	12
112	-235	180	180		45		-65	
124	-368	-354	226	213	87	119	-67	-122
134	-208		134		65		-68	
144	25	0	-15	0	-32	0	37	0

Table 15: Longitudinal stresses along beam (p.s.i.)

S&L - Scordelis & Lo[42]

S7 - finite element

X - distance along beam

7.7 Cellular bridge deck

One important type of structure in the construction industry is the cellular bridge deck. Although considerable design work has been done in the past by considering such bridges as simple beams with peculiar section properties, the present trend to shorter, wider bridges with sloping side sections and a greater attention to detail requires more sophisticated analyses.

In section 6.3.4 we considered a simply supported box beam. It was found that transverse diaphragms caused erroneous results to be produced, arising from the effect that using average rotation as a degree of freedom has on shear representation. However, provided there are no such diaphragms over the support, good results were noted.

This particular bridge structure has no such diaphragms and we can feel confident is using S7 in this analysis rather than resorting to S12. (The converse situation will be considered in chapter eight.)

The current technique of using analagous grid or space frames requires the calculation of a large number of properties not relevant to the definition of the original structure. The data preparation for this finite element method is much simpler and is thus to be preferred in those cases where the results can be guaranteed.

The sectional view of the bridge is shown in fig.73. It has a sloping section on one side only and was, in reality, one independent half of the dual carriageway bridge used at Jesmond Dene on the A1 in Newcastle-on-Tyne. There was originally a 1° transverse slope on the top slab which has been ignored in this analysis. One symmetric half of a single span was considered, divided into four elements longitudinally

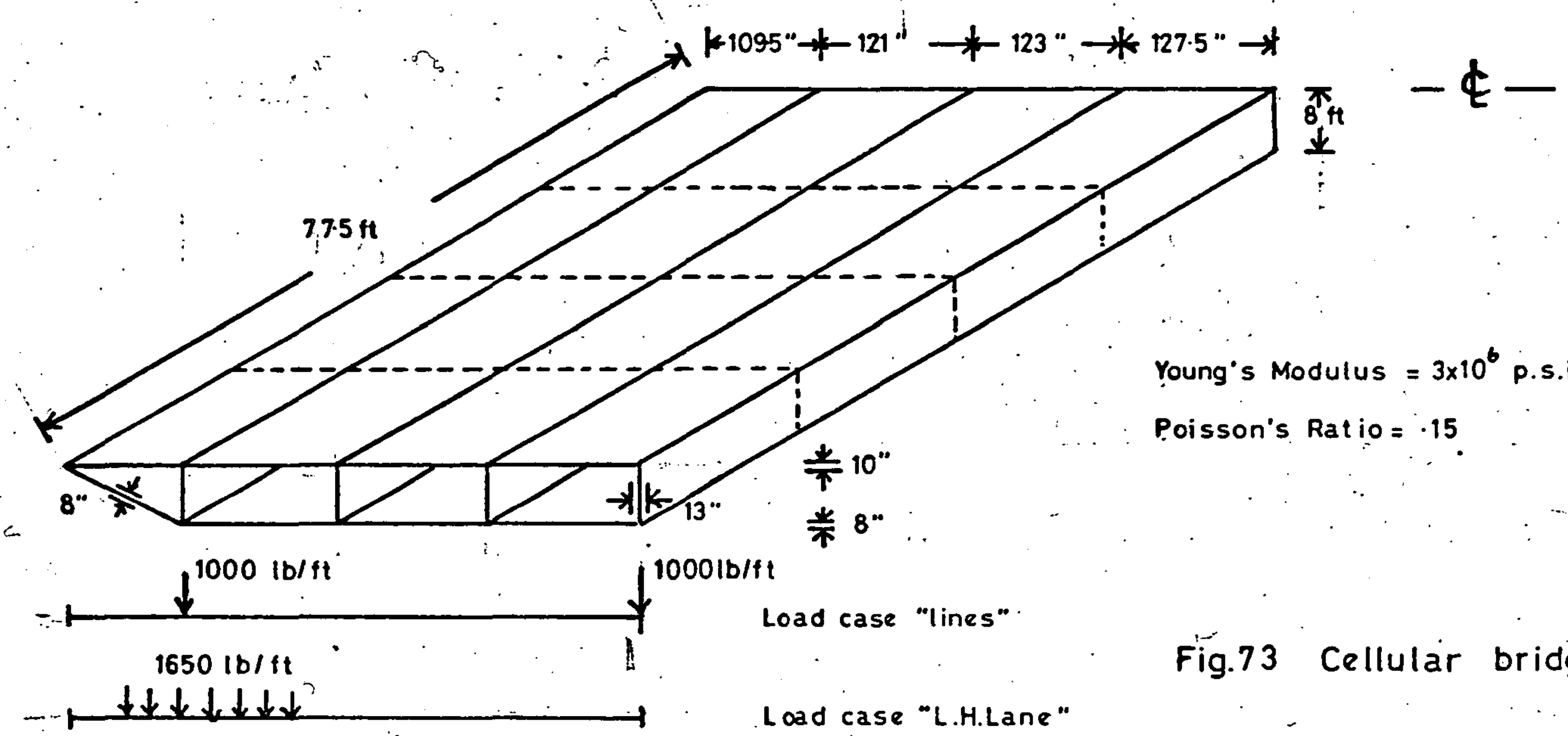

Fig.73 Cellular bridge

with rigid supports at one end and conditions of symmetry at the other.

Two loading cases are considered here. The first, the more academic case, is a pair of uniform line loads over the outer webs. The second, more realistic, represents the HA lane load on the Left hand lane. Both cases are shown in fig. 73, and were chosen in order to make a comparison with results previously obtained from a space frame analogy by Turner.(43)

These results are shown in figs. 74 - 77 and agree well. Considerable confidence may thus be placed in the use of S7 in this context.

7.8 Machine tool cantilever section

The machine tool industry also has many problems concerning the analysis of box-type members about which little systematic knowledge is currently available. As part of a research programme, one firm engaged in the design of machine tools carried out some elementary tests on a perspex model. Their concern was to extend their knowledge of the effect of the fixing of the end of a cantilever. Whilst existing theory could adequately cover the behaviour of uniform sections, there existed no such theory relating to the end fixings and the rigidity of such fixings materially affects the stability of the cutting tool.

The problem to be examined is shown in fig. 78. It consists of a uniform 5 in. square box of length 20 ins., bolted down by the bottom surface over a region of a 5 ins. square to a rigid mild steel block. The box was constructed from $\frac{1}{2}$in. thick perspex.(Young's modulus = 6.5×10^5 p.s.i. Poisson's ratio = .21) Measurements were made of the

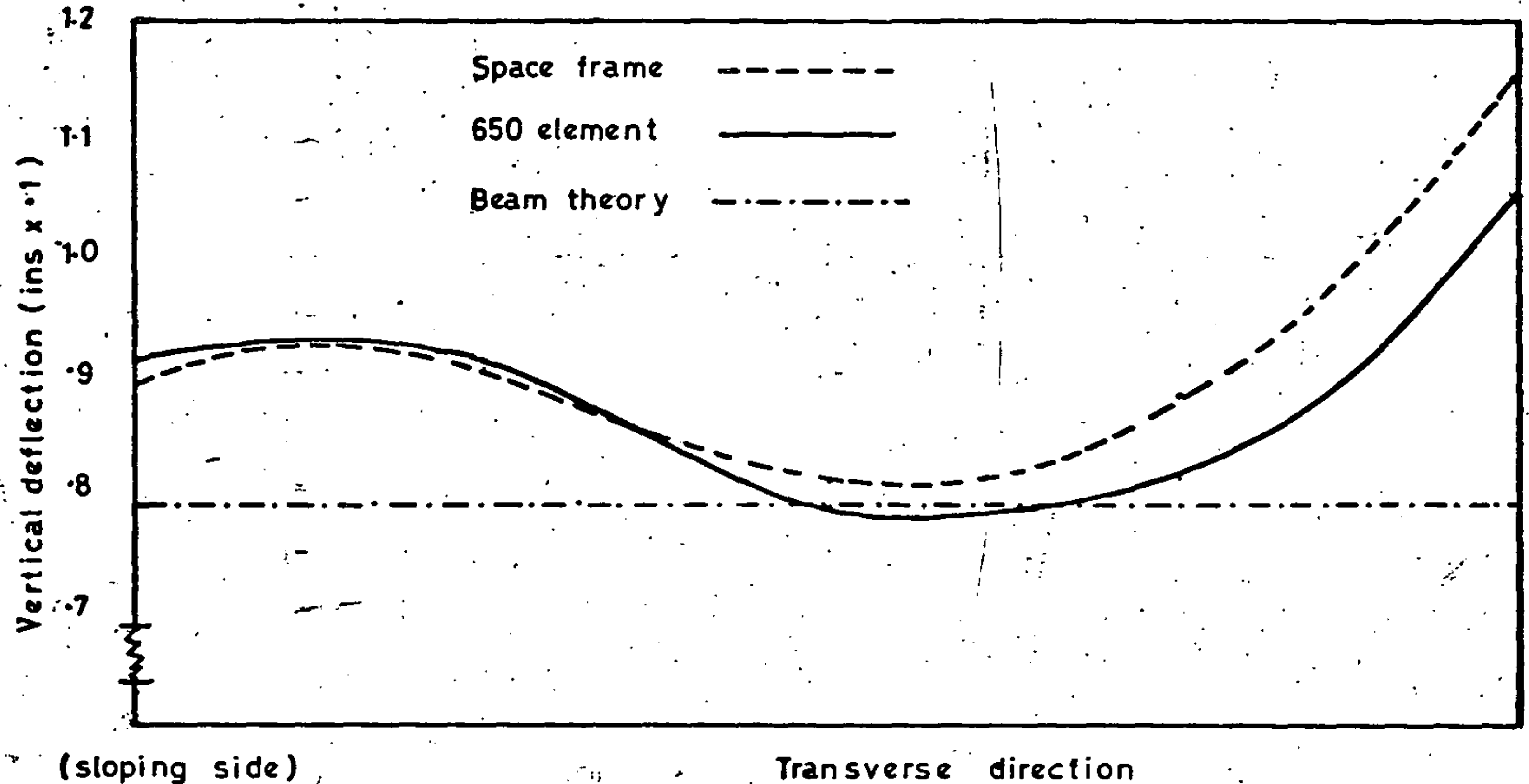

Fig. 74 Deflection of centre line ("lines" load)

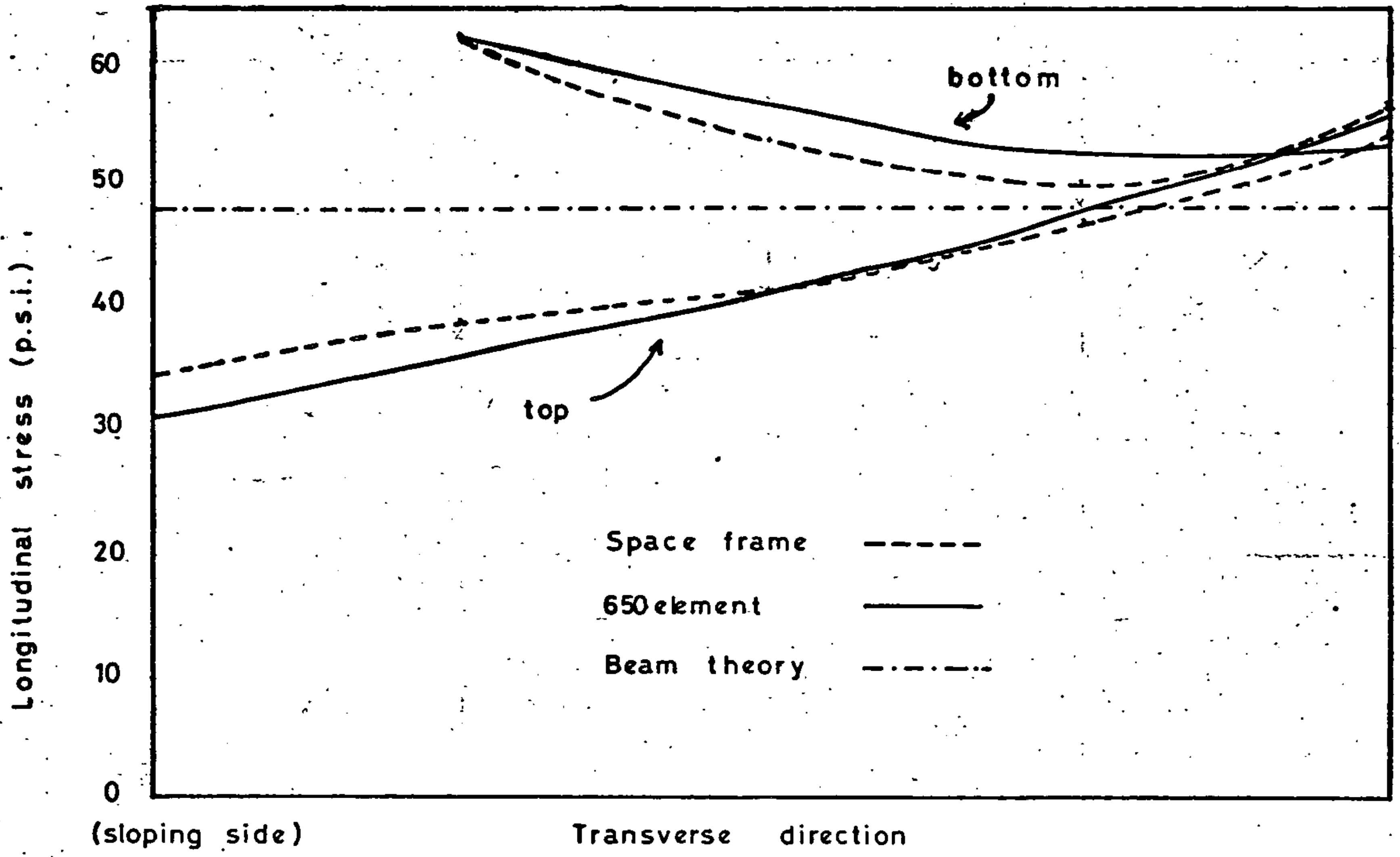

Fig. 75 Longitudinal stress across centre section (lines)

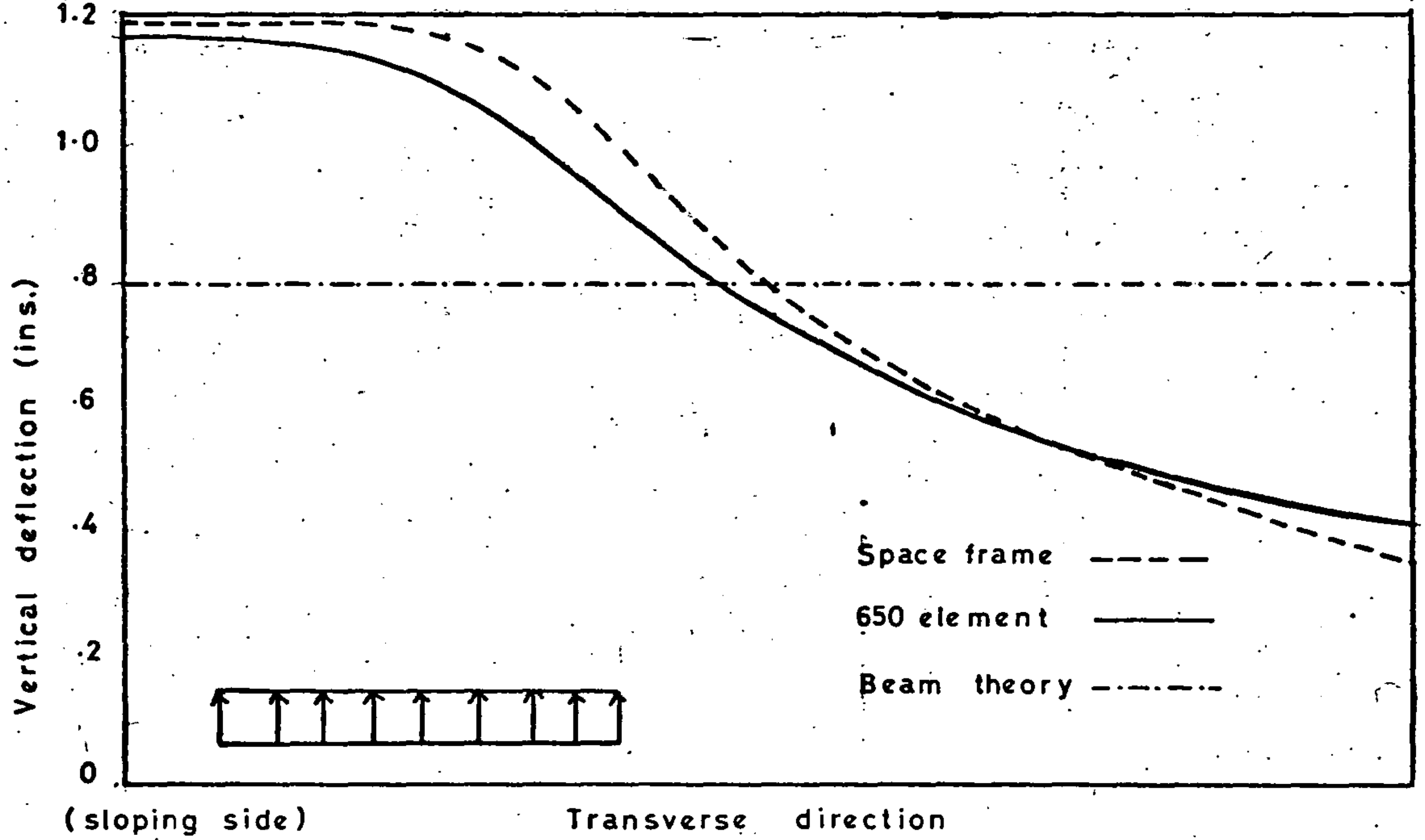

Fig. 76 Deflection of centre line (L.H. Lane load)

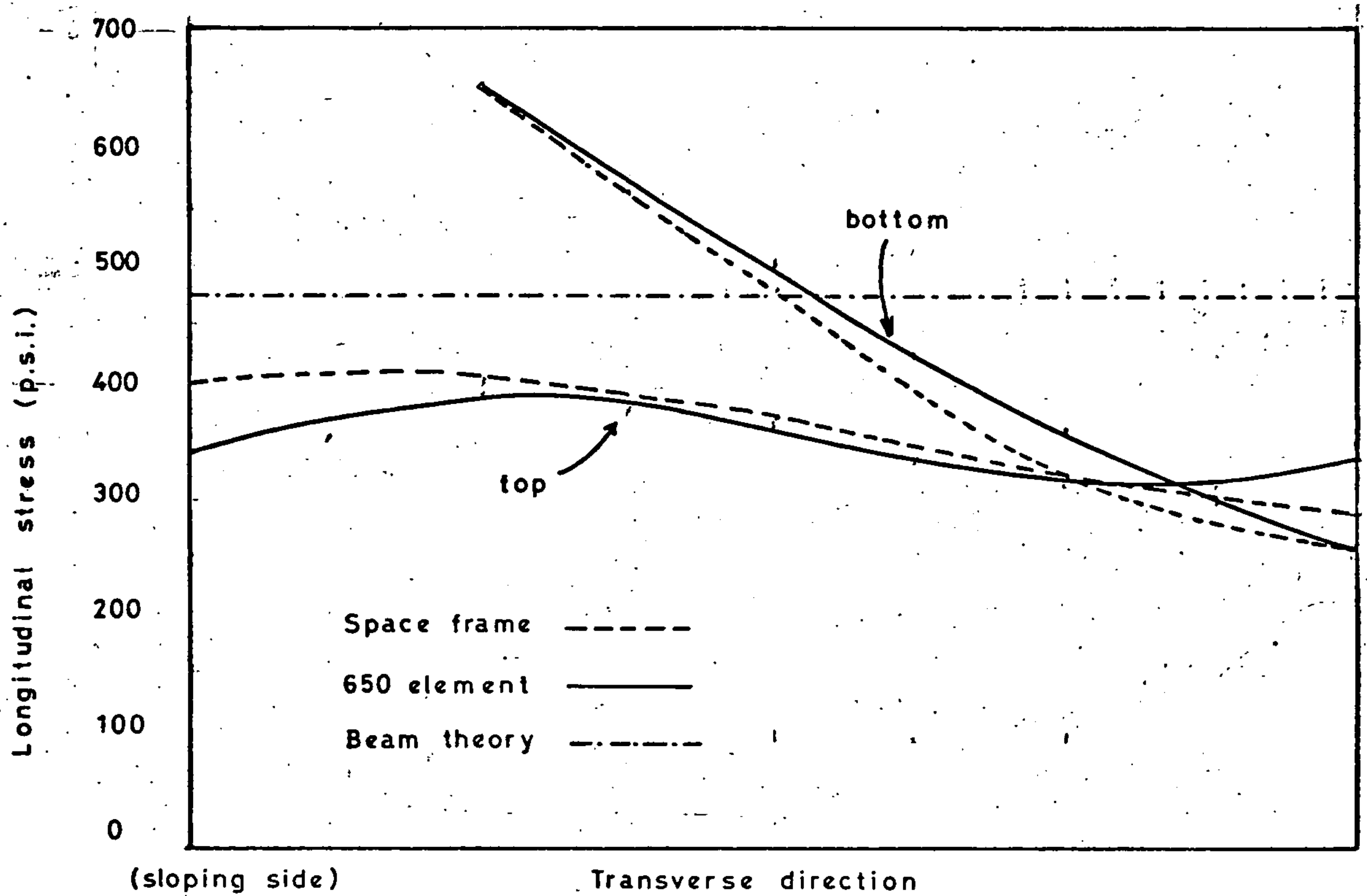

Fig.77 Longitudinal stress across centre section (L.H.Lane load)

flexibility of the end remote from the support. A sequence of additional members was considered and the actual tests compared are shown in fig. 79.

The experimental work was carried out using a "quasi-static" technique in which a load was applied sinusoidally but at such a low frequency as to make dynamic effects negligible. This approach was used in order to take advantage of existing equipment primarily designed for dynamic experiments and to overcome the effects of creep. The effects of this technique are partly exmined later.

The S7 shell element was used to carry out a finite element analysis using the mesh shown in fig. 80(a) and with load case I (see fig. 81) The finite element results are compared with the experimental values in table 16. These show that the finite element model is an accurate representation for Tests III - VI where the effect of a stiff bracing diagonal member reduces the flexibility of the base plate. In tests I & II the finite element representation does not allow the real flexibility to develop due to the support conditions. (see fig. 80(a)) The experimental model for all these tests (I - VI) had bolts which were positioned very close to the edge of the square base which was pocketed and reinforced with additional pieces of perspex.

A second experimental test of model I had been made with four plain bolts at a distance $\frac{1}{2}$in. from the edges of the base square. The result does not agree with the finite element result with a rigid base. (see table 17) It was decided that test 2 of model I would be examined in greater detail rather than test 1 of the same model. Four additional nodes were added to the base plate of the

Test	Experimental	Finite Element
I	900	512
II	750	489
III	453	378
IV	386	362
V	347	333
VI	347	328

(flexibility x 10^6 in/lb)

Table 16: Flexibility of cantilver

first series of tests.

Test	flexibility
experimental	3780
finite element	
rigid	
up	1624
down	1064
pinned	
up	6244
down	4900
average finite element	3458

flexibility x 10^6 in/lb)

Table 17: Flexibility of cantilever

test 2 model I

Point	Model I	Model III	Model VI
A_1	-3395	-2278	-1584
A_2	-2786	-1663	-1260
B	4232	2474	704

Table 18: Stresses in side of cantilever (p.s.i.)

A_1 middle of side to the immediate front of the diaphragm

A_2 similar but to the rear

B at the extreme rear end

see fig.78

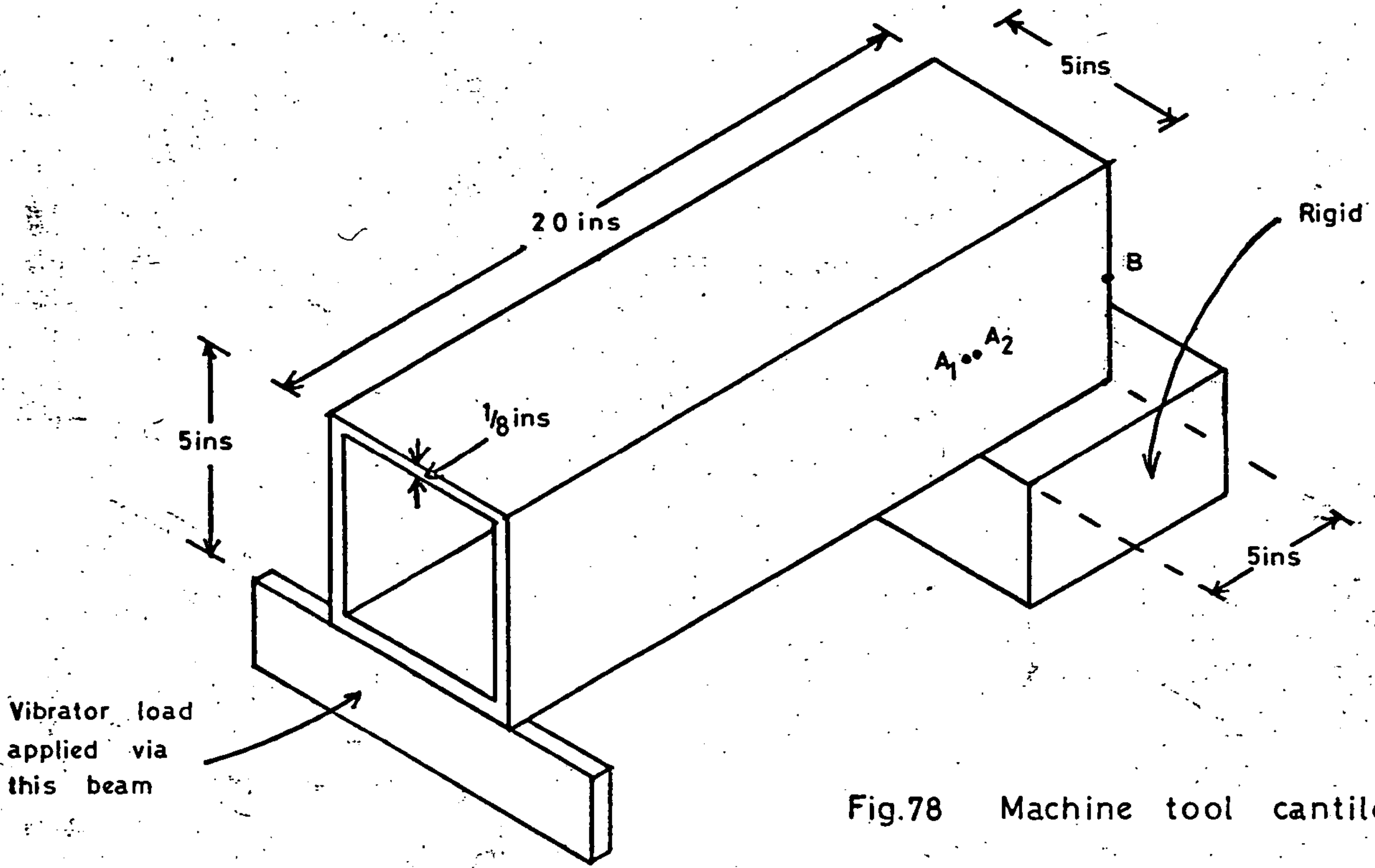

Fig.78 Machine tool cantilever

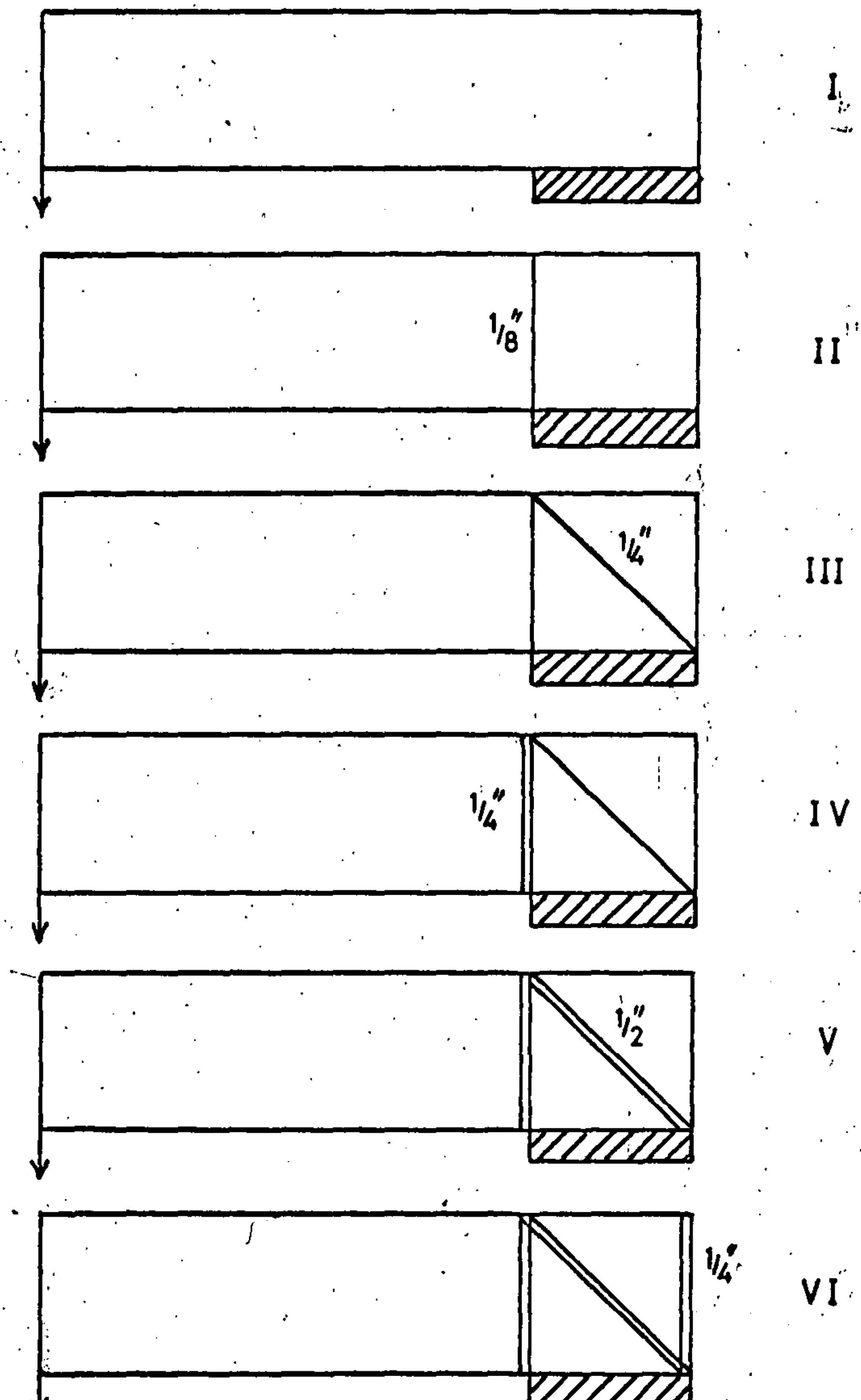

Fig. 79 Machine tool cantilever - first series of tests

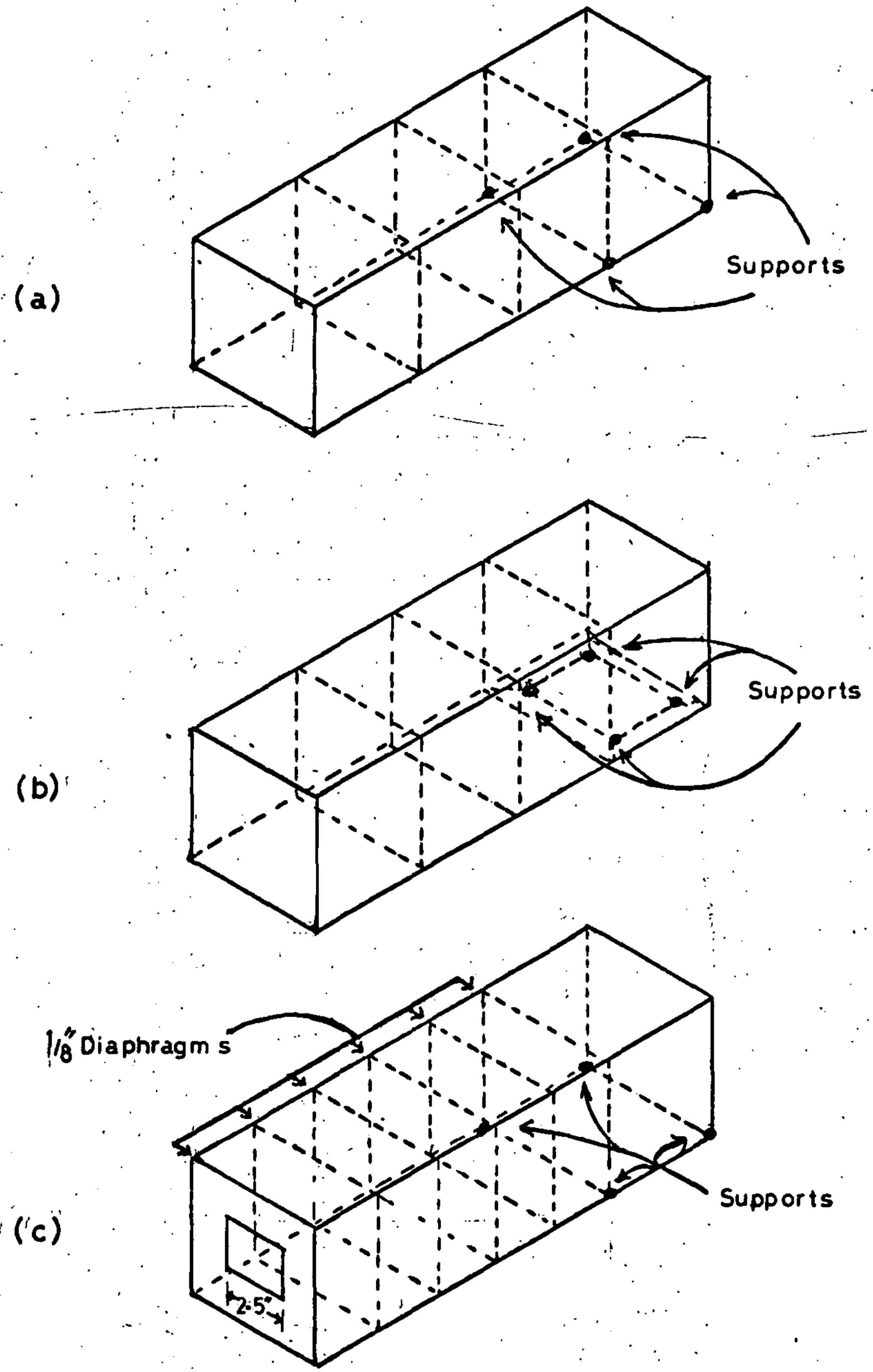

Fig. 80 Machine tool cantilever - meshes used

cantilever as shown in fig. 80(b). Four support conditions were considered. Firstly, the difference between pinned and rigid support at these four points was considered. Secondly, as mentioned above, the effect of the "quasi-static" testing was examined by taking an "up" and a "down" case with each of the pinned and rigid cases, giving four in total. The difference between "up" and "down" is the point at which the base plate lifts-off from the mild steel base. In the "down" case the rear edge lifts and the front edge is supported and vice versa for the "up" case. The flexibilities calculated for the finite element model are given in table 17. These show the considerable variation that can be generated by the details of the support condition. The fact that the average of all four cases is near the measured flexibility is probably fortuitous.

The existing theory for analysing the end section considered the contribution to stiffness by the side walls to be insignificant when the diagonal member is present. However, if we consider the stresses in the side wall for cases I, III, & VI of the finite element solution, we can see that even in the least flexible case the stresses at the extreme rear position cannot be ignored.(see table 18)

A further test was compared in which five extra diaphragms were included to examine the effects of these on the torsional flexibility of the beam. These diaphragms were $^1/_8$in. thick with a $2\frac{1}{2}$in. square hole cut out from the centre. (see fig. 80(c)) The results obtained are shown in table 19.

It is interesting to note that the difficulty earlier encountered with a diaphragm at the end of the simply supported beam does not appear to affect this problem

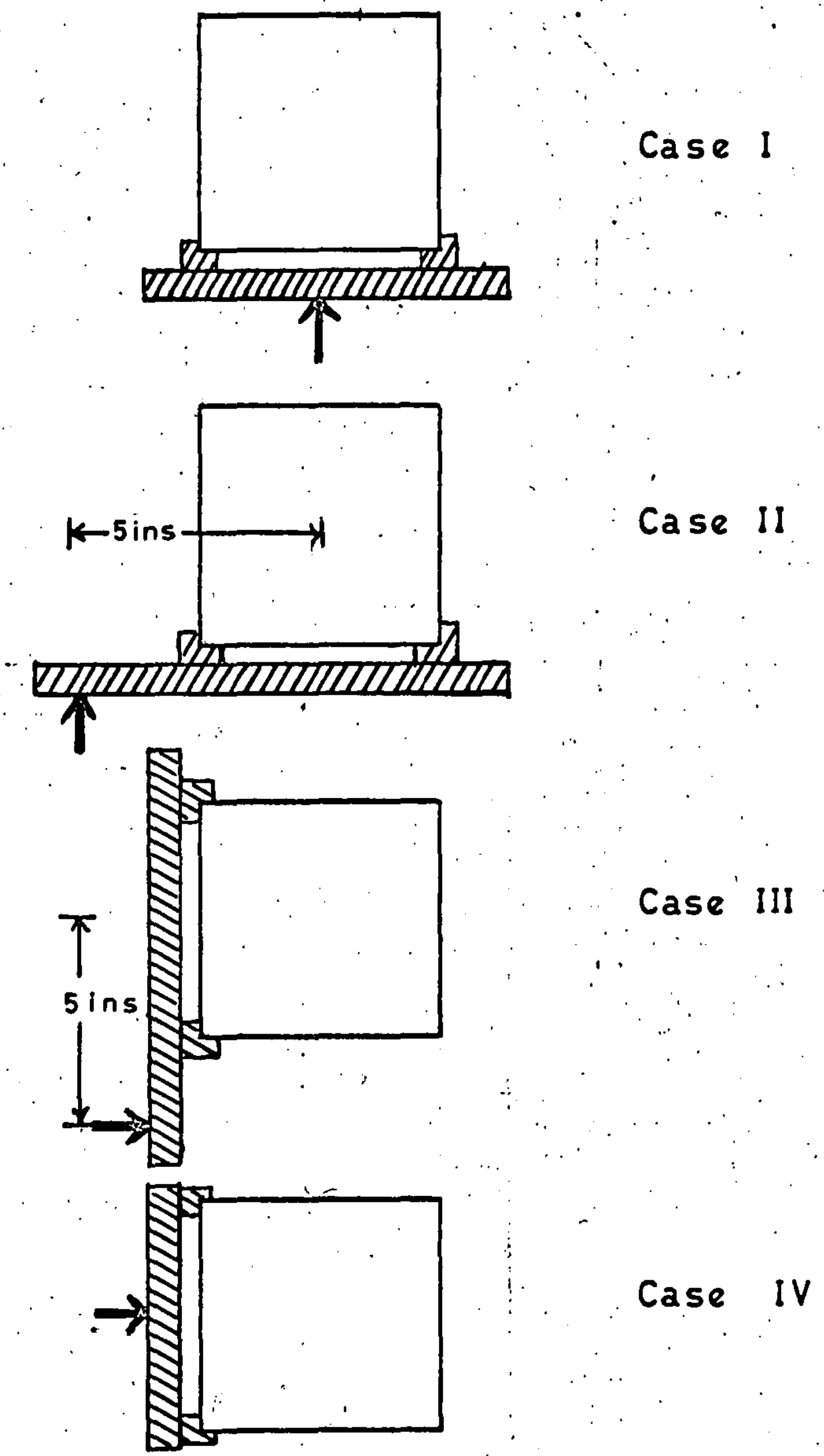

Fig.81 Machine tool cantilever - loading details

noticeably. This is largely due to the fact that at the sections where the diaphragms are included there is little or no shear between the top and bottom flanges in comparison with the bending effects. It is this shear which gives rise to the difficulty and when bending dominates no problem is seen. This is particularly important since the S7 element provided in this example exceptionally efficient and economic solutions in these series of tests which would not have been the case if the S12 element had been used.

Load case	I	II average	II at load	III	IV
Experimental	328	331	572	385	380
Finite element	331	382	463	289	288

Table 19: Flexibility of cantilever with diaphragms four load cases (10^{-6} in/lb)

Chapter Eight Gateshead Viaduct

8.1 Introduction

In this and the following chapter a detailed examination is made of a multi-cell box-type motorway bridge using the new shell elements in a practical situation. The structure is the Gateshead Viaduct on the A1(M) outside Newcastle-on-Tyne. A model analysis of this structure (fig.82) has been carried out by Turner (43) using prestressed reinforced plaster. This technique has been developed by Brock(44) primarily for ultimate load determination. However, the behaviour of the composite material, particularly when prestressed, is sufficiently linear for comparison to be made with the finite element analysis. (Details of model are shown in fig.83)

The examination of this structure is divided into two parts. The first, in this chapter, is concerned with simple loading cases, compares the finite element analysis with the model results and attempts to explain the action of the bridge in distributing stresses from the loads to the supports. The second part, in the next chapter, demonstrates the power of the finite element method by showing the changes to the stresses and deflections resulting from structural modifications chosen in the light of the results of this chapter.

8.2 Choice of shell element

It was this type of structure, simply supported box-type with end diaphragm which gave rise to errors when using the shell element S7, as shown in chapter six. It is thus necessary to use the element S12 in order to remove this difficulty. The effect of using the element S7 is demonstrated in fig. 84. This shows that the deflection at the centre of the bridge

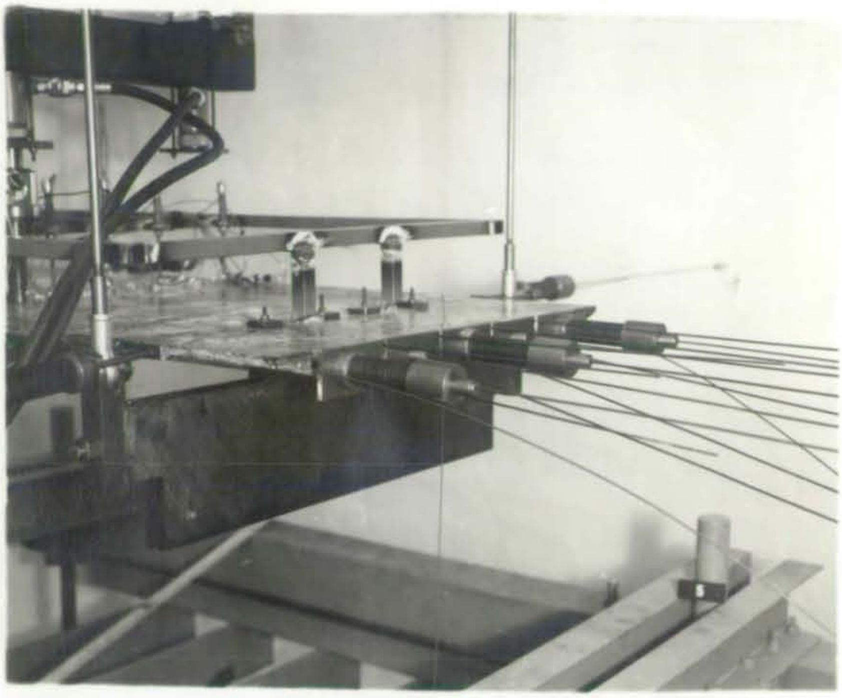

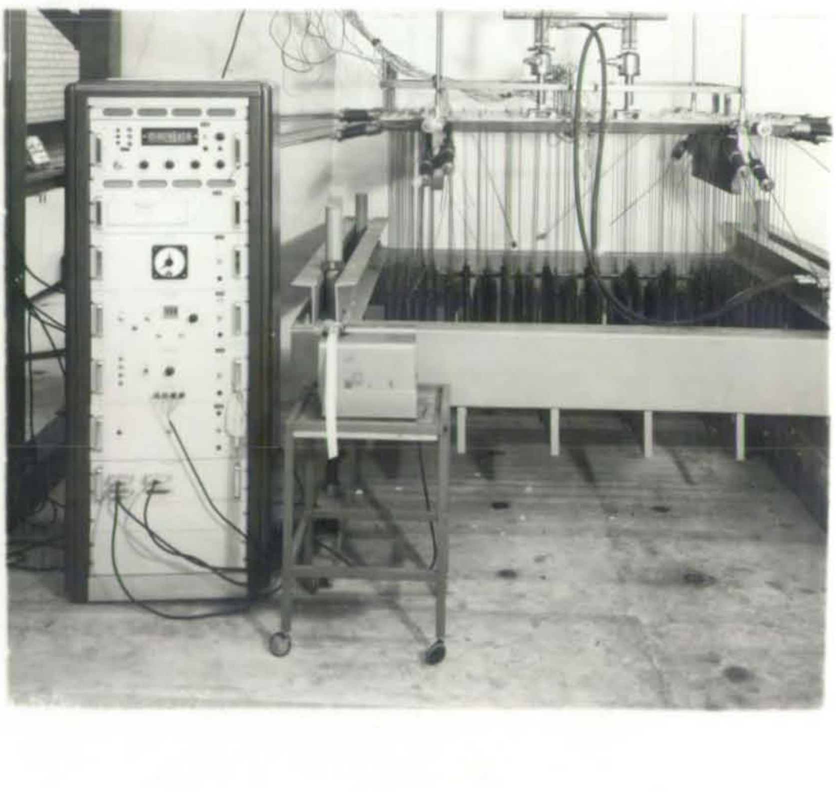

Fig. 82 Plaster model of Gateshead Viaduct

Fig. 82 (cont'd)

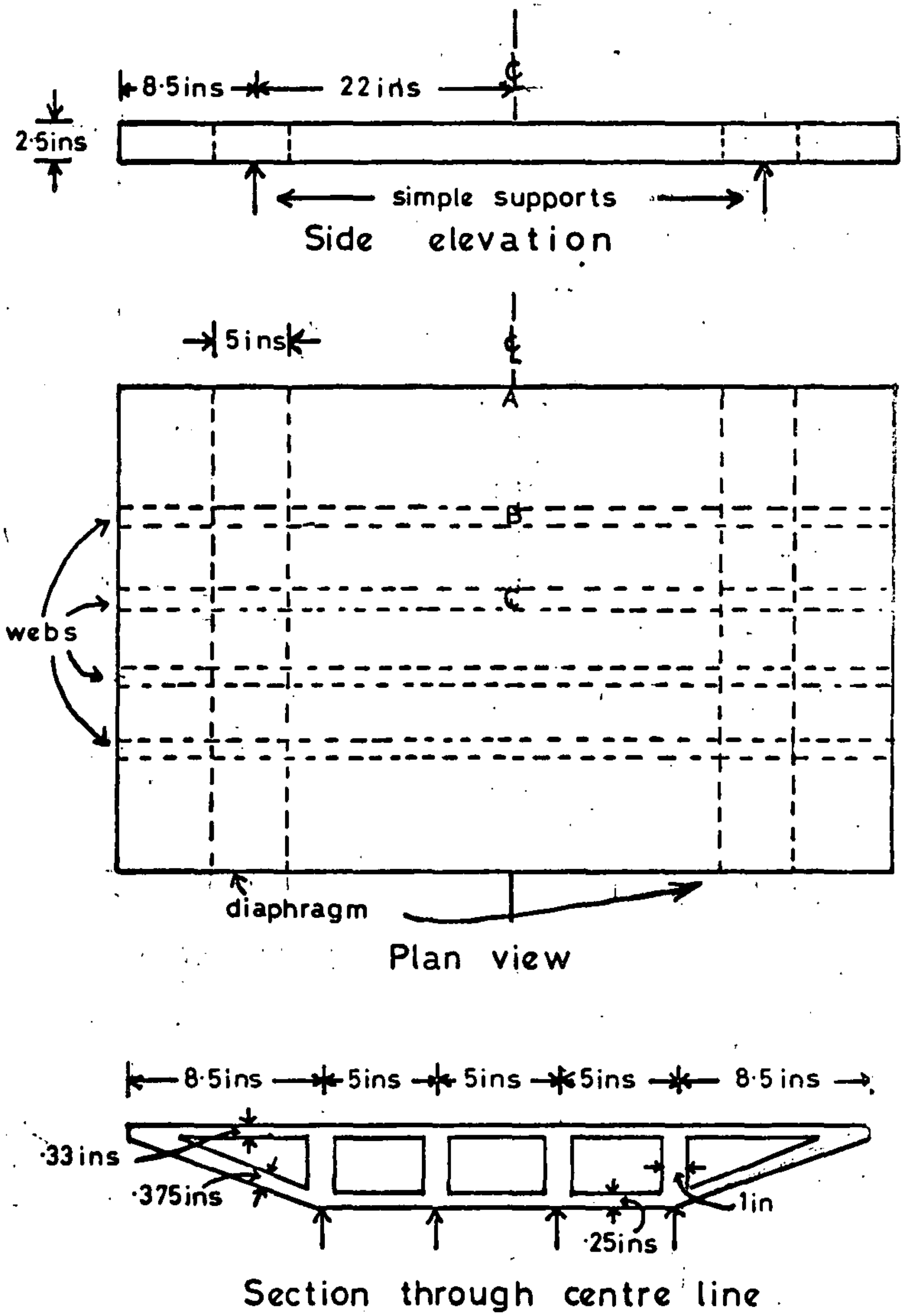

Fig. 83 Gateshead viaduct model

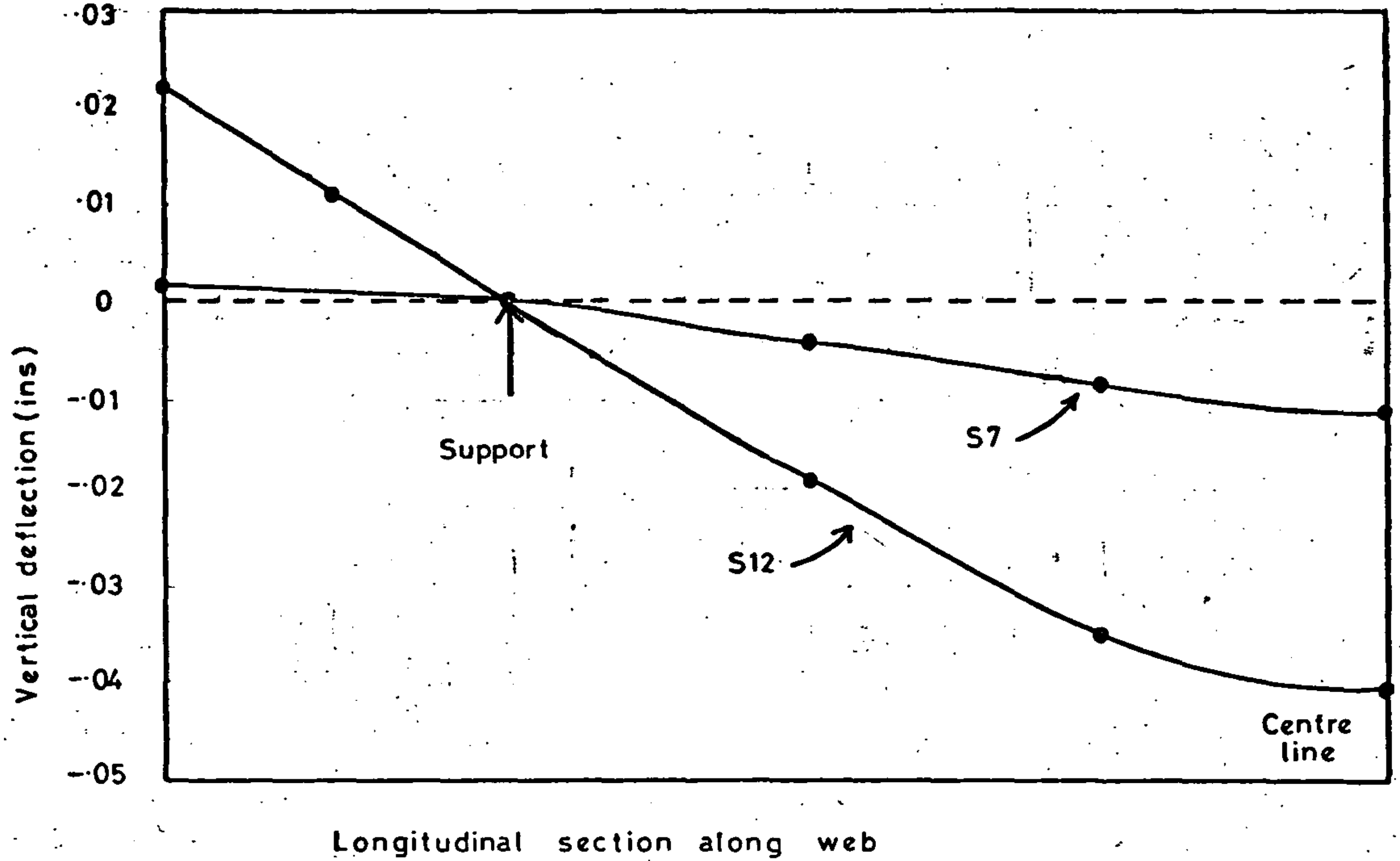

Fig.84 Vertical deflection of web using elements S7 & S12 (GHS12/1)
(Line load)

under a simple line load is about a quarter the value from considering the bridge as a simple beam. (If the end diaphragm is removed this error largely disappears.). Further, the total bending moment at the centre line is 4760 lb-in compared with the correct value of 11,000 lb-in. Similarly, the bending moment at the support should be zero but is instead -1370 lb-in. This is the result of the by now well known effect of shear at the box corner. Consequently, in the rest of this chapter and in the next all the analyses are carried out using the S12 element. This is at some extra expense, since twice as many elements are required - triangles instead of rectangles - and more equations - 864 instead of 504 - as the S7 element would have demanded. The idealisation used is shown in fig. 85. This structure will be referred to as GHS12/1 and the transverse sections through nodes will be called I,II,III,IV: I is over the support and IV the centre line. The view shown in fig. 85 is taken looking from underneath the bridge. The edge beams were represented by triangular elements as shown and although these elements are peculiar in that they are thicker than their depth, numerical problems are not expected to arise. For this first structure the four nodes indicated were supported on rollers with one node constrained transversely to prevent rigid body motion of the whole structure. Since an odd number of elements were required across the top and bottom slabs, it was not possible to use a mesh entirely symmetrical. This produced slight variations in the results at the two innermost nodes on each transverse section for the line load case. However, these were not significant.

8.3 Stresses from strains

With the S12 element the strains ϵ_{xx}, ϵ_{yy}, ϵ_{zz} are three of the independent degrees of freedom at each node. It is possible, therefore, to derive stresses from these as an alternative to the values obtained by averaging the stresses calculated in each element meeting at that node. From a practical point of view, it is considerably easier to compute the value of the stresses at any point from the strains than to extract the values from the elements and average. These two techniques are compared in fig. 86 which shows that although there is some difference between the two this is not particularly significant. If a choice is to be made on this basis, the stresses calculated from the strains are nearer the values from the simple beam theory than those from

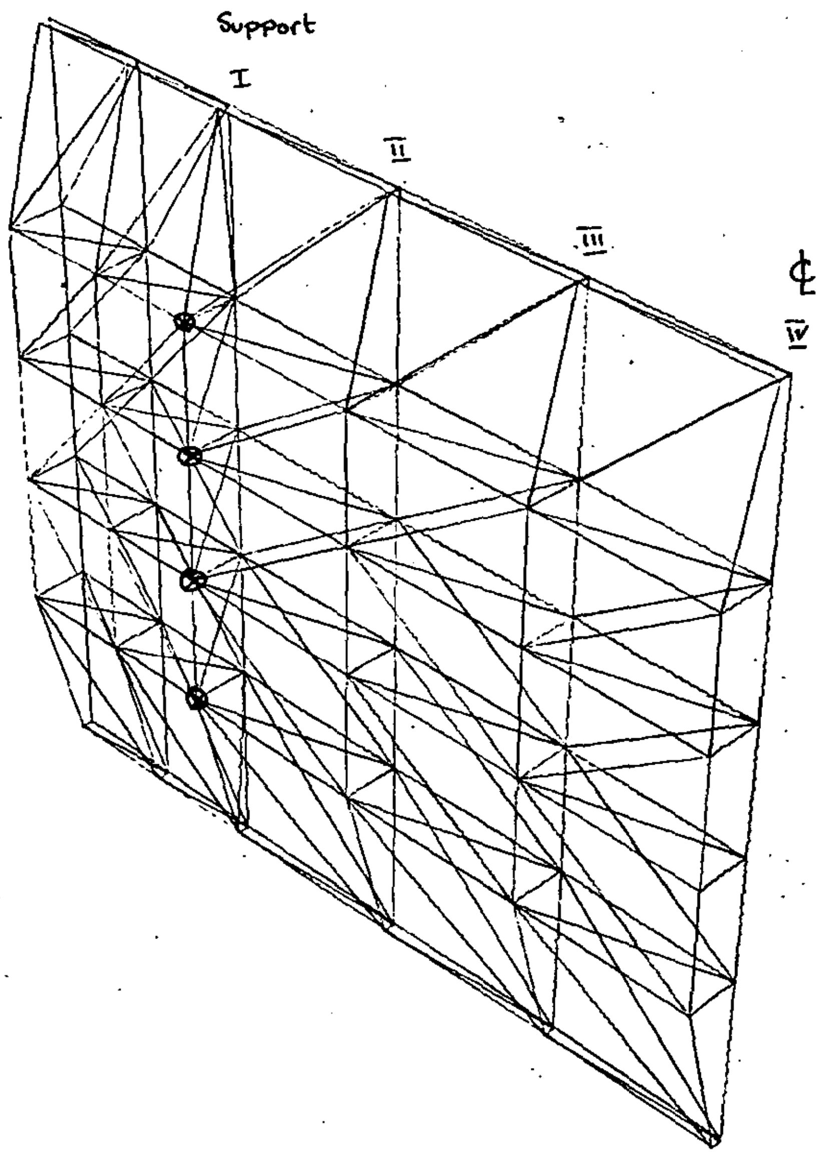

Fig. 85
Mesh used with
S12 for Gateshead
Viaduct

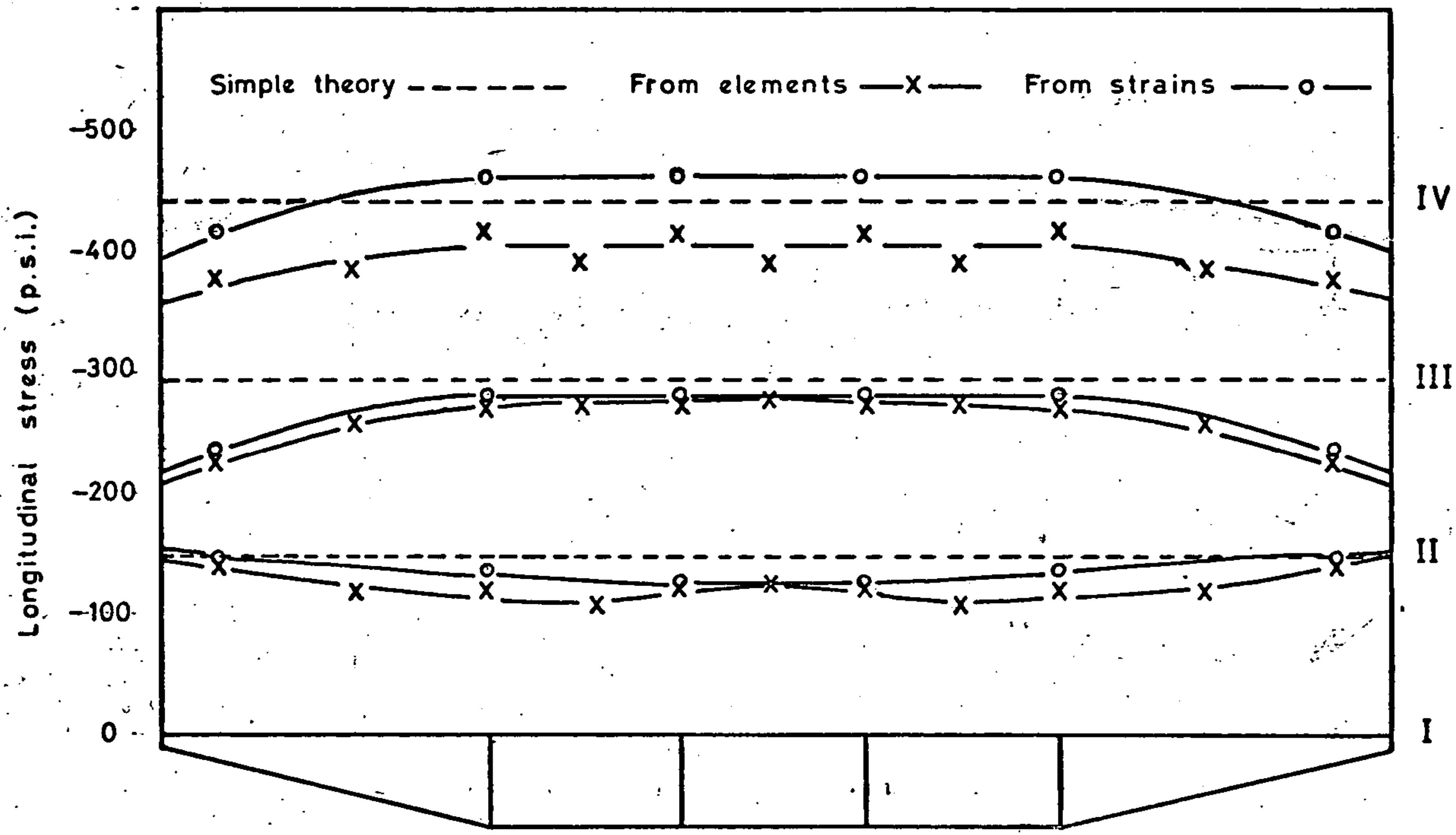

Fig.86 Comparison of longitudinal stresses on transverse sections of top slab under line load (GHS12/1)

the elements. In addition, their distributions are, where appropriate, somewhat smoother. From this, and the fact already mentioned that in,practice they are simpler to produce the subsequent calculations and results have been derived from these stresses rather than those in each element.

8.4 Comparison of results

It is a useful initial test to discover how close the finite element and model results agree with the simple beam theory for a uniform load across the centre line of the bridge. Whilst it is true that the cross section of this bridge is vastly different from a simple beam, nevertheless engineers are prepared to consider it as such for loading cases uniform across the bridge.

Vertical defelections of the four sections are shown in fig.87. and show close agreement between the finite element analysis and the simple beam theory.

The finite element analyses were carried out assuming values of Young's Modulus (= 2 x 10^6 p.s.i.) and Poisson's Ratio (= .15) which were determined experimentally by Turner[43] as the best equivalent values to take for the plaster model he used. These were obtained from a simple beam prestressed and reinforced in similar fashion to the model. The prestressing of the model produces better linearity of the stress-strain relationship than a simple reinforced model would have. The results quoted are from a best line fit through a sequence of measurements at various incremental values of the loads.

The validity of these and other underlying assumptions can best be compared initially by considering the vertical deflection of the centre line for the line load. The experimental results were for six point loads across the

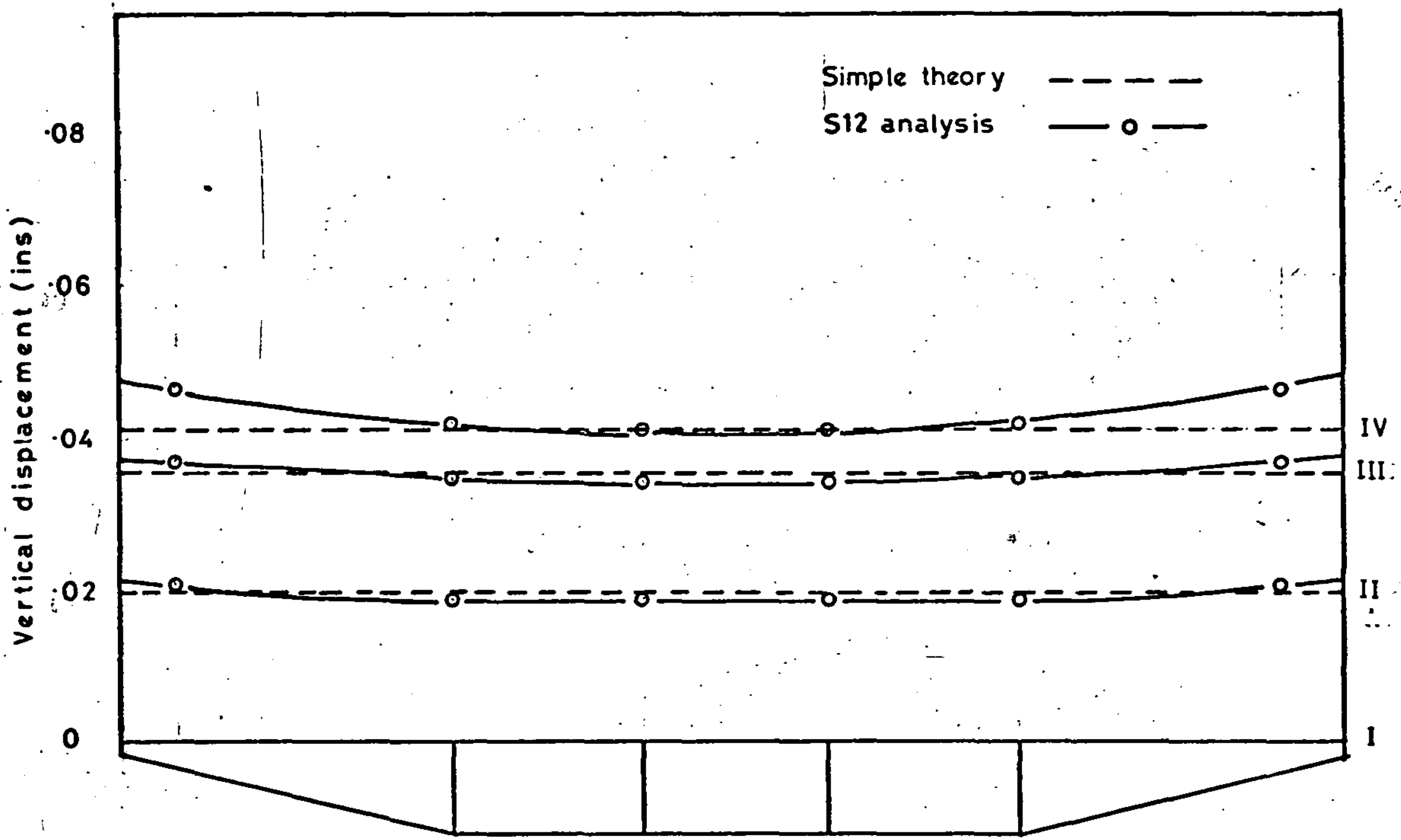

Fig.87 Vertical displacement of transverse sections under line load (GHS12/1)

centre line and are the average of tests carried out on two identical models. For the line load, an appropriate combination of these results has been taken and the comparison can be seen in fig. 88. Also shown in fig. 89 are the longitudinal strains at the centre line in the top slab for both model and finite element results. It should be borne in mind that the finite element and simple beam theory results for deflections do not include the effect due to the finite thickness of the diaphragm which reduces the effective span of the bridge. This effect in the model will tend to reduce the deflections somewhat.

The bending moments at the transverse sections can be calculated from the stresses obtained at each node. The distributions of bending moment across each section so calculated is somewhat crude due to the coarseness of the subdivision into elements. The cross section is divided into six parts and the total bending moment in each derived, which is then distributed evenly across each part. This is the distribution plotted..The simple bending moment diagram for the line load is shown in fig. 90 and can be seen to be very close to that predicted by the simple beam theory. The distribution of bending moment across the four sections is shown in fig. 91. These distributions are virtually constant apart from the outer edges where it is expected to be lower due to the sloping section.

It is also possible to consider the effect of concentrating the same total load at one outer edge node, point A on fig.83, as a point force. (This load case will be called POINT1) The corresponding results for vertical deflections are shown in figs. 92 & 93 and for the bending moment in fig. 94.

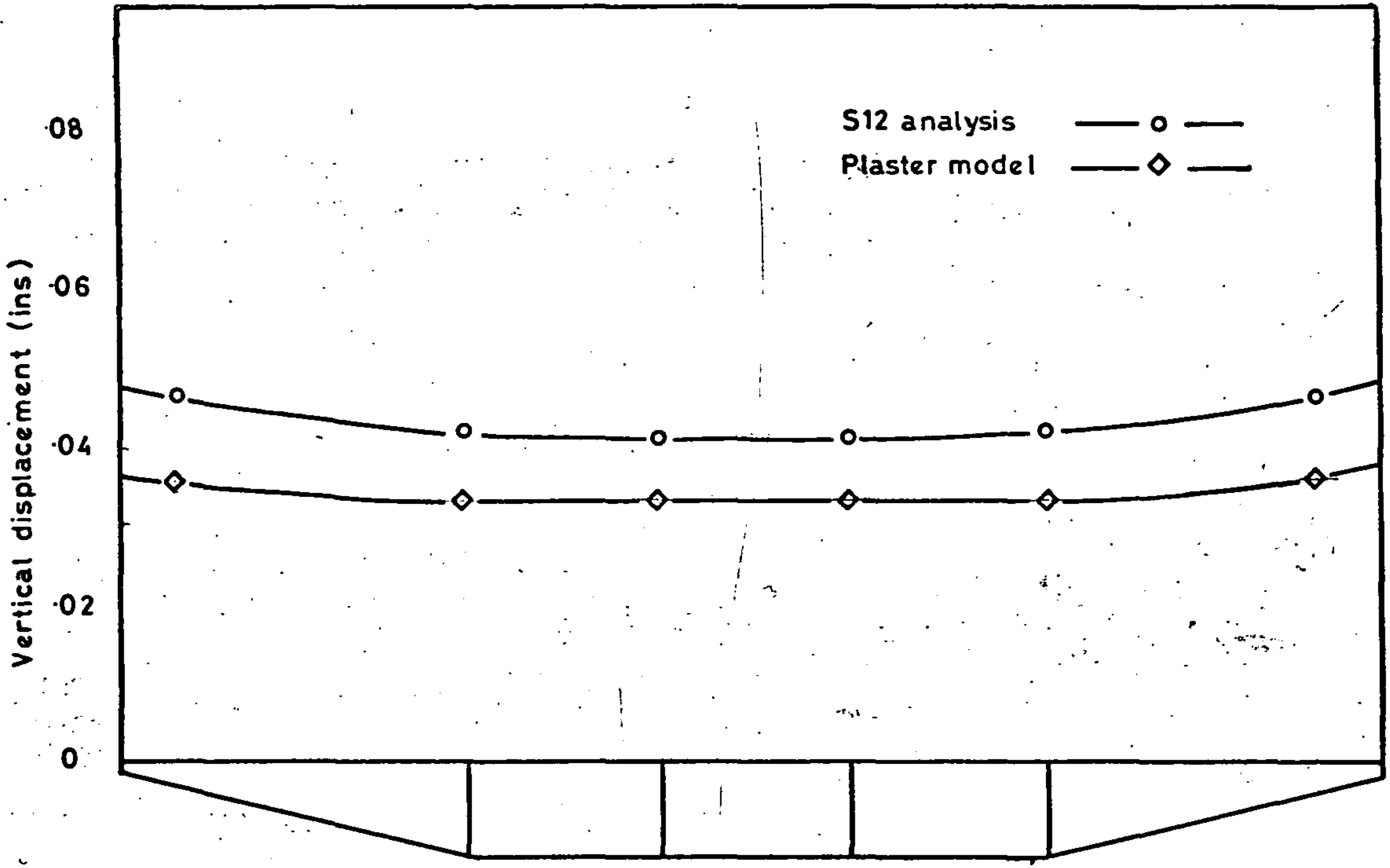

Fig.88 Vertical displacement of centre line under line load - model and finite element comparison

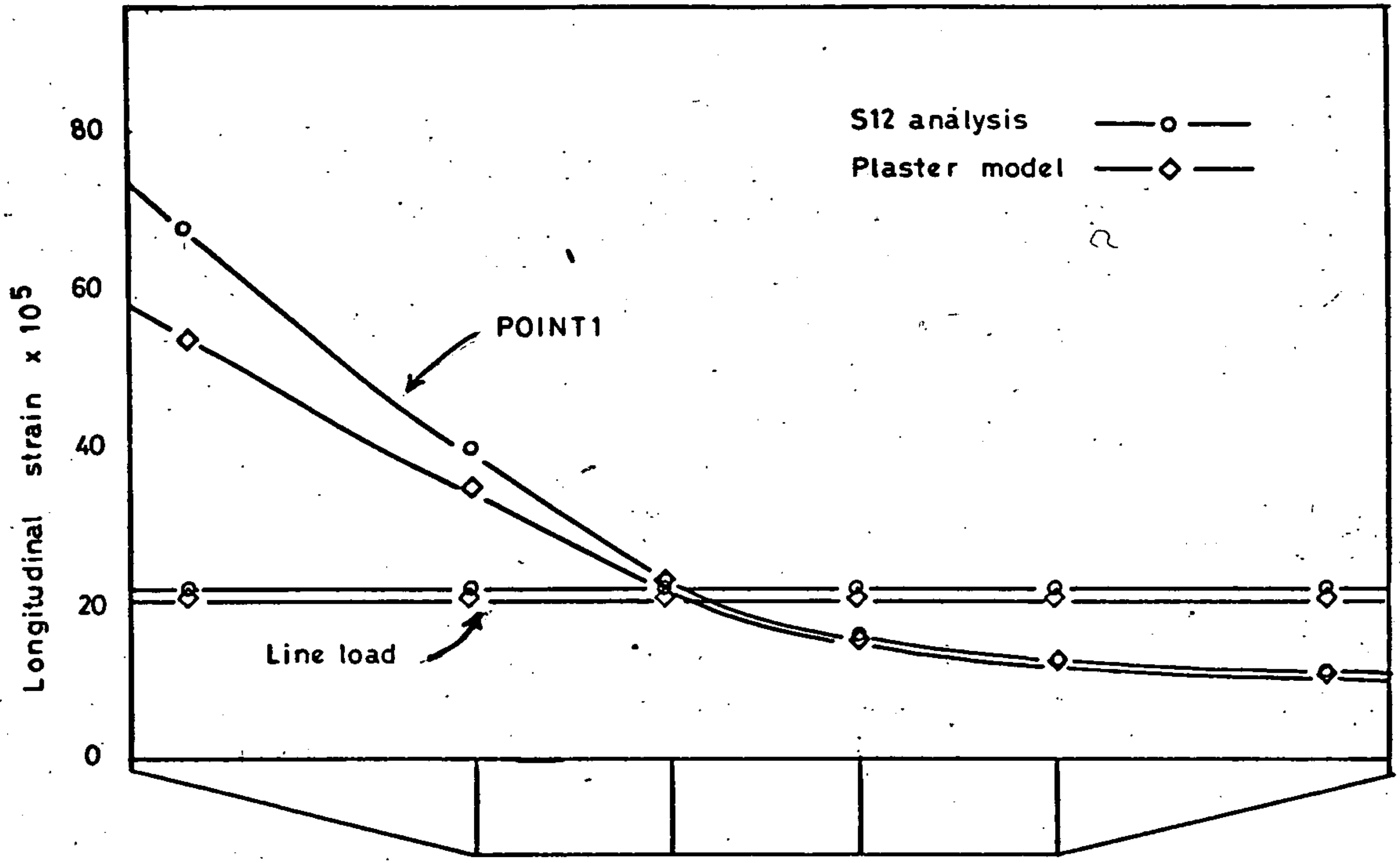

Fig. 89 Longitudinal strain across centre line - model & finite element results

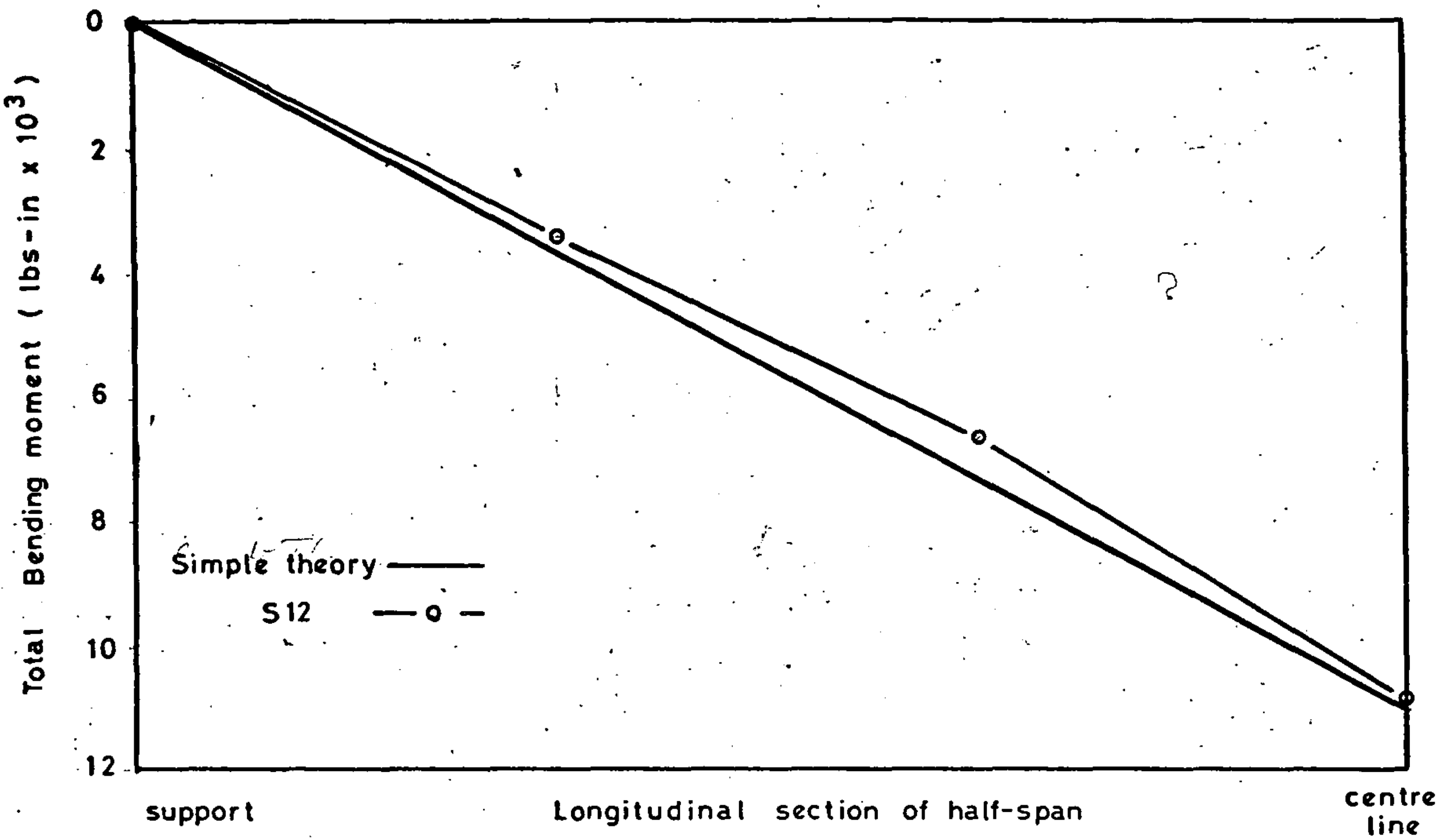

Fig. 90 Bending moment diagram for line load (GHS12/1)

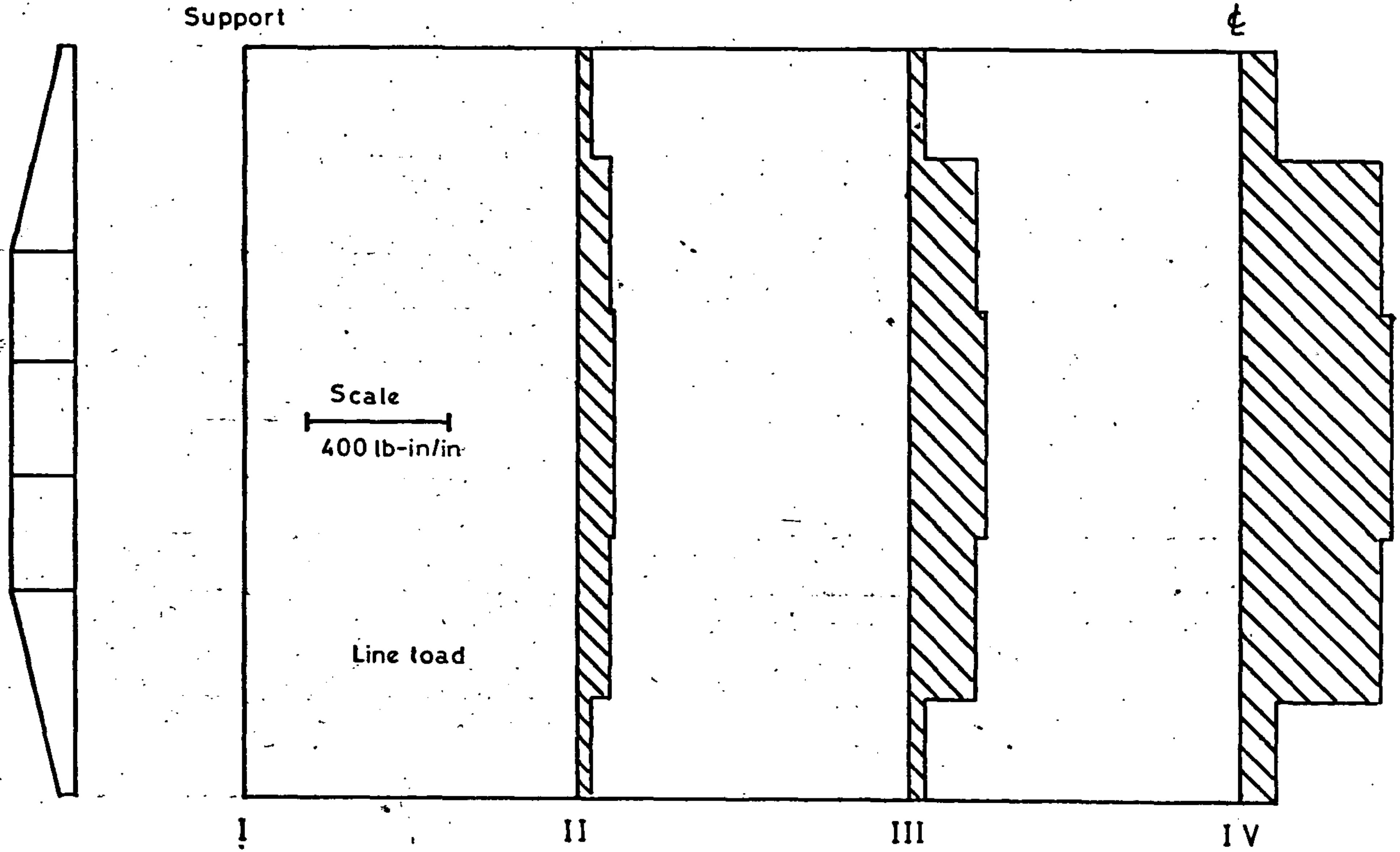

Fig. 91 Distribution of bending moment for line load (GHS12/1)

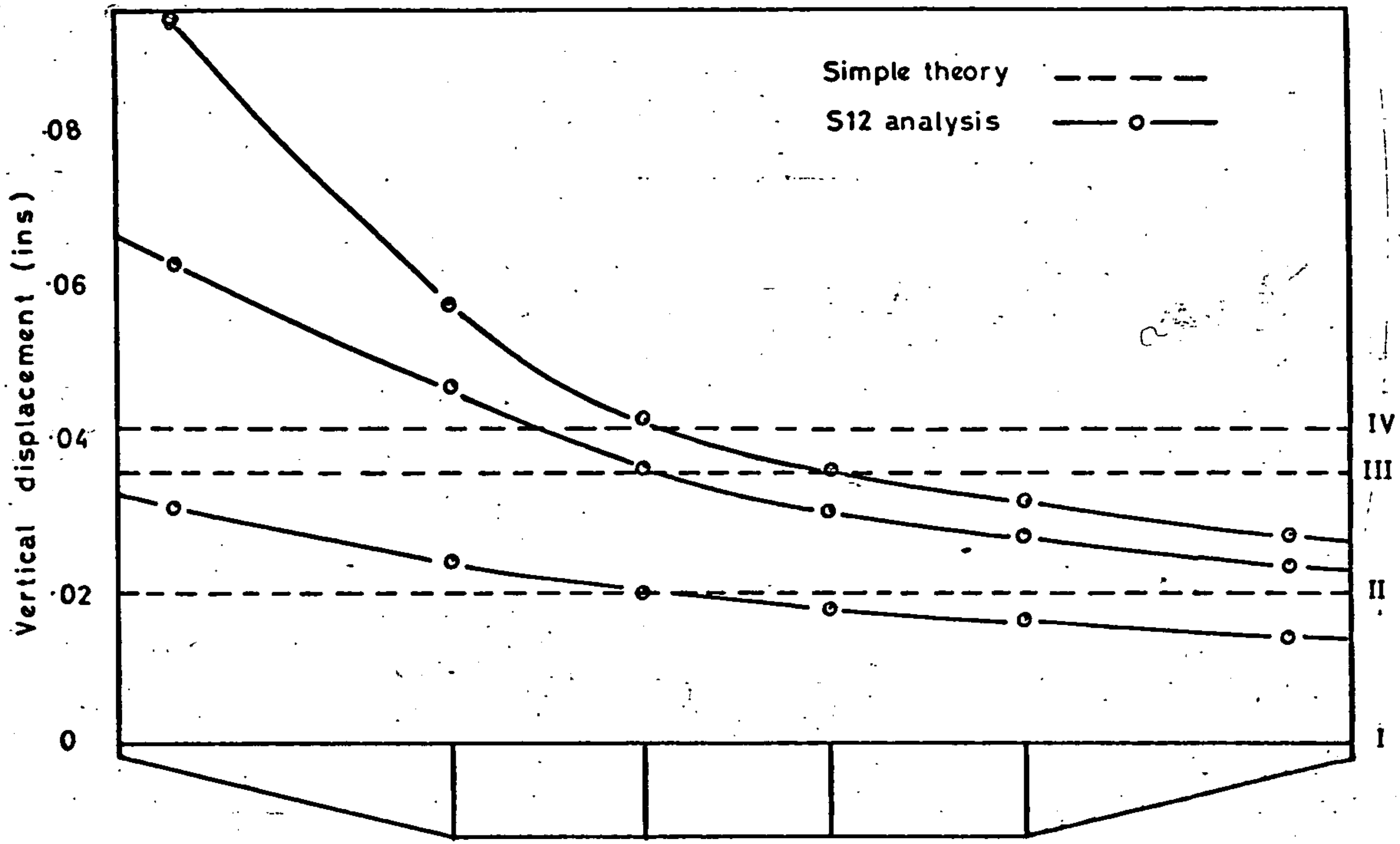

Fig.92 Vertical displacement of transverse sections under POINT1 (GHS12/1)

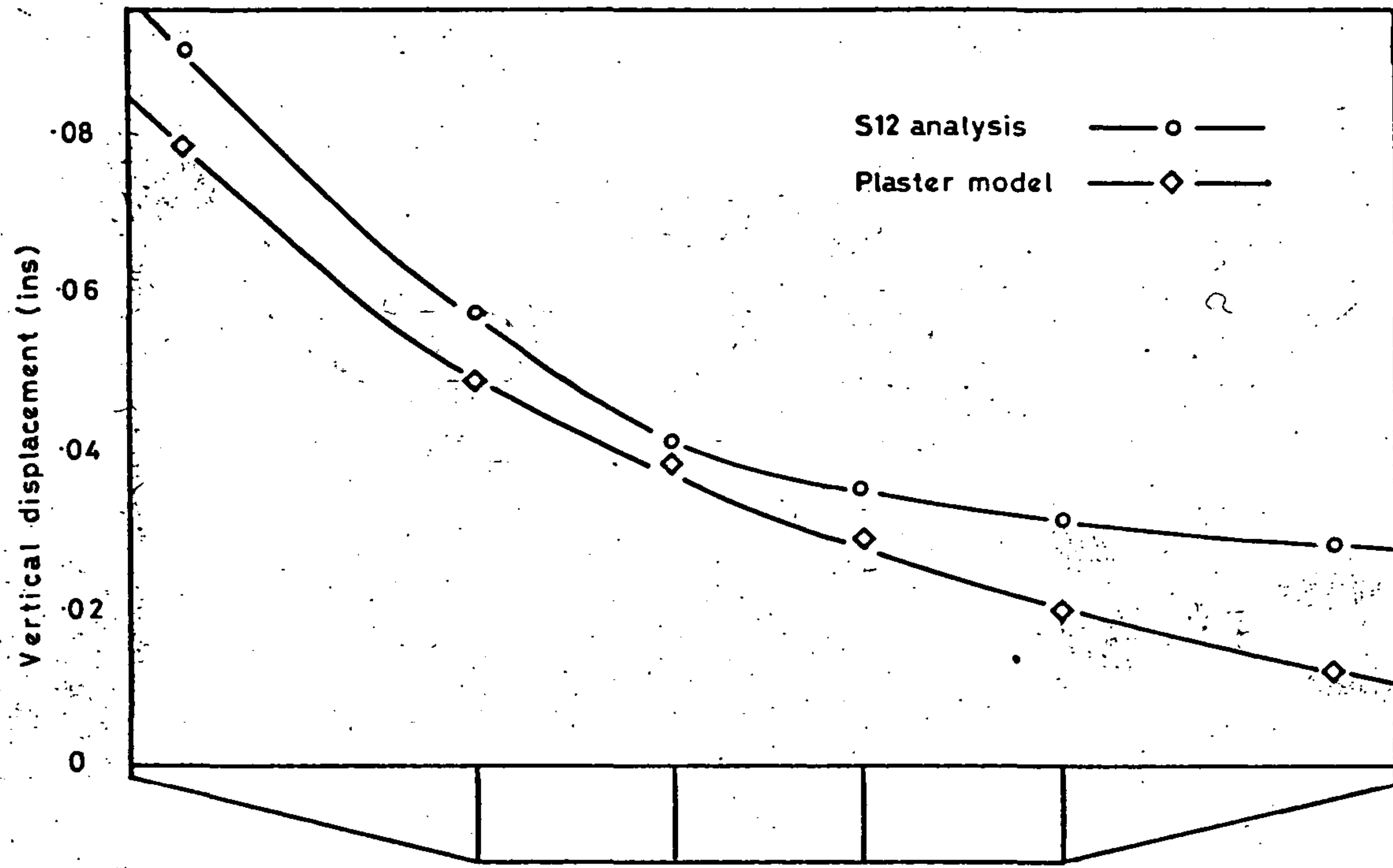

Fig. 93 Vertical displacement of centre line under load POINT1 - model & finite element comparison

(178)

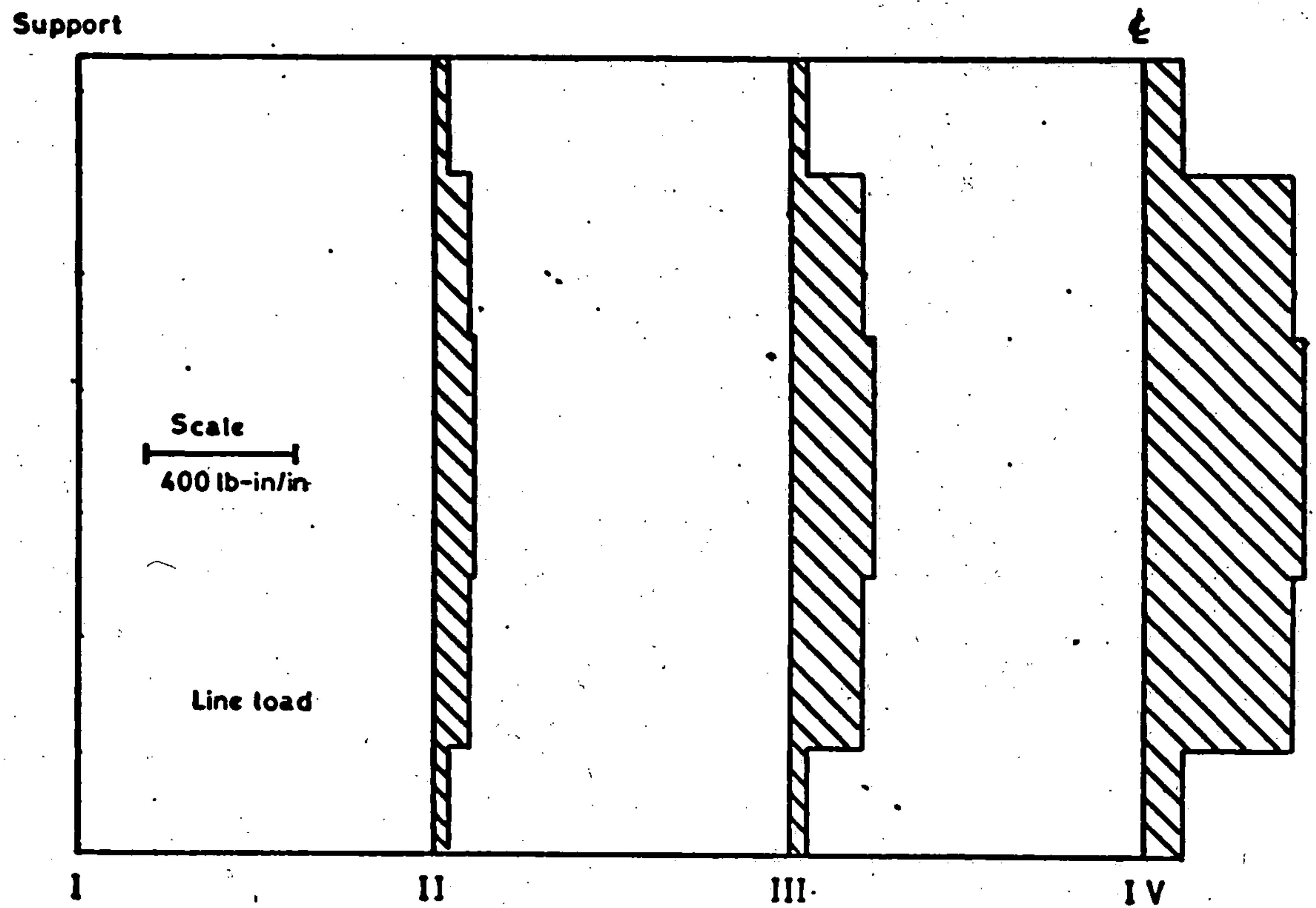

Support
℄
Scale
400 lb-in/in
Line load
I
II
III
IV

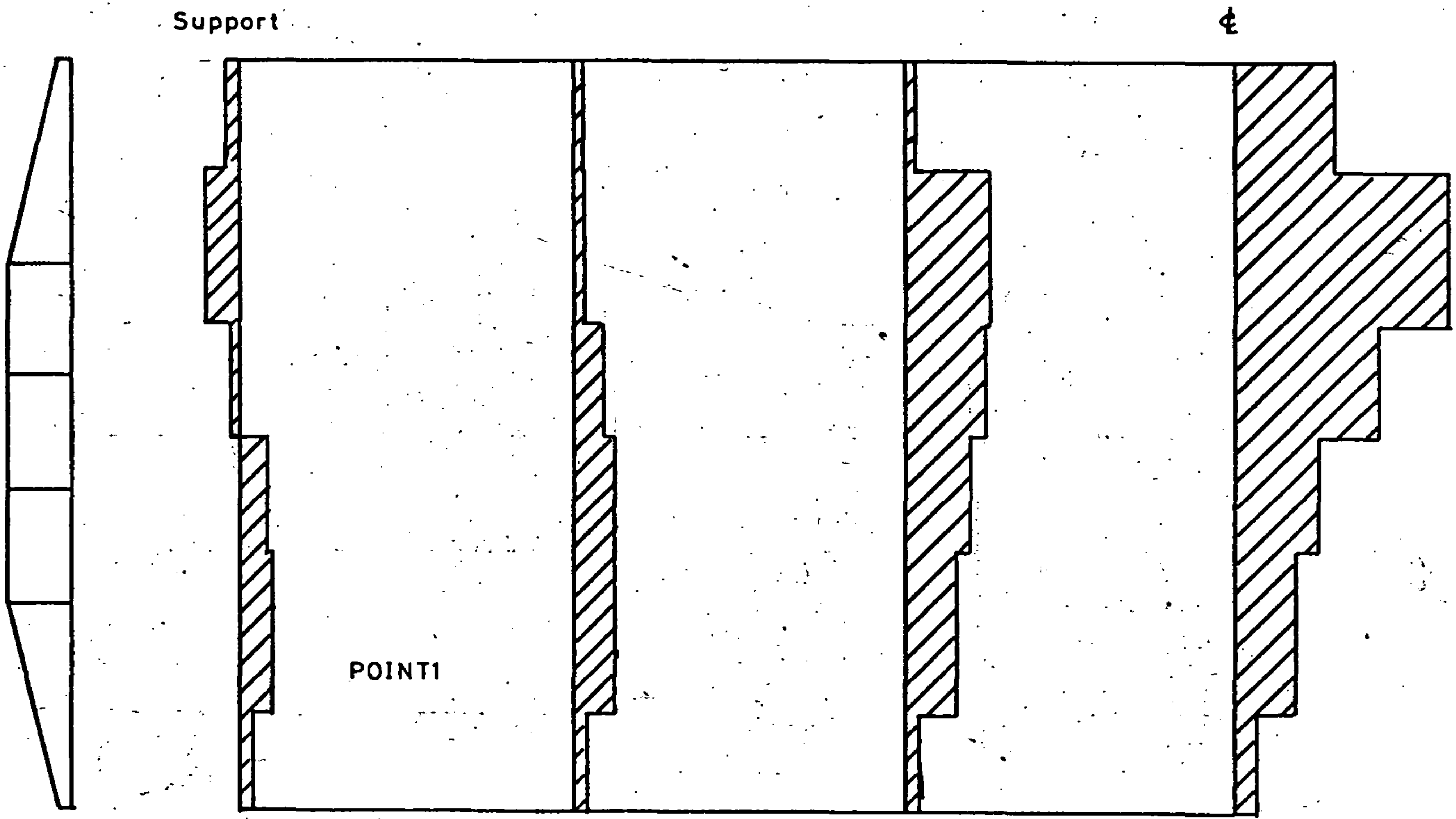

Fig. 94 Distribution of bending moment for POINT1 (GHS12/1)

From the independent rotational degrees of freedom it is also possible to compute the shear strains, in particular the in-plane shear strain distribution os shown in fig.95 for the top slab. From this it can be seen that this shear strain does not play an important part in the uniform load case but acts significantly to transfer the load from the edge to the centre in the load case POINT1.

In fig.96 the longitudinal displacements of the top slab are shown, displaying the distortion of the slab under the two load cases considered. These are consistent with the shear distributions in fig. 95.

The main point of interest to emerge from these results is the negative moment generated in part of the diaphragm over the supports for load case POINT1. The origin of this is discussed in the next section.

8.5 Action of bridge under load case POINT1

A simplified model of the bridge can be considered as composed of two independent longitudinal beams connected by the rigid diaphragm at the supports. This diaphragm has the effect of ensuring that the end rotations of each beam remain the same. The point load is supported bu one beam and the end rotation of this beam is resisted by the stiffness of the unloaded beam. This resistance reduces the deflection of the loaded side from that expected if it were simply supported and independent. This reduction causes a negative moment on the diaphragm where it is attached to the loaded beam. Detailed calculations show that only about half of the total load can be transmitted from one side to the other by this mechanism. Another action must be sought to account for the remainder.

As noted in the previous section, significant shear

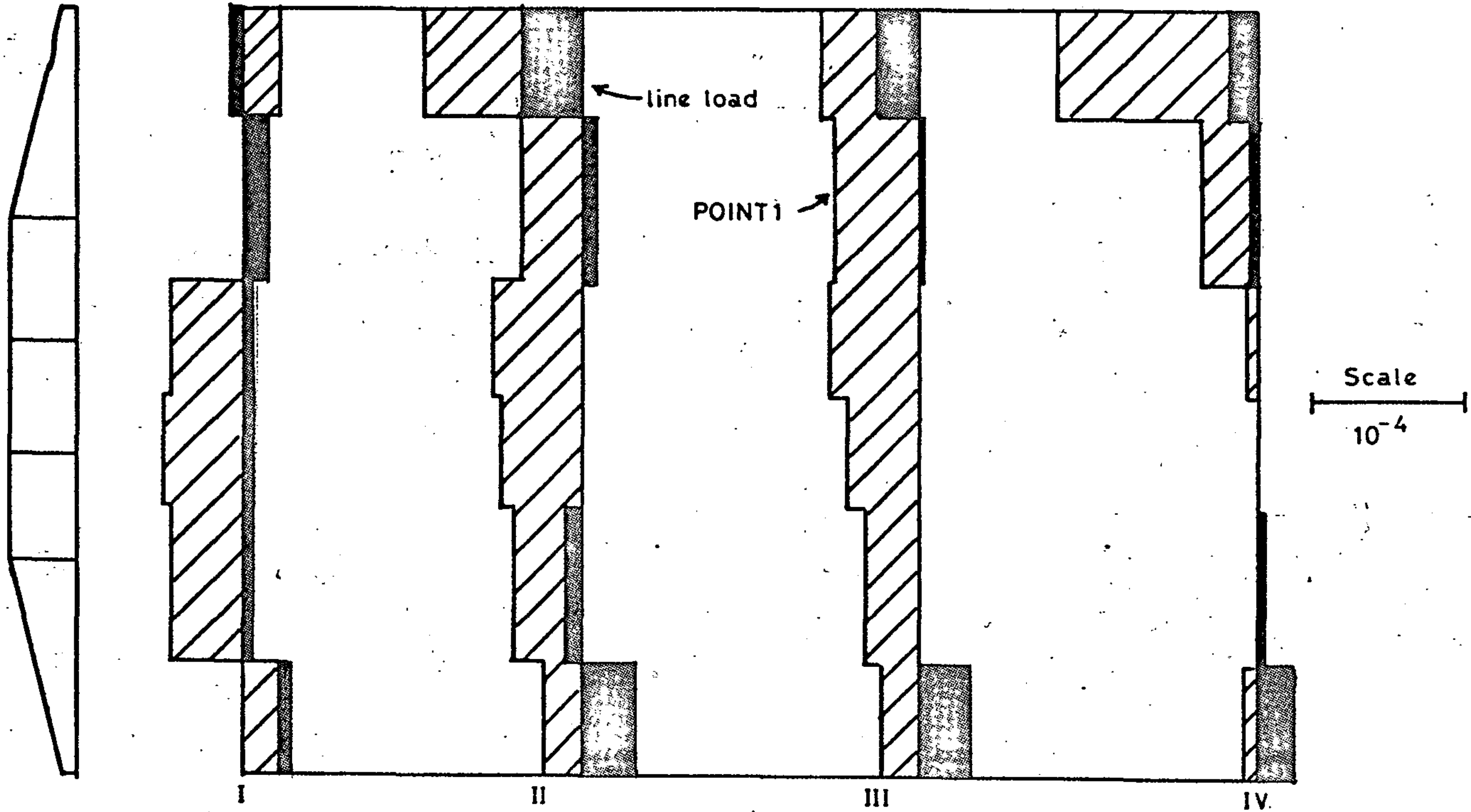

Fig. 95 Shear strain in top slab for line load & POINT1 (GHS12/1)

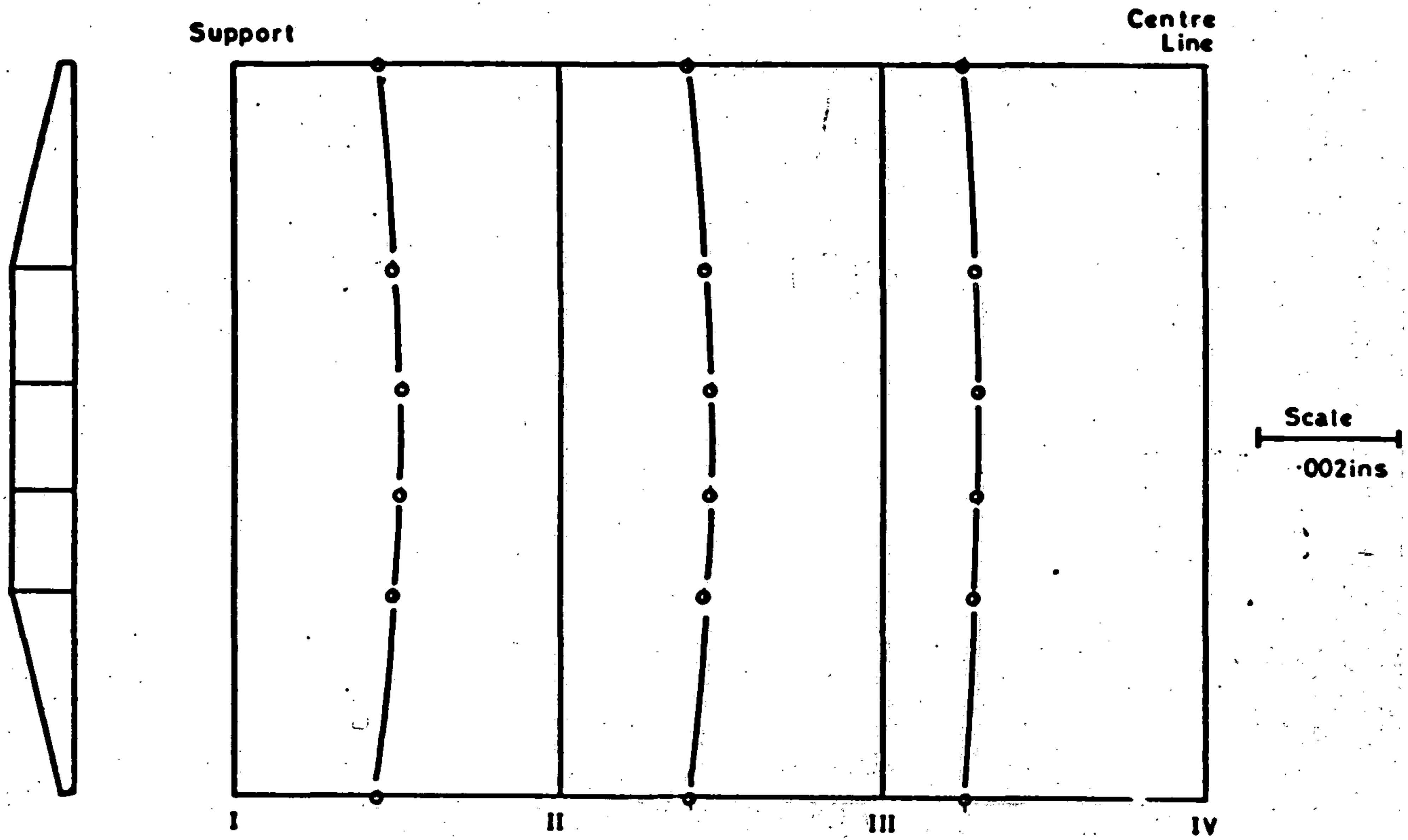

Fig.96 Longitudinal displacement of top slab under line load (GHS12/1)

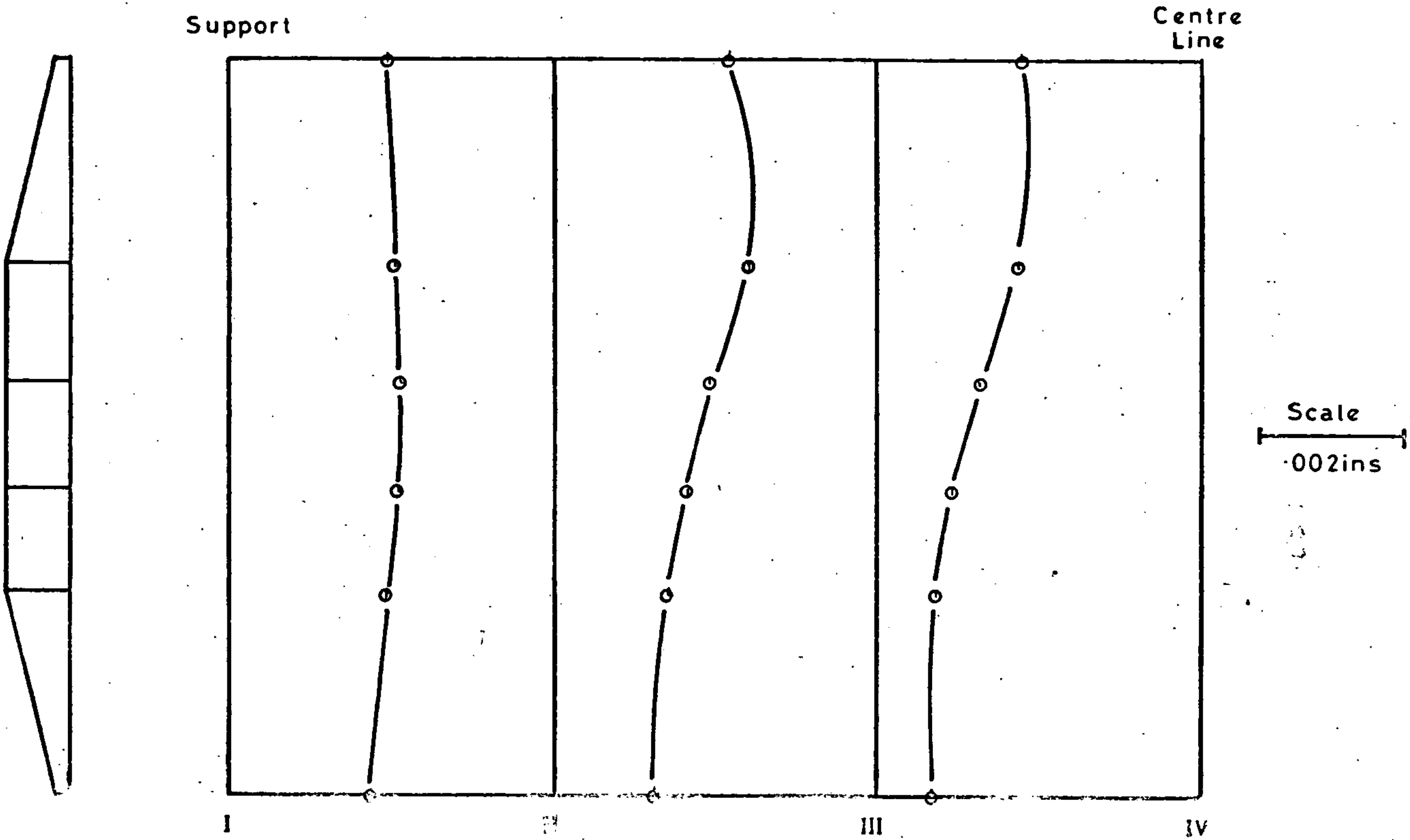

Fig. 96 Longitudinal displacement of top slab under loadcase POINT1

stresses are generated in the top and bottom slabs. If the bridge is considered "sliced" into two pieces longitudinally these shear stresses generate shear forces on the "exposed" edges which combine to result in a distributed moment along the length of the slice. This distributed moment acts to reduce the central deflection of the loaded side and transmit the load directly to the other side.

Chapter Nine   Gateshead Viaduct (modified)

9.1 Proposed structural modifications

From the results of the last chapter it is possible to suggest some modifications to the original structure and these will be examined in this chapter. In particular the effects of additional diaphragms will be considered. Such diaphragms will increase the cost of the structure due to additional labour, extra shuttering, difficulty of recovering the shuttering and other constructional reasons, thus their effectiveness in reducing stresses and deflections must be studied. It should be noted that the modifications reported below were made with only minor alterations to the original pack of data cards - no renumbering of nodes or similar changes were necessary. The ease with which these modifications can be made is part of the power of the finite element method.

Whilst the analysis reported in chapter eight used a line support across the full width of the bottom slab, the model and structure had only two point supports. (The model tests for point loads were in fact carried out with the line support but further tests used the real point supports.) For the convenience of the analysis these supports have been taken under the two inner webs. The actual model supports were 4 ins apart instead of 5 ins but considering the thickness of the webs - 1 in - this is not significant.

The action of the bridge in transmitting a load from the outer webs to the supports might be aided if more of the load were taken directly in a transverse direction to all the main webs rather than via the massive diaphragm at the supports. An extra diaphragm at the centre line should thus modify the stress distribution quite significantly. Thus for the first structural modification a centre line diaphragm of thickness 2 ins was added and to keep the volume of material more or less constant the thickness of the support diaphragm was reduced to 4 ins. This main diaphragm cannot be reduced much further as an additional design criterion is with the M.O.T. HB load directly over the diaphragm which then takes the full load as a transverse cantilever.

This process was then extended by adding further diaphragms to produce an "egg-box" type of structure. Five diaphragms were inserted at equal distances between the supports. The total volume was again kept roughly constant. Here the support diaphragm can be reduced below the previous design thickness because the length of the heavy vehicle is such that it is supported by three adjacent diaphragms acting as cantilevers. The support and centre line diaphragms were taken as 2 ins thick and the rest as 1 in thick.

To summarise, the following three structures were analysed and are to be presented below:

GHS12/2	The same structure as that in chapter eight but with two point supports instead of a line support
GHS12/3	As GHS12/2 but with a centre line diaphragm of 2 ins and a support diaphragm reduced to 4 ins thick.
GHS12/4	Centre line and support diaphragms 2 ins thick, additional diaphragms 1 in thick.

9.2 Loading cases

For this comparison four load cases were analysed, of which three were simple point and line loads and the fourth was based on MOT requirements.

The first three cases were:

LINE: uniform line load across centre line, total load 1000 lb.

POINT1: Point load of 1000 lb at A (see fig. 83)

POINT2: " " " " " B (" " ")

The last load case, referred to below as REAL, consisted of the following loads required by MOT:

(a) Dead load

The dead load of the full structure - 150 lb/cu.ft. - was scaled to the model dimensions and applied as a distributed load to the top slab. The load applied to the overhanging cantilevers was increased by a factor of 2.59 to represent the continuation of the structure over adjacent spans.

Dead load on main span = 306 lb/sq.ft.

Dead load on cantilevers = 722 lb/sq.ft.

(b) Lane loads (HA)

The full scale live loads were taken from BS153 with a load factor of 2½ and do not need scaling for the model effect. Again, the loads on the cantilevers were increased by a factor of 2.59. The main span was loaded by:

Two lanes (on carriageway with HA knife load) 515 lb/sq.ft

Fast lane (on carriageway with HB load) 398 lb/sq.ft.

Remainder of top slab 340 lb/sq.ft.

The knife edge load HA was taken as 232 lb total.

(c) Heavy vehicle.

The HB load was taken in the analysis as a total of 1440 lb and represents a full scale load of 370 tons. This load was distributed over the outside element adjacent to the centre line.

9.3 Discussion of the results

Looking first at displacements, Table 20 gives the maximum vertical displacements on the centre line. These results show that as expected the addition of a centre line diaphragm, GHS12/3, reduces the maximum displacement. The lateral distortions across sections I (over supports) to IV (at centre line) are shown in Figs. 97 to 109. Figs. 97 - 105 show vertical displacements across all sections for each separate load case and structure. The centre line displacements for each load case are combined for each structure in figs. 106 - 109. As can be seen from the latter set of figures the single additional diaphragm, GHS12/3, causes the transverse distortions to be reduced but the results from adding extra diaphragms, GHS12/4, are very similar to those for GHS12/3. These changes are most marked for the POINT load cases but are still present in all cases.

The design of the supports is dependent on the rotation of the diaphragm over the supports but it was found that this is unaffected by the structural changes.

As in chapter eight, the total bending moment at the four sections I - IV has been calculated. (Table 21.) These results provide a check on the accuracy of the calculations, both of the strains from the finite element analysis and the subsequent derivation of bending moments.

In particular the non-zero total moments at the supports for the point and line loads is a measure of the errors in the other values. The average error is about 4% of the centre line value. The corresponding simple beam solution is also shown in the table. The average error at the centre line is 2% from this solution.

Attention was drawn in chapter eight to the distribution of bending moment across transverse sections and the way in which concentrated loads are transferred to all parts of the structure. These distributions for the POINT load cases and the "REAL" loads are shown in figs. 110 - 112. In each of these figures the results for each structure are shown on a separate sheet. For ease of comparison the two modified structures - GHS12/3 and /4 are transparencies. The bottom page in each case is the result for the structure GHS12/2.

The mechanism by which loads at the outer edge of the centre line are transferred to the supports was discussed in chapter eight and was shown to generate a negative bending moment at the support. Table 22 shows how this is reduced systematically by the continued introduction of extra diaphragms, confirming the hypothesis that such structural changes would assist the distribution of such loads directly to all the main webs. Fig. 111 particularly shows how this occurs.

For the REAL load case the maximum bending moment on the centre line increases with the addition of the single central diaphragm - from 1515 lb-in/in to 1722. (see table 23.) This is due to the reduced lateral distortion, plotted in fig. 109, causing more load to be transferred to the centre webs. This change in bending moment distribution can also be seen in fig. 112.

However, the maximum bending moment an the centre line for the third structure, GHS12/4, with several diaphragms shows a reduction to 1490 lb-in/in. (Table 23) The distribution of bending moment across the centre line is now again more uniform but that at the support has become more concentrated over the supports. The support diaphragms were reduced in thickness from 5 ins for the original structure GHS12/2 to 4 ins for /3 and 2 ins for /4. The effect of a larger negative support bending moment on the central webs is to reduce the positive bending moment on the centre line.

These effects are due to the greater flexibility of the support diaphragm coupled with the more homogeneous behaviour of the structure with its "egg-box" type layout.

The plaster model referred to in chapter eight was also tested to failure under the loading case REAL. It was observed that the failure resulted from a longitudinal crack opening in the top slab adjacent to and parallel with one of the main supported webs. Table 25 shows the transverse stress in the slab calculated for this load case by the finite element analysis. These results show that this particular stress is tensile and of the same order as the major longitudinal stress at the centre line. Furthermore, this stress increases with the reduction in the thickness of the support diaphragm.

In general, these results indicate that the addition of diaphragms to this structure does not produce as significant changes in the stresses and displacements as might be expected.

	Line load	POINT1	POINT2	REAL
GHS12/2	.0476	.1012	.0612	.2164
GHS12/3	.0457	.0872	.0598	.2095
GHS12/4	.0454	.0885	.0610	.2101

Table 20: Maximum vertical displacement on Centre line (ins) (All at point A)

Section	Line load	POINT1	POINT2	REAL
I support	-369	-299	-419	-19177
	-415	-387	-464	-19357
	-453	-604	-693	-20930
	(0)	(0)	(0)	
II	3457	3919	3378	13659
	3473	3570	3730	13516
	3472	3645	3534	13770
	(3667)	(3667)	(3667)	
III	6725	6934	6681	31091
	6762	6728	6776	31363
	7235	7054	7126	31900
	(7333)	(7333)	(7333)	
IV centre line	10722	10716	10822	35438
	10695	10607	10686	35017
	11029	10829	10998	35340
	(11000)	(11000)	(11000)	

Table 21: Total bending moment (lb-in) at four transverse sections for GHS12/2 - /4 and for simple beam ( ).

	POINT1	POINT2
GHS12/2	-177	-156
GHS12/3	-148	-100
GHS12/4	-109	-76

Table 22: Maximum negative bending moment at support. (lb-in/in)

	line load	P. INT1	POINT2	REAL
GHS12/2	425	629	715	1515
GHS12/3	440	571	525	1722
GHS12/4	443	585	558	1490

Table 23: Maximum bending moment (lb-in/in) on centre line. All at Point B except for REAL which were at Point C

	Point A	Point B	Point C
GHS12/2	121	385	425
GHS12/3	112	375	440
GHS12/4	114	396	443

Table 24: Distribution of bending moment (lb-in/in) along centre line for Line load. (See fig. 83 for position of A,B &C)

	Transverse stress in top slab above support points.	Longitudinal stress in slab at Point C at centre
GHS12/2	1530	-1600
GHS12/3	1590	-1800
GHS12/4	1760	-1600

Table 25: Comparison of transverse stress in top slab above support with longitudinal stress at Point C on centre line for REAL load case (p.s.i.)

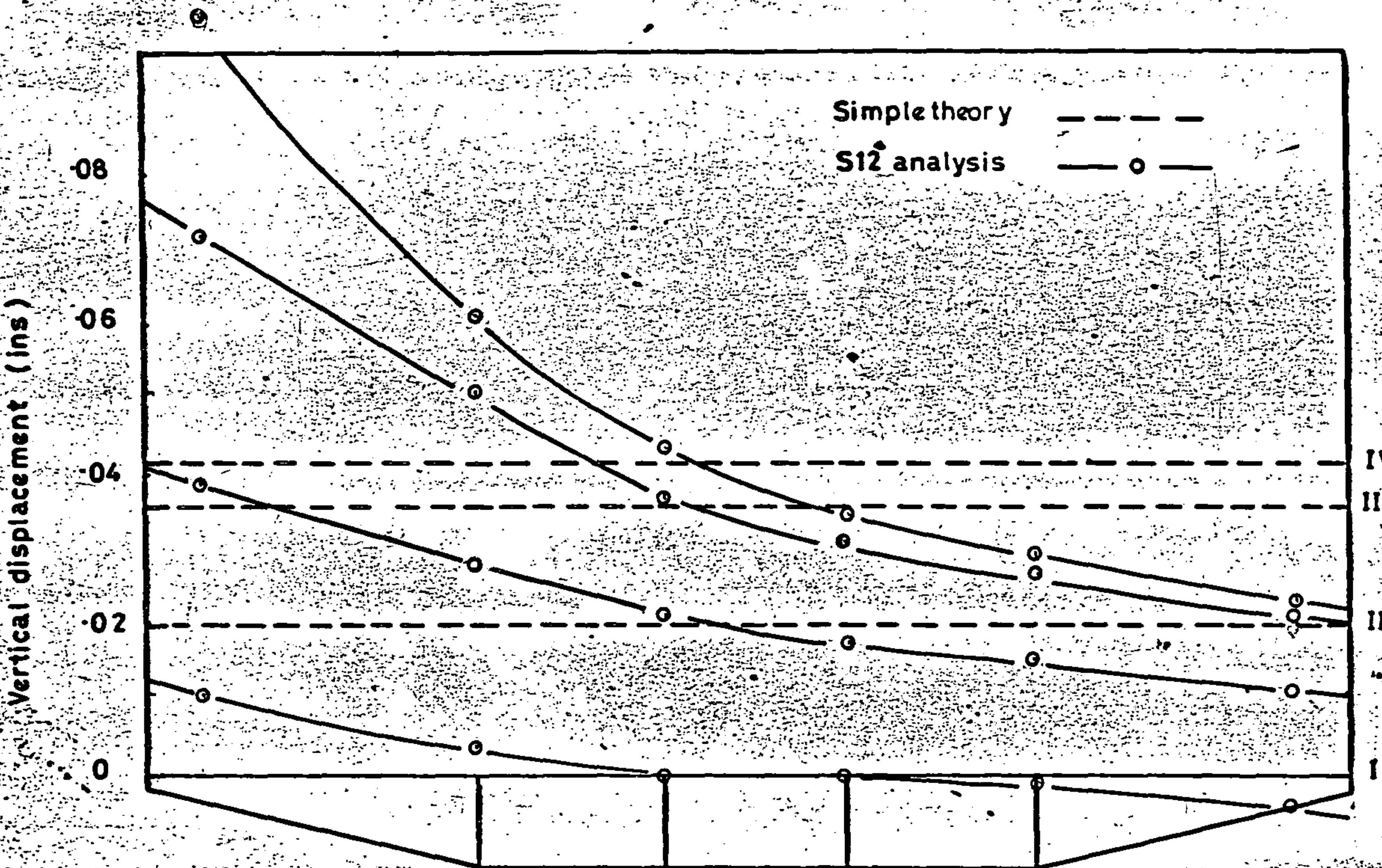

Fig. 97 Vertical displacement of transverse sections under POINT1 (GHS12/2)

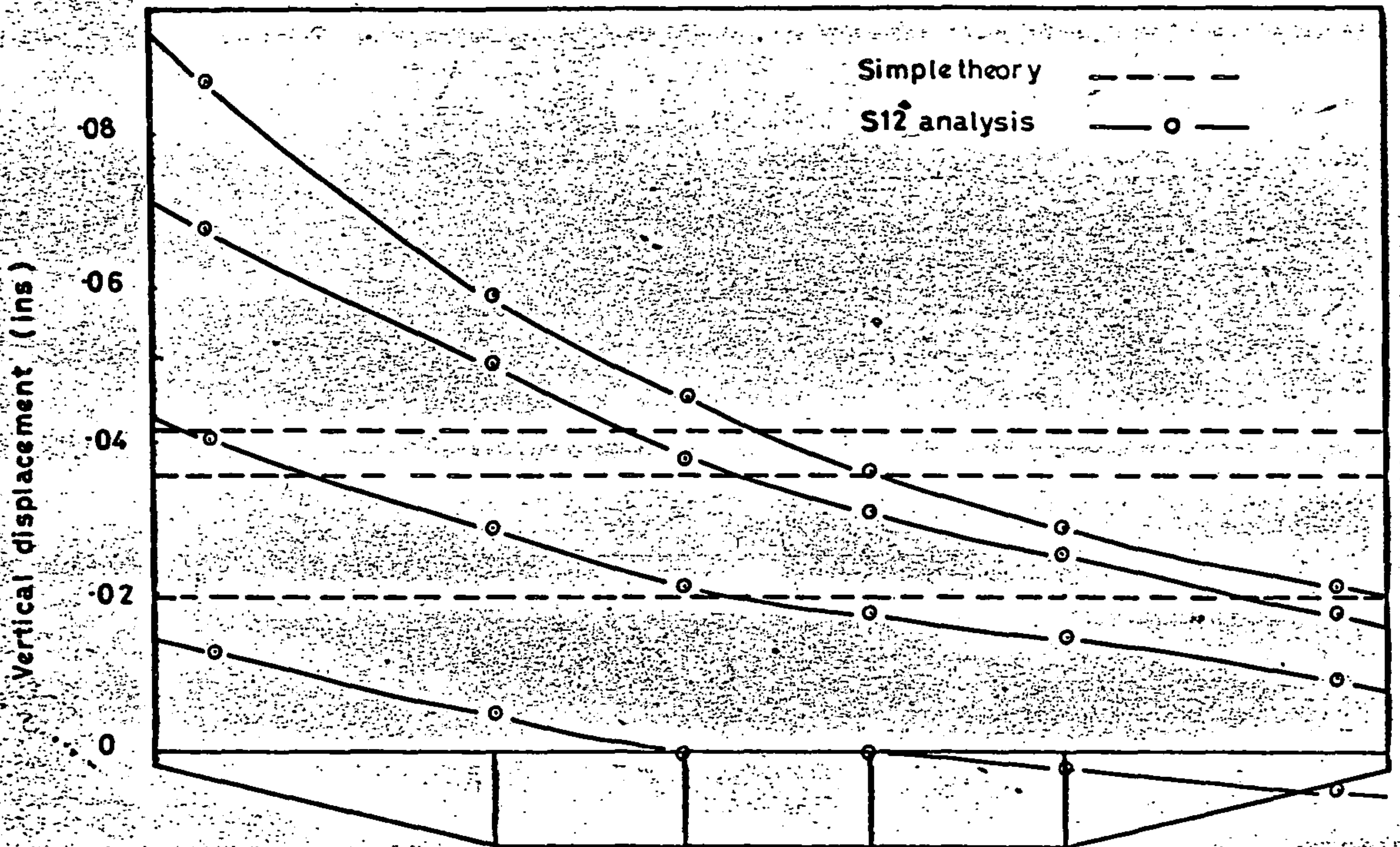

Fig. 98 Vertical displacement of transverse sections under POINT1 (GHS12/3)

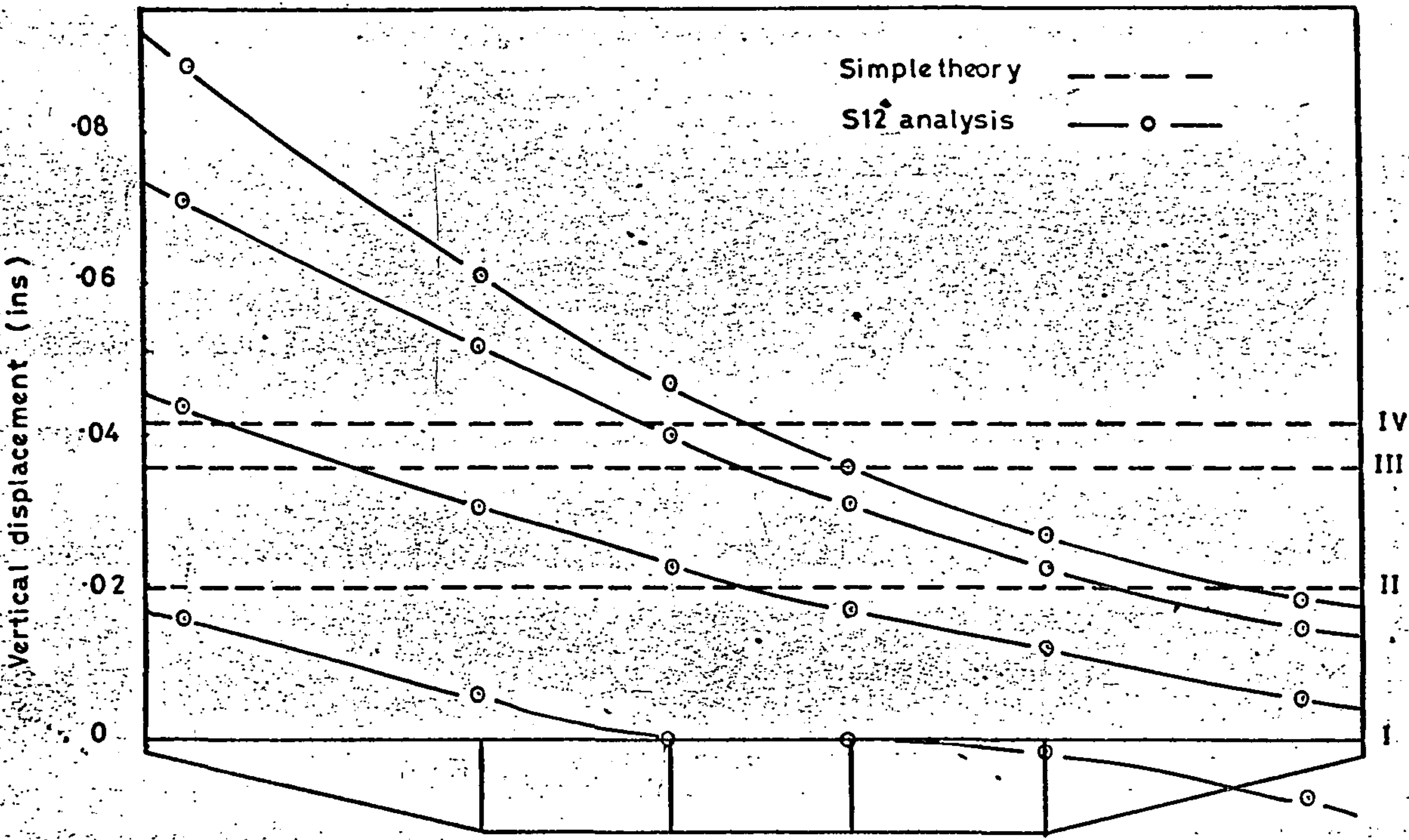

Fig. 99 Vertical displacement of transverse sections under POINT 1 (GH S12/4)

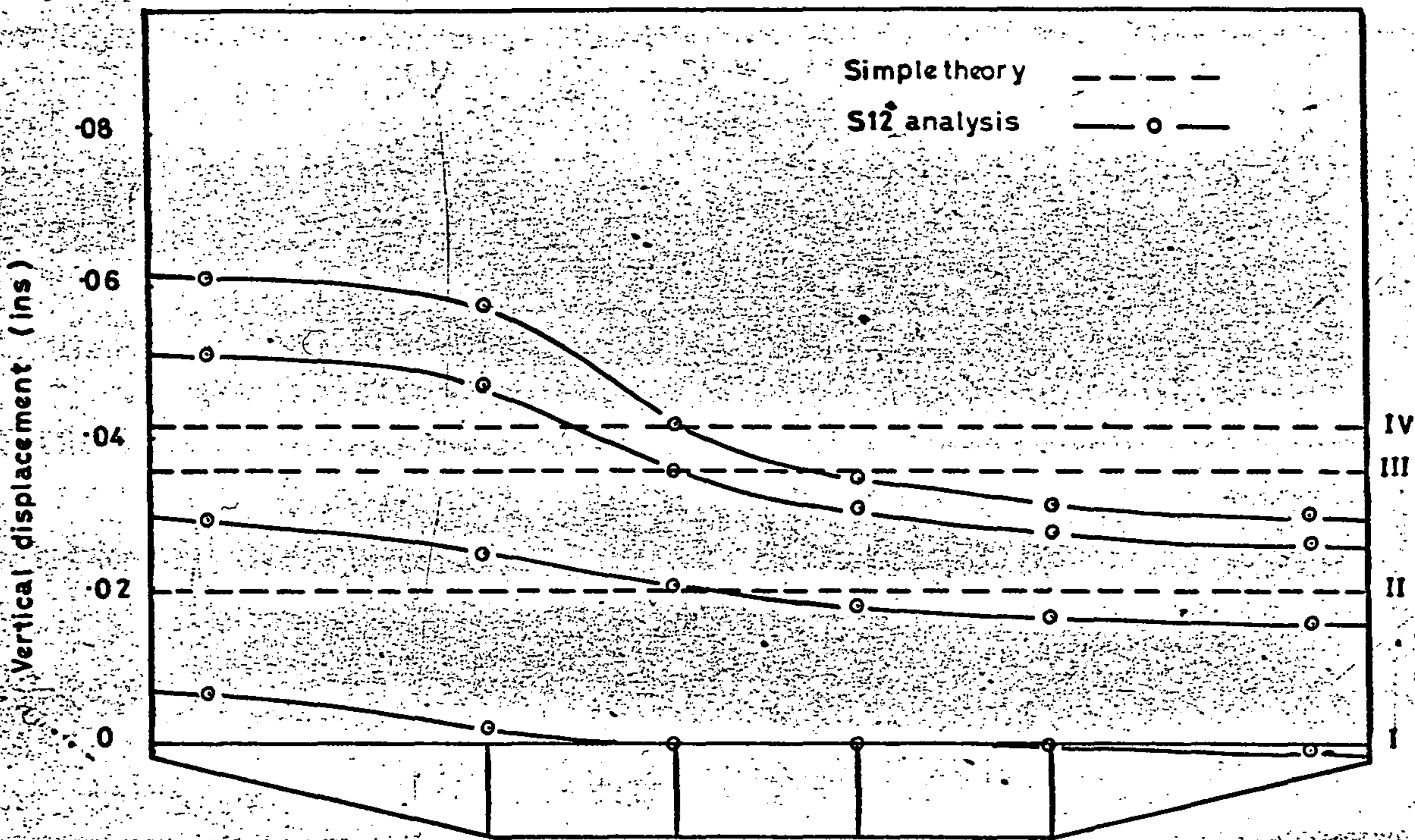

Fig.100 Vertical displacement of transverse sections under POINT 2 (GHS12/2)

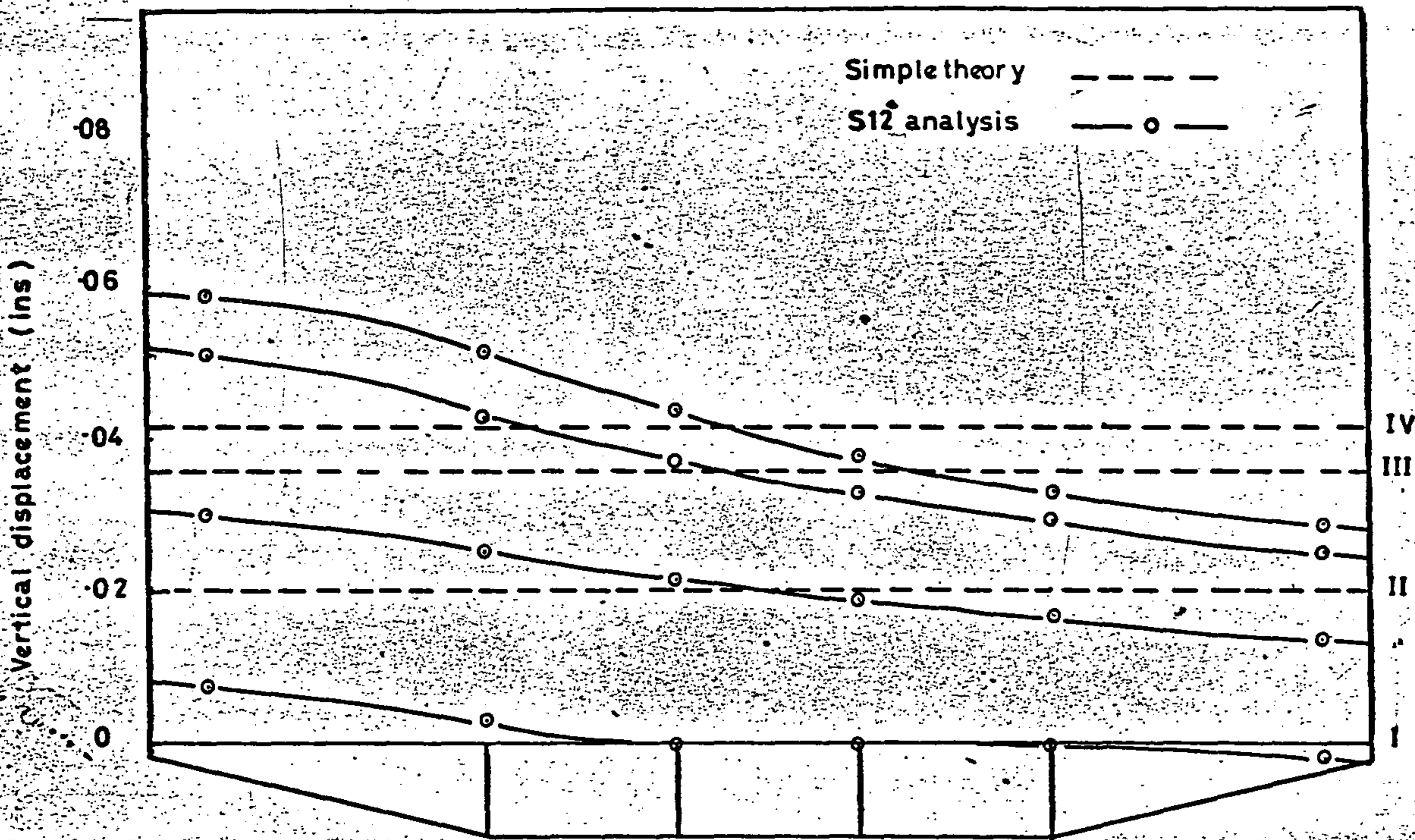

Fig.101 Vertical displacement of transverse sections under POINT 2 (GHS12/3)

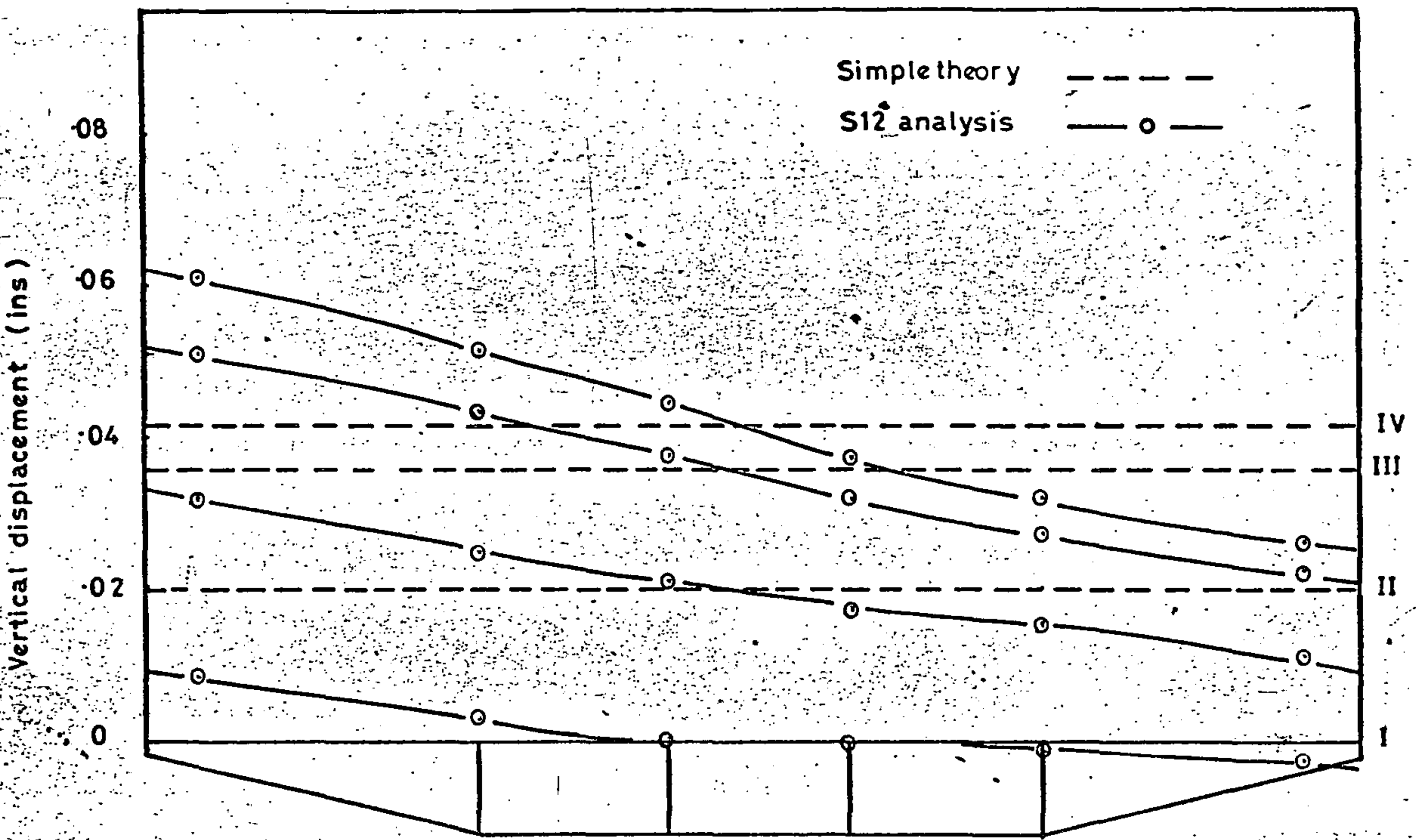

Fig.102 Vertical displacement of transverse sections under POINT2 (GHS12/4)

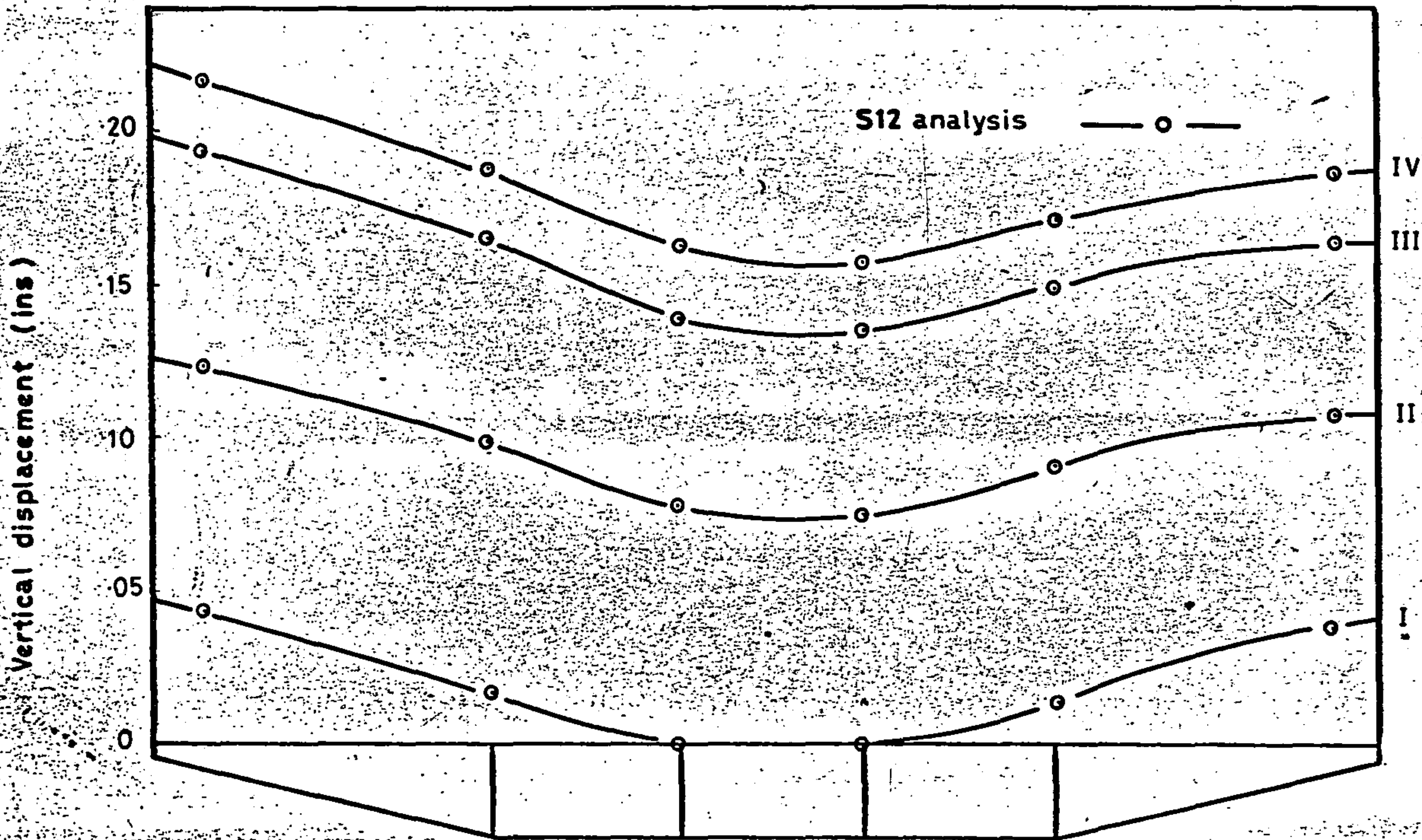

Fig.103 Vertical displacement of transverse sections under REAL load (GH S12/2)

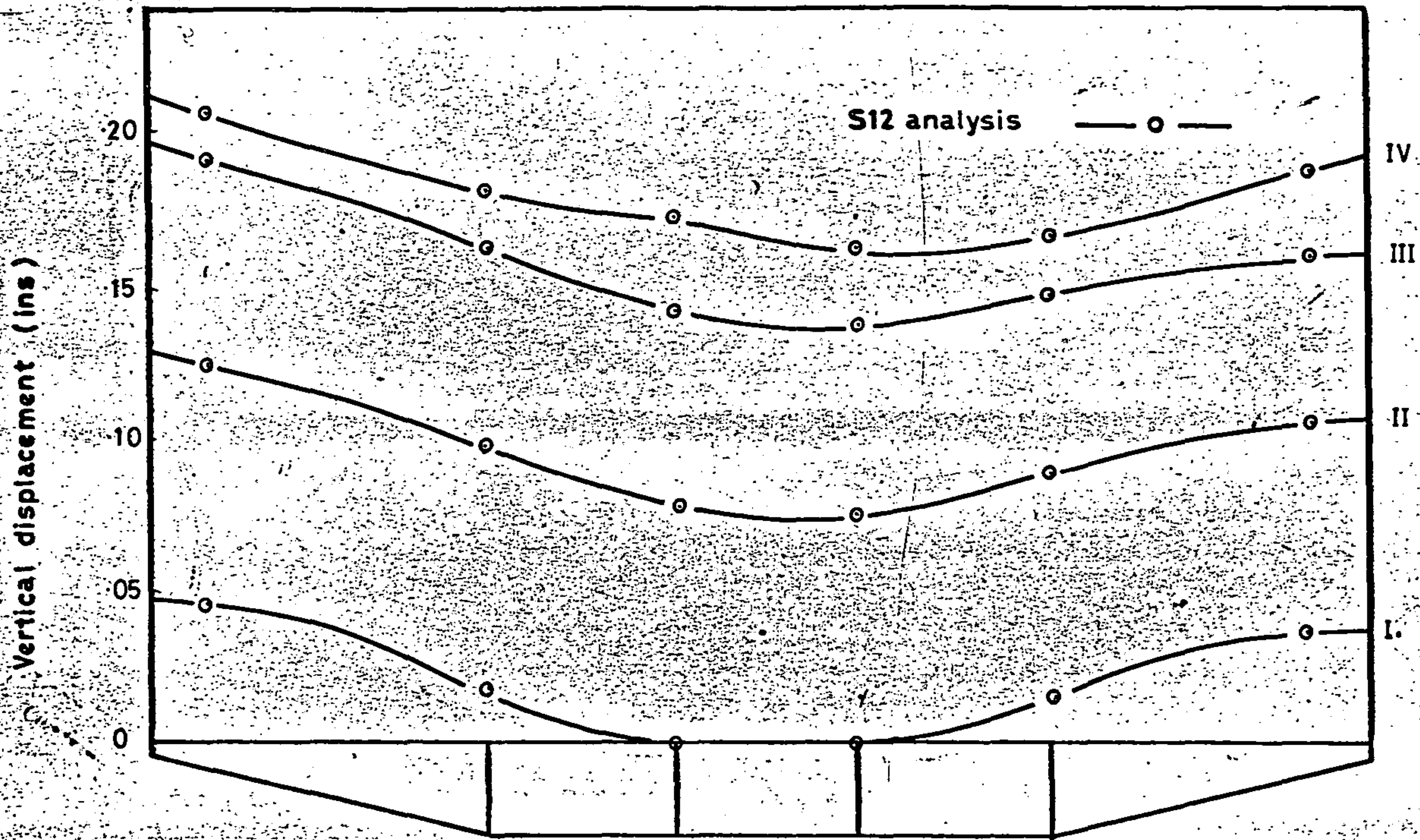

Fig. 104 Vertical displacement of transverse sections under REAL load (GH S12 / 3)

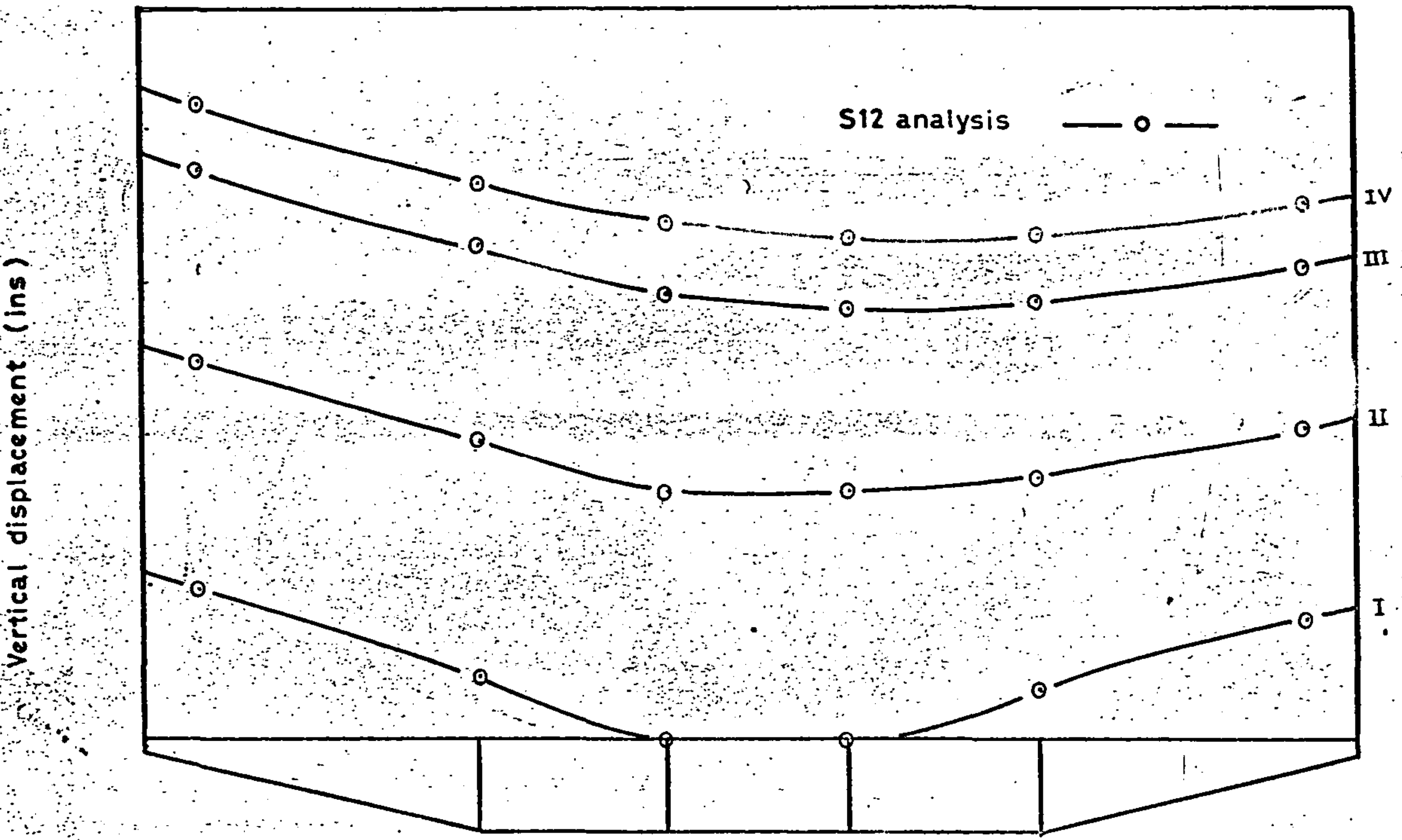

Fig.105 Vertical displacement of transverse sections under REAL (GHS12/4)

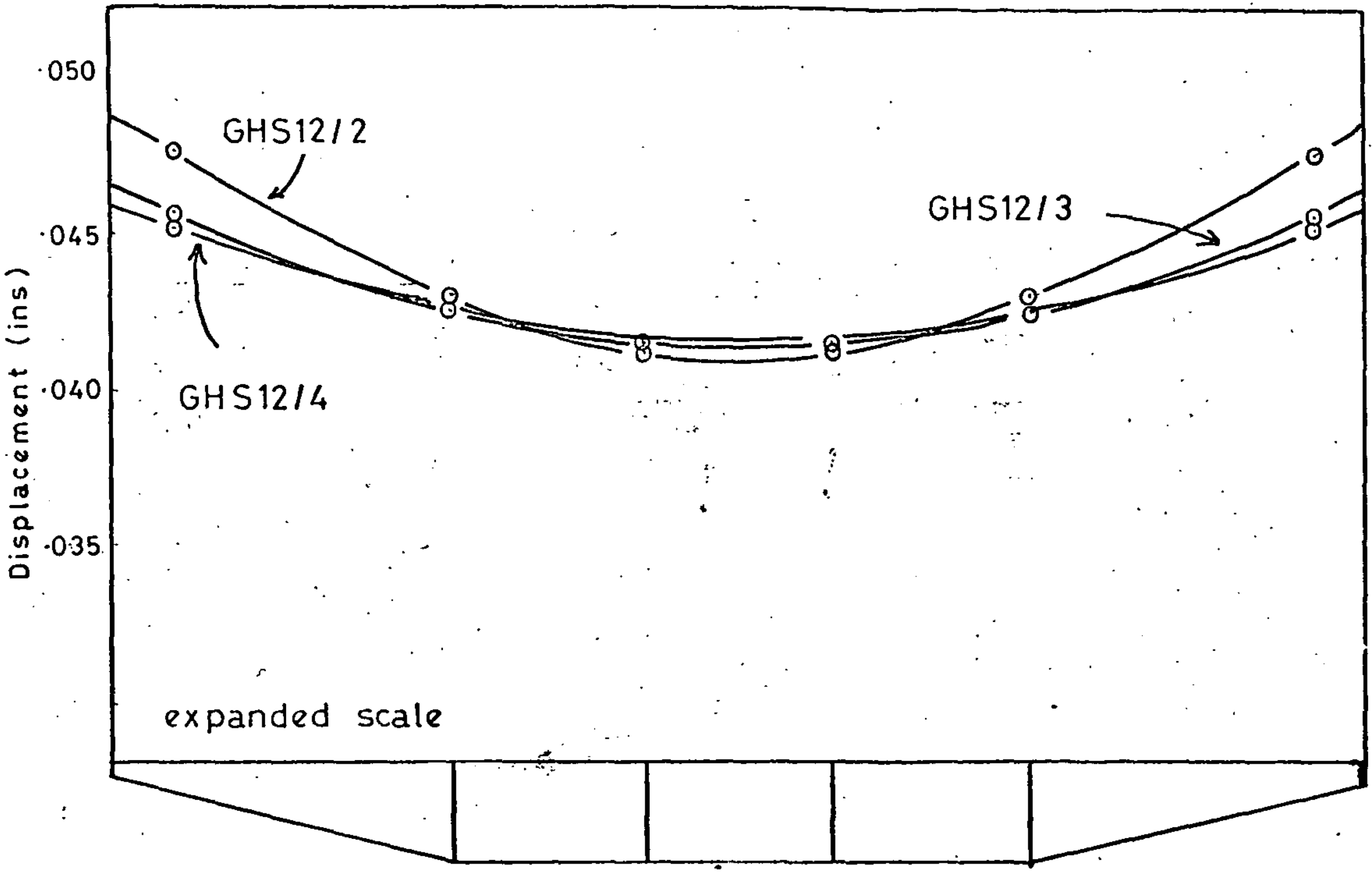

Fig. 106 Vertical displacement of centre line for Line load

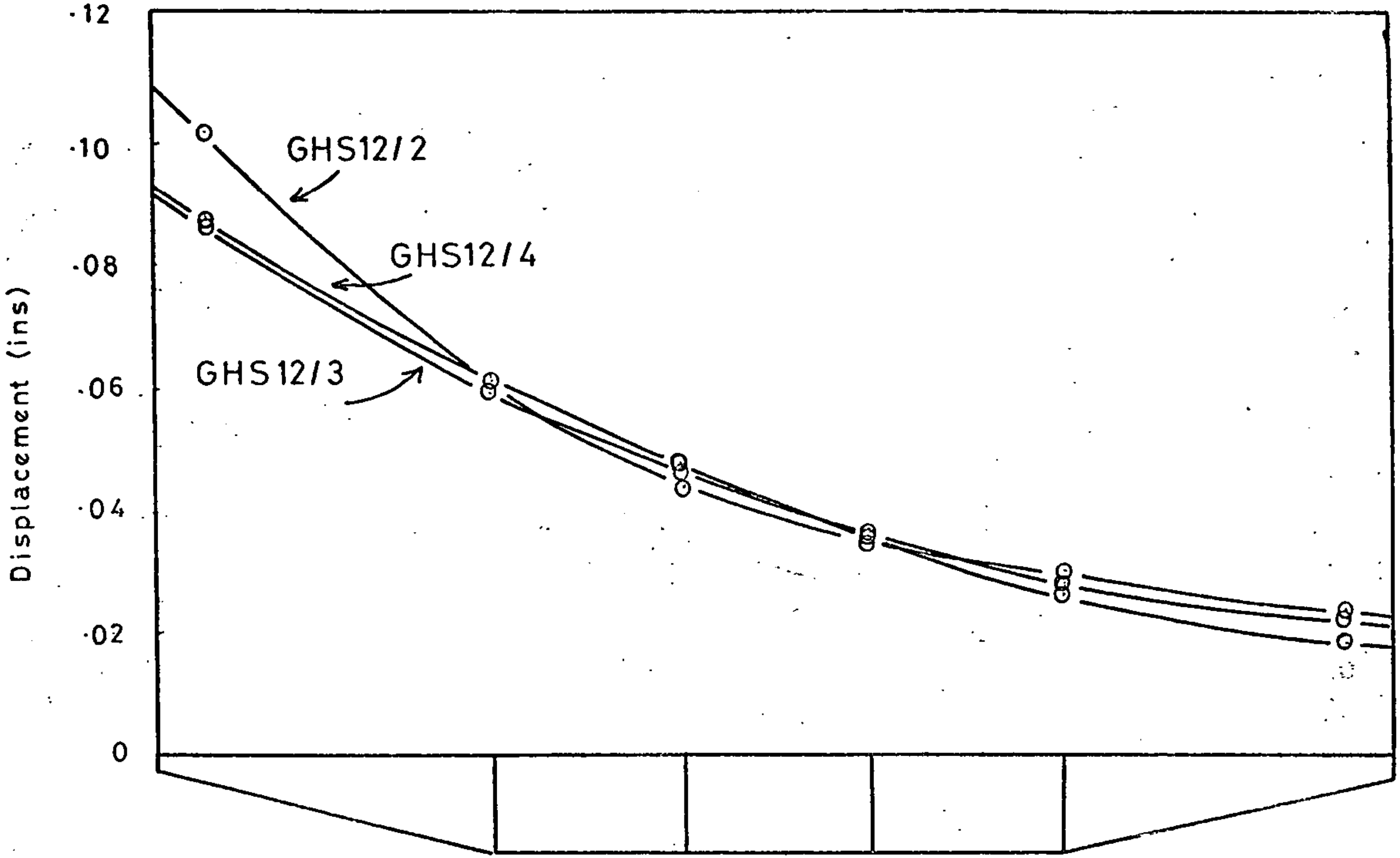

Fig. 107 Vertical displacement of centre line for POINT1

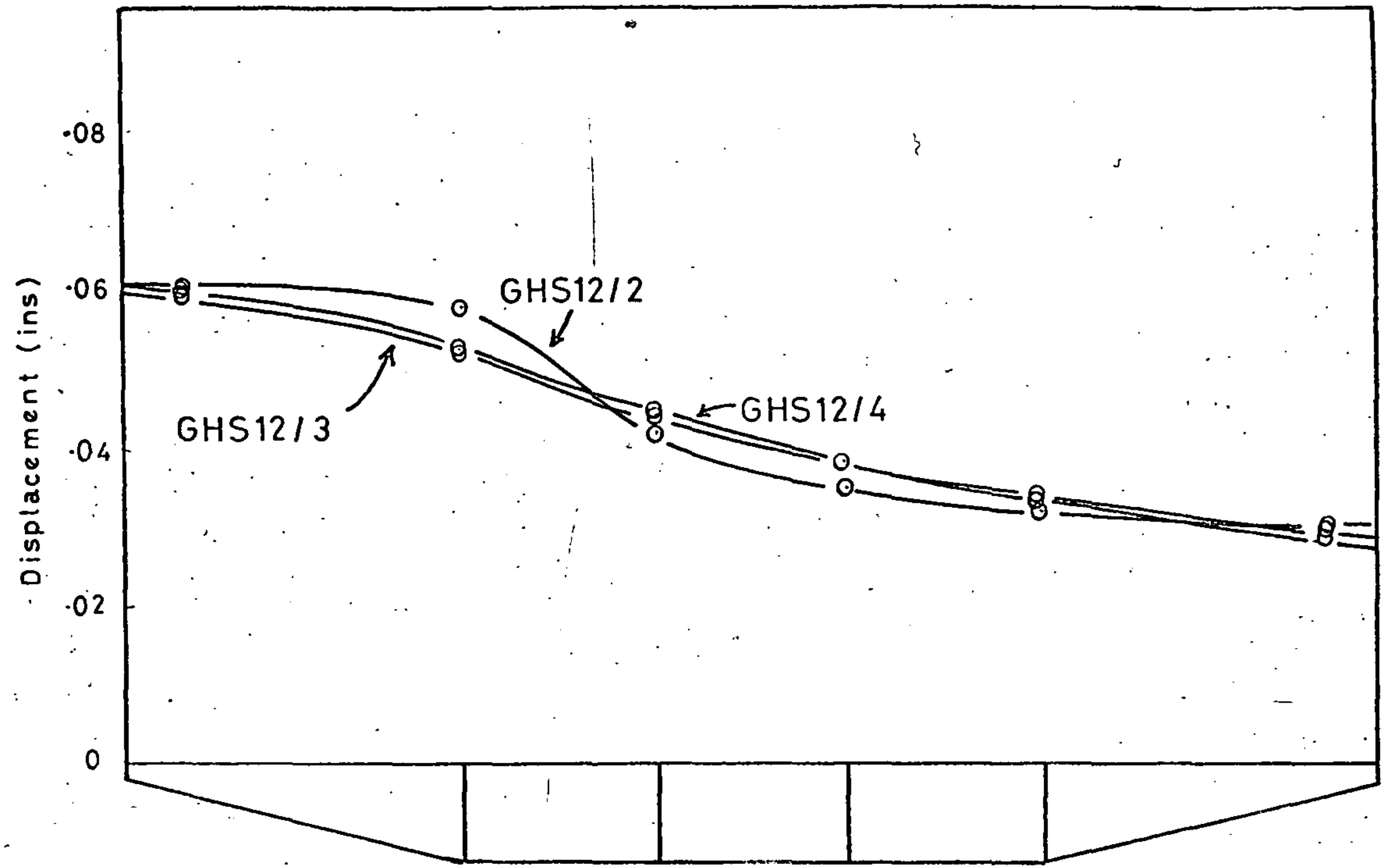

Fig. 108 Vertical displacement of centre line for POINT 2

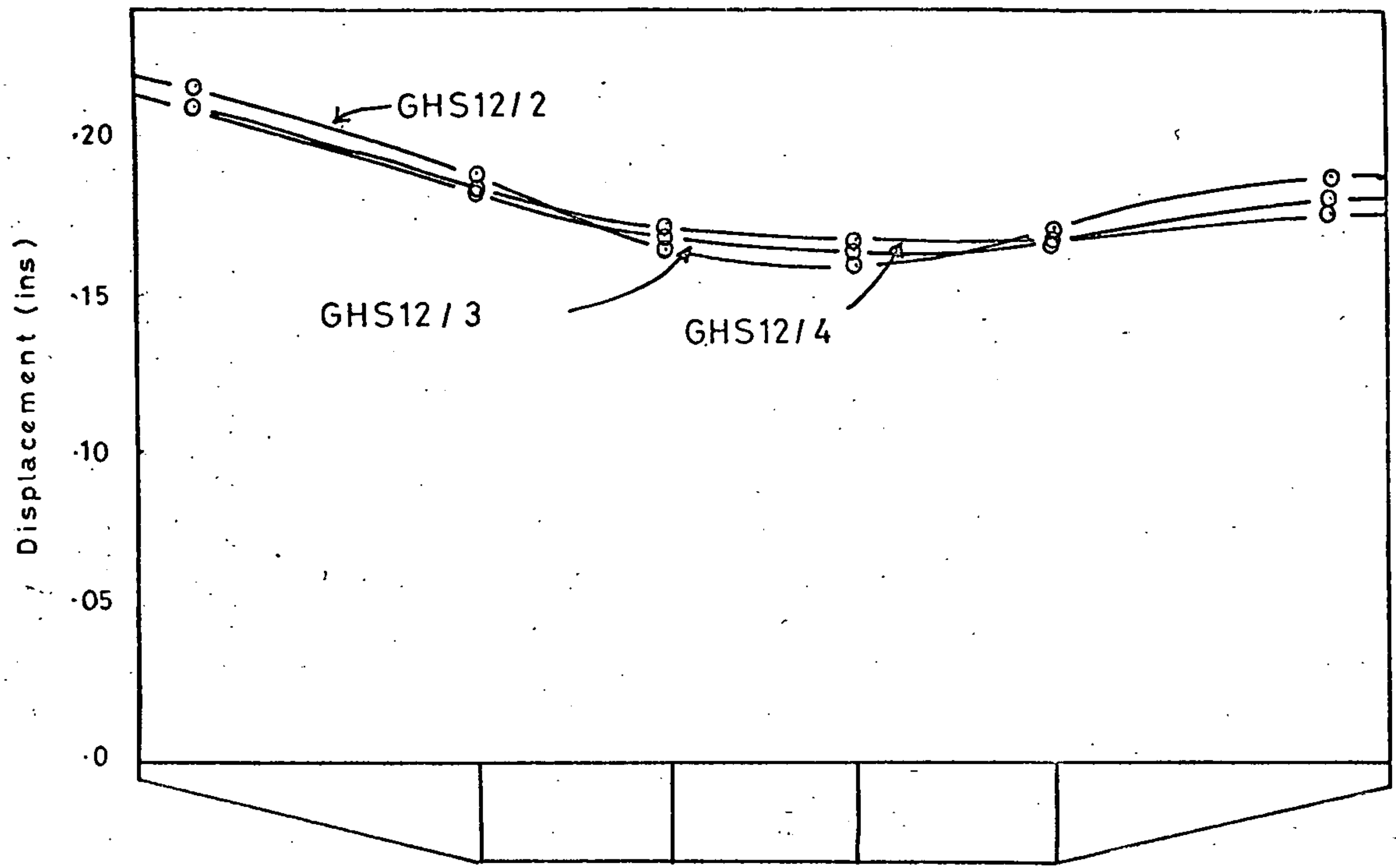

Fig. 109 Vertical displacement of centre line for REAL

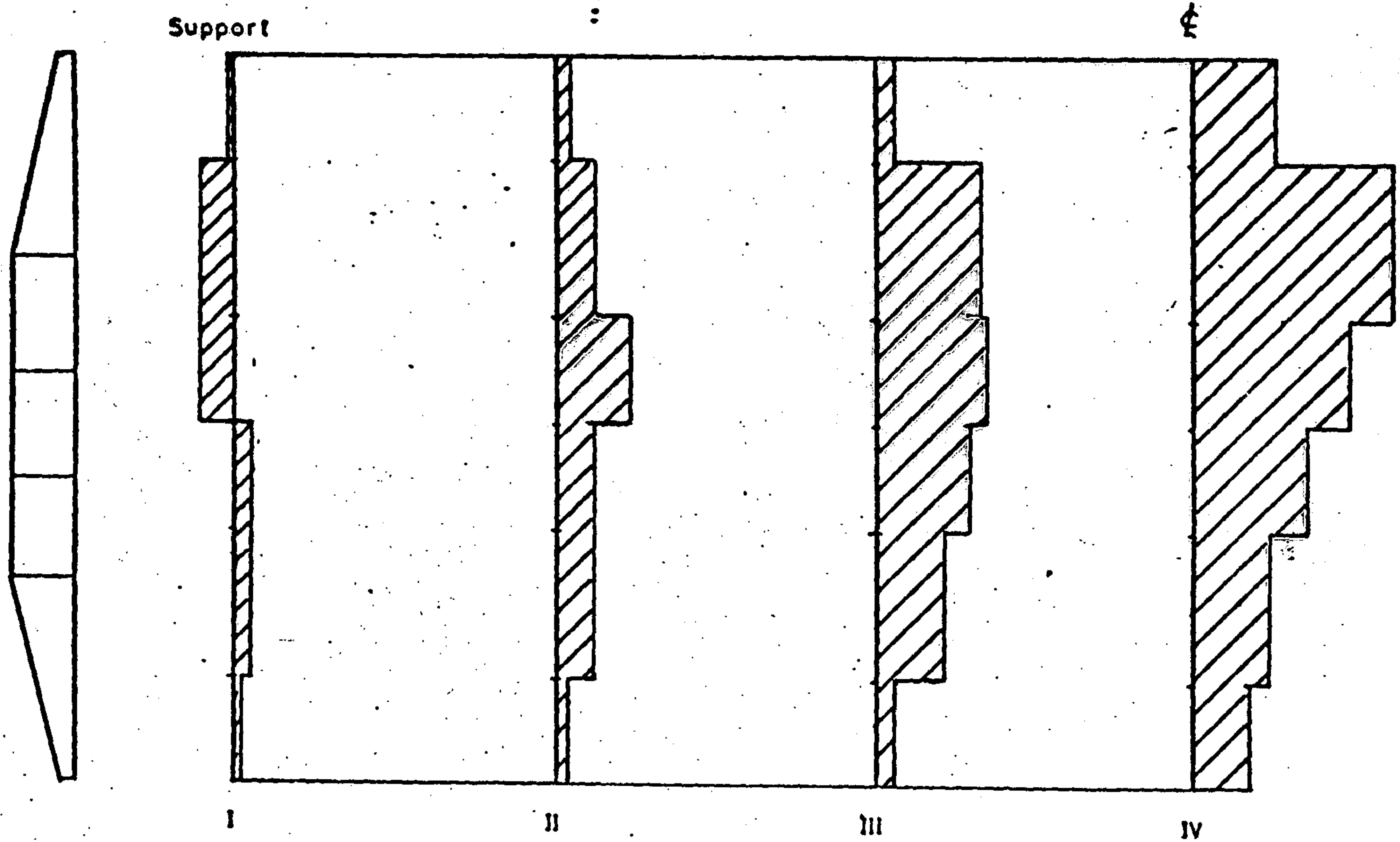

Fig. 110 Distribution of bending moment for POINT1 (GHS12/4)

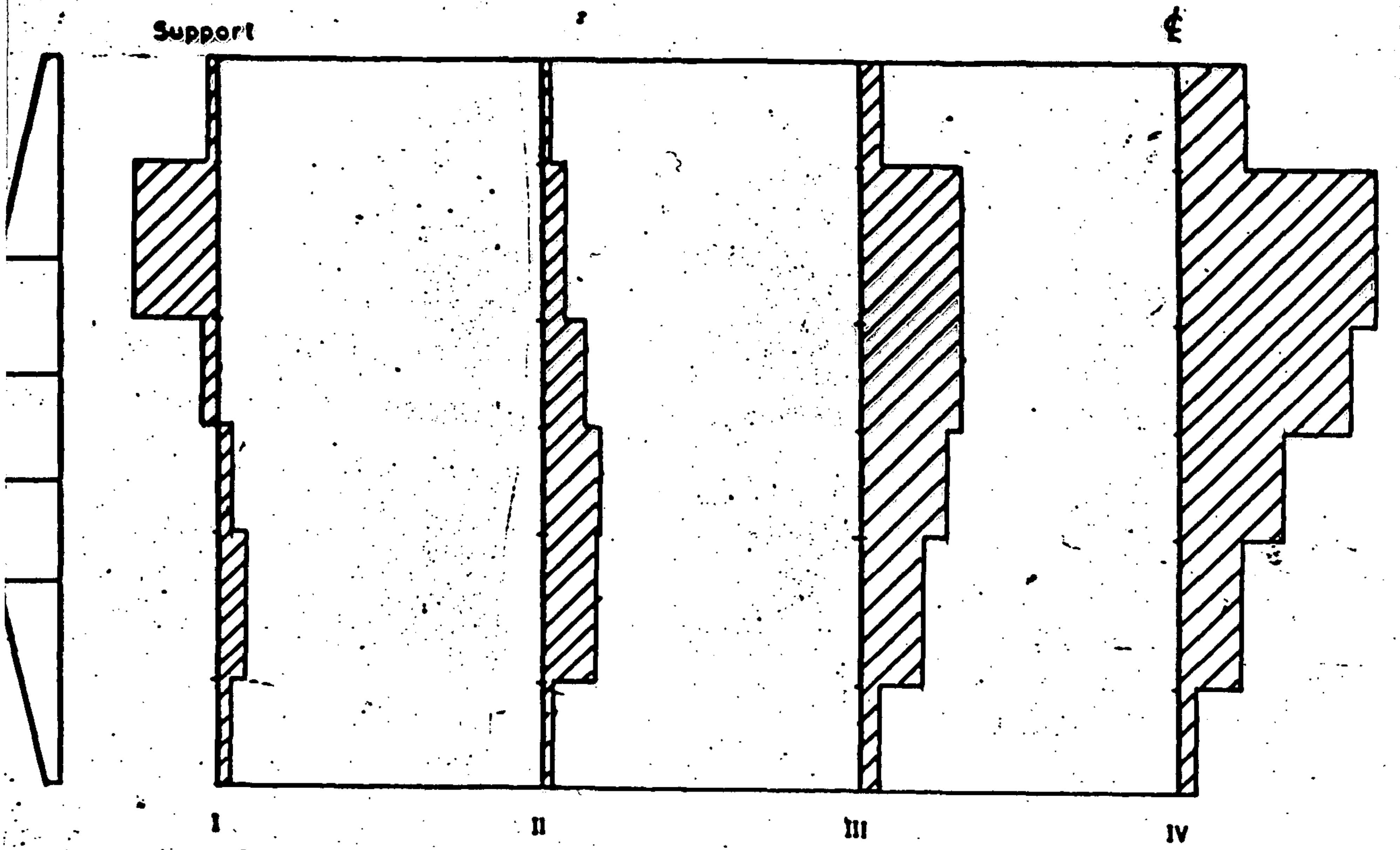

Fig. 110 Distribution of bending moment for POINT1 (GHS12/ 3)

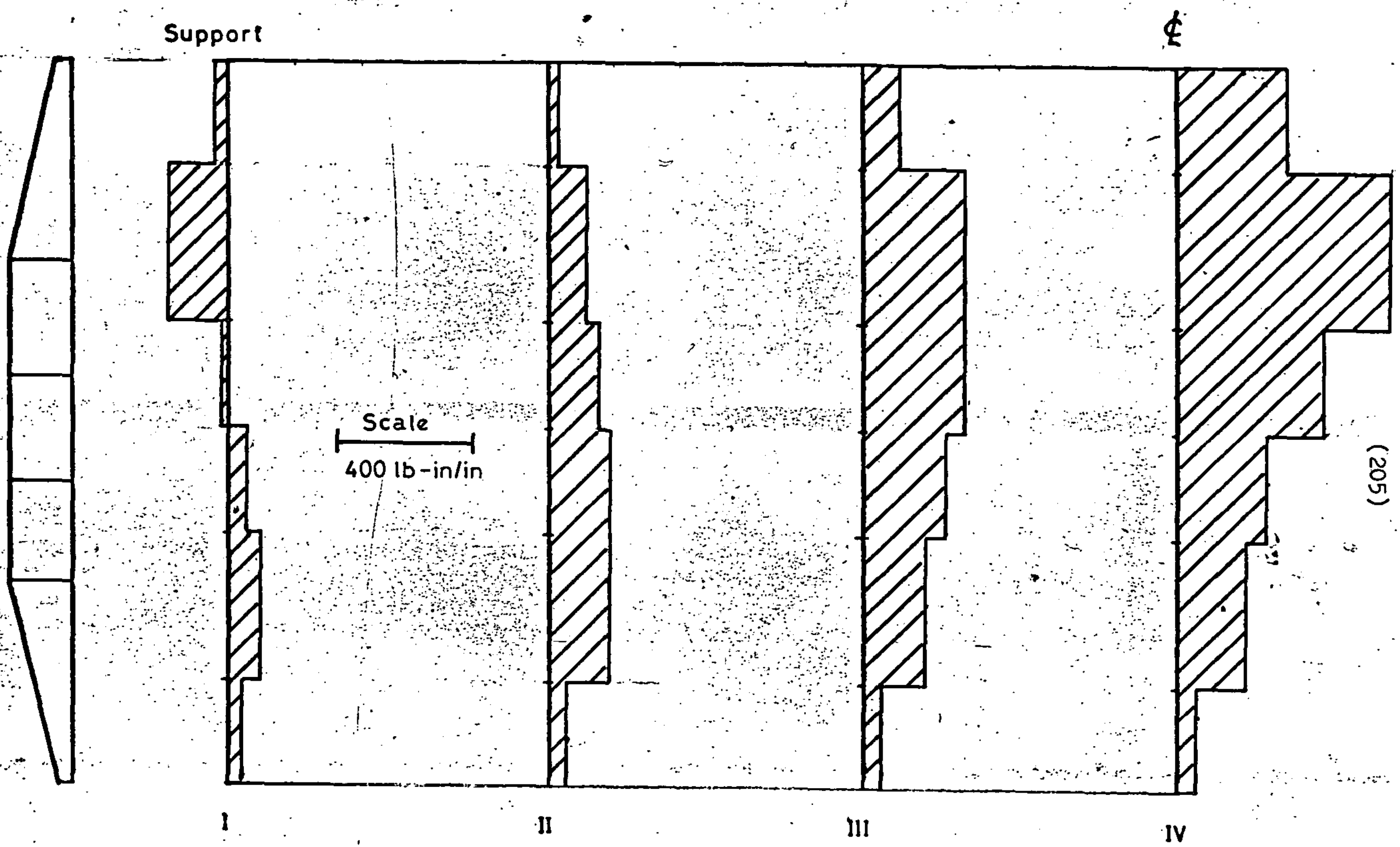

Fig.110 Distribution of bending moment for POINT 1 (GHS12/2)

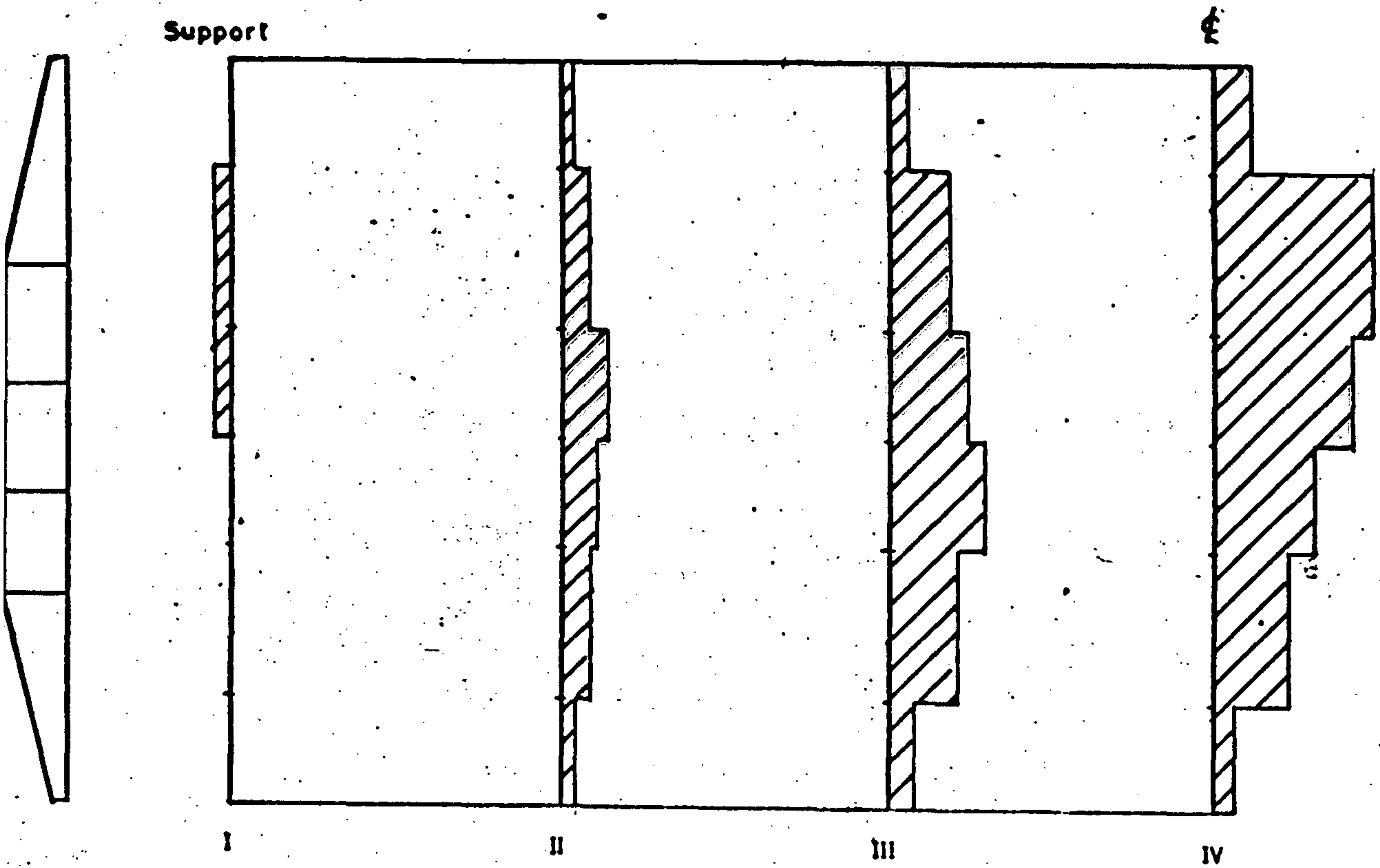

Fig. 111 Distribution of bending moment for POINT2 (GHS12/ 4)

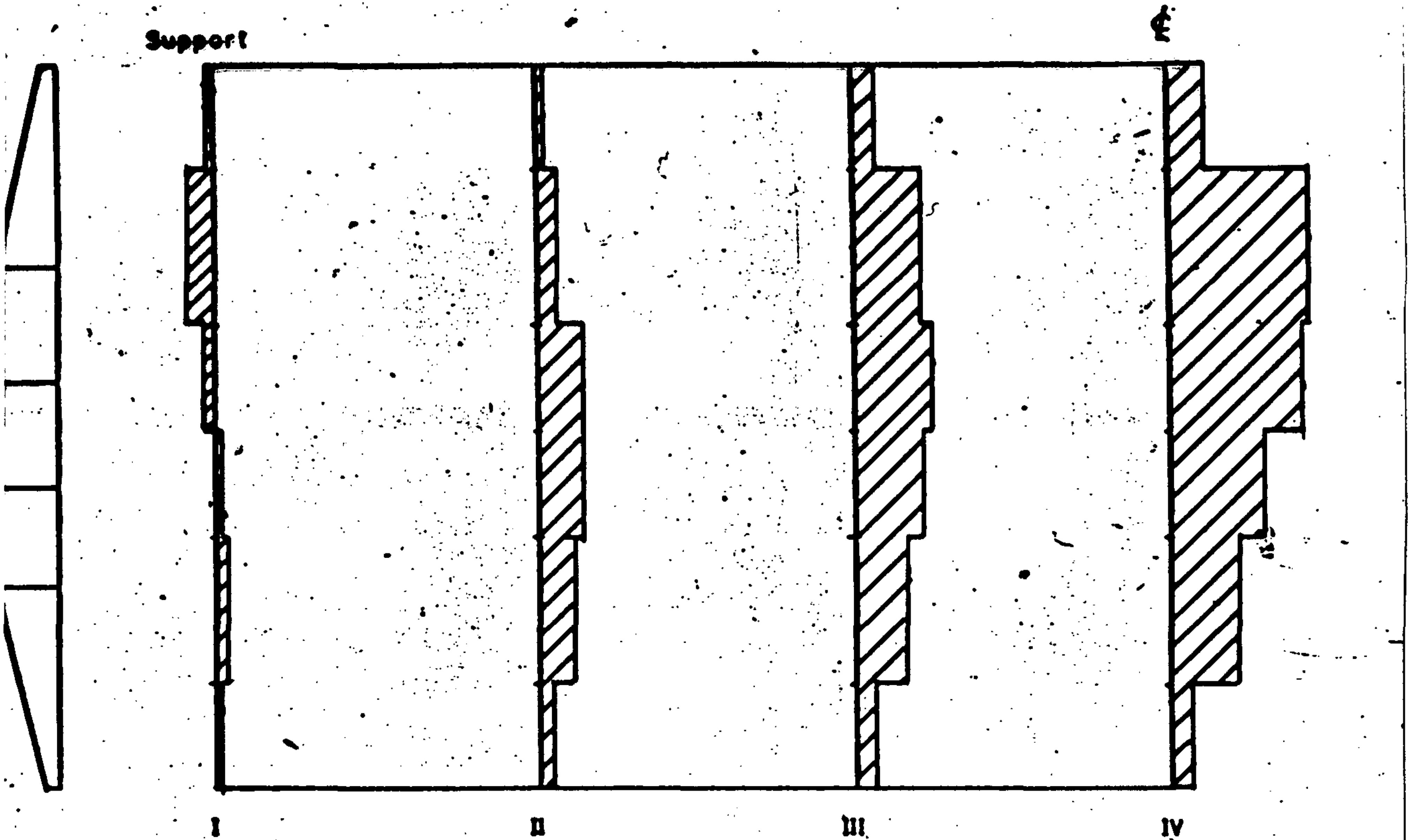

Fig.111 Distribution of bending moment for POINT 2 (GHS12 / 3)

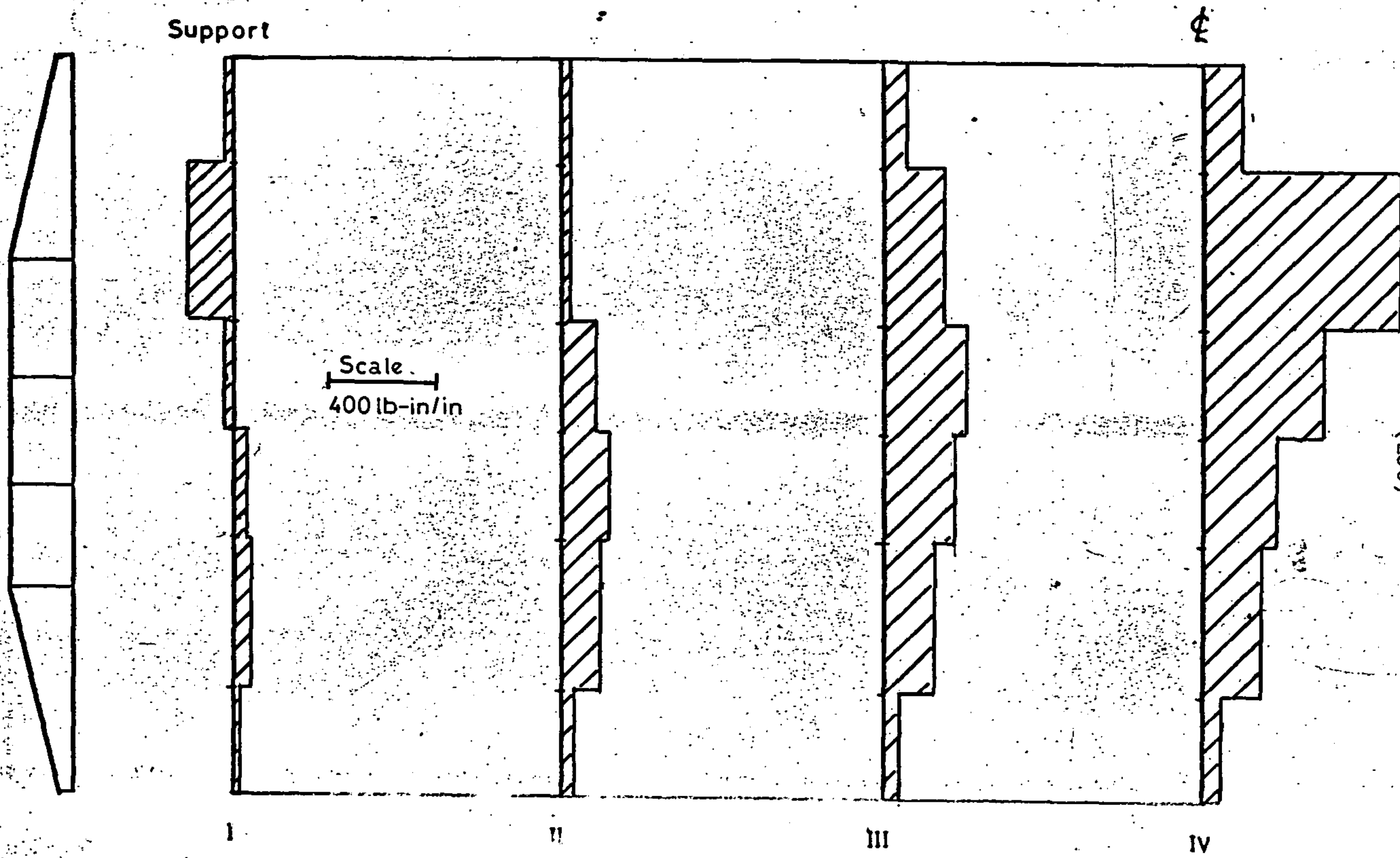

Fig 11 Distribution of be[illegible] (GHS12/2)

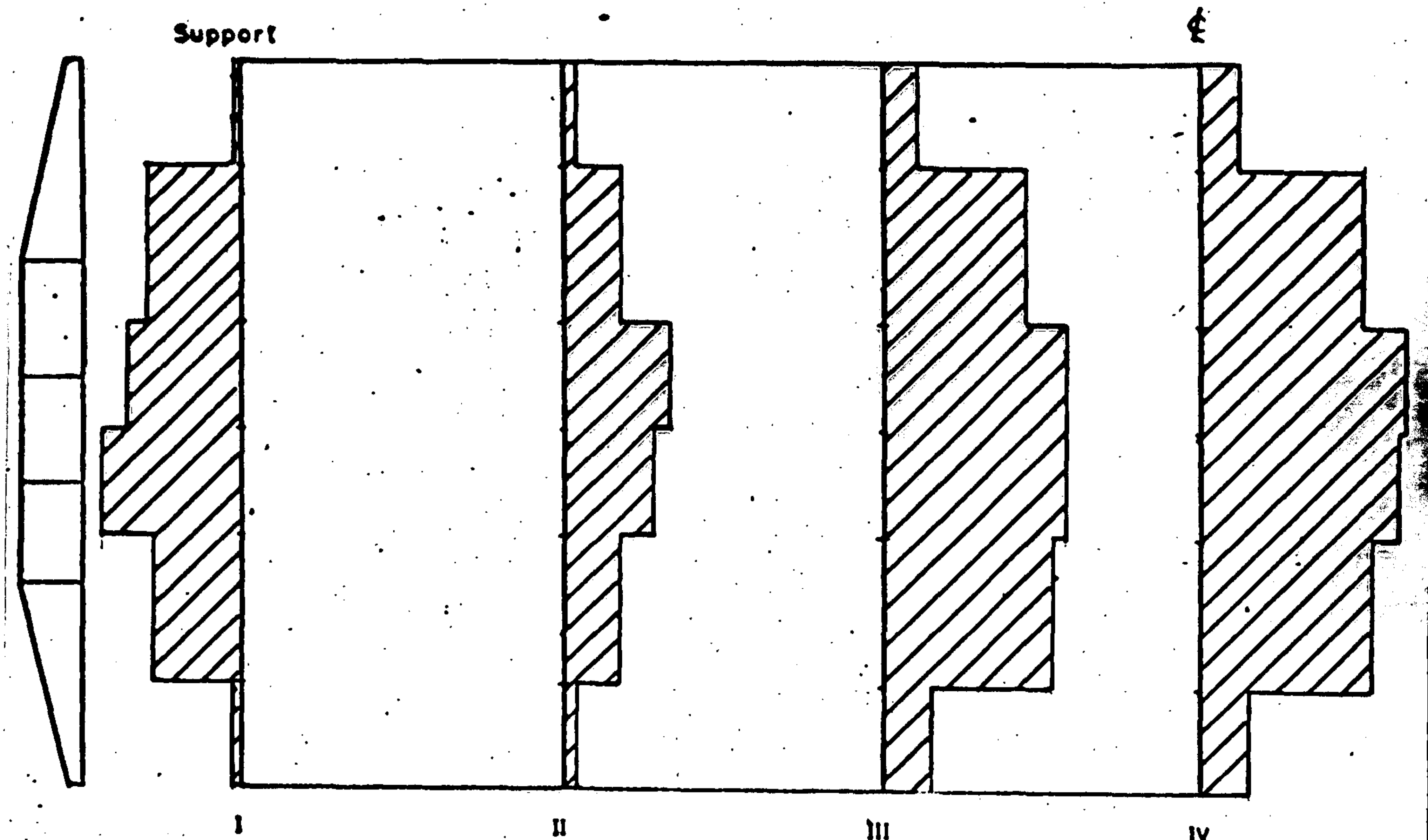

Fig.112 Distribution of bending moment for REAL (GHS12/4)

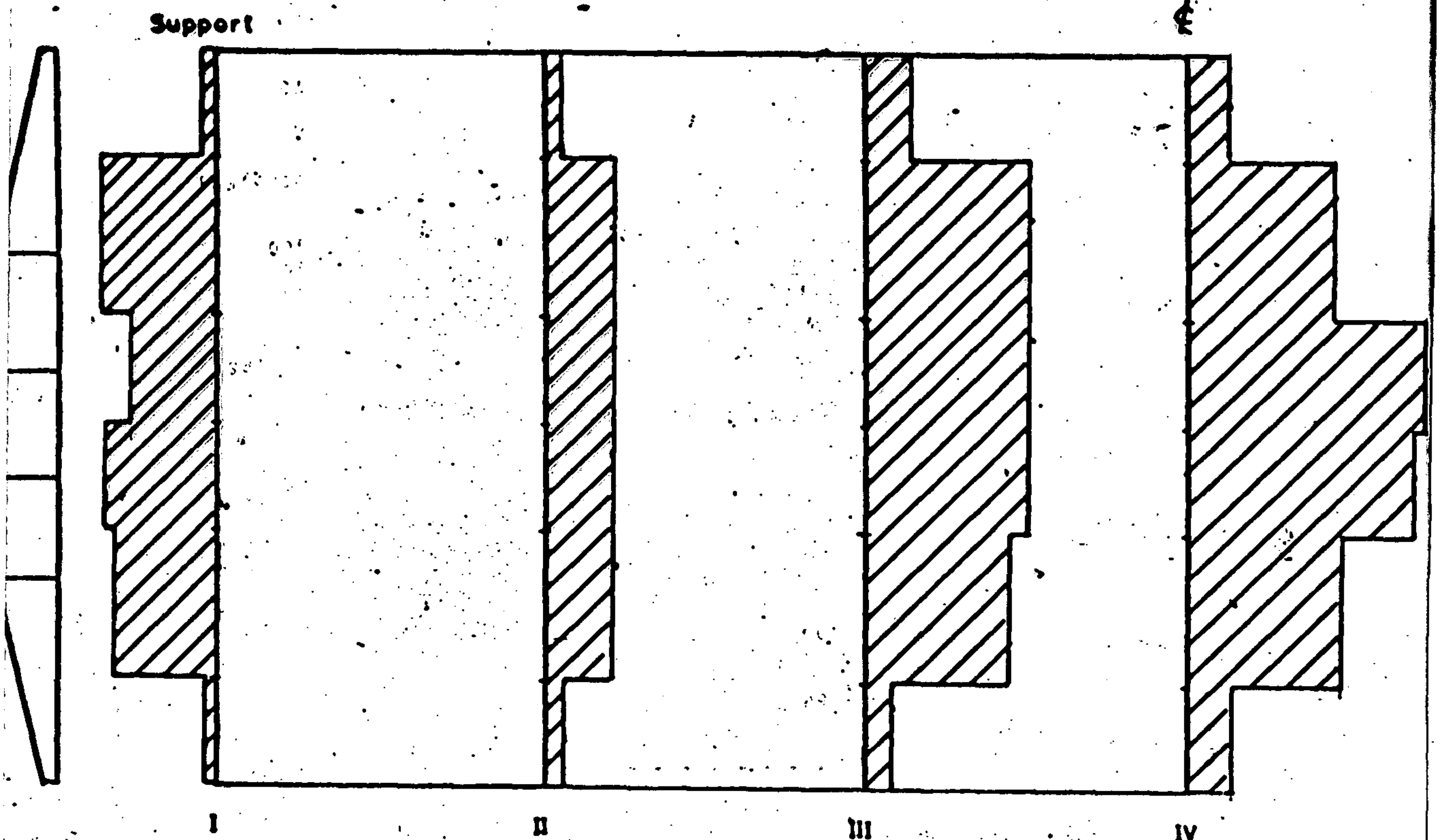

Fig.112 Distribution of bending moment for REAL (GHS12/ 3)

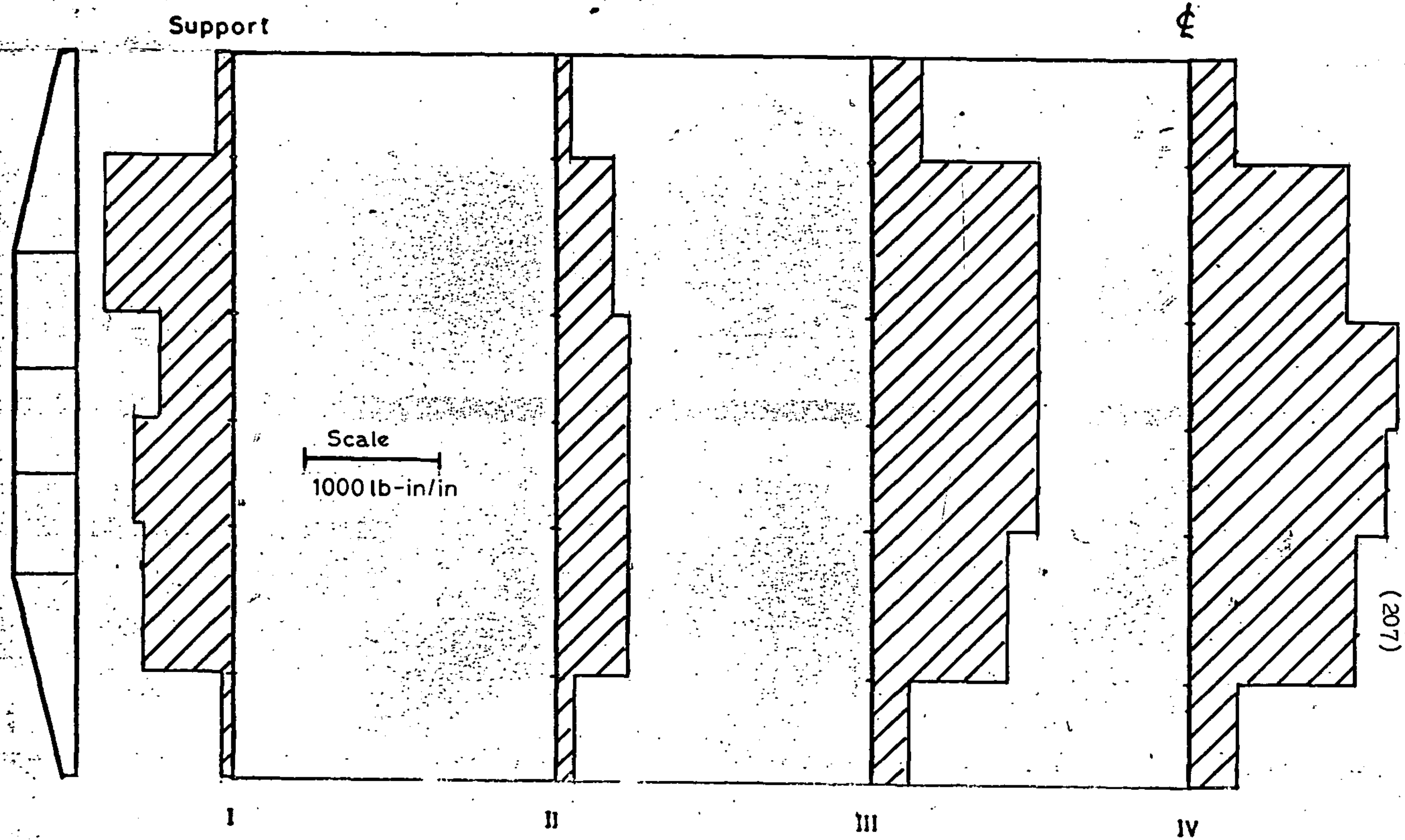

Fig.1 . Distributio of bending moment for REAI (GHS12/ 2)

Chapter Ten Conclusions

The first part of the work reported in this thesis was devoted to the development of plane stress elements, primarily with a view to the eventual combination of one of them with a plate bending element to solve shell problems. However, a secondary conclusion can be drawn from the results. There are two classes of plane stress problems which can be solved more effectively by some elements and not by others: those problems with dominant shear stress and those with dominant in-plane bending. In particular, with elements derived from assumed stress functions, an element with only two degrees of freedom per node is quite sufficient for the solution of problems which primarily involve shear effects, but is poor at representing in-plane bending. Conversely, these latter problems are well-solved with elements having three or four degrees of freedom per node, but shear effects are not now well catered for. In particular, the use of average rotation as a degree of freedom implies zero shear strain at each node. If both types of stress distribution are required to be represented satisfactorily in the same problem, it is necessary to use an element with six degrees of freedom at each node. This element combines the good features of both the two and four degree of freedom elements.

In the latter part of the work two shell elements were developed and examined in some detail, one with seven degrees of freedom per node, the other with twelve. It is perhaps fair to say at this stage that it now appears that a more conventional six degree of freedom per node element could probably have been used as effectively as the set of seven used here. However, the principal comments made in this thesis are unaffected by the choice.

Although quite straightforward for the seven degree of freedom shell element, the combination of membrane and bending elements required special consideration for the twelve degree of freedom case. In particular, a successful approach was developed to impose the three constraints which distinguish thin shells from general three dimensional stress problems, i.e. zero normal and out-of-plane shear strains.

As a result of the use of the four degree of freedom membrane component, the seven degree of freedom shell element gives zero shear strain between the planes of adjacent elements. Although, despite serious implications, correct solutions to many problems have been obtained, the deleterious effect of using average rotations as degrees of freedom was demonstrated most dramatically in Chapter Six with the analysis of a simply supported hollow box beam. The seven degree of freedom element provided an excellent solution if no end diaphragms were present, but as soon as these were added the errors involved in the solution considerably reduced the central deflection - in some cases to a third of the correct value. This same effect was also demonstrated for the Gateshead Viaduct.

In general, it appears that if significant shear strain interacts with members stiff in bending there will be serious errors. This situation commonly occurs where three elements meet at a box-type corner. This also is the case when plane elements are used to represent doubly curved shells. In these cases the twelve degree of freedom element can be used successfully, the most notable example quoted is the Gateshead Viaduct. The difficulties encountered with the seven degree of freedom element here are of course likely to be suffered when using any shell element embodying the average rotation approach.

It has not been possible to provide watertight criteria upon which to base a decision of whether or not to use the seven degree of freedom element in any particular situation. Until such criteria are available, extreme caution must be taken with the use of the above general guide lines and if there is any likelihood of the errors of the above type being significant, correct solutions can only be guaranteed with the more sophisticated twelve degree of freedom element.

Appendix One Loughborough Finite Element Program

The finite element process consists of several steps, (see fig. 113) each of which is, relatively, independent from the others. This sequence is linear in the standard case, but could be considered as re-entrant or iterative in some non-standard cases, such as material with non-linear elastic properties.

Whilst it is entirely feasible to write a program as a single unit, this can become over-large on even a moderately sized machine, introducing the need for overlay systems and complex techniques for multiple re-use of the core storage. In order to facilitate the writing and subsequent development of the program, it was found to be of considerable advantage to split the calculation into several independent sub-programs corresponding to the logical steps in the process. These programs were then linked together as a fixed linear chain or controlled by a small master program which sequenced the calls to individual programs according to input commands.

The Loughborough system splits the process into the following seven sub-processes:

1 Input of problem data
2 Output of perspective drawing on graph plotter
3 Calculation and assembly of element stiffness matrices
4 Constraining and reduction of assembled equations
5 Backsubstitution of force vetors and output of deflections on line printer
6 Calculation and output on line printer of element stresses or forces
7 Output on graph plotter of a selection of stresses

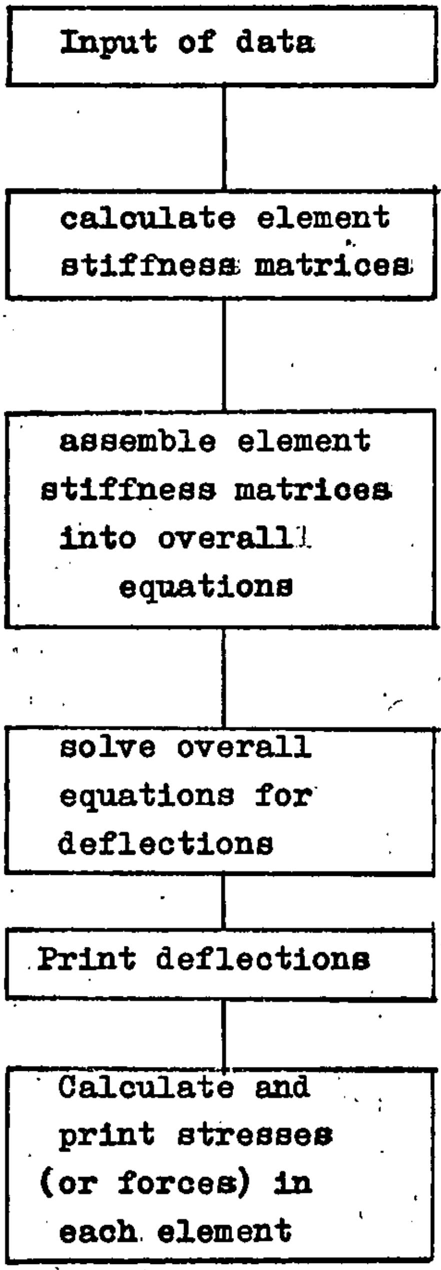

Fig. 113 Basic steps of Finite Element process

Each sub-program is independent but requires the results of any logically previous program to be left on two magnetic tapes in standard form. This concept allows several advantages, of which the following are some:

1 The development of any one sub-process can be carried out using the two magnetic tapes of results from a previous run of a test case up to the sub-process in question. This may well decrease the amount of computer time required for development quite considerably. It also means that only a small section of the total system is under alteration at any one time and the effects of any changes made are thus limited.

2 Quite apart from development work, it may also be an advantage to retain the magnetic tapes from a production run if further processing might be required. At present, two principal instances should be noted.

Firstly, the time up to the end of the reduction of the overall equations comprises the bulk of the computation and only a short time is required for the backsubstitution and output. It is possible with this system, then, to input subsequent loading cases on the same basic structure having examined the results from an initial run. The cost of these subsequent cases is much less than the first run.

Secondly, the stress results stored on the magnetic tapes can be used as input for the stress plotting program. (See Appendix 2) The selection of stresses can often be done best after a partial examination of the results.

The mathematical techniques of the system are, for the most part, standard and well-tried. However, there are points to note in one section, the solution of the equations.

The method used is a Choleski triangular decomposition as recommended by Wilkinson as likely to yield the most accurate results for a minimum of computation. The procedure adopted in this system is mathematically identical to the standard, but the computer programming involves a virtual store technique. By this means, the moving lozenge of equations required at any one stage is kept, when possible, entirely in the core store. If however, the number of degrees of freedom or the size of the bandwidth precludes this possibility, then the disc backing store is called into use. The detailed flow chart is shown in fig. 115.

The complete system as at present is shown schematically in fig.114 . The commands, which are read at run time from cards, are currently as follows:

**START **STOP **DUMP **RESTART	self-explanatory
**ANALYSE	complete finite element analysis
**PLOT	graphical output of stresses
**DRAW	perspective drawing of mesh
**RUN	

This last command is used to run an individual program. Thus sequences of programs can be built up to suit individual requirements for special circumstances or during the testing of a new program or sub-process.

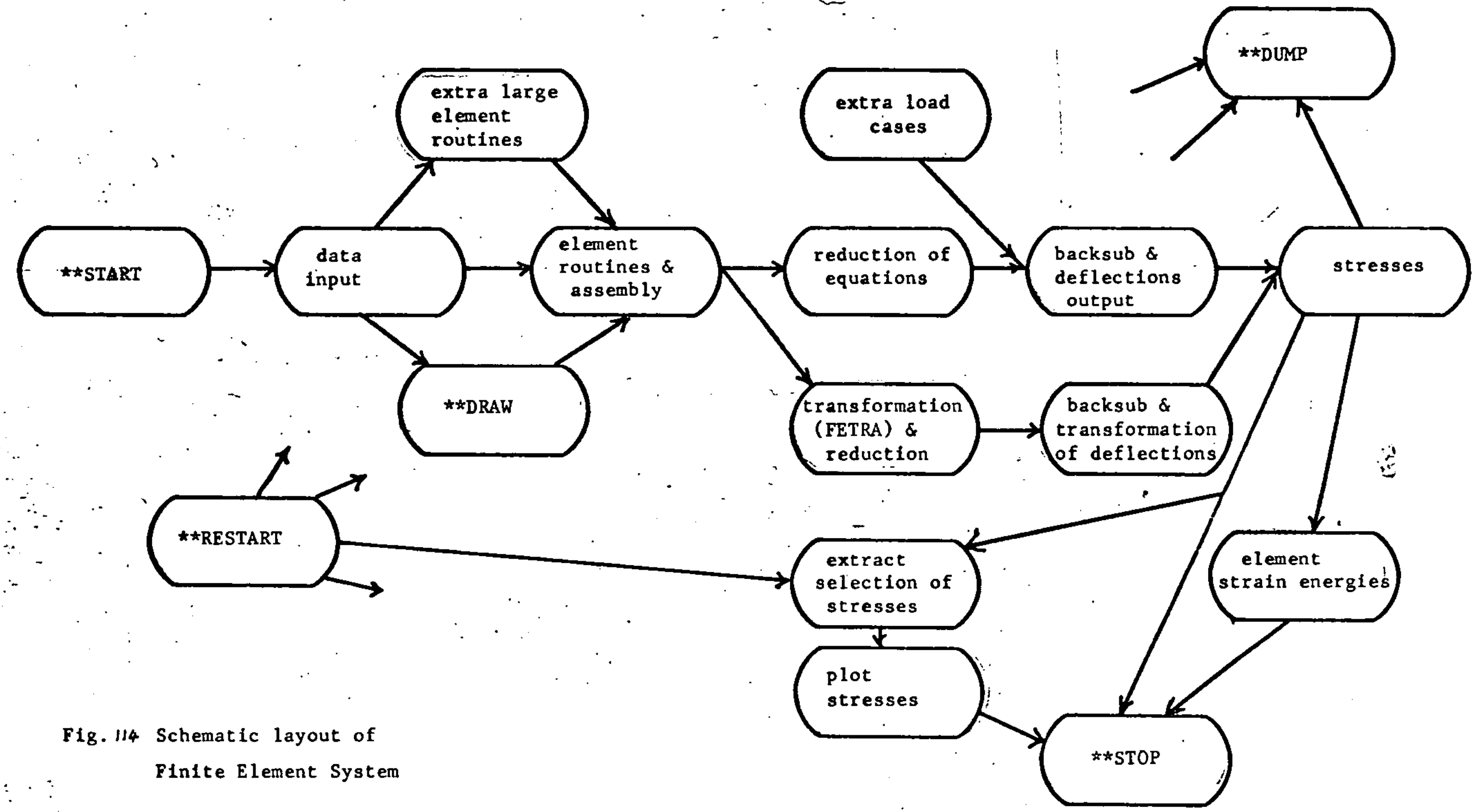

Fig. 114 Schematic layout of Finite Element System

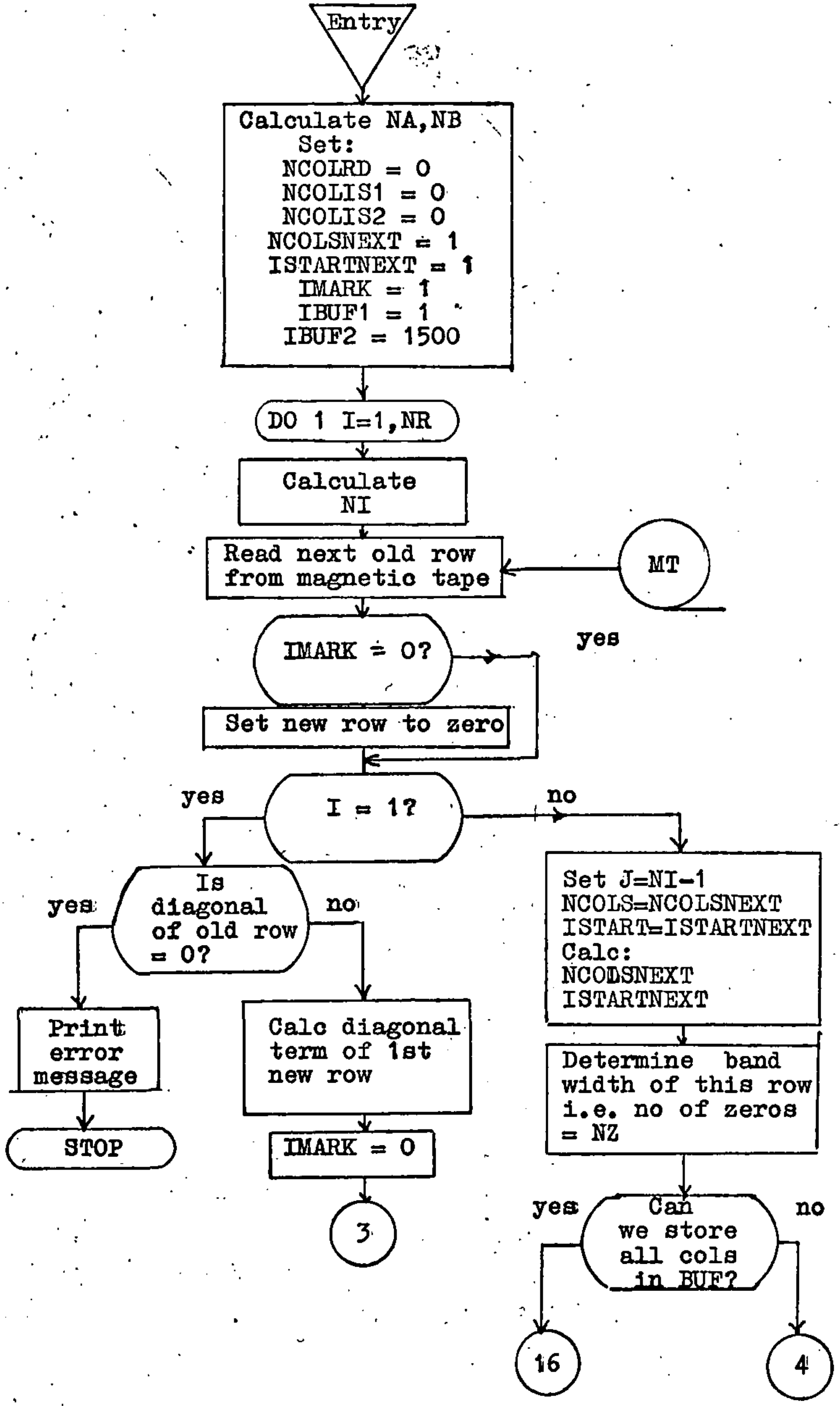

Fig.115 Flow chart of subroutine to perform Choleski decomposition

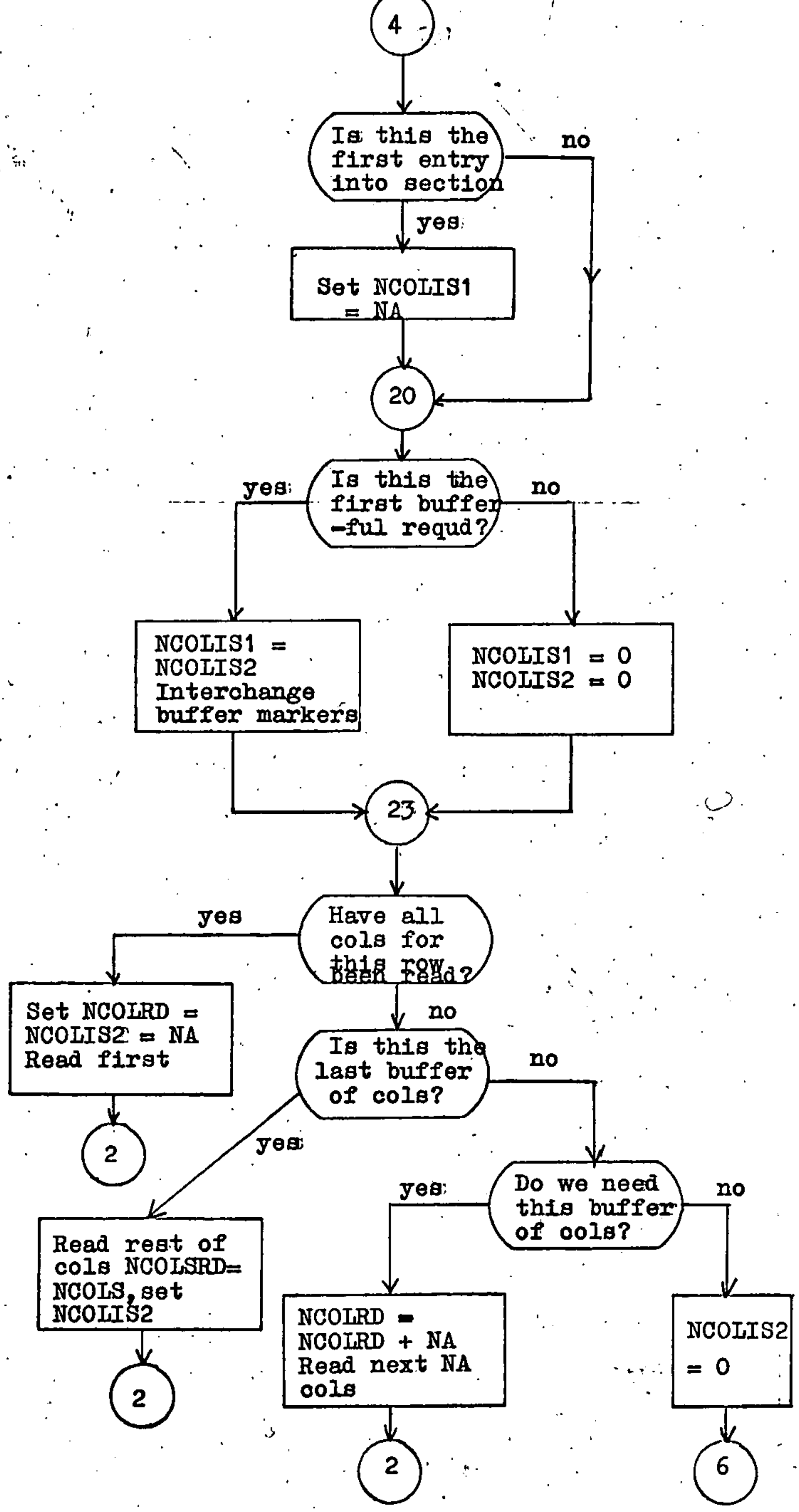
4
Is this the first entry into section
no
yes
Set NCOLIS1 = NA
20
Is this the first buffer -ful requd?
yes
no
NCOLIS1 = NCOLIS2 Interchange buffer markers
NCOLIS1 = 0 NCOLIS2 = 0
23
Have all cols for this row been read?
yes
no
Set NCOLRD = NCOLIS2 = NA Read first
2
Is this the last buffer of cols?
no
yes
Do we need this buffer of cols?
yes
no
Read rest of cols NCOLSRD= NCOLS, set NCOLIS2
2
NCOLRD = NCOLRD + NA Read next NA cols
2
NCOLIS2 = 0
6

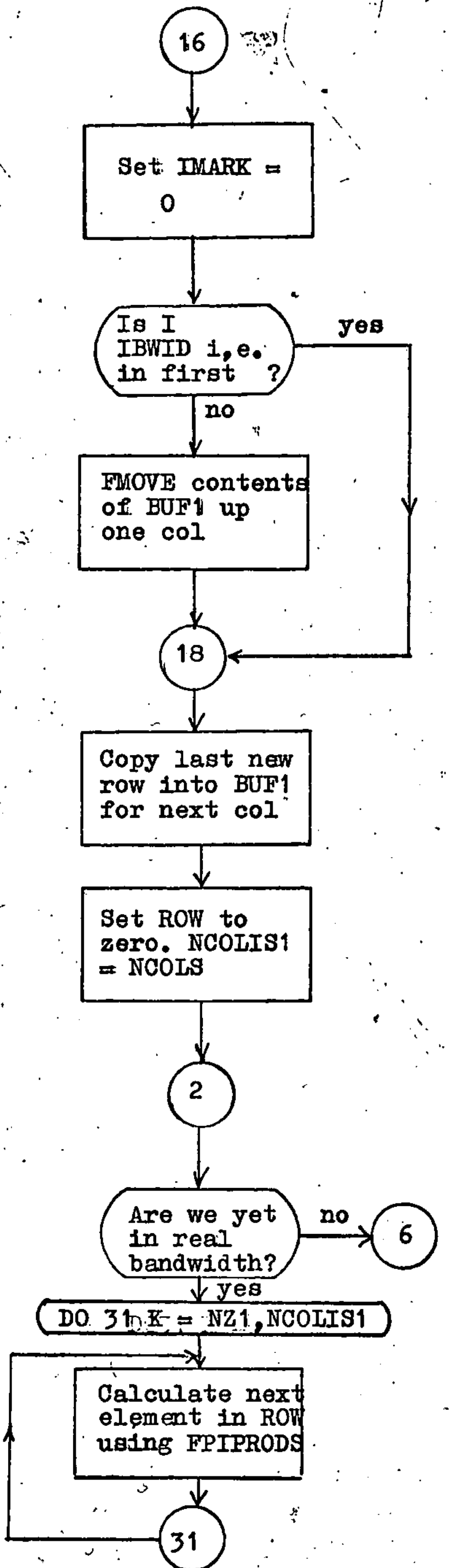
16
Set IMARK = 0
Is I IBWID i,e. in first ?
yes
no
FMOVE contents of BUF1 up one col
18
Copy last new row into BUF1 for next col
Set ROW to zero. NCOLIS1 = NCOLS
2
Are we yet in real bandwidth?
no
6
yes
DO 31 K = NZ1,NCOLIS1
Calculate next element in ROW using FPIPRODS
31

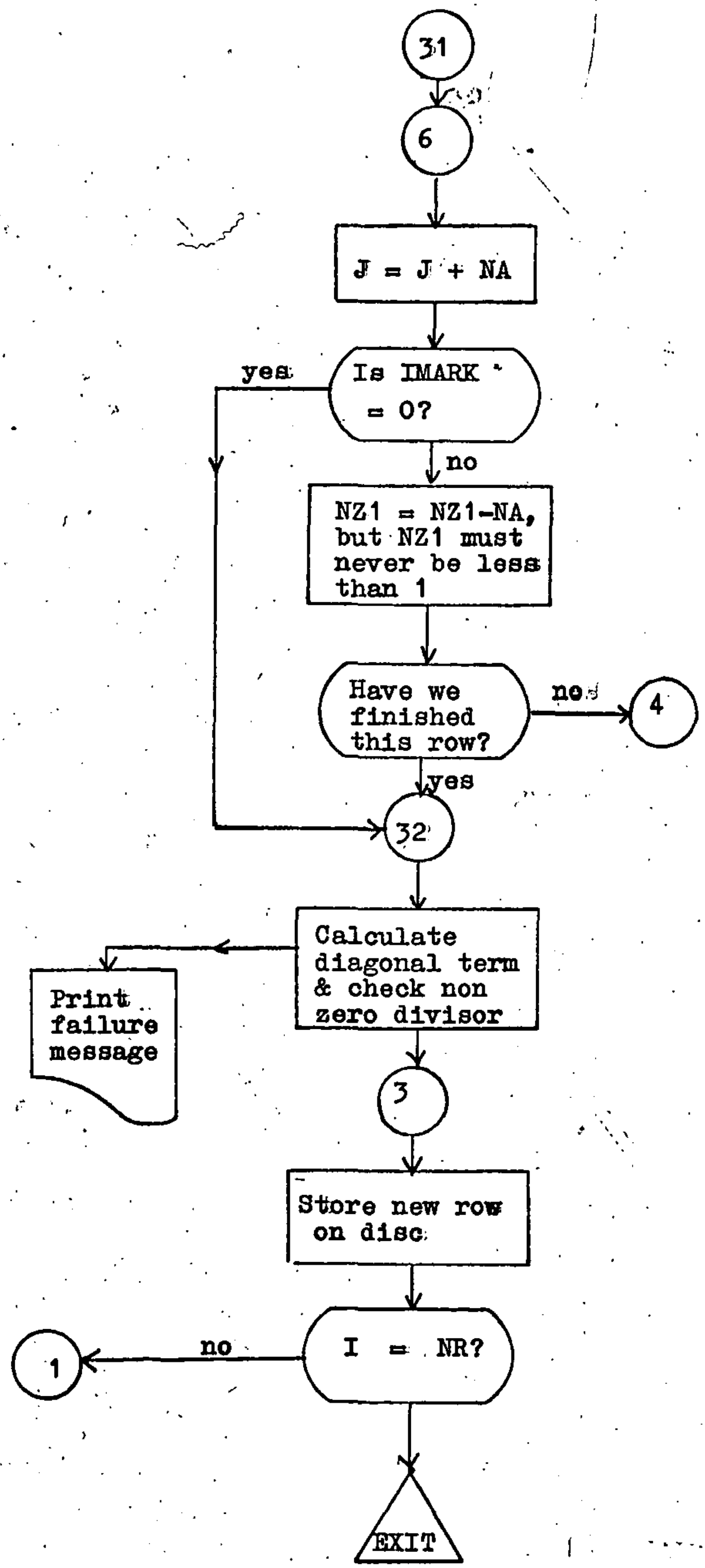
31
6
J = J + NA
Is IMARK = 0?
yes
no
NZ1 = NZ1-NA, but NZ1 must never be less than 1
Have we finished this row?
no
4
yes
32
Calculate diagonal term & check non zero divisor
Print failure message
3
Store new row on disc
I = NR?
no
1
EXIT

Appendix Two Stress Plotting

A recurrent problem which besets every user of the Finite Element Method is the interpretation of the results. Often large quantities of output are produced which have then to be digested into a form more readily understood. In particular, the averaging of stresses at nodal points and the selection of the appropriate parts of the output can consume many hours for even a relatively simple problem. It is not too difficult a task when two dimensional analyses are considered but the degree of topological complexity of which the shell elements are capable of reproducing, the Gateshead Viaduct, for example, make the design of automatic stress digesting rather difficult. Whilst the ideal is for the engineer to specify the part of the structure and the particular stress in which he is interested in a very elementary way, related as far as possible to his ordinary nomenclature, there are considerable complications in making the specification unique.

The most common way of beginning such a specification is to define a section through the structure. Having done this for a simple classical shell, such as the spherical cap, the problem is almost solved, since the resulting sectional view cah be topologically deformed into a straight line. Arbitrary, but reasonable, assumptions could be made about where to commence and end the plot, using surface distances as one coordinate. However, when the section is multi-connected, so that it cannot be deformed into a straight line, there is no unique line along which to plot the stresses. Even if the two ends of the required line were specified, there will often be more than one path between them. Obviously, the human eye would select a particular path such as the shortest, which might be, say, the top slab of a bridge deck. However, such "obvious" human decisions cannot be translated readily into computer terms. In addition, it may not always be the "obvious" path that is required.

The Loughborough system for plotting stresses has used a compromise solution. The section required is still specified and stresses are calculated in terms local to this plane and the normal to the surface, but the elements along the section which are required have to be specified manually by the user in the order required for plotting. The program does check, however, that this "chain" of elements does link together by its global coordinates and that they also lie on the specified section. These elements are specified by using the numbers printed on the element data sheet.

The program automatically averages the values at any point from adjacent elements. If a genuine discontinuity exists it is possible to specify this by commencing another sub-chain along the same section. The program allows sub-chains of up to ten elements which are averaged at all internal points but when these individual sub-chains are linked together no averaging takes place between them. There is also no need that the plane section chosen should pass through nodal points nor lie along an element edge.

Certain techniques exist for plotting smooth curves through a set of given discrete values, but these are apt to produce erratic results when a limited number of points is available. Discontinuities or sharp changes in the graph are also difficult to reproduce without absurd assumptions.

Until better methods are avilable, the values are joined by straight lines.

The axes for the plotter output have to be specified in detail by the user since the standard software available for

LOUGHBOROUGH UNIVERSITY OF TECHNOLOGY

STRESS PLOTTING

DEPARTMENT OF CIVIL ENGINEERING

DATA SHEET TYPE 7

EQUATION OF PLANE SECTION			
A	B	C	D
1 2 3 4 5 6 7 8 9 10	11 12 13 14 15 16 17 18 19 20	21 22 23 24 25 26 27 28 29 30	31 32 33 34 35 36 37 38 39 40

$Ax + By + Cz = D$

	BEGIN POINT X	Y	Z	END POINT X	Y	Z	ELEMENT NUMBERS									
1 2	3 4 5 6 7 8 9 10	11 12 13 14 15 16 17 18	19 20 21 22 23 24 25 26	27 28 29 30 31 32 33 34	35 36 37 38 39 40 41 42	43 44 45 46 47 48 49 50	51 52 53	54 55 56	57 58 59	60 61 62	63 64 65	66 67 68	69 70 71	72 73 74	75 76 77	78 79 80
EN *																

COEFFICIENTS OF STRESS TO BE PLOTTED

LOAD CASE	σ_{xI}	σ_{xo}	σ_{yI}	σ_{yo}	τ_{xyI}	τ_{xyo}	τ_{xz}	τ_{yz}	TITLE
1 2 3 4 5 6 7 8	9 10 11 12 13 14 15 16	17 18 19 20 21 22 23 24	25 26 27 28 29 30 31 32	33 34 35 36 37 38 39 40	41 42 43 44 45 46 47 48	49 50 51 52 53 54 55 56	57 58 59 60 61 62 63 64	65 66 67 68 69 70 71 72	73 74 75 76 77 78 79 80
FINISH *									

Fig. 116 Stress plotting Data sheet

* THESE TWO LINES MUST BE PUNCHED.

the drawing of axes was totally inadequate, often failing to produce a readable result. The number of tick marks, the values attached to them and the values at the origin are now under the control of the user.

This problem typifies the constant compromise in this sort of work. A conflict arises bweteen allowing the user control over the output and on the other hand reducing the amount of effort he has to use and the input to prepare for a given output.

The data sheet required for the selecting of stresses is shown in fig.116.

The data for the plotting is given in a series of commands of which four are currently available:

1 NEW AXES

2 READ

3 PLOT

4 STOP

The first is obvious in its action and is called every time axes are required to be drawn. All graphs are drawn on the same axes unless this command is interspersed with others.

The second command allows the direct input of values from cards. This can be of use if previous results are required to be plotted alongside the new calculations.

The third command takes the next chain of values from a disc file as left there by the stress selection program. These values are averaged were appropriate. There is room if in future a smoothing subroutine is required to replace the present straight line segment graph.

The last command closes the plotter and signifies the end of a run.

The NEW AXES command also requires on the following two cards these data items:

a) number of tick marks for the X axis

b) incremental value between two tick makks

c) X value at origin

d) title for X axis

e) - h) On the next card the same items but for Y axis.

In fig.117. an example of the output from these two programs is shown. The straight line graph was input using the READ command and the other by PLOT. The data required for the plotting program is as follows:

```
NEW AXES
10   ·12   0   DISTANCE ALONG X-AXIS (INS)
6    500   0   LONGITUDINAL STRESS (SXX) P.S.I.
PLOT
READ
2
0    2000    120    C
STOP
```

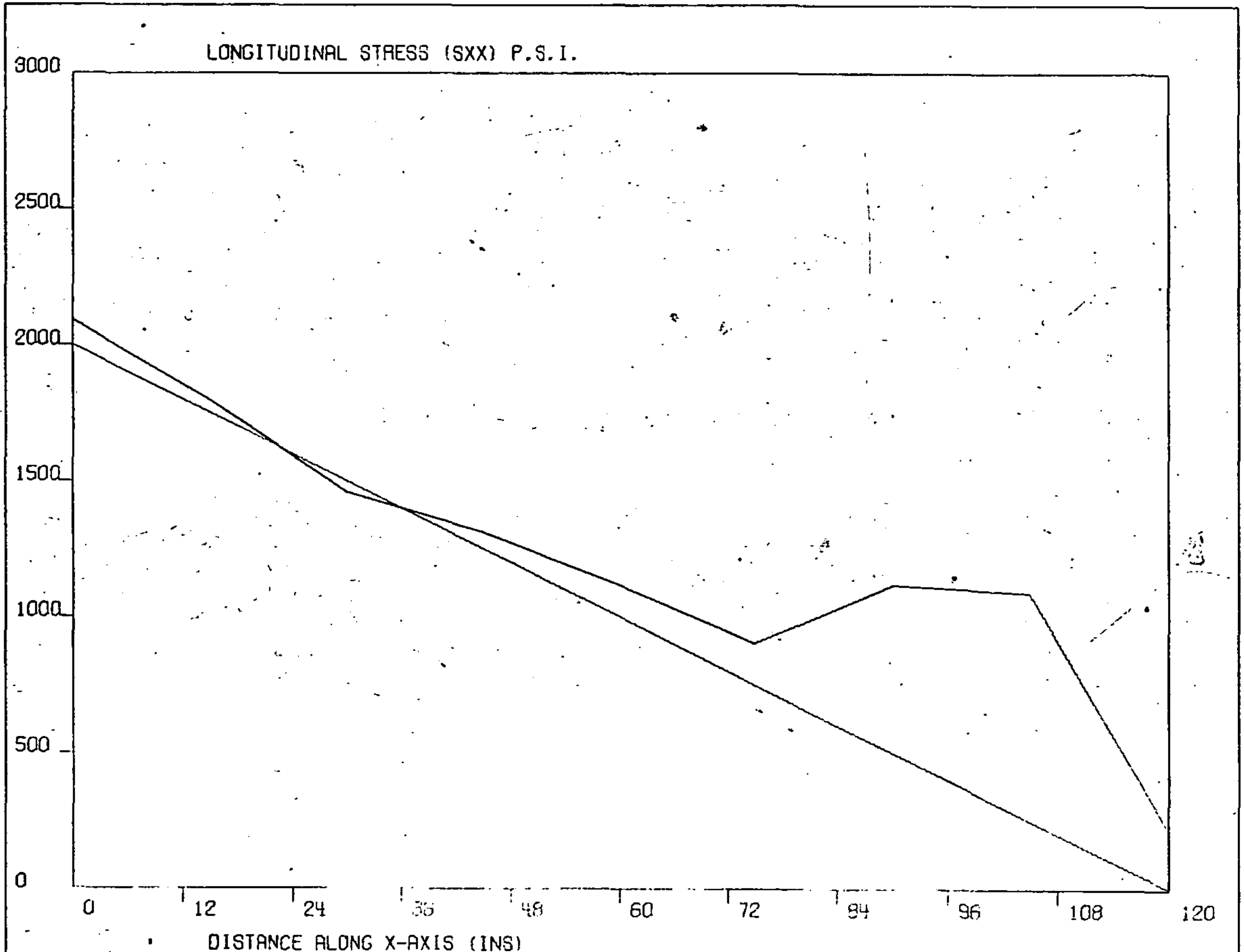

Fig.117 Sample output from stress plotting programs

Appendix Three Matrix integers and built-in functions

The following lists are the built-in functions and their corresponding reference numbers. These functions are available to all elements if required. They are selected according to the matrix integers. (see below)

Functions for matrix N (elasticity matrix)

1	1
2	-v
3	2(1+v)
4	$t^2(1+v)/5$

Functions for M matrix (transformation of stresses)

1	-2*SIN*COS
2	-SIN*COS
3	SIN*COS
4	COS*COS - SIN*SIN
5	SIN*SIN
6	COS*COS
7	-SIN
8	COS
9	SIN*SIN - COS*COS

"CONSTant" functions for L matrix (edge displacements)

1	EL
2	SIN
3	-SIN
4	COS
5	EL*COS*COS

6	-EL*SIN*SIN
7	-6/EL
8	-EL*SIN
9	EL*COS
10	-COS
11	1
12	6/EL
13	2*EL
14	-EL*SIN*COS
15	EL*SIN*SIN
16	EL*SIN*COS

Polynomial functions

All the polynomial functions for the P matrix and L matrix are stored in a linear array called FUNS. This array is set up for each element from DATA statements. This array is the same for all the plane stress elements except the PIAN element. A different array is also required for the bending element.

FUNS - for plane stress elements

function	integer	parameters						
1	1	1	1	0	0			
x	5	1	1	1	0			
y	9	1	1	0	1			
-x	13	1	-1	1	0			
-y	17	1	-1	0	1			
$y^2-\frac{1}{2}x^2$	21	2	1	0	2	-.5	2	0
$x^2-\frac{1}{2}y^2$	28	2	1	2	0	-.5	0	2
xy	35	1	1	1	1			
$-\frac{1}{2}x^2$	39	1	-.5	2	0			

$-\frac{1}{2}y^2$	43	1	-.5	0	2			
$y^3-3x^2y/2$	47	2	1	0	3	-1.5	2	1
$x^3-3xy^2/2$	54	2	1	3	0	-1.5	1	2
$-\frac{1}{2}x^3$	61	1	-.5	3	0			
$-\frac{1}{2}y^3$	65	1	-.5	0	3			
$3xy^2/2$	69	1	1.5	1	2			
$3x^2y/2$	73	1	1.5	2	1			
$\frac{1}{2}x^2y-y^3/3$	77	2	.5	2	1	-1/3	0	3
$\frac{1}{2}xy^2-x^3/3$	84	2	.5	1	2	-1/3	3	0
$-\frac{1}{2}x^2y$	91	1	-.5	2	1			
$-\frac{1}{2}xy^2$	95	1	-.5	1	2			
$xy^2-x^3/6$	99	2	1	1	2	-1/6	3	0
$x^2y-y^3/6$	106	2	1	2	1	-1/6	0	3
$2s^3-3s^2+1$	120	3	2	3	-3	2	1	0
s^3-2s^2+s	127	3	1	3	-2	2	1	1
$3s^2-2s^3$	134	2	3	2	-2	3		
s^3-s^2	139	2	1	3	-1	2		
$1-s$	144	2	1	0	-1	1		
s	149	1	1	1				
$\frac{1}{2}(s-s^2)$	152	2	.5	1	-.5	2		
$\frac{1}{2}(s^2-s)$	157	2	.5	2	-.5	1		

<u>Matrix integers</u>

For each separate element five matrices are specified by integers; Pmatrix by P1, Nmatrix by N1, M matrix by B1, L matrix by two integer matrices, CC1 & A1.
For the elements RECT4, GEN3, GEN4 & GEN6 the matrices P1, N1 & B1 are the same for each element. CC1 & A1 are however different.

P1:

$$\begin{pmatrix} 1 & 9 & 0 & 0 & 0 & 5 & 0 & 21 & 39 & 0 & 35 & 47 & 99 & 91 & 61 \\ 0 & 0 & 1 & 5 & 0 & 0 & 9 & 43 & 28 & 35 & 0 & 65 & 95 & 106 & 54 \\ 0 & 0 & 0 & 0 & 1 & 17 & 13 & 35 & 35 & 39 & 43 & 69 & 77 & 84 & 73 \end{pmatrix}$$

N1:

$$\begin{pmatrix} 1 & 2 & 0 \\ 2 & 1 & 0 \\ 0 & 0 & 3 \end{pmatrix}$$

B1:

$$\begin{pmatrix} 2 & 5 \\ 3 & 6 \\ 4 & 1 \end{pmatrix}$$

CC1:

for GEN6:

$$\begin{pmatrix} 120 & 120 & 127 & 127 & 127 & 127 & 134 & 134 & 139 & 139 & 139 & 139 \\ 120 & 120 & 127 & 127 & 127 & 127 & 134 & 134 & 139 & 139 & 139 & 139 \end{pmatrix}$$

for GEN4:

$$\begin{pmatrix} 120 & 120 & 127 & 0 & 134 & 134 & 139 & 0 \\ 120 & 120 & 0 & 127 & 134 & 134 & 0 & 139 \end{pmatrix}$$

for GEN3:

$$\begin{pmatrix} 120 & 120 & 0 & 134 & 134 & 0 \\ 120 & 120 & 127 & 134 & 134 & 139 \end{pmatrix}$$

for RECT4:

$$\begin{pmatrix} 144 & 144 & 127 & 127 & 149 & 149 & 139 & 139 \\ 120 & 120 & 127 & 127 & 134 & 134 & 139 & 139 \end{pmatrix}$$

A1:

for GEN6:

$$\begin{pmatrix} 4 & 2 & 5 & 16 & 16 & 15 & 4 & 2 & 5 & 16 & 16 & 15 \\ 3 & 4 & 14 & 6 & 5 & 16 & 3 & 4 & 14 & 6 & 5 & 16 \end{pmatrix}$$

for GEN4:

$$\begin{pmatrix} 4 & 2 & 1 & 13 & 4 & 2 & 1 & 13 \\ 3 & 4 & 1 & 13 & 3 & 4 & 1 & 13 \end{pmatrix}$$

for GEN3:

$$\begin{pmatrix} 4 & 2 & 13 & 4 & 2 & 13 \\ 3 & 4 & 13 & 3 & 4 & 13 \end{pmatrix}$$

for RECT4:

$$\begin{pmatrix} 4 & 2 & 0 & 0 & 4 & 2 & 0 & 0 \\ 3 & 4 & 5 & 6 & 3 & 4 & 5 & 6 \end{pmatrix}$$

The array FUNS and the integer matrices for PIAN and the bending element are similar to the above and are not quoted here in detail.

Details of program

To illustrate the program techniques used in the setting up of the element stiffness matrices three extracts from the program are given here. (See pages 238 , 239 , 240)
The first is taken from the subroutine to set up HI and is the section which converts the integer matrix N1 - called ENN - into a real matrix EN, using the actual values given for each element of TT (thickness) and V (Poisson's Ratio) The second and third extracts are taken from the subroutine to set up TI. The first of these is the section which generates the first algebraic product of $M^t.L$ The M matrix has already been set up in an array EM and the constants in the L matrix in an array CONST (corresponding to A1). The integers for the polynomial functions are stored in CC. The product is stored dynamically in the array STORE, with an array EML of pointers which indicate the position in STORE at which each array element of the product is stored.

The final extract is the algebraic multiplication and numerical integration of the complete product of the TI matrix. The P_s matrix is derived from the integer matrix P which points to the array FUNS.

```
      DO 60 I=1,NSTRESS          NSTRESS = number of stresses = 3 for plane stress, = 5 for bending
      DO 60 J=I,NSTRESS
      II=ENN(I,J)                pick up matrix integer
      IF(II.NE.0)GOTO 61         integer = 0 indicates zero function
      Z=0.
      GOTO 62
   61 GOTO(70,71,72,73),II           select appropriate function
   70 Z=1.
      GOTO 62
   71 Z=-V
      GOTO 62
   72 Z=2*(1+V)                          built-in functions
      GOTO 62
   73 Z=TT*TT*(1+V)/5.
   62 EN(I,J)=Z
   60 EN(J,I)=Z                            set up real matrix
```

EXTRACT ONE

```
      IP=1                                  IP = next available position in STORE
      DØ 3 I=1,NSTRESS
      DØ 3 J=1,NF                           NF = NFREE * 2
      M=0                                   M = number of terms in product result (may be zero)
      DØ 4 K=1,IS
      IB=CC(K,J)                            IB = integer pointer to polynomial in FUNS
      IF(IB.EQ.0)GØTØ 4                     IB = 0 indicates zero function and hence zero product result
      N=FUNS(IB)                            N = number of terms in polynomial
      CE=CØNST(K,J)                         CE = constant term from array element in L
      DØ 5 NN=1,N
      IJ=IB+2*(NN-1)+1
      C=EM(I,K)*FUNS(IJ)*CE                 C = constant term of product result
      IF(ABS(C).LE..0001)GØTØ 5             ignore if zero result (no need to store zero functions)
      STØRE(IP+M*2+1)=C                     }
      STØRE(IP+M*2+2)=FUNS(IJ+1)            } put result in STORE
      M=M+1
    5 CØNTINUE
    4 CØNTINUE
      EML(I,J)=0
      IF(M.EQ.0)GØTØ 3                      M = 0 after multiplication indicates zero function
      EML(I,J)=IP                           Put pointer to STORE in EML
      STØRE(IP)=M
      IP=IP+M*2+1                           update IP
    3 CØNTINUE
```


EXTRACT TWO

```
      DØ 8 I=1,NSTREC              NSTREC = number of assumed stress coefficients
      DØ 8 J=1,NF
      T=0
      DØ 10 K=1,NSTRESS
      IB=P(K,I)                    IB = integer pointer to FUNS for P
      IC=EML(K,J)                  IC = integer pointer to STORE of result product of M^t.L
      IF(IB*IC.EQ.0)GØTØ 10        ignore zero function (result is zero if either term is zero)
      NP=FUNS(IB)                  NP = number of terms in array element of P
      NE=STØRE(IC)                 NE = number of terms in array element of M^t.L
      DØ 10 IP=1,NP
      DØ 10 IE=1,NE
      C=FUNS(IB+(IP-1)*3+1)*STØRE(IC+(IE-1)*2+1)     calculate product result constant
      IF(ABS(C).LE..0001)GØTØ 10   ignore term if zero result
      IX=FUNS(IB+(IP-1)*3+2)       IX = power of X in term of polynomial for P
      IY=FUNS(IB+(IP-1)*3+3)       IY = power of Y
      ISS=STØRE(IC+(IE-1)*2+2)     ISS = power of s in term of polynomial for M^t.L
      DØ 11 IJ=1,5                 5 Gaussian points to be considered
      TEMP=(((GPTS(IJ)+1.)*.5)**ISS)*H(IJ)/2)*EL
      IF(IX.EQ.0)GØTØ 600          Ignore zero powers to avoid 0**0
      TEMP=TEMP*(X(IJ)**IX)
  600 IF(IY.EQ.0)GØTØ 601
      TEMP=TEMP*(Y(IJ)**IY)
  601 T=T+TEMP*C                   accumulate in T the numerical integral of product result
   11 CØNTINUE
   10 CØNTINUE
    8 TI(I,J)=T                    final result of array element stored in TI
```

W.M. Ltd., London, S.W.1. 3585A

EXTRACT THREE